2020

Rational design of antimicrobial nanomedicines

Adam Steven Mullis
Iowa State University

Rational design of antimicrobial nanomedicines

by

Adam Steven Mullis

A dissertation submitted to the graduate faculty

in partial fulfillment of the requirements for the degree of

DOCTOR OF PHILOSOPHY

Major: Chemical Engineering

Program of Study Committee:
Balaji Narasimhan, Co-major Professor
Bryan H. Bellaire, Co-major Professor
Thomas J. Mansell
Ian C. Schneider
Richard J. Martin
Michael J. Wannemuehler

The student author, whose presentation of the scholarship herein was approved by the program of study committee, is solely responsible for the content of this dissertation. The Graduate College will ensure this dissertation is globally accessible and will not permit alterations after a degree is conferred.

Iowa State University

Ames, Iowa

2020

DEDICATION

This work is dedicated to my parents, Anthony W. Mullis and Barbara A. Mullis, and to my wife, Kiva D. Mullis. Mom and Dad, your sacrifice and support gave me the opportunity me to chase my dreams. It must not have been easy to send me off to Raleigh, then to Ames. Thank you for being understanding when I didn't call as often as I should, and for believing in me throughout my graduate degree. You inspire me to pursue science that helps other people. Kiva, you have made the challenging course of my doctoral pursuit a smoother, more pleasant track. You have celebrated with me on good data days and built me back up when the failures became too much. You are endlessly compassionate for your students and community, which keeps me focused on the people my research is intended to help. I'm so fortunate to have you by my side. You are my closest friend, and I'm excited to see where life takes us next.

TABLE OF CONTENTS

Page

LIST OF FIGURES

Page

LIST OF TABLES

Page

ACKNOWLEDGMENTS

The dissertation presented in the following pages is not solely a personal achievement, but is the culmination of hard work, contributed expertise, and patient collaboration of many others. This work would not have been possible absent these contributions.

I wish to express my heartfelt gratitude toward my advisor and mentor, Dr. Balaji Narasimhan. The quote (attributed to Steven Spielberg), "The delicate balance of mentoring someone is not creating them in your own image, but giving them the opportunity to create themselves," crystallizes his keen eye toward training new researchers. He encouraged me to pursue new avenues to develop my own expertise and scientific communication skills. His tenacious optimism and focus on the human impact of the diseases we're trying to treat helped me persist through challenging periods. He consistently treated me with dignity, respect, and confidence in my potential. I am truly fortunate to have had the opportunity to work with him over the past six years.

I would also like to thank my co-advisor, Dr. Bryan Bellaire, and his lab members Nathan Peroutka-Bigus, Kruttika Phadke, and Dr. Andrea Binnebose. Through countless collaborations, we've gone through hundreds of nanoparticle batches and observed remarkable outcomes when pathogens are treated with nanoparticles. Their complementary perspective and frank critique challenged me to improve as a researcher, contributing to many of the innovations contained in this dissertation. Without their microbiological expertise, we would not have been able to investigate nanomedicine therapies for such harmful pathogens as *Mycobacterium tuberculosis* and *Burkholderia pseudomallei* and *mallei,* to name a few.

I would like to thank my other committee members, Dr. Thomas Mansell, Dr. Ian Schneider, Dr. Richard Martin, and Dr. Wannemuehler, for their contributed time, wisdom, and guidance. Dr. Mansell and Dr. Monica Lamm supported my development as an educator during my teaching assistantship and through the Preparing Future Faculty program.

To my lab mates, Dr. Sean Kelly, Dr. Kathleen Ross, Dr. John Goodman, Dr. Julia Vela-Ramirez, Dr. Shannon Haughney, Dr. Tim Brenza, Ben Schlichtmann, Sujata Senapati, Luman Liu, and Alaric Siddoway, thank you for your friendship, guidance, and support. The help and support of my ISU undergraduate mentees, Sarah Jacobson, Sierra Teeter, Deanna Clark, Akash Mitra, and Eden Woldesenbet, was important for shaping the directions our research pursued. A particularly big thanks goes to Sarah and Sierra for their hard work and curiosity in developing high-throughput assays to screen new nanomedicine formulations and exploring sources of variability between nanoparticle batches, respectively. Seeing the both of you grow and develop as researchers is one of my fondest memories of my time at ISU. Additionally, I would like to thank my collaborators Edmund Norris, Caleb Corona, and Dr. Joel Coats of Entomology at ISU; Lauren Washington, Fernando Marcos, and Dr. Gary Munkvold of Plant Pathology at ISU; Dr. Saurabh Verma of Biomedical Sciences at ISU; and Dr. Rohana Dassanayake of the USDA Agricultural Research Service.

Although not always an easy path, my time at Iowa State University provided valuable opportunities for professional, personal, and emotional growth and was filled with warm memories I will cherish my entire life. My final acknowledgement goes to my support network of my family since birth, my new family since marriage, and my

cherished friends at ISU. You have shaped the man I am today. I am immensely grateful for your support.

ABSTRACT

We are living in a post-antibiotic era. The miracle drugs that shaped our modern healthcare system are losing effectiveness, and we aren't developing enough new drugs to meet patient needs. Innovative strategies to kill resistant bacteria and protect our antibiotic arsenal are urgently needed. Biodegradable polyanhydride nanoparticle-based nanomedicines could shape the next generation of antimicrobial therapies by improving drug biodistribution and targeting. By controlling drug release and improving antibiotic potency, they provide dose sparing and dose frequency reduction capabilities that could improve compliance. Unfortunately, traditional screening approaches are impractical for nanomedicines due to the massive physicochemical dataspace contributed by drug, polymer, and nanoparticle properties. Additionally, the relationships between these properties and nanomedicine efficacy are complex and nonlinear, impeding first principles modeling. Improved methods of screening and modeling antimicrobial nanomedicines are needed to realize their full potential.

In this dissertation, we report the adaptation of a high-throughput method to rapidly screen a novel polyanhydride copolymer chemical space for interesting drug delivery properties. These CPTEG:SA copolymers were shown to erode more rapidly than traditional polyanhydride copolymers, resulting in rapid, chemistry-dependent drug release within three days. This rapid release could be beneficial for fast-growing pathogens by providing a quick, suppressive antibiotic dose that is maintained over several days. The high-throughput method was adapted to synthesize polymer-drug films to screen for thermodynamic mixing interactions that influence release kinetics.

These methods enabled high-throughput synthesis of antibiotic-loaded nanoparticle libraries, which were evaluated for their controlled release capabilities and antimicrobial efficacy against the opportunistic, resistant pathogen *Burkholderia cepacia*. Multivariate data analytics approaches were used to identify key polymer, drug, and nanoparticle properties that determine nanomedicine release kinetics and efficacy. Graph theory was used to reduce the dimensionality of the descriptor data while preserving nonlinear relationships between formulations, enabling interrogation of nanomedicine design pathways. The dimensionally compressed descriptor space was used to develop predictive models for nanomedicine release kinetics and efficacy. These models successfully predicted the release kinetics and encapsulation efficiency for nanoparticles encapsulating two drugs not included in the training data set. In terms of efficacy, the model successfully predicted whether untested individual nanomedicines or nanomedicine cocktails would provide improved potency over soluble drug.

From these results, we proposed two informatics-assisted frameworks to rapidly screen nanomedicine candidates capable of killing resistant bacteria and controlling drug release. Overall, this dissertation has provided the first steps toward a broader framework for the rational design of antimicrobial nanomedicines. Lead candidates identified by this framework could provide new therapies against resistant pathogens and enable repurposing of existing antibiotics limited by resistance.

CHAPTER 1. INTRODUCTION: THE RESISTANCE THREAT

We are living in a post-antibiotic era.[1] The miracle drugs that laid the foundation of the modern healthcare system are no longer broadly effective, and we are at substantial risk of losing the effectiveness of the remaining drugs. Without antibiotics, surgeries would be much riskier and organ transplants would be nearly impossible.[1] Many patients with chronic diseases would live shorter, less comfortable lives and septic infections would once again become a fatal prospect.[1] We urgently need new strategies to kill resistant bacteria and protect the potency of our existing antibiotic supply.

The discovery of penicillin by Alexander Fleming ushered in the modern antibiotic era, but in his Nobel lecture he cautioned careful stewardship of antibiotics to ward against resistance.[2] Indeed, the introduction of each new class of antibiotics into the market has been followed by discovery of organisms resistant to them (Figure 1.1).[3,4] Recently, antimicrobial resistance (AMR) rates in the U.S. and across the globe have been rising due to a combination of clinical, agricultural, industrial, and regulatory missteps. Antibiotics are overprescribed in the U.S., and studies have shown that antibiotics are inappropriately prescribed 30-50% of the time based on drug chosen, therapy duration, and indication.[3–5] Additionally, 20% of patients who take antibiotics experience adverse events,[6] which can be serious enough to hurt patient compliance.[7] Agricultural use of antibiotics has also been linked to transferring AMR bacteria from livestock to humans.[8] These improper uses of antibiotics collectively contribute to AMR by selecting for the most resistant members of a bacterial population. This selective pressure, coupled with the high capacity for mutations in bacteria and horizontal gene transfer mechanisms, provides a powerful driving force toward the cultivation of resistance.

Compounding these problems, the antibiotic development pipeline has stagnated over the past 30 years. The cost of bringing new antibiotics to market is much higher than in the past due to new FDA standards for clinical trial design.[4] Antibiotics are best used only when necessary and for the shortest time possible to prevent risk of AMR, limiting the profitability of these drugs to their manufacturers. Antibiotic stewardship guidelines mandate that new antibiotics are reserved for use only in last-resort cases, dramatically reducing the patient pool. The $2.6 billion cost of bringing a drug to market[9] coupled with the idealized low utilization of antibiotics makes research and development of new antibiotics an economically unfavorable prospect for pharmaceutical companies. Accordingly, most manufacturers have left the antibiotic space entirely,[10] resulting in an antibiotic clinical development pipeline too sparse to meet patient needs and with few new antimicrobial mechanisms.[1,11] These factors have led to a push for improved antibiotic stewardship and increased public funding for novel antimicrobials.[1]

Resistant infections have profound socioeconomic impacts. Each year in the U.S, AMR microbes cause close to three million infections, resulting in 35,900 deaths.[1] Based on a case study performed in a Chicago hospital,[12] the Alliance for the Prudent Use of Antibiotics estimates that in 2000, AMR infections caused greater than $35 billion in economic losses to U.S. families due to lost wages, length of hospital stays, and early deaths.[13] Beyond the U.S. border, AMR infections pose challenges for global healthcare systems. AMR infections are associated with higher mortality and increased healthcare costs in developing countries.[14] Globalized travel carries the risk that local shortcomings, such as limitations in AMR surveillance programs and antibiotic stewardship, prevention, and control programs,[14] become threats to every nation.

Healthcare experts and scientists have sounded a call to action to combat this dire threat. The National Academy of Engineering's "Engineer Better Medicines" grand challenge calls for improved medicines to combat AMR.[15] In 2013, the CDC issued a list of four core actions it is taking to slow and prevent AMR (Figure 1.2). Since then, the CDC has established the AR Lab Network to provide resistance testing services to healthcare facilities, launched tools to track antibiotic use and AMR through the National Healthcare Safety Network, and identified key organisms that pose AMR threats.[1]

This dissertation seeks to respond to these calls to action by developing antimicrobial nanomedicine formulations based on polyanhydride nanoparticles and existing antibiotic drugs. These nanomedicines have been shown to improve the activity of their antibiotic payloads by delivering them past complex biological barriers in a Trojan horse mechanism. However, the rules that govern the effectiveness of these nanomedicines are poorly understood. Distillation of these nanomedicine design rules would allow more effective formulations to be designed *de novo* and accelerate the rational identification of effective nanomedicines. By rationally designing nanomedicines that kill AMR microbes, the research described in this thesis could lay the foundation for new therapies to fight resistant organisms and enable repurposing of antibiotics currently limited by resistance.

1.1 References

(1) CDC. Antibiotic Resistance Threats in the United States. *Atlanta, GA, U.S. Dep. Heal. Hum. Serv. CDC* **2019**. https://doi.org/CS239559-B.

(2) Fleming, A. Penicillin, Nobel Lecture. 1945.

(3) Centers for Disease Control and Prevention. *Antibiotic Resistance Threats in the United States*; 2013. https://doi.org/CS239559-B.

(4) Ventola, C. L. The Antibiotic Resistance Crisis: Part 1: Causes and Threats. *P T A peer-reviewed J. Formul. Manag.* **2015**, *40* (4), 277–283. https://doi.org/Article.

(5) Luyt, C.-E.; Bréchot, N.; Trouillet, J.-L.; Chastre, J. Antibiotic Stewardship in the Intensive Care Unit. *Crit. Care* **2014**, *18* (5), 480. https://doi.org/10.1186/s13054-014-0480-6.

(6) Tamma, P. D.; Avdic, E.; Li, D. X.; Dzintars, K.; Cosgrove, S. E. Association of Adverse Events with Antibiotic Use in Hospitalized Patients. *JAMA Intern. Med.* **2017**, *177* (9), 1308–1315. https://doi.org/10.1001/jamainternmed.2017.1938.

(7) Kishor, K.; Dhasmana, N.; Kamble, S.; Sahu, R. Linezolid Induced Adverse Drug Reactions - An Update. *Curr. Drug Metab.* **2015**, *16* (7), 553–559. https://doi.org/10.2174/1389200216666151001121004.

(8) Bartlett, J. G.; Gilbert, D. N.; Spellberg, B. Seven Ways to Preserve the Miracle of Antibiotics. *Clin. Infect. Dis.* **2013**, *56* (10), 1445–1450. https://doi.org/10.1093/cid/cit070.

(9) DiMasi, J. A.; Grabowski, H. G.; Hansen, R. W. Innovation in the Pharmaceutical Industry: New Estimates of R&D Costs. *J. Health Econ.* **2016**, *47*, 20–33. https://doi.org/10.1016/j.jhealeco.2016.01.012.

(10) Young, R. *Hunting the Nightmare Bacteria*; Frontline, Public Broadcasting Service, 2013.

(11) The Pew Charitable Trusts. Tracking the Global Pipeline of Antibiotics in Development https://www.pewtrusts.org/en/research-and-analysis/issue-briefs/2019/09/tracking-the-global-pipeline-of-antibiotics-in-development.

(12) Roberts, R. R.; Hota, B.; Ahmad, I.; Scott II, R. D.; Foster, S. D.; Abbasi, F.; Schabowski, S.; Kampe, L. M.; Ciavarella, G. G.; Supino, M.; et al. Hospital and Societal Costs of Antimicrobial-Resistant Infections in a Chicago Teaching Hospital: Implications for Antibiotic Stewardship. *Clin. Infect. Dis.* **2009**, *49* (8), 1175–1184. https://doi.org/10.1086/605630.

(13) Alliance for the Prudent Use of Antibiotics. *The Cost of Antibiotic Resistance to U.S. Families and the Health Care System*; 2010.

(14) Founou, R. C.; Founou, L. L.; Essack, S. Y. Clinical and Economic Impact of Antibiotic Resistance in Developing Countries: A Systematic Review and Meta-Analysis. *PLoS One* **2017**, *12* (12), e0189621. https://doi.org/10.1371/journal.pone.0189621.

(15) National Academy of Engineering. *Engineer Better Medicines*; 2018.

1.2 Figures

Figure 1.1 Timeline of antibiotic introduction and resistance.[3] Introduction of new antibiotics is followed by discovery of organisms resistant to them.

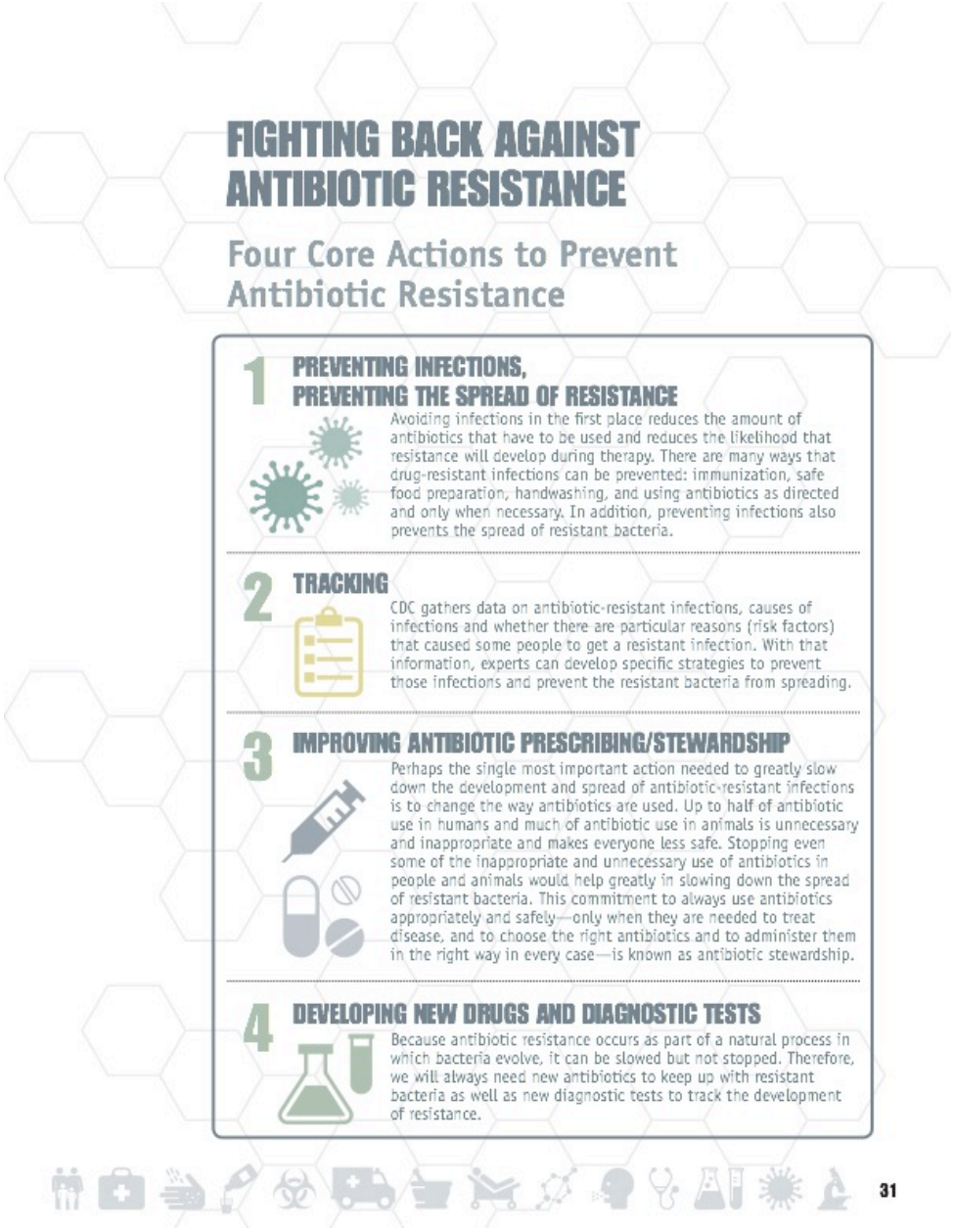

Figure 1.2 CDC core action plan for combatting antimicrobial resistance.[3]

CHAPTER 2. LITERATURE REVIEW

Adapted with modifications from Mullis, A.; Schlichtmann, B. W.; Narasimhan, B.; Cademartiri, R.; Mallapragada, S. K. Ligand-Cascading Nano-Delivery Devices to Enable Multiscale Targeting of Anti-Neurodegenerative Therapeutics. *Biomed. Mater.* **2018**, *13* (3).[1]

As discussed in the previous chapter, antimicrobial resistance (AMR) is a defining challenge for our modern healthcare system. This threat requires innovative solutions to preserve our existing antibiotic supply and provide new therapies against resistant pathogens. This chapter will begin by introducing major classes of antimicrobial compounds and their respective limitations in Section 2.1. Section 2.2 will introduce drug delivery platforms and concepts that have been used to improve the activity of antimicrobial drugs. As many AMR pathogens inhabit locations where the biodistribution of drugs is poor, Section 2.3 will discuss strategies for targeting and crossing complex biological barriers.

2.1 Antimicrobial Therapies and Antimicrobial Resistance Mechanisms

The activity of antibiotics against bacteria is dependent on the physiology of the bacteria. Gram-positive bacteria have a plasma single membrane and a thick peptidoglycan cell wall (Figure 2.1). Gram-negative bacteria have a thinner peptidoglycan layer which is sandwiched between two plasma membranes (Figure 2.1). The outer plasma membrane of Gram-negative bacteria is an additional barrier to drug diffusion (relative to Gram-positive bacteria) and is a major reason many Gram-positive compounds show poor efficacy against Gram-negative bacteria.[2]

2.1.1 Antibiotic Classification

Antibiotics can be broadly divided into five major categories based on their targets and mechanism of action (Figure 2.2). These targets include the bacterial cell wall,

metabolism and cofactor synthesis, DNA synthesis, RNA synthesis, and protein synthesis. The categories are further broken down into drug classes consisting of a parent compound and its derivatives.

Many successful antibiotics target the bacterial cell wall. β-lactams contribute the majority of these compounds, yielding over 100 clinically-relevant antibiotics in the last 75 years.[3] β-lactams target transpeptidases, which are responsible for linking and rearranging peptidoglycan in the bacterial cell wall.[2] Blocking transpeptidase activity inhibits cell wall repair, resulting in weak structural stability and eventual cell lysis.[4] Four major classes of β-lactams exist: penicillin and its derivatives, cephalosporins, carbapenems, and monobactams. β-lactams have a broad-spectrum of activity, meaning that they generally have activity against both Gram-positive and Gram-negative bacteria.[2] Carbapanems have the most potency and widest spectrum of all β-lactams, and are the quintessential last-line antibiotics that are used when front line drugs are not effective.[5] Glycopeptides also target cell wall repair by binding to terminal D-alanyl-D-alanine units on peptidoglycan,[4] which prevents transpeptidase recognition of the peptidoglycan and results in similar outcomes as β-lactams. Lipopeptides are a newer class of antibiotics that are often categorized with β-lactams and glycopeptides, however they target the cell membrane instead of the cell wall. Although some aspects of the mechanism remain unclear, they generally act by insertion of a hydrophobic tail into the plasma membrane, which causes pore formation and cell death by ion leakage.[6] Both glycopeptides and lipopeptides are indicated for Gram-positive infections.[2]

Sulfonamides and trimethoprim comprise an antibiotic category that inhibits the production of bacterial cofactors. Both antibiotics inhibit enzymes along the metabolic

pathway converting folate to tetrahydrofolate.[4,7] Notably, tetrahydrofolate is a cofactor in amino acid and nucleic acid metabolism.[8] Therefore sulfonamides and trimethoprim interfere with the bacterial production of biomolecules essential for life.

Some antibiotics target enzymatic machinery that maintains and manipulates DNA. Quinolones are a class of broad-spectrum bactericidal and bacteriostatic compounds that target DNA gyrase and DNA topoisomerase IV, inhibiting DNA replication and cell growth.[9] Early quinolones generally require protein synthesis and aerobic conditions.[4] Fluoroquinolones are a second-generation set of quinolone derivatives that show improved potency and a broader spectrum than the first generation quinolones.[2] These have shown efficacy against bacteria in hypoxic conditions[4] and slow-growing bacteria that can survive with DNA gyrase only, such as *Mycobacterium tuberculosis*.[9]

Rifamycins comprise the sole major class of drugs that target RNA synthesis. These drugs inhibit transcription by interacting with RNA polymerase, interfering with the initiation step but not elongation or termination.[4] Rifampicin, a rifamycin derivative, is a front-line drug for tuberculosis.[10] Rifamycins cover a broad spectrum, but are typically used for Gram-positive infections.[4]

Many antibiotic classes act by interfering with ribosome function, thereby inhibiting protein biosynthesis at the translation step. The ribosome is comprised of 30S and 50S subunits, both of which are antibiotic targets. The 30S subunit is targeted by tetracyclines and aminoglycosides, but are not effective against anaerobic bacteria.[4] Tetracyclines bind the 30S subunit to block the binding of tRNA to the ribosome-mRNA complex, which inhibits further translation.[4] Aminoglycosides induce conformational changes in the ribosome that limit proofreading, which can result in protein truncation due to aberrant stop codons.[4]

Odilorhabdins, a recently discovered class of antibiotics isolated from *Xenorhabdus* bacteria, operate on a similar mechanism as aminoglycosides.[11] Tetracyclines, aminoglycosides and odilorhabdins have a wide spectrum of activity, although the latter has only been tested in rodent models to date.[2,11]

The 50S ribosomal subunit is targeted by macrolides, oxazolidinones, phenicols, and lincosamides. Macrolides and phenicols bind domain V of the 23S rRNA of the 50S subunit, inhibiting aminoacyl-tRNAs binding the mRNA-ribosome complex.[4] Oxazolidinones also bind the 23S rRNA of the 50S subunit,[4] and are the most recent synthetic antibiotic class to be introduced to the clinic.[12] Lincosamides also bind the 23S rRNA,[13] and are used for Gram-positive infections.[2] Macrolides, oxazolidinones, and amphenicols show a broad spectrum of activity.

2.1.2 Antimicrobial Resistance Mechanisms

Bacteria have developed multiple mechanisms of resisting antimicrobial therapies. These mechanisms, as well as the factors that influence their prevalence in bacterial populations, are important to consider when developing therapies against AMR microbes.

Some bacteria have evolved means of preventing antibiotics from reaching their targets. Gram-negative bacteria have a second outer membrane which acts as a permeability barrier that hinders the activity of Gram-positive drugs.[14,15] Some Gram-negative bacteria such as Enterobacteriaceae, Pseudomonads, and *Acinetobacter* spp. modify the expression or type of porins in the outer membrane, which changes the ability of antibiotics to diffuse across the membrane.[14,16] Additionally, some antibiotics require certain enzymatic machinery for activity. For example, anaerobic bacteria are not susceptible to aminoglycosides because those compounds require a functional electron transport chain for activity.[4] A major mechanism of acquired AMR involves bacterial efflux pumps, which actively export toxic

compounds outside the bacterium. Of particular interest are the multidrug resistance (MDR) efflux pumps, which are capable of transporting a broad range of drugs. ATP-binding cassette (ABC) family transporters constitute one subset of MDR efflux pumps that use ATP to drive drug efflux.[15] A second class of these transporters uses the cell membrane electrochemical potential to pump out antibiotics; notable groups of this class include the resistance nodulation division (RND), small multidrug resistance (SMR), and multidrug and toxic compound extrusion (MATE) families and the major facilitator superfamily (MFS).[15] The RND family contains many clinically important export pumps, like the AcrAB-TolC in *Escherichia coli* and *Salmonella enterica*, as well as highly homologous systems in *P. aeruginosa*, *A. baumannii*, *and Neisseria gonorrhoeae*.[14,15]

Other AMR bacteria prevent antibiotic activity by mutating or modifying the drug targets. The high mutation rate that many pathogenic bacteria have can result in multiple functional genetic copies of an antibiotic target, which can enable bacterial survival when the drug has limited affinity for the mutated copy. For example, *Pseudomonas aeruginosa* resistance to the antibacterial agent triclosan has been shown to be due to an alternative duplicate of the *fabI* gene, which encodes the enzymatic target of the drug.[17] Additionally, bacteria can express enzymes that chemically modify the drug targets, which reduces antibiotic binding. Chloramphenicol-florfenicol resistant methyltransferase, which has been identified in *Staphylococcus aureus* and *E. coli*, methylates the 23S rRNA of the 50S subunit, which causes resistance to drugs that target this site (e.g. phenicols, oxazolidonones).[14]

Bacteria can also degrade or chemically modify antibiotics to interfere with their ability to bind targets. β-lactamases are a classic example of this mechanism, and act by

hydrolytically cleaving the β-lactam ring.[2] Since the 1970s, a class of antibiotic adjuvants called β-lactamase inhibitors have been developed to competitively bind or permanently inactivate β-lactamases, allowing β-lactam antibiotics to reach penicillin binding proteins and mediate cell killing.[18] Carbapenems showed the remarkable capacity to simultaneously act as a β-lactamase inhibitor and inhibit penicillin binding proteins, giving them remarkable potency and breadth of spectrum.[19] Unfortunately, highly active β-lactamases with reduced susceptibility to β-lactamase inhibitors, known as carbapenemases, have been recently and increasingly identified in multidrug resistant bacteria like *Klebsiella pneumoniae*.[5,20] These carbapenem resistant Enterobacteriaceae (CRE) infections are hard to treat and highly lethal, and are listed as an urgent threat by the CDC.[20,21] By a similar mechanism of chemical modulation-mediated inactivation as β-lactams, aminoglycosides are particularly vulnerable to transferase-mediated modification with acyl, phosphate, nucleotidyl, and ribotyl moieties due to their reactive hydroxyl and amide groups.[14] Rifamycin can also be deactivated by a rifamycin phosphotransferase that has been recently discovered in Actinomycetes.[14]

2.1.3 Acquisition of and Selection for Antimicrobial Resistance

Mobile genetic elements are a major source of AMR trait acquisition. Bacteria can exchange DNA, including resistance genes, that are encoded on plasmids and transposons via conjugation.[22] Carbapenemases like OXA-48 and *K. pneumonia* carbapenemase are often encoded on plasmids.[20,23] Transduction is a mechanism of acquired AMR in which bacterial DNA is loaded into bacteriophages and transferred to another bacterium. Additionally, bacteria can take up loose DNA, including mobile genetic elements, in their environment in a process called transformation.[22] Genetic recombination machinery, including integrons, allows bacteria to rearrange their genetic material, which can activate AMR genes or allow

transfer to other bacteria via plasmids or transposons.[22] The free exchange of superbug genes, including MDR efflux pumps and carbapenemase, between bacteria enables rapid spread of these traits in the clinic, in the environment, and even in the absence of human hosts.[23,24]

Bacterial populations are genetically diverse prior to antimicrobial treatment. Treatment with antibiotics will kill or inhibit the growth of susceptible strains of the population, enriching the percentage of the population that is resistant to the therapy. However, these resistant traits come with some evolutionary fitness cost, meaning that susceptible strains are typically advantaged in the absence of antibiotics.[25] At a certain sub-therapeutic drug concentration, the selective pressure of the antibiotic balances out the fitness detriment of the resistant strains, above which the resistant strains gain a competitive advantage.[22] These resistance-favoring, sub-therapeutic concentrations can occur at the start and end of the therapy due to pharmacokinetics, and in tissues where the drug poorly distributes.

2.2 Countering Antimicrobial Resistance

To meet the pressing need for effective therapies against AMR bacteria, two predominant goals have risen to the fore. Firstly, new bactericidal and bacteriostatic compounds and derivatives need to synthesized, developed, tested, and brought into the clinic. This strategy is limited due to its potential for further AMR, but is necessary in the interim until better means of preventing resistance can be implemented. Secondly, approaches for improving the activity of existing antibiotics and blocking key resistance pathways need to developed. This allows repurposing of existing antibiotics, which leverages the considerable effort and cost of bringing them to market.

2.2.1 Synthesis of Novel Bioactive Compounds

Classical antibiotic screening platforms have been, with a few notable exceptions, unable generate successful new antibiotic classes since the golden age of antibiotics. Improvements to the screening approach could yield new useful drugs. New approaches have enabled *in situ* growth and screening of "unculturable" bacteria by creating a blended agar-soil (or water) medium diffusion chamber, which could effectively bypass the cultivability limitation of classical screening.[26] Additionally, the continual decrease in the cost of transcriptomics experiments can aid compound identification in strains that show inhibitory activity.[26] Prodrugs have been effective in treating challenging intracellular infections, like *M. tuberculosis*, due to their ability to kill persisters.[26] Since all of the prodrugs were discovered in 1950s, it is likely that the much-larger modern compound libraries could harbor promising new candidates.[26] The approach of synthesizing new bioactive compounds is also severely limited by the current regulatory and economic environment. Due to high risk of toxicity compared to other therapeutic compounds, high cost of clinical trials, and limited profitability, it remains challenging to bring a brand new antibiotic to market.[27,28]

Recently, antimicrobial peptides (AMPs) have been proposed as a supplement to conventional antibiotics. Generally, AMPs are a set of eukaryotic peptides that are cationic and contain a high proportion of hydrophobic moieties.[29] They exhibit a broad spectrum by acting on general targets like the cell membrane and DNA,[30] which contrasts the molecular specificity exhibited by small molecule antibiotics. This could potentially reduce the risk of resistance. AMPs are currently limited in their high cost, proteolytic degradability, and limited understanding of their molecular mechanism.[29] As of 2018, no AMP has reached clinical testing.[31]

2.2.2 Improving Activity of Existing Antimicrobials

2.2.2.1 Antibiotic adjuvants

Antibiotic adjuvants are a set of compounds that improve the activity of antibiotics. They can be divided into Class I, which act on bacteria, and Class II, which act on the host. β-lactamase inhibitors comprise a large subset of Class I adjuvants. Clavulanic acid was the first antibiotic adjuvant to be clinically approved, and acts by irreversibly inactivating Ser-β-lactamases.[32] Multiple new Ser-β-lactamase inhibitor-antibiotic combinations have successfully passed clinical trials in the last five years.[32] Metallo-β-lactamases appear to be more challenging targets, as there are few adjuvants that show efficacy in animal models.[32] Other Class I antibiotic adjuvants interfere with passive resistance mechanisms. Loperamide, for example, interferes with the cell membrane electrochemical potential to drive an increased tetracycline permeability.[33] Other adjuvants, such as PAβN, can inhibit efflux pumps, which improve the activity of multiple classes of antibiotics.[32]

Class II adjuvants improve innate host defense mechanisms to assist antibiotic activity. LL-37 is an immunomodulatory peptide that stimulates the innate immune system's antimicrobial capabilities.[32] Another example is streptazolin, which has been shown to stimulate macrophages by NF-κB activation, resulting in improved macrophage phagocytosis and subsequent killing of *S. mutans*.[34] Increased induction of the adaptive immune response by improving phagocytosis of pathogenic bacteria could provide a complementary antimicrobial mechanism to existing antibiotic therapies.

2.2.2.2 Drug delivery vehicles

Polymeric nano-delivery devices offer another solution to improving antimicrobial activity. These nano-delivery devices can alter the biodistribution of the antibiotic and direct

its localization at target tissues within the host, which improves their efficacy and reduces their toxicity.[35] Increasing dosing frequency is correlated with poorer antibiotic regimen compliance.[36] The controlled release capabilities of many of these devices can reduce the number of administrations needed, and therefore improve compliance. The main classes of these (polymeric) devices include dendrimers, micelles, nanoparticles, nanotubes, liposomes, and polymersomes.[37] These devices typically encapsulate or chemically link a drug payload, which is protected from physiological degradation by a biocompatible material.[38] Additionally, the devices offer suitable chemistries for facile linkage of functional groups, or targeting ligands to navigate the hurdles associated with brain drug delivery.[38,39] The ability to link targeting ligands to these devices provides a "plug-and-play" capability in that a functionalization used on one device can often be replicated on another to exploit that device's physical properties.

Dendrimers contain many functional groups that allow for the ability to conjugate therapeutics and significantly improve bioavailability, which makes them very versatile.[40,41] Additionally, dendrimers have demonstrated high biocompatibility and enhanced the circulation times of conjugated therapeutics.[40,42] Liposomes are also biocompatible and can be functionalized, but additionally possess lipophilic properties that may be well suited for adsorptive-mediated strategies.[37] Micelles have a hydrophilic shell and hydrophobic core, which gives them amphiphilic properties; this can enable high encapsulation of hydrophobic therapeutics.[37]

Polymeric nanoparticles, based on biodegradable polymer such as polyesters and polyanhydrides, can provide precisely controlled sustained therapeutic release properties and easily tailor-able chemistries.[43–49] Carbon nanotubes exhibit a high surface area to volume

ratio that enables high loading capacity;[50] this unique property could be beneficial when multiple therapeutics are to be used for the same treatment. Polymersomes, which self-assemble in water, also feature easily tunable size and chemistry.[51]

Metallic nano-delivery devices are also available. While less biocompatible than polymeric devices and not biodegradable, they can be made to a smaller size. For example, iron oxide nanoparticles can be made with a diameter of less than 50 nm whereas most polymeric nanoparticles are limited to sizes of 50 nm or greater.[52–57] These small sizes can enable more flexibility in organelle targeting by allowing passive NPC transport. Additionally, research has demonstrated high levels of internalization of such devices by phagocytic immune cells, indicating their promise for cell-mediated delivery.[55,58] While an extensive review of these core nano-delivery device technologies is outside the scope of this paper, Jia et al. and Shadab et al. have written reviews on nano-delivery device technologies.[59,60]

Polyanhydride nanoparticles represent a promising drug delivery platform. They are biodegradable,[61] show high biocompatibility,[62,63] and are synthesized from the same parent materials as an FDA-approved device for treating malignant gliomas, the Gliadel® wafer.[64] Their erosion rate, and therefore their rate of payload release, can be tuned by altering the copolymer molar composition.[65,66] Typical polyanhydride carriers for drug and vaccine delivery are formulated using monomer such as sebacic acid (SA), 1,3-bis-(*p*-carboxyphenoxy)propane (CPP),1,6-bis-(*p*-carboxyphenoxy)hexane (CPH), and 1,8-bis-(*p*-carboxyphenoxy)-3,6-dioxaoctane (CPTEG). Polymer-drug thermodynamic mixing interactions are known to influence polyanhydride film and microparticle release kinetics.[67,68] Favorable interactions lead to diffuse drug distribution within the device resulting in erosion-

controlled release, while unfavorable interactions induce precipitation and localization of the drug at the device surface, resulting in a burst release.[67,69,70] The tunable release kinetics exhibited by polyanhydride particles allows them to be adapted for different therapeutic scenarios. Their extended release capabilities could reduce the number of therapeutic administrations requires, enhancing patient compliance.

Polyanhydride nanoparticles have been used to successfully deliver antibiotics past complex biological barriers. Phanse et al. showed that nanoparticle chemistries that achieved high internalization in phagocytic cells were able kill intracellular *Brucella abortus* by delivering doxycycline.[71] Rifampicin-encapsulating polyanhdride nanoparticles showed improved elimination of *Brucella melitensis* infecting macrophages, and protected against *B. melitensis infection* following nanoparticle pretreatment compared to soluble drug *in vitro*.[72] *In vivo*, weekly doses of these nanoparticles provided comparable reductions in liver and spleen *B. melitensis* colonization after three weeks as daily soluble drug, a seven fold reduction in antibiotic dose.[72] Binnebose et al. demonstrated that 20:80 CPTEG:CPH nanoparticles could effectively co-deliver ivermectin, a hydrophobic antiparasitic, and doxycycline to kill filarial worms *in vitro*.[73] In adult female worms, they observed a 4000x dose sparing effect in the nanoparticles compared to soluble drug. These results support the hypothesis that the use of such nano-carriers can improve the activity of existing antimicrobial drugs.

2.3 Intracellular Drug Delivery

In many cases, therapeutic efficacy can be maximized by delivering the therapeutic payload to an organelle inside the target cell.[74] The scale of impact in organelle delivery is significantly smaller than that at the cellular internalization level; host phagocytic cells can have a surface area on the order of tens to hundreds of square microns, but the mitochondria

and nucleus typically have surface areas of one to tens of square microns. Specifically, mitochondria are typically 0.75-3.0 square microns in size, which limits the functional surface area for interaction.[75] Whereas cell internalization relies on protein-ligand or membrane interactions; size, morphology, and charge are the primary determinants of intracellular organelle accumulation.

2.3.1 Surviving the Endocytic Pathway

The primary concern in designing organelle-specific nano-delivery devices is escaping the endocytic pathway. Nano-delivery devices that exploit receptor-mediated endocytosis to achieve internalization must be able to protect their payload from acidic hydrolysis and escape from endosomes and lysosomes into the cytosol. Several techniques for endosomal escape of delivery devices have therefore been developed (Figure 2.3, Table 2.1). Cationic amphiphilic peptides, like melittin, a major component of bee venom, and KALA, a synthetic peptide derived from influenza hemagglutinin, associate strongly with the endosomal membrane.[76–79] This association disrupts stabilizing tension forces, which causes pore formation.[80] Alternatively, photoreactive molecules can be released that degrade the endosomal membrane via production of reactive oxygen species.[80] Another well-studied technique is to decorate the device with buffering agents such as quaternary and tertiary amines that causes an immense inflow of ions and water and ruptures the endosome membrane due to osmotic pressure; this is commonly referred to as the “proton sponge effect”.[80]

2.4 Conclusions

Antimicrobial resistance is a rising threat to the modern healthcare system. Due to complex economic, social, and regulatory factors, the clinical supply pipeline is too sparsely populated to meet current or future patient needs.[28] At the same time, the existing supply of

antibiotics is being rendered ineffective by resistance. There is an urgent need for new antimicrobial therapies and strategies that repurpose existing antibiotics. Polyanhydride nanoparticles can improve the activity of encapsulated antibiotics by delivering them to their site of action, generating a dose sparing effect. Reducing the dose needed to clear an infection can reduce the patient's risk of toxicity. Gradually releasing drugs over a long period of time can reduce the number of administrations, and thereby improve compliance. In these ways, antimicrobial-loaded polyanhydride nanoparticles could shape the next generation of antimicrobial therapies. These "nanomedicines" have shown the potential to contribute new therapies against resistant organisms, and could enable repurposing of antibiotics limited by resistance.

2.5 References

(1) Mullis, A. S.; Schlichtmann, B. W.; Narasimhan, B.; Cademartiri, R.; Mallapragada, S. K. *Ligand-Cascading Nano-Delivery Devices to Enable Multiscale Targeting of Anti-Neurodegenerative Therapeutics*; IOP Publishing, 2018; Vol. 13, p 034102. https://doi.org/10.1088/1748-605X/aaa778.

(2) Singh, S. B.; Young, K.; Silver, L. L. What Is an "Ideal" Antibiotic? Discovery Challenges and Path Forward. *Biochemical Pharmacology*. Elsevier June 1, 2017, pp 63–73. https://doi.org/10.1016/j.bcp.2017.01.003.

(3) Page, M. G. P. Beta-Lactam Antibiotics BT - Antibiotic Discovery and Development. In *Antibiotic Discovery and Development*; Dougherty, T. J., Pucci, M. J., Eds.; Springer US: Boston, MA, 2012; pp 79–117. https://doi.org/10.1007/978-1-4614-1400-1_3.

(4) Carlson-Banning, K. M.; Zechiedrich, L. Antibiotic Classes and Mechanisms of Resistance. In *Encyclopedia of Metagenomics*; Highlander, S. K., Rodriguez-Valera, F., White, B. A., Eds.; Springer US: Boston, MA, 2013; pp 1–13. https://doi.org/10.1007/978-1-4614-6418-1_55-1.

(5) Queenan, A. M.; Bush, K. Carbapenemases: The Versatile β-Lactamases. *Clin. Microbiol. Rev.* **2007**, *20* (3), 440–458. https://doi.org/10.1128/CMR.00001-07.

(6) Steenbergen, J. N.; Alder, J.; Thorne, G. M.; Tally, F. P. Daptomycin: A Lipopeptide Antibiotic for the Treatment of Serious Gram-Positive Infections. *J. Antimicrob. Chemother.* **2005**, *55* (3), 283–288. https://doi.org/10.1093/jac/dkh546.

(7) Sköld, O. Resistance to Trimethoprim and Sulfonamides. In *Veterinary Research*; EDP Sciences, 2001; Vol. 32, pp 261–273. https://doi.org/10.1051/vetres:2001123.

(8) Wishart, D. S.; Feunang, Y. D.; Guo, A. C.; Lo, E. J.; Marcu, A.; Grant, J. R.; Sajed, T.; Johnson, D.; Li, C.; Sayeeda, Z.; et al. DrugBank 5.0: A Major Update to the DrugBank Database for 2018. *Nucleic Acids Res.* **2018**, *46* (D1), D1074–D1082. https://doi.org/10.1093/nar/gkx1037.

(9) Jacoby, G. A.; Hooper, D. C. Review of the Quinolone Family BT - Antibiotic Discovery and Development. In *Antibiotic Discovery and Development*; Dougherty, T. J., Pucci, M. J., Eds.; Springer US: Boston, MA, 2012; pp 119–146. https://doi.org/10.1007/978-1-4614-1400-1_4.

(10) Seung, K. J.; Keshavjee, S.; Rich, M. L. Drug-Resistant Tuberculosis. *Cold Spring Harb Perspect Med* **2015**, *5*, 1–20.

(11) Pantel, L.; Florin, T.; Dobosz-Bartoszek, M.; Racine, E.; Sarciaux, M.; Serri, M.; Houard, J.; Campagne, J. M.; de Figueiredo, R. M.; Midrier, C.; et al. Odilorhabdins, Antibacterial Agents That Cause Miscoding by Binding at a New Ribosomal Site. *Mol. Cell* **2018**, *70* (1), 83-94.e7. https://doi.org/10.1016/j.molcel.2018.03.001.

(12) Chellat, M. F.; Raguž, L.; Riedl, R. Targeting Antibiotic Resistance. *Angew. Chemie - Int. Ed.* **2016**, *55* (23), 6600–6626. https://doi.org/10.1002/anie.201506818.

(13) Spížek, J.; Řezanka, T. Lincosamides: Chemical Structure, Biosynthesis, Mechanism of Action, Resistance, and Applications. *Biochemical Pharmacology*. 2017, pp 20–28. https://doi.org/10.1016/j.bcp.2016.12.001.

(14) Blair, J. M. A.; Webber, M. A.; Baylay, A. J.; Ogbolu, D. O.; Piddock, L. J. V. Molecular Mechanisms of Antibiotic Resistance. *Nat. Rev. Microbiol.* **2011**, *47* (14), 4055–4061. https://doi.org/10.1039/c0cc05111j.

(15) Blair, J. M.; Richmond, G. E.; Piddock, L. J. Multidrug Efflux Pumps in Gram-Negative Bacteria and Their Role in Antibiotic Resistance. *Future Microbiol.* **2014**, *9* (10), 1165–1177. https://doi.org/10.2217/fmb.14.66.

(16) Tamber, S.; Hancock, R. E. W. On the Mechanism of Solute Update in Pseudomonas. *Front. Biosci* **2003**, *8*, 472–483.

(17) Zhu, L.; Lin, J.; Ma, J.; Cronan, J. E.; Wang, H. Triclosan Resistance of Pseudomonas Aeruginosa PAO1 Is Due to FabV, a Triclosan-Resistant Enoyl-Acyl Carrier Protein Reductase. *Antimicrob. Agents Chemother.* **2010**, *54* (2), 689–698. https://doi.org/10.1128/AAC.01152-09.

(18) Drawz, S. M.; Bonomo, R. A. Three Decades of β-Lactamase Inhibitors. *Clin. Microbiol. Rev.* **2010**, *23* (1), 160–201. https://doi.org/10.1128/CMR.00037-09.

(19) Papp-Wallace, K. M.; Endimiani, A.; Taracila, M. A.; Bonomo, R. A. Carbapenems: Past, Present, and Future. *Antimicrob. Agents Chemother.* **2011**, *55* (11), 4943–4960. https://doi.org/10.1128/AAC.00296-11.

(20) McCann, E.; Srinivasan, A.; Andrew DeRyke, C.; Ye, G.; DePestel, D. D.; Murray, J.; Gupta, V. Carbapenem-Nonsusceptible Gram-Negative Pathogens in ICU and Non-ICU Settings in US Hospitals in 2017: A Multicenter Study. *Open Forum Infect. Dis.* **2018**, *5* (10), 1–7. https://doi.org/10.1093/ofid/ofy241.

(21) CDC. Antibiotic Resistance Threats in the United States. *Atlanta, GA, U.S. Dep. Heal. Hum. Serv. CDC* **2019**. https://doi.org/CS239559-B.

(22) Van Hoek, A. H. A. M.; Mevius, D.; Guerra, B.; Mullany, P.; Roberts, A. P.; Aarts, H. J. M. Acquired Antibiotic Resistance Genes: An Overview. *Frontiers in Microbiology*. Frontiers Media SA 2011, p 203. https://doi.org/10.3389/fmicb.2011.00203.

(23) Bonomo, R. A.; Burd, E. M.; Conly, J.; Limbago, B. M.; Poirel, L.; Segre, J. A.; Westblade, L. F. Carbapenemase-Producing Organisms: A Global Scourge. *Clinical Infectious Diseases*. April 3, 2018, pp 1290–1297. https://doi.org/10.1093/cid/cix893.

(24) Young, R. *Hunting the Nightmare Bacteria*; Frontline, Public Broadcasting Service, 2013.

(25) Hughes, D. Selection and Evolution of Resistance to Antimicrobial Drugs. *IUBMB Life*. Wiley-Blackwell August 2014, pp 521–529. https://doi.org/10.1002/iub.1278.

(26) Lewis, K. Platforms for Antibiotic Discovery. *Nature Reviews Drug Discovery*. Nature Publishing Group May 1, 2013, pp 371–387. https://doi.org/10.1038/nrd3975.

(27) DiMasi, J. A.; Grabowski, H. G.; Hansen, R. W. Innovation in the Pharmaceutical Industry: New Estimates of R&D Costs. *J. Health Econ.* **2016**, *47*, 20–33. https://doi.org/10.1016/j.jhealeco.2016.01.012.

(28) The Pew Charitable Trusts. Tracking the Global Pipeline of Antibiotics in Development https://www.pewtrusts.org/en/research-and-analysis/issue-briefs/2019/09/tracking-the-global-pipeline-of-antibiotics-in-development.

(29) da Costa, J. P.; Cova, M.; Ferreira, R.; Vitorino, R. Antimicrobial Peptides: An Alternative for Innovative Medicines? *Applied Microbiology and Biotechnology*. Springer Berlin Heidelberg March 15, 2015, pp 2023–2040. https://doi.org/10.1007/s00253-015-6375-x.

(30) Nguyen, L. T.; Haney, E. F.; Vogel, H. J. The Expanding Scope of Antimicrobial Peptide Structures and Their Modes of Action. *Trends in Biotechnology*. Elsevier Current Trends September 1, 2011, pp 464–472. https://doi.org/10.1016/j.tibtech.2011.05.001.

(31) AB Naafs, M. The Antimicrobial Peptides: Ready for Clinical Trials? *Biomed. J. Sci. Tech. Res.* **2018**, *7* (4), 6038–6042. https://doi.org/10.26717/bjstr.2018.07.001536.

(32) Wright, G. D. Antibiotic Adjuvants: Rescuing Antibiotics from Resistance. *Trends Microbiol.* **2016**, *24* (11), 862–871. https://doi.org/10.1016/j.tim.2016.06.009.

(33) Ejim, L.; Farha, M. A.; Falconer, S. B.; Wildenhain, J.; Coombes, B. K.; Tyers, M.; Brown, E. D.; Wright, G. D. Combinations of Antibiotics and Nonantibiotic Drugs Enhance Antimicrobial Efficacy. *Nat. Chem. Biol.* **2011**, *7* (6), 348–350. https://doi.org/10.1038/nchembio.559.

(34) Perry, J. A.; Koteva, K.; Verschoor, C. P.; Wang, W.; Bowdish, D. M.; Wright, G. D. A Macrophage-Stimulating Compound from a Screen of Microbial Natural Products. *J. Antibiot. (Tokyo).* **2015**, *68* (1), 40–46. https://doi.org/10.1038/ja.2014.83.

(35) Narasimhan, B.; Goodman, J. T.; Vela Ramirez, J. E. Rational Design of Targeted Next-Generation Carriers for Drug and Vaccine Delivery. *Annu. Rev. Biomed. Eng* **2016**, *18* (1), 25–49. https://doi.org/10.1146/annurev-bioeng-082615-030519.

(36) Falagas, M. E.; Karagiannis, A. K. A.; Nakouti, T.; Tansarli, G. S. Compliance with Once-Daily versus Twice or Thrice-Daily Administration of Antibiotic Regimens: A Meta-Analysis of Randomized Controlled Trials. *PLoS One* **2015**, *10* (1), 1–15. https://doi.org/10.1371/journal.pone.0116207.

(37) Wong, H. L.; Wu, X. Y.; Bendayan, R. Nanotechnological Advances for the Delivery of CNS Therapeutics. *Adv. Drug Deliv. Rev.* **2012**, *64* (7), 686–700. https://doi.org/10.1016/j.addr.2011.10.007.

(38) Chen, Y.; Liu, L. Modern Methods for Delivery of Drugs across the Blood-Brain Barrier. *Adv. Drug Deliv. Rev.* **2012**, *64* (7), 640–665. https://doi.org/10.1016/j.addr.2011.11.010.

(39) Wong, H. L.; Chattopadhyay, N.; Wu, X. Y.; Bendayan, R. Nanotechnology Applications for Improved Delivery of Antiretroviral Drugs to the Brain. *Adv. Drug Deliv. Rev.* **2010**, *62* (4–5), 503–517. https://doi.org/10.1016/j.addr.2009.11.020.

(40) Bielski, E. R.; Zhong, Q.; Brown, M.; Da Rocha, S. R. P. Effect of the Conjugation Density of Triphenylphosphonium Cation on the Mitochondrial Targeting of Poly(Amidoamine) Dendrimers. *Mol. Pharm.* **2015**, *12* (8), 3043–3053. https://doi.org/10.1021/acs.molpharmaceut.5b00320.

(41) Pathak, R. K.; Kolishetti, N.; Dhar, S. Targeted Nanoparticles in Mitochondrial Medicine. *Wiley Interdiscip. Rev. Nanomedicine Nanobiotechnology* **2015**, *7* (3), 315–329. https://doi.org/10.1002/wnan.1305.

(42) Biswas, S.; Dodwadkar, N. S.; Piroyan, A.; Torchilin, V. P. Surface Conjugation of Triphenylphosphonium to Target Poly(Amidoamine) Dendrimers to Mitochondria. *Biomaterials* **2012**, *33* (18), 4773–4782. https://doi.org/10.1016/j.biomaterials.2012.03.032.

(43) Kumar, N.; Langer, R. S.; Domb, A. J. Polyanhydrides: An Overview. *Adv. Drug Deliv. Rev.* **2002**, *54*, 889–910.

(44) Göpferich, A.; Tessmar, J. Polyanhydride Degradation and Erosion. *Adv. Drug Deliv. Rev.* **2002**, *54* (7), 911–931. https://doi.org/10.1016/S0169-409X(02)00051-0.

(45) Narasimhan, B.; Kipper, M.; Larobina, D.; Mensitieri, G. Bioerodible Polyanhydrides with Tailored Microstructure for Controlled Drug Delivery. In *Proceedings of the 2002 IEEE Engineering in Medicine and Biology 24th Annual Conference and the 2002 Fall Meeting of the Biomedical Engineering Society (BMES / EMBS)*; Department of Chemical Engineering, Iowa State University, Ames, IA, United States, 2002; Vol. 1, pp 468–469.

(46) Larobina, D.; Mensitieri, G.; Kipper, M. J.; Narasimhan, B. Mechanistic Understanding of Degradation in Bioerodible Polymers for Drug Delivery. *AIChE J.* **2002**, *48* (12), 2960–2970. https://doi.org/10.1002/aic.690481221.

(47) Nowacek, A. S.; Miller, R. L.; Mcmillan, J.; Kanmogne, G.; Mosley, R. L.; Ma, Z.; Graham, S.; Chaubal, M.; Rabinow, B.; Dou, H.; et al. NanoART Synthesis, Characterization, Uptake, Release and Toxicology for Human Oocyte-Macrophage Drug Delivery. *Nanomedicine (Lond)* **2009**, *4* (8), 903–917. https://doi.org/10.2217/nnm.09.71.

(48) Puligujja, P.; Balkundi, S. S.; Kendrick, L. M.; Baldridge, H. M.; Hilaire, J. R.; Bade, A. N.; Dash, P. K.; Zhang, G.; Poluektova, L. Y.; Gorantla, S.; et al. Pharmacodynamics of Long-Acting Folic Acid-Receptor Targeted Ritonavir-Boosted Atazanavir Nanoformulations. *Biomaterials* **2015**, *41*, 141–150. https://doi.org/10.1016/j.biomaterials.2014.11.012.

(49) Kanmogne, G. D.; Singh, S.; Roy, U.; Liu, X.; McMillan, J. E.; Gorantla, S.; Balkundi, S.; Smith, N.; Alnouti, Y.; Gautam, N.; et al. Mononuclear Phagocyte Intercellular Crosstalk Facilitates Transmission of Cell-Targeted Nanoformulated Antiretroviral Drugs to Human Brain Endothelial Cells. *Int. J. Nanomedicine* **2012**, *7*, 2373–2388. https://doi.org/10.2147/IJN.S29454.

(50) Ren, J.; Shen, S.; Wang, D.; Xi, Z.; Guo, L.; Pang, Z.; Qian, Y.; Sun, X.; Jiang, X. The Targeted Delivery of Anticancer Drugs to Brain Glioma by PEGylated Oxidized Multi-Walled Carbon Nanotubes Modified with Angiopep-2. *Biomaterials* **2012**, *33* (11), 3324–3333. https://doi.org/10.1016/j.biomaterials.2012.01.025.

(51) Tian, X.; Nyberg, S.; S Sharp, P.; Madsen, J.; Daneshpour, N.; Armes, S. P.; Berwick, J.; Azzouz, M.; Shaw, P.; Abbott, N. J.; et al. LRP-1-Mediated Intracellular Antibody Delivery to the Central Nervous System. *Sci. Rep.* **2015**, *5*, 11990. https://doi.org/10.1038/srep11990.

(52) Krais, A.; Wortmann, L.; Hermanns, L.; Feliu, N.; Vahter, M.; Stucky, S.; Mathur, S.; Fadeel, B. Targeted Uptake of Folic Acid-Functionalized Iron Oxide Nanoparticles by Ovarian Cancer Cells in the Presence but Not in the Absence of Serum. *Nanomedicine Nanotechnology, Biol. Med.* **2014**, *10* (7), 1421–1431. https://doi.org/10.1016/j.nano.2014.01.006.

(53) Durán-Lobato, M.; Martín-Banderas, L.; Gonçalves, L. M. D.; Fernández-Arévalo, M.; Almeida, A. J. Comparative Study of Chitosan- and PEG-Coated Lipid and PLGA Nanoparticles as Oral Delivery Systems for Cannabinoids. *J. Nanoparticle Res.* **2015**, *17* (2), 1–17. https://doi.org/10.1007/s11051-015-2875-y.

(54) Chen, J.; Zhang, C.; Liu, Q.; Shao, X.; Feng, C.; Shen, Y.; Zhang, Q.; Jiang, X. Solanum Tuberosum Lectin-Conjugated PLGA Nanoparticles for Nose-to-Brain Delivery: In Vivo and in Vitro Evaluations. *J. Drug Target.* **2012**, *20* (2), 174–184. https://doi.org/10.3109/1061186X.2011.622396.

(55) Beduneau, A.; Ma, Z.; Grotepas, C. B.; Kabanov, A.; Rabinow, B. E.; Gong, N.; Mosley, R. L.; Dou, H.; Boska, M. D.; Gendelman, H. E. Facilitated Monocyte-Macrophage Uptake and Tissue Distribution of Superparmagnetic Iron-Oxide Nanoparticles. *PLoS One* **2009**, *4* (2), 1–12. https://doi.org/10.1371/journal.pone.0004343.

(56) Sun, Z.; Yathindranath, V.; Worden, M.; Thliveris, J. A.; Chu, S.; Parkinson, F. E.; Hegmann, T.; Miller, D. W. Characterization of Cellular Uptake and Toxicity of Aminosilane-Coated Iron Oxide Nanoparticles with Different Charges in Central Nervous System-Relevant Cell Culture Models. *Int. J. Nanomedicine* **2013**, *8*, 961–970. https://doi.org/10.2147/IJN.S39048.

(57) Mathew, A.; Aravind, A.; Brahatheeswaran, D.; Fukuda, T.; Nagaoka, Y.; Hasumura, T.; Iwai, S.; Morimoto, H.; Yoshida, Y.; Maekawa, T.; et al. Amyloid-Binding Aptamer Conjugated Curcumin-PLGA Nanoparticle for Potential Use in Alzheimer's Disease. *Bionanoscience* **2012**, *2* (2), 83–93. https://doi.org/10.1007/s12668-012-0040-y.

(58) Gendelman, H. E.; Anantharam, V.; Bronich, T.; Ghaisas, S.; Jin, H.; Kanthasamy, A. G.; Liu, X.; McMillan, J. E.; Mosley, R. L.; Narasimhan, B.; et al. Nanoneuromedicines for Degenerative, Inflammatory, and Infectious Nervous System Diseases. *Nanomedicine Nanotechnology, Biol. Med.* **2015**, *11* (3), 751–767. https://doi.org/10.1016/j.nano.2014.12.014.

(59) Jia, F.; Liu, X.; Li, L.; Mallapragada, S.; Narasimhan, B.; Wang, Q. Multifunctional Nanoparticles for Targeted Delivery of Immune Activating and Cancer Therapeutic Agents. *J. Control. Release* **2013**, *172* (3), 1020–1034. https://doi.org/10.1016/j.jconrel.2013.10.012.

(60) Md, S.; Bhattmisra, S. K.; Zeeshan, F.; Shahzad, N.; Mujtaba, M. A.; Srikanth Meka, V.; Radhakrishnan, A.; Kesharwani, P.; Baboota, S.; Ali, J. Nano-Carrier Enabled Drug Delivery Systems for Nose to Brain Targeting for the Treatment of Neurodegenerative Disorders. *J. Drug Deliv. Sci. Technol.* **2018**, *43*, 295–310. https://doi.org/10.1016/j.jddst.2017.09.022.

(61) Leong, K. W.; Brott, B. C.; Langer, R. Bioerodible Polyanhydrides as Drug-carrier Matrices. I: Characterization, Degradation, and Release Characteristics. *J. Biomed. Mater. Res.* **1985**, *19* (8), 941–955. https://doi.org/10.1002/jbm.820190806.

(62) Huntimer, L.; Ramer-Tait, A. E.; Petersen, L. K.; Ross, K. a.; Walz, K. a.; Wang, C.; Hostetter, J.; Narasimhan, B.; Wannemuehler, M. J. Evaluation of Biocompatibility and Administration Site Reactogenicity of Polyanhydride-Particle-Based Platform for Vaccine Delivery. *Adv. Healthc. Mater.* **2013**, *2* (2), 369–378. https://doi.org/10.1002/adhm.201200181.

(63) Vela-Ramirez, J. E.; Goodman, J. T.; Boggiatto, P. M.; Roychoudhury, R.; Pohl, N. L.; Hostetter, J. M.; Wannemuehler, M. J.; Narasimhan, B. Safety and Biocompatibility of Carbohydrate-Functionalized Polyanhydride Nanoparticles. *AAPS J* **2014**. https://doi.org/10.1208/s12248-014-9699-z.

(64) Westphal, M.; Ram, Z.; Riddle, V.; Hilt, D.; Bortey, E. Gliadel® Wafer in Initial Surgery for Malignant Glioma: Long-Term Follow-up of a Multicenter Controlled Trial. *Acta Neurochir. (Wien).* **2006**, *148* (3), 269–275. https://doi.org/10.1007/s00701-005-0707-z.

(65) Göpferich, A.; Tessmar, J. Polyanhydride Degradation and Erosion. *Adv. Drug Deliv. Rev.* **2002**, *54* (7), 911–931. https://doi.org/10.1016/S0169-409X(02)00051-0.

(66) Petersen, L. K.; Sackett, C. K.; Narasimhan, B. Novel, High Throughput Method to Study in Vitro Protein Release from Polymer Nanospheres. *J. Comb. Chem.* **2010**, *12* (1), 51–56. https://doi.org/10.1021/cc900116c.

(67) Shen, E.; Kipper, M. J.; Dziadul, B.; Lim, M.-K.; Narasimhan, B. Mechanistic Relationships between Polymer Microstructure and Drug Release Kinetics in Bioerodible Polyanhydrides. *J. Control. Release* **2002**, *82* (1), 115–125. https://doi.org/10.1016/S0168-3659(02)00125-6.

(68) Kipper, M. J.; Hou, S.-S.; Seifert, S.; Thiyagarajan, P.; Schmidt-Rohr, K.; Narasimhan, B. Nanoscale Morphology of Polyanhydride Copolymers. *Macromolecules* **2005**, *38* (20), 8468–8472. https://doi.org/10.1021/ma051267r.

(69) Shen, E.; Pizsczek, R.; Dziadul, B.; Narasimhan, B. Microphase Separation in Bioerodible Copolymers for Drug Delivery. *Biomaterials* **2001**, *22* (3), 201–210. https://doi.org/10.1016/S0142-9612(00)00175-7.

(70) Berkland, C.; Kipper, M. J.; Narasimhan, B.; Kim, K.; Pack, D. W. Microsphere Size, Precipitation Kinetics and Drug Distribution Control Drug Release from Biodegradable Polyanhydride Microspheres. *J. Control. Release* **2004**, *94* (1), 129–141. https://doi.org/10.1016/j.jconrel.2003.09.011.

(71) Phanse, Y.; Lueth, P.; Ramer-Tait, A. E.; Carrillo-Conde, B. R.; Wannemuehler, M. J.; Narasimhan, B.; Bellaire, B. H. Cellular Internalization Mechanisms of Polyanhydride Particles: Implications for Rational Design of Drug Delivery Vehicles. *J. Biomed. Nanotechnol.* **2016**, *12* (7), 1544–1552. https://doi.org/10.1166/jbn.2016.2259.

(72) Lueth, P.; Haughney, S. L.; Binnebose, A. M.; Mullis, A. S.; Peroutka-Bigus, N.; Narasimhan, B.; Bellaire, B. H. Nanotherapeutic Provides Dose Sparing and Improved Antimicrobial Activity against Brucella Melitensis Infections. *J. Control. Release* **2019**, *294*, 288–297. https://doi.org/10.1016/j.jconrel.2018.12.024.

(73) Binnebose, A. M.; Haughney, S. L.; Martin, R.; Imerman, P. M.; Narasimhan, B.; Bellaire, B. H. Polyanhydride Nanoparticle Delivery Platform Dramatically Enhances Killing of Filarial Worms. *PLoS Negl. Trop. Dis.* **2015**, *9* (10), e0004173. https://doi.org/10.1371/journal.pntd.0004173.

(74) Biswas, S.; Torchilin, V. P. Nanopreparations for Organelle-Specific Delivery in Cancer. *Adv. Drug Deliv. Rev.* **2014**, *66*, 26–41. https://doi.org/10.1016/j.addr.2013.11.004.

(75) Wiemerslage, L.; Lee, D. Quantification of Mitochondrial Morphology in Neurites of Dopaminergic Neurons Using Multiple Parameters. *J. Neurosci. Methods* **2016**, *262*, 56–65. https://doi.org/10.1016/j.jneumeth.2016.01.008.

(76) Legendre, J. Y.; Szoka, F. C. Cyclic Amphipathic Peptide-DNA Complexes Mediate High-Efficiency Transfection of Adherent Mammalian Cells. *Proc. Natl. Acad. Sci. U. S. A.* **1993**, *90* (3), 893–897. https://doi.org/10.1073/pnas.90.3.893.

(77) Boeckle, S.; Fahrmeir, J.; Roedl, W.; Ogris, M.; Wagner, E. Melittin Analogs with High Lytic Activity at Endosomal PH Enhance Transfection with Purified Targeted PEI Polyplexes. *J. Control. Release* **2006**, *112* (2), 240–248. https://doi.org/10.1016/j.jconrel.2006.02.002.

(78) Min, S. H.; Lee, D. C.; Lim, M. J.; Park, H. S.; Kim, D. M.; Cho, C. W.; Yoon, D. Y.; Yeom, Y. Il. A Composite Gene Delivery System Consisting of Polyethylenimine and an Amphipathic Peptide KALA. *J. Gene Med.* **2006**, *8* (12), 1425–1434. https://doi.org/10.1002/jgm.973.

(79) Wyman, T. B.; Nicol, F.; Zelphati, O.; Scaria, P. V.; Plank, C.; Szoka, F. C. Design, Synthesis, and Characterization of a Cationic Peptide That Binds to Nucleic Acids and Permeabilizes Bilayers. *Biochemistry* **1997**, *36* (10), 3008–3017. https://doi.org/10.1021/bi9618474.

(80) Varkouhi, A. K.; Scholte, M.; Storm, G.; Haisma, H. J. Endosomal Escape Pathways for Delivery of Biologicals. *J. Control. Release* **2011**, *151* (3), 220–228. https://doi.org/10.1016/j.jconrel.2010.11.004.

(81) Langley, M.; Ghosh, A.; Charli, A.; Sarkar, S.; Ay, M.; Luo, J.; Zielonka, J.; Brenza, T.; Bennett, B.; Jin, H.; et al. Mito-Apocynin Prevents Mitochondrial Dysfunction, Microglial Activation, Oxidative Damage, and Progressive Neurodegeneration in MitoPark Transgenic Mice. *Antioxid. Redox Signal.* **2017**, *27* (14), 1048–1066. https://doi.org/10.1089/ars.2016.6905.

(82) Torchilin, V. P. Recent Approaches to Intracellular Delivery of Drugs and DNA and Organelle Targeting. *Annu. Rev. Biomed. Eng.* **2006**, *8*, 343–375. https://doi.org/10.1146/annurev.bioeng.8.061505.095735.

(83) Augusto, A.; Looney, E.; Del Cañizo, C.; Bowden, S. G.; Buonassisi, T. Thin Silicon Solar Cells: Pathway to Cost-Effective and Defect-Tolerant Cell Design, 2017. https://doi.org/10.1016/j.egypro.2017.09.346.

(84) Vela-Ramirez, J. E.; Goodman, J. T.; Boggiatto, P. M.; Roychoudhury, R.; Pohl, N. L. B.; Hostetter, J. M.; Wannemuehler, M. J.; Narasimhan, B. Safety and Biocompatibility of Carbohydrate-Functionalized Polyanhydride Nanoparticles. *AAPS J.* **2015**, *17* (1), 256–267. https://doi.org/10.1208/s12248-014-9699-z.

(85) Phanse, Y.; Carrillo-Conde, B. R.; Ramer-Tait, A. E.; Roychoudhury, R.; Broderick, S.; Pohl, N.; Rajan, K.; Narasimhan, B.; Wannemuehler, M. J.; Bellaire, B. H. Functionalization Promotes Pathogen-Mimicking Characteristics of Polyanhydride Nanoparticle Adjuvants. *J. Biomed. Mater. Res. - Part A* **2017**, *105* (10), 2762–2771. https://doi.org/10.1002/jbm.a.36128.

(86) Brenza, T. M.; Ghaisas, S.; Ramirez, J. E. V.; Harischandra, D.; Anantharam, V.; Kalyanaraman, B.; Kanthasamy, A. G.; Narasimhan, B. Neuronal Protection against Oxidative Insult by Polyanhydride Nanoparticle-Based Mitochondria-Targeted Antioxidant Therapy. *Nanomedicine Nanotechnology, Biol. Med.* **2017**, *13* (3), 809–820. https://doi.org/10.1016/j.nano.2016.10.004.

(87) Carrillo-Conde, B. R.; Darling, R. J.; Seiler, S. J.; Ramer-Tait, A. E.; Wannemuehler, M. J.; Narasimhan, B. Sustained Release and Stabilization of Therapeutic Antibodies Using Amphiphilic Polyanhydride Nanoparticles. *Chem. Eng. Sci.* **2015**, *125*, 98–107. https://doi.org/10.1016/j.ces.2014.08.015.

(88) Huntimer, L.; Wilson Welder, J. H.; Ross, K.; Carrillo-Conde, B.; Pruisner, L.; Wang, C.; Narasimhan, B.; Wannemuehler, M. J.; Ramer-Tait, A. E. Single Immunization with a Suboptimal Antigen Dose Encapsulated into Polyanhydride Microparticles Promotes High Titer and Avid Antibody Responses. *J. Biomed. Mater. Res. - Part B Appl. Biomater.* **2013**, *101 B* (1), 91–98. https://doi.org/10.1002/jbm.b.32820.

(89) Ulery, B. D.; Kan, H. .-M. H. M.; Williams, B. A.; Narasimhan, B.; Lo, K. W. H. K. W. .-H.; Nair, L. S.; Laurencin, C. T. Facile Fabrication of Polyanhydride/Anesthetic Nanoparticles with Tunable Release Kinetics. *Adv. Healthc. Mater.* **2014**, *3* (6), 843–847. https://doi.org/10.1002/adhm.201300521.

(90) Petersen, L. K.; Determan, A. S.; Westgate, C.; Bendickson, L.; Nilsen-Hamilton, M.; Narasimhan, B. Lipocalin-2-Loaded Amphiphilic Polyanhydride Microparticles Accelerate Cell Migration. *J. Biomater. Sci. Polym. Ed.* **2011**, *22* (9), 1237–1252. https://doi.org/10.1163/092050610X502776.

(91) Determan, A. S.; Trewyn, B. G.; Lin, V. S.-Y. V. S. Y.; Nilsen-Hamilton, M.; Narasimhan, B. Encapsulation, Stabilization, and Release of BSA-FITC from Polyanhydride Microspheres. *J. Control. Release* **2004**, *100* (1), 97–109. https://doi.org/10.1016/j.jconrel.2004.08.006.

(92) Shen, E.; Kipper, M. J.; Dziadul, B.; Lim, M. K. M.-K.; Narasimhan, B. Mechanistic Relationships between Polymer Microstructure and Drug Release Kinetics in Bioerodible Polyanhydrides. *J. Control. Release* **2002**, *82* (1), 115–125. https://doi.org/10.1016/S0168-3659(02)00125-6.

(93) Dranka, B. P.; Gifford, A.; McAllister, D.; Zielonka, J.; Joseph, J.; O'Hara, C. L.; Stucky, C. L.; Kanthasamy, A. G.; Kalyanaraman, B. A Novel Mitochondrially-Targeted Apocynin Derivative Prevents Hyposmia and Loss of Motor Function in the Leucine-Rich Repeat Kinase 2 (LRRK2R1441G) Transgenic Mouse Model of Parkinson's Disease. *Neurosci. Lett.* **2014**, *583*, 159–164. https://doi.org/10.1016/j.neulet.2014.09.042.

(94) Wongrakpanich, A.; Geary, S. M.; Joiner, M. A.; Anderson, M. E.; Salem, A. K. Mitochondria-Targeting Particles. *Nanomedicine (Lond).* **2014**, *9* (16), 2531–2543. https://doi.org/10.2217/nnm.14.161.

(95) Denora, N.; Laquintana, V.; Lopalco, A.; Iacobazzi, R. M.; Lopedota, A.; Cutrignelli, A.; Iacobellis, G.; Annese, C.; Cascione, M.; Leporatti, S.; et al. In Vitro Targeting and Imaging the Translocator Protein TSPO 18-KDa through G(4)-PAMAM-FITC Labeled Dendrimer. *J. Control. Release* **2013**, *172* (3), 1111–1125. https://doi.org/10.1016/j.jconrel.2013.09.024.

(96) Chan, M. S.; Tam, D. Y.; Dai, Z.; Liu, L. S.; Ho, J. W.-T.; Chan, M. L.; Xu, D.; Wong, M. S.; Tin, C.; Lo, P. K. Mitochondrial Delivery of Therapeutic Agents by Amphiphilic DNA Nanocarriers. *Small* **2016**, *12* (6), 770–781. https://doi.org/10.1002/smll.201503051.

(97) Wei, Y.; Zhou, F.; Zhang, D.; Chen, Q.; Xing, D. A Graphene Oxide Based Smart Drug Delivery System for Tumor Mitochondria-Targeting Photodynamic Therapy. *Nanoscale* **2016**, *8* (6), 3530–3538. https://doi.org/10.1039/c5nr07785k.

(98) Kabachinski, G.; Schwartz, T. U. The Nuclear Pore Complex - Structure and Function at a Glance. *J. Cell Sci.* **2015**, *128* (3), 423–429. https://doi.org/10.1242/jcs.083246.

(99) van der Aa, M. A. E. M.; Mastrobattista, E.; Oosting, R. S.; Hennink, W. E.; Koning, G. A.; Crommelin, D. J. A. The Nuclear Pore Complex: The Gateway to Successful Nonviral Gene Delivery. *Pharm. Res.* **2006**, *23* (3), 447–459. https://doi.org/10.1007/s11095-005-9445-4.

(100) Pouton, C. W.; Wagstaff, K. M.; Roth, D. M.; Moseley, G. W.; Jans, D. A. Targeted Delivery to the Nucleus. *Adv. Drug Deliv. Rev.* **2007**, *59* (8), 698–717. https://doi.org/10.1016/j.addr.2007.06.010.

(101) Shi, J.; Chou, B.; Choi, J. L.; Ta, A. L.; Pun, S. H. Investigation of Polyethylenimine/DNA Polyplex Transfection to Cultured Cells Using Radiolabeling and Subcellular Fractionation Methods. *Mol. Pharm.* **2013**, *10* (6), 2145–2156. https://doi.org/10.1021/mp300651q.

(102) Lanford, R. E.; Kanda, P.; Kennedy, R. C. Induction of Nuclear Transport with a Synthetic Peptide Homologous to the SV40 T Antigen Transport Signal. *Cell* **1986**, *46* (4), 575–582. https://doi.org/10.1016/0092-8674(86)90883-4.

(103) Escriou, V.; Carrière, M.; Scherman, D.; Wils, P. NLS Bioconjugates for Targeting Therapeutic Genes to the Nucleus. *Adv. Drug Deliv. Rev.* **2003**, *55* (2), 295–306. https://doi.org/10.1016/S0169-409X(02)00184-9.

(104) Vives, E.; Brodin, P.; Lebleu, B. A Truncated HIV-1 Tat Protein Basic Domain Rapidly Translocates through the Plasma Membrane and Accumulates in the Cell Nucleus. *J. Biol. Chem.* **1997**, *272* (25), 16010–16017. https://doi.org/10.1074/jbc.272.25.16010.

(105) Bogacheva, M.; Egorova, A.; Slita, A.; Maretina, M.; Baranov, V.; Kiselev, A. Arginine-Rich Cross-Linking Peptides with Different SV40 Nuclear Localization Signal Content as Vectors for Intranuclear DNA Delivery. *Bioorganic Med. Chem. Lett.* **2017**, *27* (21), 4781–4785. https://doi.org/10.1016/j.bmcl.2017.10.001.

(106) Tammam, S. N.; Azzazy, H. M. E.; Lamprecht, A. The Effect of Nanoparticle Size and NLS Density on Nuclear Targeting in Cancer and Normal Cells; Impaired Nuclear Import and Aberrant Nanoparticle Intracellular Trafficking in Glioma. *J. Control. Release* **2017**, *253*, 30–36. https://doi.org/10.1016/j.jconrel.2017.02.029.

(107) Tammam, S. N.; Azzazy, H. M. E.; Breitinger, H. G.; Lamprecht, A. Chitosan Nanoparticles for Nuclear Targeting: The Effect of Nanoparticle Size and Nuclear Localization Sequence Density. *Mol. Pharm.* **2015**, *12* (12), 4277–4289. https://doi.org/10.1021/acs.molpharmaceut.5b00478.

(108) Namvar, A.; Bolhassani, A.; Khairkhah, N.; Motevalli, F. Physicochemical Properties of Polymers: An Important System to Overcome the Cell Barriers in Gene Transfection. *Biopolymers* **2015**, *103* (7), 363–375. https://doi.org/10.1002/bip.22638.

(109) Rass, U.; Ahel, I.; West, S. C. Defective DNA Repair and Neurodegenerative Disease. *Cell* **2007**, *130* (6), 991–1004. https://doi.org/10.1016/j.cell.2007.08.043.

(110) Chaturbedy, P.; Kumar, M.; Salikolimi, K.; Das, S.; Sinha, S. H.; Chatterjee, S.; Suma, B. S.; Kundu, T. K.; Eswaramoorthy, M. Shape-Directed Compartmentalized Delivery of a Nanoparticle-Conjugated Small-Molecule Activator of an Epigenetic Enzyme in the Brain. *J. Control. Release* **2015**, *217*, 151–159. https://doi.org/10.1016/j.jconrel.2015.08.043.

(111) Maity, A. R.; Stepensky, D. Delivery of Drugs to Intracellular Organelles Using Drug Delivery Systems: Analysis of Research Trends and Targeting Efficiencies. *Int. J. Pharm.* **2015**, *496* (2), 268–274. https://doi.org/10.1016/j.ijpharm.2015.10.053.

(112) Chen, Z.; Zhang, L.; Song, Y.; He, J.; Wu, L.; Zhao, C.; Xiao, Y.; Li, W.; Cai, B.; Cheng, H.; et al. Hierarchical Targeted Hepatocyte Mitochondrial Multifunctional Chitosan Nanoparticles for Anticancer Drug Delivery. *Biomaterials* **2015**, *52*, 240–250. https://doi.org/10.1016/j.biomaterials.2015.02.001.

(113) Li, Z.; Dong, K.; Huang, S.; Ju, E.; Liu, Z.; Yin, M.; Ren, J.; Qu, X. A Smart Nanoassembly for Multistage Targeted Drug Delivery and Magnetic Resonance Imaging. *Adv. Funct. Mater.* **2014**, *24* (23), 3612–3620. https://doi.org/10.1002/adfm.201303662.

2.6 Tables

Table 2.1 Intracellular targeting strategies for CNS anti-neurodegenerative therapeutic delivery. Reproduced with permission from Mullis et al.[1]

Strategy	Mechanism	General Characteristics	Examples	Pros	Cons	References
Endosomal Escape	**Proton Sponge Effect**	buffering at pH 7.2-5	- Polyethyl-enimine - imidazole			70,105,106
	Release of Reactive Oxygen Species	photo-sensitizer, singlet oxygen production	- $TPPS_4$ - $AlPcS_{2a}$ - dendrimer - pthalo-cyanine			70
	Pore Formation	cationic amphiphilic peptides	- penton base - melittin			70
Targeting the Nucleus	**Passive NPC Transport**	< 9 nm		- fewer chemical modifications	- steric limitation	92
	Active NPC Transport	40-60 nm, NLS		- greater size capacity	- steric limitation	95–97
	Mitotic Vulner-abilities	replicating cells		- greater size capacity	- exclusive to mitotic cells	101,102
	Shape-Directed Localization	biconcave, spherical morphology		- fewer chemical modifications - greater size capacity	- device material dependence	103
Targeting the Mitochon-dria	**Electrostatic Attraction**	cationic amphiphilic peptides	- TPP - TAT	- increased cytoplasmic transport	- toxicity - protein aggregation	64
	Receptor-Mediated Transport	mitochondrial receptor ligand	- TSPO ligand	- high selectivity		88

2.7 Figures

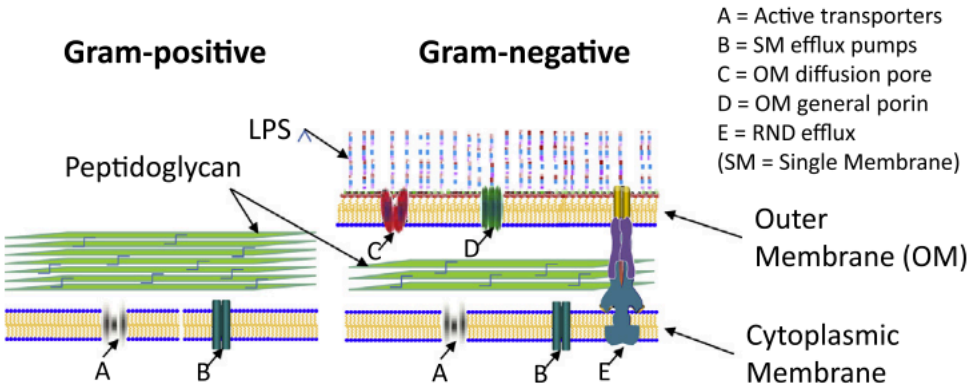

Figure 2.1 Gram-positive and Gram-negative biological barriers. Reproduced with permission from Singh et al.[5]

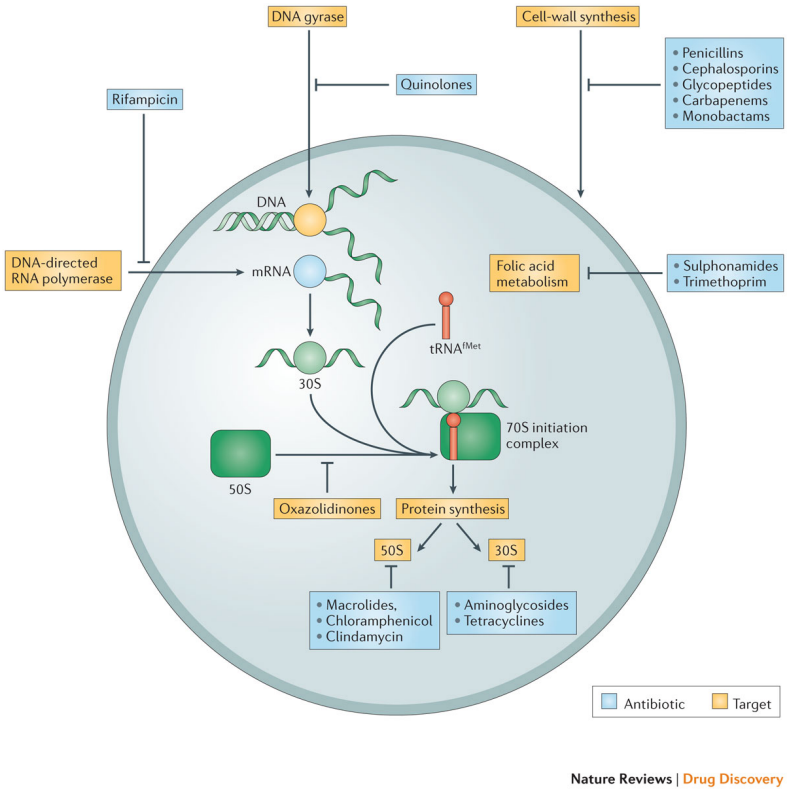

Figure 2.2 Antibiotic drug targets. Reproduced with permission from Lewis.[21]

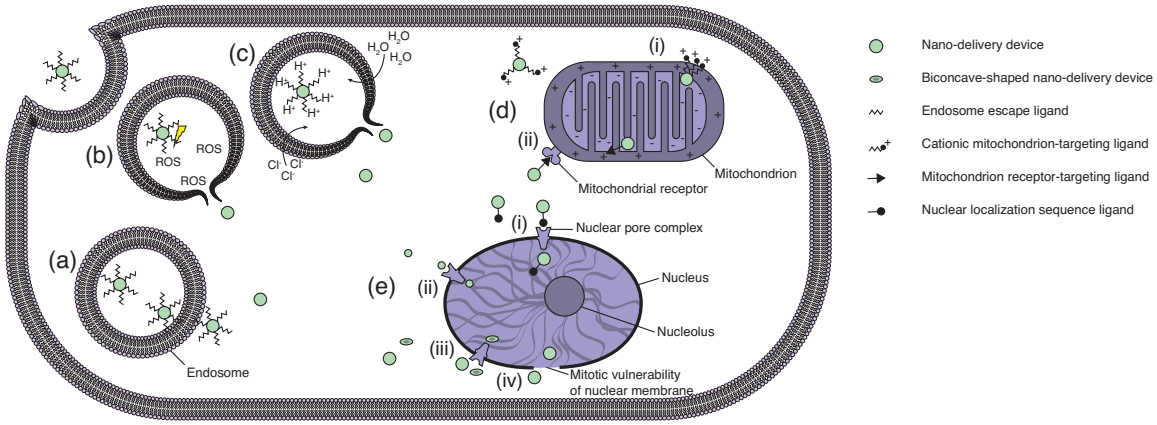

Figure 2.3 Organelle targeting mechanisms for intracellular drug delivery. After internalization into the diseased cell, the nanoscale delivery devices must escape the endosome to avoid acidic degradation of their payload and enable organelle localization. Delivery devices can escape the endosome via (a) partitioning into and disrupting the endosomal membrane, (b) device release of reactive oxygen species from photoreactive molecules, and (c) rupturing the endosome through osmotic pressure differences (i.e, the proton sponge effect). After escaping the endosome, the delivery device can target their cargo's organelles of interest with functionalizations. (d) The mitochondrion can be targeted via (i) electrostatic attraction of positively-charged devices, or through (ii) functionalization with mitochondria receptor ligands. (e) The nucleus can be targeted through (i) functionalization with an NLS ligand, (ii) passive diffusion through the NPC, (iii) shape-directed localization, or through (iv) mitotic vulnerabilities in the nuclear membrane. Reproduced with minor modifications and permission from Mullis et al.[1]

CHAPTER 3. RESEARCH OBJECTIVES AND THESIS ORGANIZATION

3.1 Research Objectives

The overall goal of this dissertation is to develop a new framework for rationally designing nanomedicine formulations for antimicrobial therapies and targeted drug delivery. While individual antimicrobial nanoparticle formulations have been shown to provide sustained drug release and improve antibiotic activity, the factors that influence nanoparticle effectiveness are poorly understood. In the past, traditional screening approaches have identified lead antibiotic candidates through brute force testing. However, these methods are unlikely to show the same level of success for nanoparticles due to the massively larger dataspace contributed by polymer and nanoparticle properties, as well as their interactions with drug properties. The research described in this dissertation seeks to clarify the physicochemical rules governing antimicrobial nanoparticle efficacy. This could streamline screening of nanoparticle formulations by identifying candidates with a high likelihood of success.

This dissertation is organized into three specific goals to develop this framework for antimicrobial nanoparticle design:

SG1: Deconvolute complex relationships between polymer chemistry, physicochemical properties of payload, encapsulation efficiency, and release kinetics from polyanhydride nanoparticles using materials analytics-based approaches.

SG2: Develop a high-throughput methodology to rapidly synthesize and screen libraries of novel nanoparticle formulations encapsulating small molecule payloads.

SG3: Use the materials analytics approaches from SG1 to investigate polymer, payload, and nanoparticle properties that impact biological efficacy in antimicrobial therapies and targeted drug delivery.

The relationships between carrier chemistry, payload physicochemical properties, drug release kinetics, encapsulation efficiency, and biological activity are complex and nonlinear. In SG1, we generated release data from multiple polyanhydride nanoparticle-based chemistries, payloads, and loading, and employed a materials analytics approach to deconvolute these complex relationships. This analysis enabled the design of a predictive algorithm for first-pass *in silico* screening of new antimicrobial nanoparticle formulations. In SG2, we utilized a high-throughput synthesis and screening method to characterize new rapid-release nanoparticle formulations based on CPTEG:SA copolymers. By pairing *in silico* and *in vitro* thermodynamic mixing predictions, we demonstrated that copolymer chemistry and polymer-drug mixing thermodynamics can be used to explain trends in release kinetics data. In SG3, we investigated the ability of individual nanoparticle formulations and cocktails of multiple formulations to improve the efficacy of their antibiotic payload against *Burkholderia cepacia* relative to soluble controls. Using a materials analytics approach, we identified key attributes of these formulations that govern functional efficacy. This enabled predictive modeling of the antimicrobial activity of untested nanoparticle formulations and cocktails.

3.2 Dissertation Organization

The following three chapters in the dissertation address these specific goals. Chapter 4 focuses on SG1, discussing the development of structure function relationships for release kinetics and a predictive model to program release kinetics. SG2 is addressed in Chapter 5, describing the adaptation of a high-throughput method to rapidly synthesize libraries of small

molecule-loaded nanoparticles. Chapter 6 outlines SG3, wherein libraries of nanoparticles are synthesized via the Chapter 5 method and evaluated for antimicrobial activity. The Chapter 4 informatics approach is applied to these data, and structure function relationships and a predictive model are derived for nanoparticle antimicrobial activity. Chapter 7 summarizes the outcomes of this dissertation, and highlight ongoing and future work using polyanhydride nanoparticles as carriers for small molecule drugs.

CHAPTER 4. A DATA ANALYTICS APPROACH FOR RATIONAL DESIGN OF NANOMEDICINES WITH PROGRAMMABLE DRUG RELEASE

A paper published in Molecular Pharmaceutics, April 2019

*Adam S. Mullis[1], Scott R. Broderick[2], Andrea Binnebose[3,4], Nathan Peroutka-Bigus[3,4], Bryan Bellaire[3,4,5], Krishna Rajan[2,5], Balaji Narasimhan[1,5]**

[1]Department of Chemical and Biological Engineering, Iowa State University, Ames, Iowa 50011, United States

[2]Department of Materials Design and Innovation, University at Buffalo, Buffalo, NY 14260, United States

[3]Department of Veterinary Microbiology and Preventive Medicine, Iowa State University, Ames, Iowa 50011, United States

[4]Interdepartmental Microbiology Graduate Program, Iowa State University, Ames, Iowa 50011, United States

[5]Nanovaccine Institute, Iowa State University, Ames, Iowa 50011, United States

KEYWORDS: polyanhydrides, degradable biomaterials, drug delivery, drug release kinetics, informatics, data mining

4.1 Abstract

Drug delivery vehicles can improve the functional efficacy of existing antimicrobial therapies by improving biodistribution and targeting. A critical property of such nanomedicine formulations is their ability to control the release kinetics of their payloads. The combination of (and interactions between) polymer, drug, and nanoparticle properties gives rise to nonlinear behavioral relationships and a large data space. These factors complicate both first-principles modeling and screening of nanomedicine formulations.

Predictive analytics may offer a more efficient approach toward rational design of nanomedicines by identifying key descriptors and correlating them to nanoparticle release behavior. In this work, antibiotic release kinetics data were generated from polyanhydride nanoparticle formulations with varying copolymer compositions, encapsulated drug type, and drug loading. Four antibiotics, doxycycline, rifampicin, chloramphenicol, and pyrazinamide, were used. Linear manifold learning methods were used to relate drug release properties with polymer, drug, and nanoparticle properties, and key descriptors were identified that are highly correlated with release properties. However, these linear methods could not predict release behavior. Non-linear multivariate modeling based on graph theory was then used to deconvolute the governing relationships between these properties, and predictive models were generated to rapidly screen lead nanomedicine formulations with desirable release properties with minimal nanoparticle characterization. Release kinetics predictions of two drugs containing atoms not included in the model showed good agreement with experimental results, validating the model and indicating its potential to virtually explore new polymer and drug pairs not included in training data set. The models were shown to be robust after inclusion of these new formulations in that the new inclusions did not significantly change model regression. This approach provides the first steps towards development of a framework that can be used to rationally design nanomedicine formulations by selecting the appropriate carrier for a drug payload to program desirable release kinetics.

4.2 Introduction

Intracellular bacterial infections are challenging to treat using traditional antimicrobial therapies due to the difficulty in achieving high enough local drug concentration for antimicrobial activity without inducing host cell toxicity.[1] Elimination of soluble drugs through host metabolism and excretion pathways act to reduce bioavailable

amounts of antimicrobials requiring repeated dosing to maintain therapeutic concentrations to mitigate the development of antibiotic resistant in pathogens.[2,3] Drug delivery vehicles can improve the efficacy and potency of antimicrobials by altering the drug biodistribution with improved intracellular localization and delivery of cargo to the pathogen's intracellular niche within host cells.[4,5] Biodegradable polyanhydride nanoparticles show passive targeting and payload stabilization properties that make them uniquely suited for antibiotic delivery for intracellular infections.[4,6] These particles are internalized efficiently by phagocytic cells using multiple mechanisms, and have been used to deliver antibiotics to kill intracellular *Brucella abortus.*[7] Additionally, polyanhydride nanoparticles mediated efficient killing of filarial parasites by co-delivering an antiparasitic with an antibiotic targeting an intracellular endosymbiotic bacterium that supports parasite health and reproduction.[8]

A key feature of the effectiveness of these nanomedicine formulations is their ability to control payload release rate, however rationally designing nanomedicines with programmable release remains elusive. Release kinetics are influenced by drug distribution within a device and/or a particle, which is in turn influenced by polymer-drug thermodynamic interactions.[9–11] These interactions give rise to nonlinear release behavior which is difficult to predict *a priori.* Screening nanomedicine formulations is challenging as polymer and nanoparticle properties (e.g., polymer chemistry, nanoparticle size, polydispersity, release kinetics, and encapsulation efficiency) yield a large number of additional variables beyond drug-specific properties. This large dataspace, coupled with the multiple length scales at play, poses difficulties for generalizing conclusions to other nanoparticle systems and impedes first principles modeling of nanoparticle behavior.[12,13]

Hierarchical modeling may be a more efficient approach for such systems, wherein key descriptors are identified and correlated to performance parameters.

Informatics methods encompass several tools for such hierarchical modeling. Data mining techniques can deconvolute complex behavior, unraveling relationships that lie on non-Euclidian surfaces,[14] which enables pattern recognition and prediction through the development of quantitative structure-property relationships (QSPRs).[15] To this end, previous informatics analyses from our laboratories has enabled identification of polyanhydride chemistry and structural factors that influence protein release from films[16] and enable pathogen-mimicking nanoparticle processing by immune cells.[17–20]

The focus of this work was to develop an informatics-based framework that determines how polymer, drug, and nanoparticle characteristics influence drug encapsulation efficiency and release kinetics. We sought to generate predictive models that can virtually test potential new polymer and drug combinations for desirable release kinetics. Our long-term goal is to develop a predictive analytics framework to enable rational design of nanomedicine formulations for different types of therapeutic and prophylactic applications.

4.3 Experimental Methods

4.3.1 Materials

Sebacic acid (SA) was purchased from Sigma Aldrich (St. Louis, MO). Triethylene glycol, 4-*p*-hydroxybenzoic acid, 1- methyl-2-pyrrolidinone, and 1,6-dibromohexane were purchased from Sigma Aldrich for 1,8-bis(p-carboxyphenoxy)-3,6-dioxaoctane (CPTEG) and 1,6-bis(p-carboxyphenoxy)hexane (CPH) monomer synthesis. Potassium carbonate, dimethyl formamide, toluene, acetonitrile, acetic acid, sulfuric acid, N,N-dimethylacetamide, and acetic anhydride were purchased from Fisher Scientific (Fairlawn, NJ) for monomer and polymer synthesis. 4-*p*-fluorobenzonitrile was purchased from Apollo Scientific (Cheshire,

UK) for use in monomer synthesis. Methylene chloride, pentane, and hexanes were purchased from Fisher Scientific for polymer purification and nanoparticle synthesis. Doxycycline (DOX), rifampicin (RIF), and pyrazinamide (PZA) were purchased from Sigma Aldrich, and chloramphenicol (CAM) was purchased from Fisher Scientific. Meropenem (MEM) was purchased from Ark Pharm, Inc. (Arlington Heights, IL) and ceftazidime (CAZ) was purchased from Acros Organics (NJ). ^{1}H NMR analysis used deuterated chloroform purchased from Cambridge Isotope Laboratories (Andover, MA). Drug quantification used UV-transparent microplates from Greiner Bio-One (Kremsmünster, Austria), HPLC grade acetonitrile, methanol, and tetrahydrofuran from Fisher Scientific, and phosphoric acid from Sigma Aldrich.

4.3.2 Polymer and Nanoparticle Synthesis

CPTEG and CPH diacid were synthesized as described previously.[10,21,22] CPTEG:CPH and CPH:SA copolymers were synthesized as described previously.[10,21] Briefly, monomers were weighed in appropriate molar ratios and added to a round bottom flask. The monomers were acetylated in excess acetic acid at 125°C for 30 min, and rotary evaporation was used to remove excess solvent from the resulting prepolymer. CPTEG:CPH was reacted for six hours at 140°C at <0.1 Torr and CPH:SA was reacted for 30 min at 180°C at <0.3 Torr. Polymers were purified by precipitation in chilled hexanes. Copolymer composition and number average molecular weight (M_n) was confirmed from ^{1}H NMR spectra acquired on a Varian MR-400 (Varian, Inc. Palo Alto, CA) and thermal properties of the copolymers was characterized by DSC (Q2000, TA Instruments, New Castle, DE).

Antibiotic-loaded nanoparticles were synthesized as described previously.[7,8] Polymer and drug were weighed in separate scintillation vials at appropriate %w/w ratios. Enough methylene chloride to dissolve the polymer at 20 mg/mL was added to the drug vial to

dissolve/disperse the drug, then transferred to the polymer vial. The combined drug and polymer solution was poured into a pentane antisolvent bath at room temperature (CPH:SA) or -10°C (CPTEG:CPH) at a solvent:anti-solvent ratio of 1:250 and nanoparticles were recovered by vacuum filtration. CPTEG:CPH nanoprecipitation was carried out in a cold room at 4°C. A total of 68 nanoformulations were tested, spanning drug loadings between 1% and 20% loading (% w/w). All drugs were tested in 20:80 CPH:SA and 20:80 CPTEG:CPH nanoparticles, and rifampicin was additionally tested in 10:90, 30:70, and 50:50 CPTEG:CPH. ^{1}H NMR spectra of empty 20:80 CPTEG:CPH and 20:80 CPH:SA nanoparticles indicated undetectable amounts of methylene chloride and trace amounts of pentane (data not shown).

To validate the informatics analysis, nanoparticles encapsulating meropenem or ceftazidime were synthesized using a high-throughput method adapted from Goodman et al.[23] Briefly, polymer and drugs were dissolved/dispersed in methylene chloride and dispensed via high-throughput robot into 10 mL borosilicate tubes at a final polymer concentration of 20 mg/mL. The robot sonicated and dispensed the combined polymer and drug solution into 50 mL conical polypropylene tubes containing 45 mL pentane (1:18 solvent:anti-solvent ratio) at the temperatures listed above. Multiple particle batches were pooled and recovered by vacuum filtration. Scanning electron microscopy (SEM, FEI Quanta 250, Hillsboro, OR) was used to image all nanoparticles, and size distributions were calculated using Fiji image analysis software[24] and the ParticleSizer plugin script for Fiji. Nanoparticle zeta potential was measured using a Zetasizer Nano (Malvern Instruments Ltd., Worcester, UK).

4.3.3 Drug Release Kinetics

Nanoparticles (9-11 mg) were dispersed in 0.5 mL PBS, pH 7.4 and suspended by sonication (VCX 130 PB, Sonics & Materials, Inc., Newtown, CT). At each time point, the

nanoparticles were pelleted by centrifugation and supernatant was collected for drug quantification. Fresh PBS was added to maintain perfect sink conditions and the nanoparticles were dispersed by sonication. At the end of the release experiment, 40 mM sodium hydroxide was added to accelerate polymer degradation and extract the remaining encapsulated drug as described previously.[25]

The drug mass released at each time point was determined by spectrophotometry (SpectraMax M3, Molecular Devices, San Jose, CA) and UV-HPLC (1200 series, Agilent Technologies, Santa Clara, CA). Doxycycline, rifampicin, and chloramphenicol were quantified by absorbance in UV-transparent 96-well plates at 350, 333, and 293 nm, respectively. Pyrazinamide release and base extraction samples were separated using a Phenomenex Kinetex 2.6-micron C18 100Å 100x4.6mm column and a 30:5:65 acetonitrile:methanol:water mobile phase adjusted to pH 5.2 with phosphoric acid.[26] The flow rate was 0.6 mL/min and pyrazinamide was quantified at 268 nm. Meropenem and ceftazidime release and base extraction samples were separated using a Zorbax Eclipse XDB-C8 5-micron 4.6x150 mm column, monitoring at 299 nm and 246 nm, respectively. Meropenem release samples used a mobile phase gradient ramping from 0.1/99.9 (%v/v) methanol/water to 50/50 over 15 min. Meropenem base extraction samples used a gradient ramping from 0.1/99.9 acetonitrile 0.1% trifluoroacetic acid/ water 0.1% trifluoroacetic acid to 50/50 over 15 min. Ceftazidime release samples used a mobile phase protocol with an isocratic step at 0.1/99.9 methanol/water for 5 minutes followed by a gradient ramping to 50/50 over 10 min. Ceftazidime base extraction samples used an isocratic step at 15/85 from 0.1/99.9 acetonitrile 0.1% trifluoroacetic acid/ water 0.1% trifluoroacetic acid for 1 min

followed by a gradient ramping to 40/60 over 5 min. All meropenem and ceftazidime HPLC protocols used a flow rate of 1 mL/min.

The small mass of drug and large volume of antisolvent used in nanoparticle synthesis render the non-encapsulated drug concentration below the limit of detection of the analytical methods used in this study. Therefore encapsulation efficiency (EE) was calculated from the cumulative sum of detected drug mass released in PBS and base extraction samples using Eq. 1.[25] In a minority of formulations >100% EE was observed, which could arise from the presence of drug nanocrystals[27] (which was not detected on nanoparticle surfaces by SEM), gravimetric inaccuracies due to static charge of the nanoparticles, or residual error in the drug concentration quantification assays. Drug release kinetics are presented as fraction released, where the cumulative drug mass release is normalized by the total encapsulated drug mass. Prism 7 (Graphpad Software, La Jolla, CA) was used to generate release kinetics figures.

Eq. 1)

$$\frac{EE}{100\%} = \frac{cumulative\ drug\ mass\ from\ release\ \&\ base\ extraction}{nanoparticle\ mass * drug\ loading\ fraction\left(\frac{wt}{wt}\right)}$$

4.3.4 Informatics Analysis

Release behavior parameters, along with polymer, drug, and nanoparticle properties, were normalized and mean-centered. Three different informatics approaches were integrated and applied to analyze the data in this work. Linear manifold learning approaches, such as principal component analysis (PCA),[28–30] permit us to identify the right projection of data from which meaningful features associated with the input data can be identified. PCA performs an eigenvector decomposition and defines a new set of linear combinations of descriptors which maximize the amount of unique information in a minimal set of orthogonal

axes, termed principal components (PCs). The original data is decomposed into two matrices of interest for this work: the scores and loadings. The scores describe the different conditions (i.e., nanoparticle and drug chemistry), while the loadings describe the different descriptors and properties. The interpretation of these matrices is provided here with the relevant results, and an additional term called the variable importance projection (VIP) is calculated from the loadings matrix using Eq. 2.

Eq. 2)

$$VIP = \frac{PC_x^T * PC_x^i}{\sum PC_x^T * PC_x^i}$$

In this case, x = 5 because 5 PCs captured >90% of the variance in the data. The analysis was performed for T = encapsulation efficiency, drug released @2 h, and fraction released/day (Figure 4.6). Partial Least Squares (PLS) is a multi-linear regression approach which accounts for co-linearity in the data, and therefore limits bias and develops more robust quantitative relationships.[31–34] PLS performs separate PC analyses on the predictor variables (i.e., descriptors) and the predicted variables (i.e., properties). These therefore represent linear manifold learning approaches which provide qualitative and quantitative design relationships.

In order to model the drug release properties accurately and robustly, we found that non-linearity needed to be accounted for in the modeling. Therefore, we first developed non-linear parameterization of the data through non-linear manifold learning, based on graph theory, using the Isomap algorithm.[14,35] This approach generates a graph connecting data points on a high dimensional space to their nearest neighbors, mapped out in the high dimensional space, and then fit to a low dimensional manifold. The assumption here is that the graph Euclidean distance between the points in high dimensions closely approximates the

curvilinear distances along the low dimensional manifold. Through dimensionality reduction the manifold unravels into two or three dimensions allowing it to be visualized. The result of such dimensionality reduction is a weighted graph of the original data points where the edges are weighted according to the geodesic distances. Like in PCA, we develop a set of parameters for each set of conditions, although in this case the parameters are based on a non-linear combination of descriptors.

4.4 Results

4.4.1 Building Descriptor Library

To generate the data set, we focused on nanoparticles composed of CPTEG, CPH, and SA copolymers (Figure 4.1a,b). Nanoparticles synthesized from these polyanhydride copolymers have been shown to kill intracellular bacteria because of their high internalization rates by phagocytic cells,[7,36] localization in intracellular compartments that harbor these bacteria,[17,36] and improved antimicrobial activity of encapsulated drugs.[6–8] In addition to the structural descriptors defined by Li et al.,[16] we included molecular weight and compositional data from ^{1}H NMR and thermal characterization from DSC analysis. The release kinetics of four antibiotics, doxycycline (Figure 4.1c), rifampicin (Figure 4.1d), chloramphenicol (Figure 4.1e), and pyrazinamide (Figure 4.1f), were studied. The choice of the drug library was motivated by multiple factors. These drugs were selected due to their diversity of molecular weight, chemical structure, and hydrophobicity, among other physicochemical differences. All are FDA-approved drugs and belong to separate antibiotic classes, target distinct bacterial structures, and have well-characterized pharmacokinetics/pharmacodynamics. Experimental and predicted physicochemical properties for each of these drugs were gathered from the Drugbank database.[37] Predicted

drug properties from this database were calculated by ALGOPS and ChemAxon methodologies.

These drugs were encapsulated in polyanhydride nanoparticles by flash nanoprecipitation, and zeta potential, size distributions, and polydispersity index were obtained. Release profiles and encapsulation efficiencies were obtained from *in vitro* experiments in PBS, pH 7.4 (Figure 4.2). Figure 4.2 shows representative release kinetics data for multiple drugs, selected from a total of 68 nanoformulations that were tested. The formulations depicted in Figure 4.2 were selected to show the diversity of release behavior in the data set. CPH:SA-doxycycline nanoformulations tended to show a higher burst than CPTEG:CPH nanoformulations, and the lower loading in the CPH:SA nanoformulations tended to have a greater sustained release slope (Figure 4.2a). The chemistry trend was reversed in the rifampicin nanoformulations, where the CPTEG:CPH chemistries tended to show a higher burst release than the CPH:SA chemistries, and increasing the loading increased the burst (Figure 4.2b). For chloramphenicol, both 20:80 CPH:SA and CPTEG:CPH nanoformulations tended to generate a large burst release followed by a slow rate of drug release (Figure 4.2c). Pyrazinamide formulations generated a large burst from the 20:80 CPH:SA nanoparticles followed by a steady rate of drug release (Figure 4.2d). In contrast, the 20:80 CPTEG:CPH nanoparticles encapsulating pyrazinamide showed a small burst and slow rate of drug release and did not release more than 20% of the payload in one week. These results add to the body of literature[9–11,38] that indicates that copolymer chemistry, drug type, and drug loading influence drug release kinetics from biodegradable particles and other devices.

4.4.2 Identifying Factors that Influence Drug Release

The drug release profiles were parameterized using three attributes: (i) fraction released at two hours (FR (2h)); (ii) fraction released in one day (FR (24h)), both of which characterized the burst effect; and (iii) the slope of the release profile between 2 and 7 days to characterize the sustained release (Table 4.1). The normalized and mean-centered data are represented in the form of a heat map to provide an overview and to ensure that no outliers are biasing the results (Figure 4.3, Supporting Tables 4.1-2). In this step, no data specific to particle chemistry was included so as to not bias the analysis. A clustering analysis, based on Euclidian distance, was used to visualize broad trends in the data set between descriptors and nanoformulations, and is represented in Figure 4.3 by dendrograms which define the correlative indices. The clustering along the y-axis of Figure 4.3 can be visualized as plotting each nanoformulation in multidimensional space, where each dimension is a different descriptor. Encompassing n-dimensional "spheres" are defined at the locations of the nanoformulations, and as the radii of the spheres increase additional nanoformulations are encompassed. The relative sphere size needed to encompass multiple descriptors is comparable to the height of the branch in the dendrogram. Nanoformulations or descriptors grouped lower in the dendrograms are likely to show relatively strong, positive correlations. Branches higher in the dendrograms are more likely to show weak, positive correlations or inverse correlations.

From Figure 4.3, we find that the primary difference is between CPH:SA and CPTEG:CPH, given that the two chemistries branch off at the lowest correlation node. Therefore, particle chemistry is the key discriminator for nanoformulation behavior. Within each node, the compounds then group based on drug type, and then finally branch off based on theoretical drug loading and molar monomer ratios within the copolymer. This defines the

order of importance on release properties with CPH:SA versus CPTEG:CPH as the most important and the theoretical drug loading having less importance. For CPH:SA nanoparticles, rifampicin and pyrazinamide grouped together strongly, whereas doxycycline and chloramphenicol grouped together within the CPTEG:CPH chemistries. The CPTEG:CPH-chloramphenicol and -pyrazinamide nanoformulations clustered together, and diverged from the CPTEG:CPH-rifampicin and -doxycycline nanoformulations. Considering correlations to the release properties, the fraction released at two hours and 24 hours are strongly correlated with the polymer melting point (T_m) and zeta potential. The fraction released/day clustered with nanoparticle diameter and PDI polymer DOP and M_n. The relatively low branching of these properties in the dendrogram indicates moderate to strong correlation. Encapsulation efficiency (EE) was most strongly correlated with water solubility, followed by fraction released/day. This (weak) correlation to water solubility is expected, as incompatibility between polymer and drug hydrophobicity/hydrophilicity can result in drug partitioning more strongly in the antisolvent than the polymer matrix. The drug release properties (burst release, slope of release, and encapsulation efficiency) appeared relatively isolated from each other within the dendrogram, suggesting potential for independent control of these properties in designing nanoformulations.

A dimensionality reduction analysis, specifically principal component analysis (PCA), was then applied to the data of Figure 4.3, with descriptors specific to the particle and drug chemistry added to the data set (Supporting Table 4.3). Plots of formulation mapping and descriptor mapping within the dimensionally-reduced space are shown in Figures 4.4 and 4.5, respectively. In these figures, the principal components (PC) are ordered in terms of decreasing variability captured. PC1, the most important PC, captured particle chemistry

properties (41.3%); therefore, differences in particle chemistry descriptors explain more variance in release behavior than other descriptor sets. The next most important PC, PC2, captured differences in drug-specific descriptors (27.9%). The scores plot (Figure 4.4), which maps individual nanoparticle formulations onto these PC's (which, between them, allow us to reliably capture correlations in those two dimensions), shows a clear separation between CPTEG:CPH and CPH:SA particle chemistries. Within each polymer, doxycycline, chloramphenicol, and pyrazinamide clustered together, whereas rifampicin formulations formed a cluster isolated from the other drugs, indicating potentially different types of interactions with the particle carriers.

The loadings plot (Figure 4.5), which maps the descriptor variables onto the PC's shows that the role of the particle and the drug bank descriptors have been isolated (i.e., particle data lies along the PC1 axis and drug bank data is along the PC2 axis). Given that PC1 is the most important axis, we are capturing that the particle chemistry is the critical characteristic for predicting particle release behavior. The drug release properties do not adhere exclusively to either PC1 or PC2 axes, indicating that they are influenced by both polymer and drug characteristics. The ability to isolate the different controls allows us to assess, model, and design by the material characteristics.

To further quantify the correlation between descriptors and release properties, we calculated the VIP. In all, a total of 36 descriptors were used in the VIP analysis (as shown in Table 4.2), describing nanoparticle (1-3), polymer (4-13), and drug properties (14-36). The encapsulation efficiency was most strongly correlated with zeta potential (-), % Cl (drug) (+), % O (drug) (+), $T_{m,drug}$ (-), predicted water solubility (-), pKa (strongest base) (-), and drug rotatable bond count (+). As seen in Figure 4.3, the two-hour burst and slope of release were

highly correlated with each other, and showed similar correlations with the descriptors. Both the two-hour burst and slope of release were most strongly correlated with % Cl (drug) (+), % O (drug) (+), water solubility (-), % N (drug) (-), pKa (strongest acid) (-), and rotatable bond count (+). The identification of several highly correlated descriptors allows for reduction of the descriptor space to a minimum number and defines the number of descriptors necessary for performing high throughput calculations. This minimization is an important objective in computational modeling to improve model robustness. The purpose of VIP analysis is to assess the descriptors that contribute significant information as well as to identify correlated descriptors. While we identify the drug-related descriptors as having the highest individual impact, the particle-related descriptors collectively contribute the largest amount of information as seen in Figure 4.4.

4.4.3 Modeling Release Behavior

Beyond only observing the correlation of data, we wanted to identify similarities and design pathways between the various nanoformulations. This connectivity defines samples which have the most similar behavior and can provide information on potential replacements and design. In order to accomplish this, we performed a graph theory analysis (Figure 4.7). For the CPH:SA particle chemistries, there is a high connectivity (illustrated by black lines) and tight clustering within individual drugs. For the CPTEG:CPH particle chemistries, chloramphenicol, doxycycline, and pyrazinamide showed a high internal connectivity, but rifampicin branched out significantly. Each drug showed some degree of connectivity between the CPH:SA and CPTEG:CPH particle chemistries and doxycycline appeared to be the most interconnected across particle chemistries.

The degree of similarity can be defined by the number of connections required to connect two points. The distance along the two-dimensional projection also indicates the

similarity of formulations. Pyrazinamide and chloramphenicol generated the least similarity in release behavior, as they required 4-6 connections, and lie far from each other along the projection. Within each particle chemistry, doxycycline showed the most similarity to rifampicin and pyrazinamide, and rifampicin showed the most similarity to doxycycline and chloramphenicol. The branched region of the CPTEG:CPH-rifampicin nanoformulations indicates some dissimilarity from the other rifampicin nanoformulations and some unique behavior that will need to be explored more systematically using experiments. Of note, the rifampicin formulations with altered molar composition of CPTEG:CPH (from the 20:80 that makes up most of the data set) showed high similarity to the 20:80 CPTEG:CPH nanoformulations within the cluster. This would suggest that nano-carrier copolymer compositions can be interchanged within these rifampicin-loaded formulations without major impact.

This graph theory mapping in Figure 4.7 yielded notably different drug clustering within each nano-carrier chemistry compared to PCA (Figure 4.4). Rifampicin and chloramphenicol formulations are closely related in this map, while they were distant from each other in the PCA scores plot. Strikingly, chloramphenicol and pyrazinamide are most distant in the graph theory map, while they were clustered closely in the PCA scores plot. These clustering differences are likely due to PCA's limited ability to capture non-linear relationships. Non-linear modeling techniques like graph theory are better equipped to capture the non-linear release behavior arising from interactions between polymer and drug properties. In summary, the graph theory mapping defined similarity and connectivity between different nanoparticle formulations, while capturing non-linearity in relationships that can be lost in linear analysis.

As PCA projects data onto a linear manifold, it has difficulty explaining non-linear relationships. To this end, PCA demonstrated insufficient capability to accurately predict release properties in this data set. By contrast, graph theory can be used to project the data onto a non-linear manifold. This provides high-throughput modeling that accounts for non-linearity without requiring so many terms as to reduce the robustness of analysis. Therefore, the input into the predictions defines the graph theory values of Figure 4.7, which reflects a non-linear combination of descriptors, and a multi-linear regression between these values and the drug release properties was developed. It should be noted that the drug release properties were not included in the non-linear parameterization used for the prediction input, because that would result in predicting a property as a function of itself. The result of the high throughput modeling is shown in Figure 4.8. This represents a model with non-linear parameters that are a function of nanoparticle chemistry and theoretical drug loading and is defined generally so as to be applied to a wide range of chemistries. These models are fairly accurate, with R^2 values ranging between 70.0% and 75.5%. Cross validation was applied to ensure an even trade-off between robustness and accuracy. Since these methods are based on descriptors that can be generated for potential new nanoparticle formulations, the models provide a method to virtually explore a large search space. This method can guide experimentation by predicting target properties for a desired release profile, suggesting chemistries that match the targeted properties for testing.

4.4.3 Model Validation

To evaluate the robustness and accuracy of the multilinear models, nanoparticles encapsulating two new antibiotic drugs (not included in the training data set), meropenem and ceftazidime, were synthesized and characterized. Importantly, these drugs contain sulfur atoms (Supporting Figure 4.1) which are not present in the four drugs used in the original

model training. The models in Figure 4.8 were used to predict the release properties for these new formulations (Table 4.3). Based on these predictions, it is expected that all eight formulations would show a high (>80%) burst release at 2h and 24h and minimal sustained release over d2-d7. With the exception of the 20:80 CPH:SA–meropenem formulation, all other nanoformulations are expected to show near-100% encapsulation efficiency.

Strikingly, these predictions match experimental results closely. These new nano-formulations displayed similar release profiles characterized by a >90% burst release within two hours, followed by small amounts of drug released over the following two weeks (Supporting Figure 4.2, Table 4.3). For this data set, the models tended to under-predict the burst release and over-predict the sustained release behavior of the nano-formulations. The EE model was relatively accurate for 20:80 CPH:SA formulations, within 5%-20% of the measured EE's. The EE model showed more deviation from measured values for 20:80 CPTEG:CPH formulations, at circa 15-35% differences from the experimental values.

To test the robustness of the models when adding new, untrained chemistries, eight nano-formulations were included in the models (compositional percentages were calculated including sulfur atoms, but without a separate descriptor for sulfur) and new regressions were calculated. We found R^2 values for EE, FR (2h), FR (24h) and d2-d7 slope after these inclusions to be 74.3%, 75.5%, 69.9%, and 74.6%, respectively. The small changes in regression from the original model data in Figure 4.8 indicates that the analytics methodology was able to incorporate new drug chemistries with minor impacts on the models. This confirms the robustness of the model and its capability to screen drug and polymer chemistries not included in the model development.

4.5 Discussion

Due to the wide diversity of microbial infections, nanomedicines need to be customizable. Infections that are responsive to antibiotics may benefit from sustained release-skewing formulations by leveraging the dose sparing properties, limiting the risk of off-target effects, reducing the number of administrations, and enhancing patient compliance.[4,8,39] Polyanhydride nanoparticles represent an attractive and adaptable nanomedicine platform by virtue of their tunable degradation and payload release rates,[25,40] high biocompatibility,[41,42] and efficient internalization by phagocytic cells.[7]

Predictive analytics approaches have the potential to accelerate nanomedicine clinical translation, but the application of such informatics and data mining techniques to nanomedicine design has been slow to develop.[13] To date, the majority of such efforts has focused on either linear dimensionality reduction through PCA and regression through PLS,[27] which provides insight into relationships between formulations and variables but has limited capacity to capture nonlinear behavior, or else artificial neural network "black box" models,[43–45] which can capture nonlinear behavior but obscure interpretation of the structure of the model and dataspace. As the long-term goal of this research is to facilitate rational design of nanomedicine formulations, interpretation of the relationships between formulations is important. Accordingly, the dimensionality reduction approach was selected for this research, and paired with graph theory mapping to overcome the linearity limitations of PCA.

A hybrid data mining approach was employed to deconvolute the complex polymer and drug relationships and develop QSPRs that describe release kinetics and encapsulation efficiency. We correlated antibiotic release properties from varying polyanhydride chemistries, encapsulated drug types, and drug loading within the nanoparticles. Through

PCA analysis, we showed that release properties are dependent on both copolymer chemistry properties and drug properties, with polymer properties being more important. VIP analysis identified key polymer and drug descriptors that predicted drug release and encapsulation properties, but PCA was insufficient to predict release behavior from these formulations.

Graph theory was used to characterize the multilinear connectedness and similarity of formulations, which can guide selection of replacement formulations with similar release behavior. For example, it is expected that 20:80 CPH:SA rifampicin-loaded nanoparticles (Figure 4.2b) would demonstrate similar release behavior (including burst release, slope of release between days 2-7, and encapsulation efficiency) as 20:80 CPH:SA doxycycline-loaded nanoparticles (Figure 4.2a) based on their close connections and proximal distance on the map (Figure 4.7). Similarly, 20:80 CPTEG:CPH pyrazinamide-loaded nanoparticles (Figure 4.2d) would be expected to show large differences in release behavior from 20:80 CPH:SA chloramphenicol-loaded nanoparticles (Figure 4.2c) due to the large number of lines needed to connect them and far distance on the map (Figure 4.7). The descriptors identified by VIP analysis were paired with the multilinear mapping from graph theory to generate predictive models for *a priori* screening of nanoparticle formulations with desired release kinetics and high encapsulation efficiency.

The physicochemical properties of compounds influence their distribution, either in blood plasma or a polymer matrix. To this effect, VIP analysis (Figure 4.6) indicated that the descriptors most strongly correlated with release properties were both polymer and drug properties. This is expected, as favorable mixing thermodynamics allows distribution of the drugs inside the polymer device.[10,46] In polyanhydride nanoparticles, such a distribution allows an erosion-controlled release profile, which tends toward sustained release.[9,11] In

contrast, poor mixing between the polymer and drug induces thermodynamic partitioning of the drug into polymer microdomains and/or localization at the particle surface, which skews the release profile toward a high-burst, diffusion-dominated regime.[11] Many of these same drug properties were correlated with encapsulation efficiency, supporting the notion that polymer-drug mixing influences the carrying capacity of delivery devices. As empty polyanhydride nanoparticles have a moderately negative zeta potential,[23] the strong negative correlation between zeta potential and encapsulation efficiency could reflect a strong surface localization of positively charged drugs. If this were the case, however, we would expect a strong positive correlation between zeta potential and the two-hour burst release, which was not observed. Regardless, the predictive power of this descriptor could support the use of zeta potential as a quality control metric to ensure consistent encapsulation efficiencies of lead formulations. While it is not surprising that these drug properties affect encapsulation and release kinetics, this informatics analysis provides a sense of their relative impact. Reducing the data space in this way can help guide rational selection of antibiotic and polymer carrier pairs for nanomedicine formulations. These observations underline the complexity of these relationships and provide support for the use of data analytics approaches to enable rational design of nanomedicines.

It should be noted that we can only confidently make quantitative predictions in chemical spaces represented in our training data. While the additional testing of drugs containing sulfur, which was not represented in our training data, resulted in approximately no change in accuracy, materials that have unique behavior but with chemistries outside our training data may not be quantitatively described by this approach. However, even in these cases, our approach has significant impact. While the objective for the systems described by

our training data is to predict properties with high accuracy, the objective for systems containing groups and elements not in our training data is to identify polymer and drug combinations which have the most promising characteristics and identify where additional experiments are needed. This leads to an iterative approach where necessary experiments are identified, thus feeding back to the analysis.

From all of these results, we propose a framework for rational design and rapid testing of nanomedicine formulations (Figure 4.9). In the first step, selected antibiotic drug candidates are encapsulated within nanoparticles of various polymer chemistries (potentially using high throughput techniques,[23] as demonstrated in section 3.4), and characterization of size distribution by SEM and zeta potential is obtained. These nanoparticle characteristics, along with polymer properties and drug properties, can then be fed into the multilinear graph theory model to predict encapsulation efficiencies and release kinetics. Nanomedicine candidates that demonstrate insufficient encapsulation and/or undesirable drug release profiles can be discarded. The *in vitro* performance of the lead nanomedicine candidates that emerge from this step can then be validated using drug release kinetics assays. A feedback reformulation loop allows gradual optimization of nanomedicine formulations and iterative updates to the models when release behavior deviates from predictions. In theory, this framework could be expanded to include other performance metrics, including internalization by appropriate cells and biological efficacy. As this methodology uses standard polymer and nanoparticle characterization techniques used in nano-carrier drug delivery research and publicly available drug information, this approach could be expanded to include other types of polymeric materials and other classes of small molecule drugs. This data analytics

framework constitutes the first steps toward the rational design of nanomedicine formulations for antimicrobial therapies.

4.6 Conclusions

A multivariate data analytics approach was used to correlate drug release profiles from nanomedicine formulations based on different polyanhydride chemistries, encapsulated antibiotic drug type, and varying drug loading. We showed that both drug and polymer properties influence the drug encapsulation efficiency within the nanoparticles, the prevalence of burst in the drug release profile, and the slope of post-burst release. Polymer and drug properties that significantly impacted drug encapsulation efficiency and release kinetics were identified and defined a minimum descriptor set. The informatics analysis captured and preserved non-linear behavior governing relationships between drug type, polymer chemistry, and nanoparticle release properties, enabling interrogation of nanomedicine design pathways. We developed predictive models for drug release kinetics of untested drugs, using data from the Drugbank database and nano-carrier characterization as inputs. Release kinetics predictions of two drugs containing atoms not included in the model showed good agreement with experimental results, validating the model and indicating its potential to virtually explore new polymer and drug pairs not included in training data set. The models were shown to be robust after inclusion of these new formulations in that there were no significant changes in the model regressions. This multilinear modeling approach provides the first steps towards development of a framework that can be used to rationally design nanomedicine formulations by selecting the appropriate carrier for a drug payload to program desirable release kinetics profiles.

4.7 References

(1) Arora, D.; Sharma, N.; Sharma, V.; Abrol, V.; Shankar, R.; Jaglan, S. An Update on Polysaccharide-Based Nanomaterials for Antimicrobial Applications. *Appl. Microbiol. Biotechnol.* **2016**, *100* (6), 2603–2615. https://doi.org/10.1007/s00253-016-7315-0.

(2) Vorachit, M.; Chongtrakool, P.; Arkomsean, S.; Boonsong, S. Antimicrobial Resistance in Burkholderia Pseudomallei. *Acta Trop* **2000**, *74* (2–3), 139–144. https://doi.org/S0001-706X(99)00063-7 [pii].

(3) Seung, K. J.; Keshavjee, S.; Rich, M. L. Drug-Resistant Tuberculosis. *Cold Spring Harb Perspect Med* **2015**, *5*, 1–20.

(4) Narasimhan, B.; Goodman, J. T.; Vela Ramirez, J. E. Rational Design of Targeted Next-Generation Carriers for Drug and Vaccine Delivery. *Annu. Rev. Biomed. Eng* **2016**, *18* (1), 25–49. https://doi.org/10.1146/annurev-bioeng-082615-030519.

(5) Chan, C.-F.; Huang, K.-S.; Lee, M.-Y.; Yang, C.-H.; Wang, C.-Y.; Lin, Y.-S. Applications of Nanoparticles for Antimicrobial Activity and Drug Delivery. *Curr. Org. Chem.* **2014**, *18* (2), 204–215. https://doi.org/10.2174/1385272813176660144.

(6) Lueth, P.; Haughney, S. L.; Binnebose, A. M.; Mullis, A. S.; Peroutka-Bigus, N.; Narasimhan, B.; Bellaire, B. H. Nanotherapeutic Provides Dose Sparing and Improved Antimicrobial Activity against Brucella Melitensis Infections. *J. Control. Release* **2019**, *294*, 288–297. https://doi.org/10.1016/j.jconrel.2018.12.024.

(7) Phanse, Y.; Lueth, P.; Ramer-Tait, A. E.; Carrillo-Conde, B. R.; Wannemuehler, M. J.; Narasimhan, B.; Bellaire, B. H. Cellular Internalization Mechanisms of Polyanhydride Particles: Implications for Rational Design of Drug Delivery Vehicles. *J. Biomed. Nanotechnol.* **2016**, *12* (7), 1544–1552. https://doi.org/10.1166/jbn.2016.2259.

(8) Binnebose, A. M.; Haughney, S. L.; Martin, R.; Imerman, P. M.; Narasimhan, B.; Bellaire, B. H. Polyanhydride Nanoparticle Delivery Platform Dramatically Enhances Killing of Filarial Worms. *PLoS Negl. Trop. Dis.* **2015**, *9* (10), e0004173. https://doi.org/10.1371/journal.pntd.0004173.

(9) Shen, E.; Kipper, M. J.; Dziadul, B.; Lim, M.-K.; Narasimhan, B. Mechanistic Relationships between Polymer Microstructure and Drug Release Kinetics in Bioerodible Polyanhydrides. *J. Control. Release* **2002**, *82* (1), 115–125. https://doi.org/10.1016/S0168-3659(02)00125-6.

(10) Shen, E.; Pizsczek, R.; Dziadul, B.; Narasimhan, B. Microphase Separation in Bioerodible Copolymers for Drug Delivery. *Biomaterials* **2001**, *22* (3), 201–210. https://doi.org/10.1016/S0142-9612(00)00175-7.

(11) Berkland, C.; Kipper, M. J.; Narasimhan, B.; Kim, K.; Pack, D. W. Microsphere Size, Precipitation Kinetics and Drug Distribution Control Drug Release from Biodegradable Polyanhydride Microspheres. *J. Control. Release* **2004**, *94* (1), 129–141. https://doi.org/10.1016/j.jconrel.2003.09.011.

(12) Barnard, A. S. Challenges in Modelling Nanoparticles for Drug Delivery. *J. Phys. Condens. Matter* **2016**, *28* (2), 023002. https://doi.org/10.1088/0953-8984/28/2/023002.

(13) Jones, D. E.; Ghandehari, H.; Facelli, J. C. A Review of the Applications of Data Mining and Machine Learning for the Prediction of Biomedical Properties of Nanoparticles. *Comput. Methods Programs Biomed.* **2016**, *132*, 93–103. https://doi.org/10.1016/j.cmpb.2016.04.025.

(14) Tenenbaum, J.; Silva, V.; Langford, J. A Global Geometric Framewok for Nonlinear Dimensionality Reduction. *Science (80-.).* **2000**, *290* (December), 2319–2323.

(15) Broderick, S.; Rajan, K. Informatics Derived Materials Databases for Multifunctional Properties. *Sci. Technol. Adv. Mater.* **2015**, *16* (1), 1–8. https://doi.org/10.1088/1468-6996/16/1/013501.

(16) Li, X.; Petersen, L.; Broderick, S.; Narasimhan, B.; Rajan, K. Identifying Factors Controlling Protein Release from Combinatorial Biomaterial Libraries via Hybrid Data Mining Methods. *ACS Comb. Sci.* **2011**, *13* (1), 50–58. https://doi.org/10.1021/co100019d.

(17) Ulery, B. D.; Petersen, L. K.; Phanse, Y.; Kong, C. S.; Broderick, S. R.; Kumar, D.; Ramer-Tait, A. E.; Carrillo-Conde, B.; Rajan, K.; Wannemuehler, M. J.; et al. Rational Design of Pathogen-Mimicking Amphiphilic Materials as Nanoadjuvants. *Sci. Rep.* **2011**, *1*, 1–9. https://doi.org/10.1038/srep00198.

(18) Petersen, L. K.; Ramer-Tait, A. E.; Broderick, S. R.; Kong, C. S.; Ulery, B. D.; Rajan, K.; Wannemuehler, M. J.; Narasimhan, B. Activation of Innate Immune Responses in a Pathogen-Mimicking Manner by Amphiphilic Polyanhydride Nanoparticle Adjuvants. *Biomaterials* **2011**, *32* (28), 6815–6822. https://doi.org/10.1016/j.biomaterials.2011.05.063.

(19) Phanse, Y.; Carrillo-Conde, B. R.; Ramer-Tait, A. E.; Roychoudhury, R.; Pohl, N. L. B.; Narasimhan, B.; Wannemuehler, M. J.; Bellaire, B. H. Functionalization of Polyanhydride Microparticles with Di-Mannose Influences Uptake by and Intracellular Fate within Dendritic Cells. *Acta Biomater.* **2013**, *9* (11), 8902–8909. https://doi.org/10.1016/j.actbio.2013.06.024.

(20) Phanse, Y.; Carrillo-Conde, B. R.; Ramer-Tait, A. E.; Roychoudhury, R.; Broderick, S.; Pohl, N.; Rajan, K.; Narasimhan, B.; Wannemuehler, M. J.; Bellaire, B. H. Functionalization Promotes Pathogen-Mimicking Characteristics of Polyanhydride Nanoparticle Adjuvants. *J. Biomed. Mater. Res. - Part A* **2017**, *105* (10), 2762–2771. https://doi.org/10.1002/jbm.a.36128.

(21) Torres, M. P.; Vogel, B. M.; Narasimhan, B.; Mallapragada, S. K. Synthesis and Characterization of Novel Polyanhydrides with Tailored Erosion Mechanisms. *J. Biomed. Mater. Res. - Part A* **2006**, *76* (1), 102–110. https://doi.org/10.1002/jbm.a.30510.

(22) Conix, A. Poly[1,3-Bis(p-Carboxyphenoxy)-Propane Anhydride]. *Macromol. Synth.* **1966**, *2*, 95–98.

(23) Goodman, J. T.; Mullis, A. S.; Dunshee, L.; Mitra, A.; Narasimhan, B. Automated High-Throughput Synthesis of Protein-Loaded Polyanhydride Nanoparticle Libraries. *ACS Comb. Sci.* **2018**, *20* (5), 298–307. https://doi.org/10.1021/acscombsci.8b00008.

(24) Schindelin, J.; Arganda-Carreras, I.; Frise, E.; Kaynig, V.; Longair, M.; Pietzsch, T.; Preibisch, S.; Rueden, C.; Saalfeld, S.; Schmid, B.; et al. Fiji: An Open-Source Platform for Biological-Image Analysis. *Nat. Methods* **2012**, *9* (7), 676–682. https://doi.org/10.1038/nmeth.2019.

(25) Carrillo-Conde, B. R.; Darling, R. J.; Seiler, S. J.; Ramer-Tait, A. E.; Wannemuehler, M. J.; Narasimhan, B. Sustained Release and Stabilization of Therapeutic Antibodies Using Amphiphilic Polyanhydride Nanoparticles. *Chem. Eng. Sci.* **2015**, *125*, 98–107. https://doi.org/10.1016/j.ces.2014.08.015.

(26) Prasanthi, B.; Ratna, J. V.; Phani, R. S. C. Development and Validation of RP-HPLC Method for Simultaneous Estimation of Rifampicin, Isoniazid and Pyrazinamide in Human Plasma. *J. Anal. Chem.* **2015**, *70* (8), 1015–1022. https://doi.org/10.1134/S1061934815080146.

(27) Silva, J.; Mendes, M.; Cova, T.; Sousa, J.; Pais, A.; Vitorino, C. Unstructured Formulation Data Analysis for the Optimization of Lipid Nanoparticle Drug Delivery Vehicles. *AAPS PharmSciTech* **2018**, *19* (5), 1–12. https://doi.org/10.1208/s12249-018-1078-0.

(28) Broderick, S. R.; Suh, C.; Provine, J.; Roper, C. S.; Maboudian, R.; Howe, R. T.; Rajan, K. Application of Principal Component Analysis to a Full Profile Correlative Analysis of FTIR Spectra. *Surf. Interface Anal.* **2012**, *44* (3), 365–371. https://doi.org/10.1002/sia.3813.

(29) Ashton, M.; Hennig, R. G.; Broderick, S. R.; Rajan, K.; Sinnott, S. B. Computational Discovery of Stable M2AX Phases. *Phys. Rev. B* **2016**, *94* (5), 054116. https://doi.org/10.1103/PhysRevB.94.054116.

(30) Ericksson, L.; Byrne, T.; Johansson, E.; Trygg, J.; Vikstrom, C. *Multi- and Megavariate Data Analysis : Basic Principles and Applications*; Umetrics Ab,: Umea, 2001.

(31) Wold, S.; Sjöström, M.; Eriksson, L. PLS-Regression: A Basic Tool of Chemometrics. *Chemom. Intell. Lab. Syst.* **2001**, *58* (2), 109–130. https://doi.org/10.1016/S0169-7439(01)00155-1.

(32) Nguyen, D. V.; Rocke, D. M. Tumor Classification by Partial Least Squares Using Microarray Gene Expression Data. *Bioinformatics* **2002**, *18* (1), 39–50. https://doi.org/10.1093/bioinformatics/18.1.39.

(33) Balachandran, P. V.; Broderick, S. R.; Rajan, K. Identifying the "inorganic Gene" for High-Temperature Piezoelectric Perovskites through Statistical Learning. *Proc. R. Soc. A Math. Phys. Eng. Sci.* **2011**, *467* (2132), 2271–2290. https://doi.org/10.1098/rspa.2010.0543.

(34) Wodo, O.; Broderick, S.; Rajan, K. Microstructural Informatics for Accelerating the Discovery of Processing-Microstructure-Property Relationships. *MRS Bull.* **2016**, *41* (8), 603–609. https://doi.org/10.1557/mrs.2016.161.

(35) Srinivasan, S.; Broderick, S. R.; Zhang, R.; Mishra, A.; Sinnott, S. B.; Saxena, S. K.; LeBeau, J. M.; Rajan, K. Mapping Chemical Selection Pathways for Designing Multicomponent Alloys: An Informatics Framework for Materials Design. *Sci. Rep.* **2015**, *5*, 1–8. https://doi.org/10.1038/srep17960.

(36) Ulery, B. D.; Phanse, Y.; Sinha, a.; Wannemuehler, M. J.; Narasimhan, B.; Bellaire, B. H. Polymer Chemistry Influences Monocytic Uptake of Polyanhydride Nanospheres. *Pharm. Res.* **2009**, *26* (3), 683–690. https://doi.org/10.1007/s11095-008-9760-7.

(37) Wishart, D. S.; Feunang, Y. D.; Guo, A. C.; Lo, E. J.; Marcu, A.; Grant, J. R.; Sajed, T.; Johnson, D.; Li, C.; Sayeeda, Z.; et al. DrugBank 5.0: A Major Update to the DrugBank Database for 2018. *Nucleic Acids Res.* **2018**, *46* (D1), D1074–D1082. https://doi.org/10.1093/nar/gkx1037.

(38) Kipper, M. J.; Shen, E.; Determan, A.; Narasimhan, B. Design of an Injectable System Based on Bioerodible Polyanhydride Microspheres for Sustained Drug Delivery. *Biomaterials* **2002**, *23* (22), 4405–4412. https://doi.org/10.1016/S0142-9612(02)00181-3.

(39) Thomas, S. N.; Schudel, A. Overcoming Transport Barriers for Interstitial-, Lymphatic-, and Lymph Node-Targeted Drug Delivery. *Curr. Opin. Chem. Eng.* **2015**, *7*, 65–74. https://doi.org/10.1016/j.coche.2014.11.003.

(40) Petersen, L. K.; Sackett, C. K.; Narasimhan, B. Novel, High Throughput Method to Study in Vitro Protein Release from Polymer Nanospheres. *J. Comb. Chem.* **2010**, *12* (1), 51–56. https://doi.org/10.1021/cc900116c.

(41) Huntimer, L.; Ramer-Tait, A. E.; Petersen, L. K.; Ross, K. a.; Walz, K. a.; Wang, C.; Hostetter, J.; Narasimhan, B.; Wannemuehler, M. J. Evaluation of Biocompatibility and Administration Site Reactogenicity of Polyanhydride-Particle-Based Platform for Vaccine Delivery. *Adv. Healthc. Mater.* **2013**, *2* (2), 369–378. https://doi.org/10.1002/adhm.201200181.

(42) Adler, A. F.; Petersen, L. K.; Wilson, J. H.; Torres, M. P.; Thorstenson, J. B.; Gardner, S. W.; Mallapragada, S. K.; Wannemuehler, M. J.; Narasimhan, B. High Throughput Cell-Based Screening of Biodegradable Polyanhydride Libraries. *Comb. Chem. High Throughput Screen.* **2009**, *12* (7), 634–645. https://doi.org/10.2174/138620709788923764.

(43) Metwally, A. A.; Hathout, R. M. Computer-Assisted Drug Formulation Design: Novel Approach in Drug Delivery. *Mol. Pharm.* **2015**, *12* (8), 2800–2810. https://doi.org/10.1021/mp500740d.

(44) Shalaby, K. S.; Soliman, M. E.; Casettari, L.; Bonacucina, G.; Cespi, M.; Palmieri, G. F.; Sammour, O. A.; El Shamy, A. A. Determination of Factors Controlling the Particle Size and Entrapment Efficiency of Noscapine in PEG/PLA Nanoparticles Using Artificial Neural Networks. *Int. J. Nanomedicine* **2014**, *9* (1), 4953–4964. https://doi.org/10.2147/IJN.S68737.

(45) Husseini, G. A.; Mjalli, F. S.; Pitt, W. G.; Abdel-Jabbar, N. M. Using Artificial Neural Networks and Model Predictive Control to Optimize Acoustically Assisted Doxorubicin Release from Polymeric Micelles. *Technol. Cancer Res. Treat.* **2009**, *8* (6), 479–488. https://doi.org/10.1177/153303460900800609.

(46) Marsac, P. J.; Shamblin, S. L.; Taylor, L. S. Theoretical and Practical Approaches for Prediction of Drug–Polymer Miscibility and Solubility. *Pharm. Res.* **2006**, *23* (10), 2417–2426. https://doi.org/10.1007/s11095-006-9063-9.

4.8 Tables

Table 4.1 Representative antibiotic release properties

Nano-formulation	EE	FR (2h)	FR (24h)	FR slope (FR/day)
20:80 CPH:SA 5% DOX	64.9% ± 5.8%	0.878 ± 0.005	0.921 ± 0.007	0.00003 ± 0.00016
20:80 CPH:SA 1% DOX	159.0% ± 9.3%	0.675 ± 0.025	0.702 ± 0.010	0.02963 ± 0.97909
20:80 CPTEG:CPH 1% DOX	71.6% ± 5.8%	0.329 ± 0.023	0.462 ± 0.159	0.00082 ± 0.00014
50:50 CPTEG:CPH 10% RIF	86.7% ± 2.6%	0.818 ± 0.008	0.872 ± 0.004	0.00087 ± 0.20502
20:80 CPH:SA 3% RIF	29.8% ± 2.4%	0.240 ± 0.013	0.335 ± 0.009	0.06993 ± 0.96020
20:80 CPH:SA 1% RIF	49.3% ± 2.8%	0.106 ± 0.011	0.168 ± 0.010	0.06285 ± 0.96084
20:80 CPH:SA 20% CAM	59.8% ± 0.4%	0.886 ± 0.009	0.927 ± 0.006	0.00192 ± 0.47169
20:80 CPTEG:CPH 20% CAM	123.5% ± 13.0%	0.766 ± 0.020	0.782 ± 0.018	0.00055 ± 0.00821
20:80 CPH:SA 5% PZA	34.9% ± 4.8%	0.298 ± 0.053	0.449 ± 0.069	0.02168 ± 0.30458
20:80 CPTEG:CPH 5% PZA	89.7% ± 36.6%	0.057 ± 0.013	0.086 ± 0.020	0.00879 ± 0.33933

FR (2h) fraction released in two-hour burst, FR (24h) fraction released in 24-hour burst. Data are presented as mean ± SD.

Table 4.2 List of descriptors used in VIP analysis

1	Zeta potential	13	Tg (°C)	25	logP (predicted, ChemAxon)
2	Diameter	14	% C (Drug)	26	logS (predicted, ALGOPS)
3	PDI	15	% H (Drug)	27	pKa (Strongest Acidic)
4	Water contact angle	16	% Cl (Drug)	28	pKa (Strongest Basic)
5	Backbone O	17	% N (Drug)	29	Physiological charge
6	Aliphatic C	18	% O (Drug)	30	Hydrogen acceptor count
7	Aromatic C	19	molar mass	31	Hydrogen donor count
8	% O	20	Tm (°C, Drug)	32	Polar surface area
9	% H	21	water solubility (experimental)	33	Rotatable bond count
10	% C	22	logP (experimental)	34	Refractivity
11	DOP	23	water solubility (predicted, ALGOPS)	35	Polarizability
12	Mn (Da)	24	logP (predicted, ALGOPS)	36	Number of rings

Table 4.3 Parameterized release properties of nanoparticles encapsulating two drugs (meropenem and ceftazidime) not included in training data set

	EE		FR (2h)		FR (24h)		FR slope (FR/day)	
Nano-formulation	predicted	measured	predicted	measured	predicted	measured	predicted	measured
20:80 CPTEG:CPH 5% meropenem	159%	195.0%	0.83	0.9406	0.84	0.9408	0.0033	0.000853
20:80 CPTEG:CPH 10% meropenem	128%	140.9%	0.81	0.9616	0.86	0.9617	0.0026	0.000271
20:80 CPH:SA 5% meropenem	29%	34.5%	0.95	0.9933	0.90	0.9933	0.0011	0.000656
20:80 CPH:SA 10% meropenem	49%	61.7%	0.98	0.9965	0.91	0.9967	0.0014	0.000168
20:80 CPTEG:CPH 5% ceftazidime	175%	156.8%	0.92	0.9997	0.88	1.0000	0.0019	0.000001
20:80 CPTEG:CPH 10% ceftazidime	190%	159.9%	0.91	0.9997	0.87	1.0000	0.0041	0.000004
20:80 CPH:SA 5% ceftazidime	114%	91.8%	0.97	0.9915	0.91	0.9952	0.0031	0.000771
20:80 CPH:SA 10% ceftazidime	129%	112.7%	0.94	0.9910	0.91	0.9941	0.0051	0.000686

FR (2h) fraction released in two-hour burst, FR (24h) fraction released in 24-hour burst.

4.9 Figures

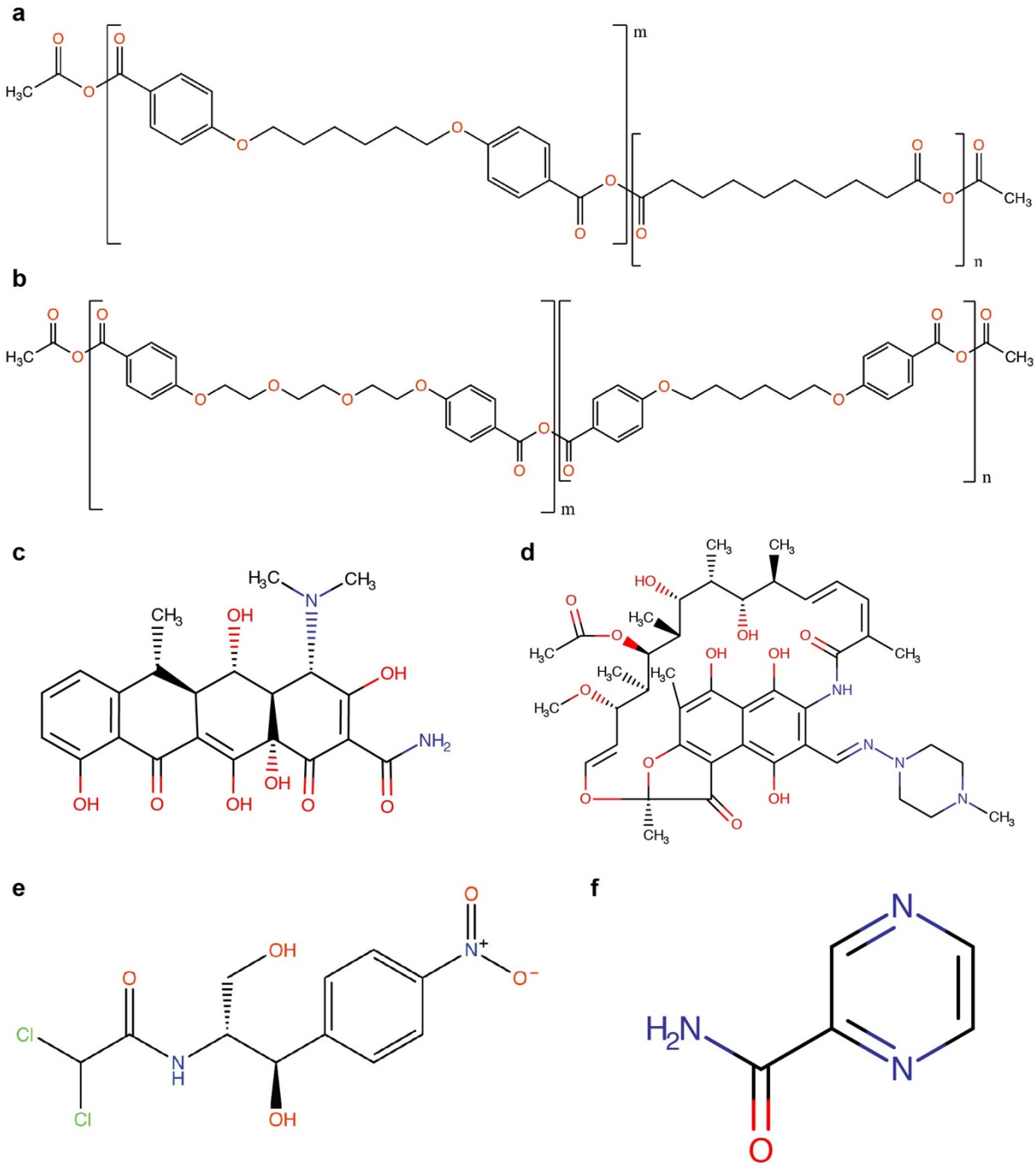

Figure 4.1 Polymer and antibiotic chemical structures. (a,b) Structures of CPH:SA (a) and CPTEG:CPH (b) copolymers, where m and n are the number of repeats for each unit. (c-f) Structure of doxycycline (DOX, a), rifampicin (RIF, b), chloramphenicol (CAM, c), and pyrazinamide (PZA, d).

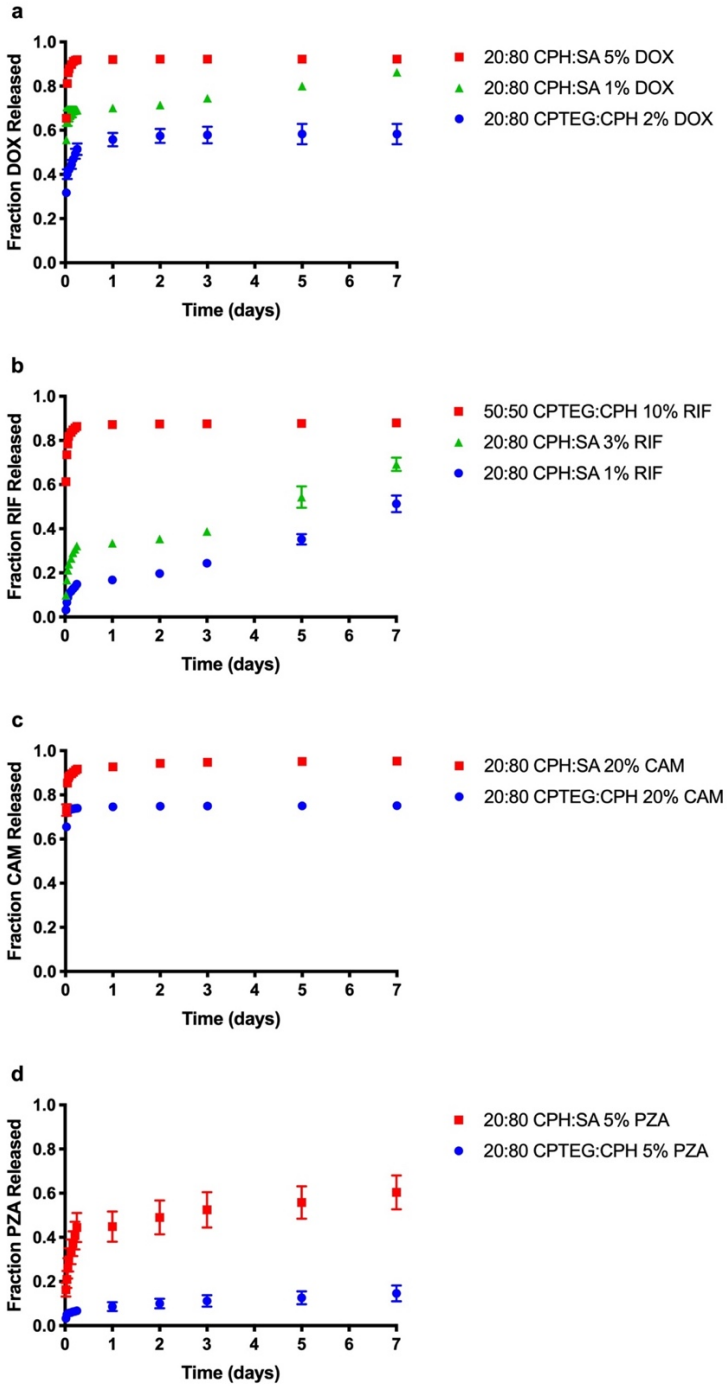

Figure 4.2 Representative antibiotic release kinetics from nanoparticles encapsulating doxycycline (DOX, a), rifampicin (RIF, b), chloramphenicol (CAM, c), and pyrazinamide (PZA, d). The depicted nanoformulations represent a subset of the 68 formulations tested and were selected to display the diversity of release behavior in the data set. Data are presented as mean ± SD. Error bars are not depicted in cases where the error bar height is smaller than the symbol. Release profiles were parameterized into two-hour burst, one day burst, and 2-7 day sustained release slope.

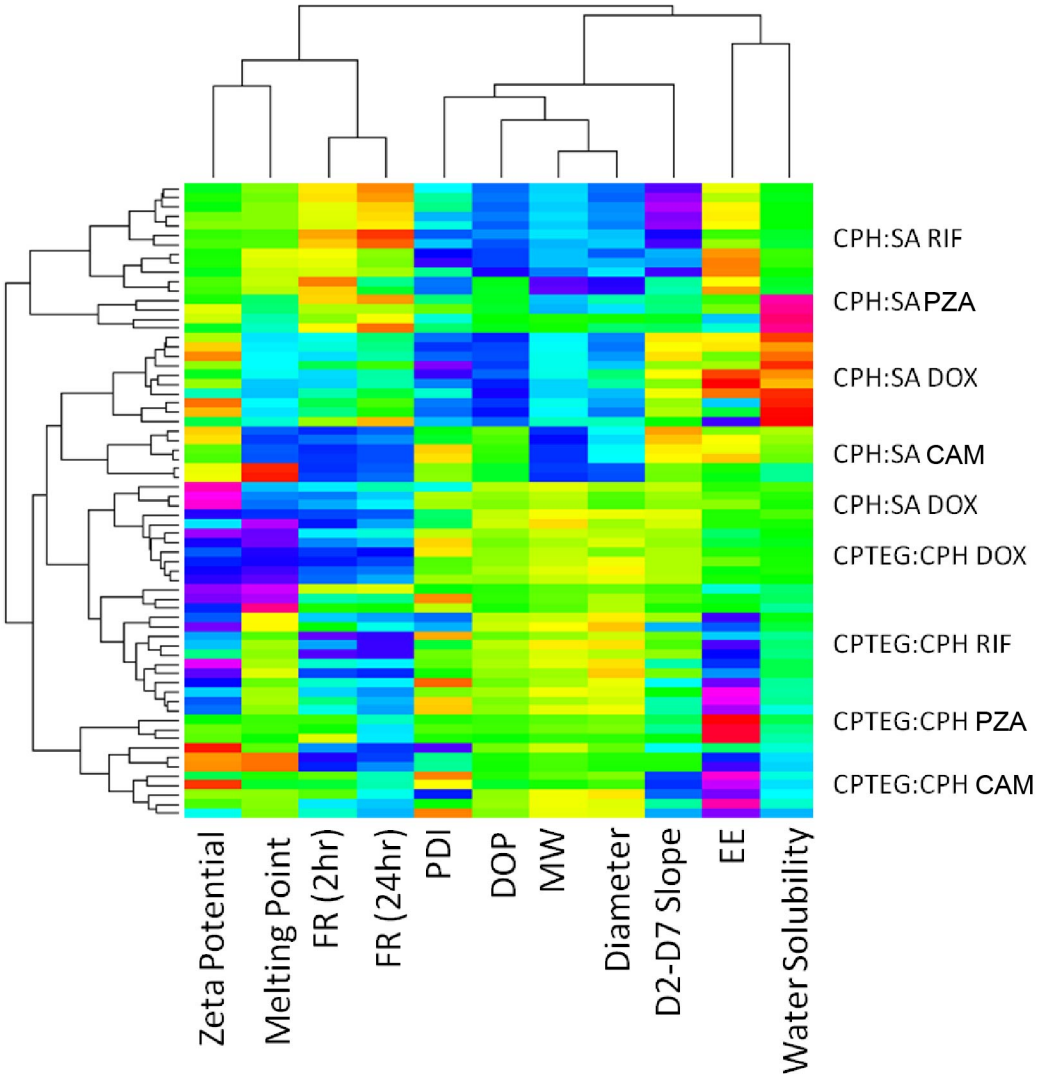

Figure 4.3 Representation of correlations in data using Euclidian distance-based clustering, with the dendrograms defining the degree of correlation (i.e., branches at the bottom of the dendrogram have high correlation and correlation decreases as moving along the branches). From the dendrograms, the key discriminators among nanoformulations (vertical axis) in the order of importance are carrier chemistry (CPTEG:CPH versus CPH:SA), drug type, and theoretical drug loading. Concerning correlations between drug release properties and descriptors (horizontal axis), nanoparticle burst release (FR (2hr) and FR (24 hr)) was most strongly correlated with zeta potential and drug melting point. The release slope was most strongly correlated with the nanoparticle and polymer size properties. Encapsulation efficiency was most strongly correlated with the water solubility of the drug. That these data fall within comparable ranges demonstrates the robustness of the method and data set, enabling interrogation of nanoformulation behavior. Drug abbreviations: doxycycline (DOX), rifampicin (RIF), chloramphenicol (CAM), and pyrazinamide (PZA). Raw and processed input data are included in Supporting Tables 4.1-2.

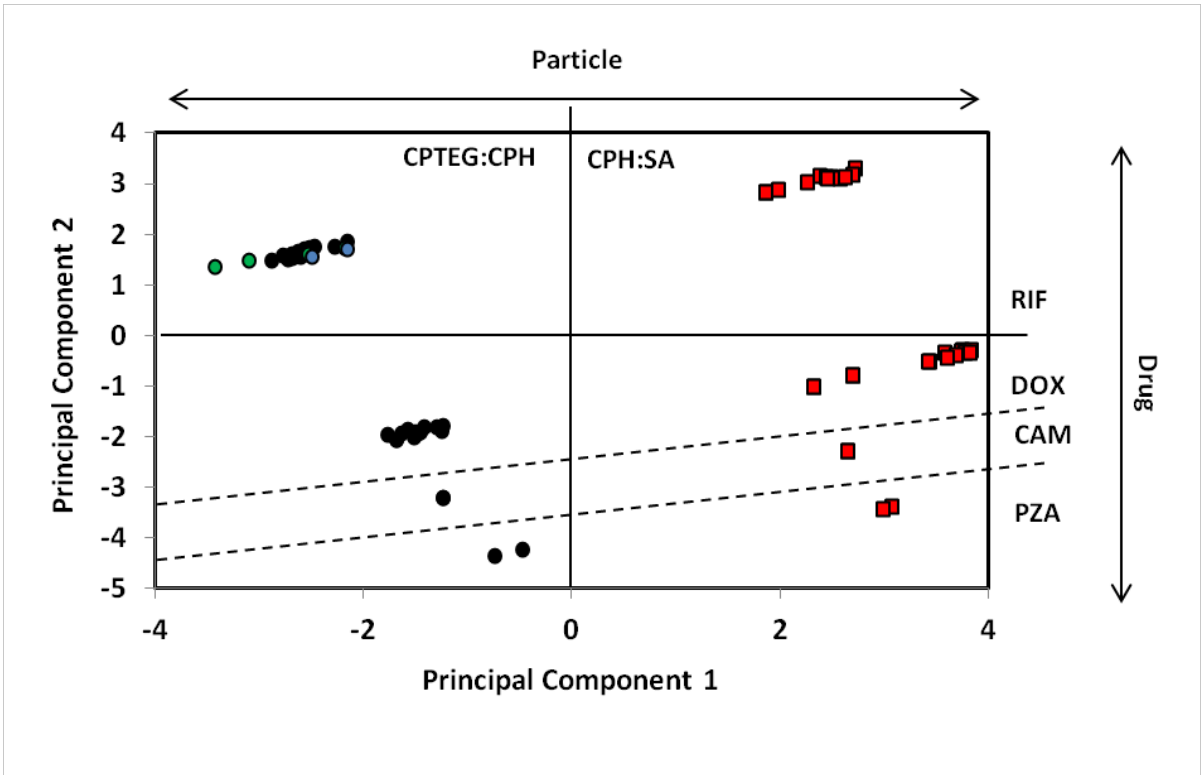

Figure 4.4 PCA scores plot. PC1 captures differences due to particle chemistry (10:90 CPTEG:CPH in blue, 20:80 CPTEG:CPH in black, and >30:<70 CPTEG:CPH in green) and PC2 captures the differences due to drug. There is a clear separation of formulations due to different chemistries, with a demonstrated capability to isolate the effects of particle chemistry from drug properties. PC1 and PC2 captured 43.1% and 27.9% of variability, respectively. Drug abbreviations: doxycycline (DOX), rifampicin (RIF), chloramphenicol (CAM), and pyrazinamide (PZA). Raw input data are provided in Supporting Table 4.3.

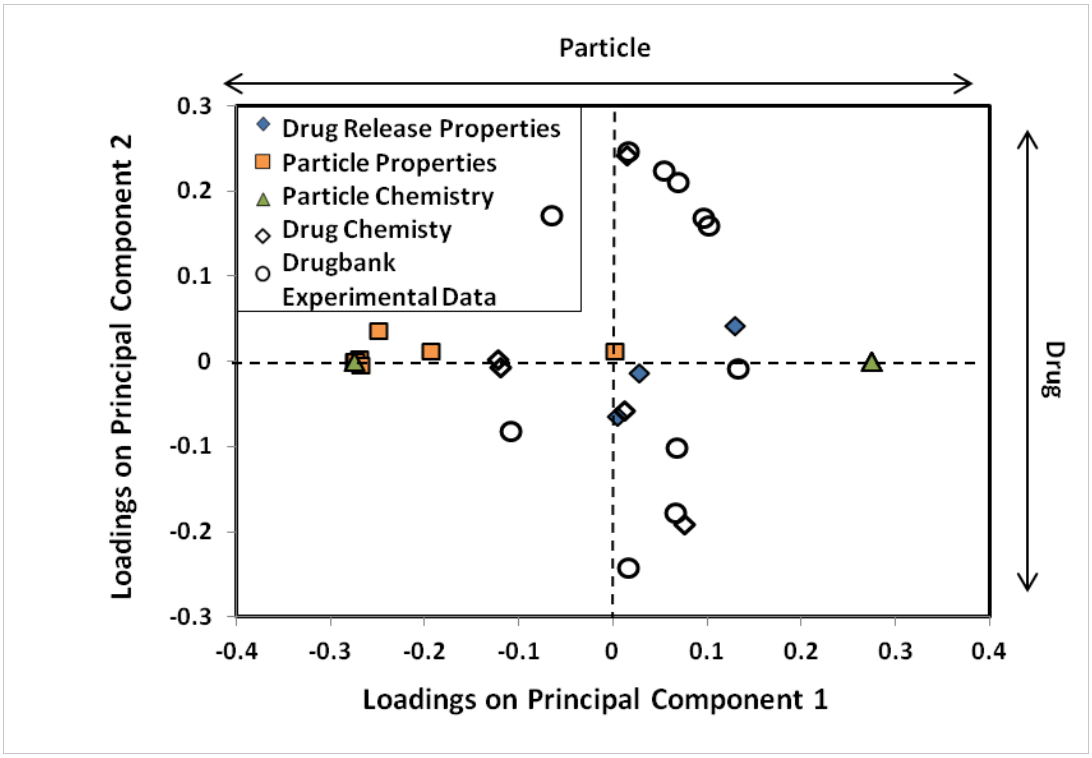

Figure 4.5 PCA loadings plot. Particle descriptors lie along the PC1 axis and drug descriptors lie along the PC2 axis. Drug release properties lie along both axes, indicating some dependence on both particle and drug descriptors. PC1 and PC2 captured 43.1% and 27.9% of variability, respectively. Raw input data are provided in Supporting Table 4.3.

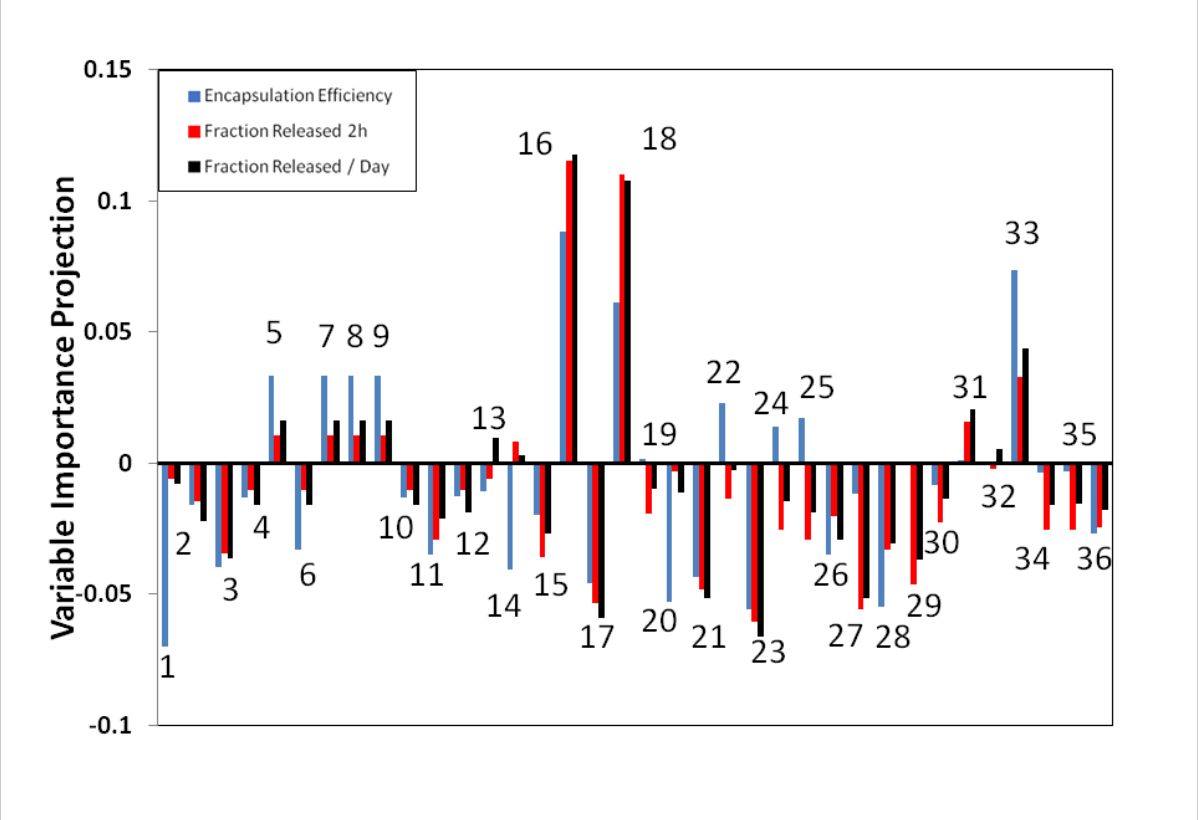

Figure 4.6 Variable importance projection of descriptors with respect to drug release properties. Descriptors are listed in Table 4.2. Positive VIP values correspond to positive correlation, and negative values to inverse correlation.

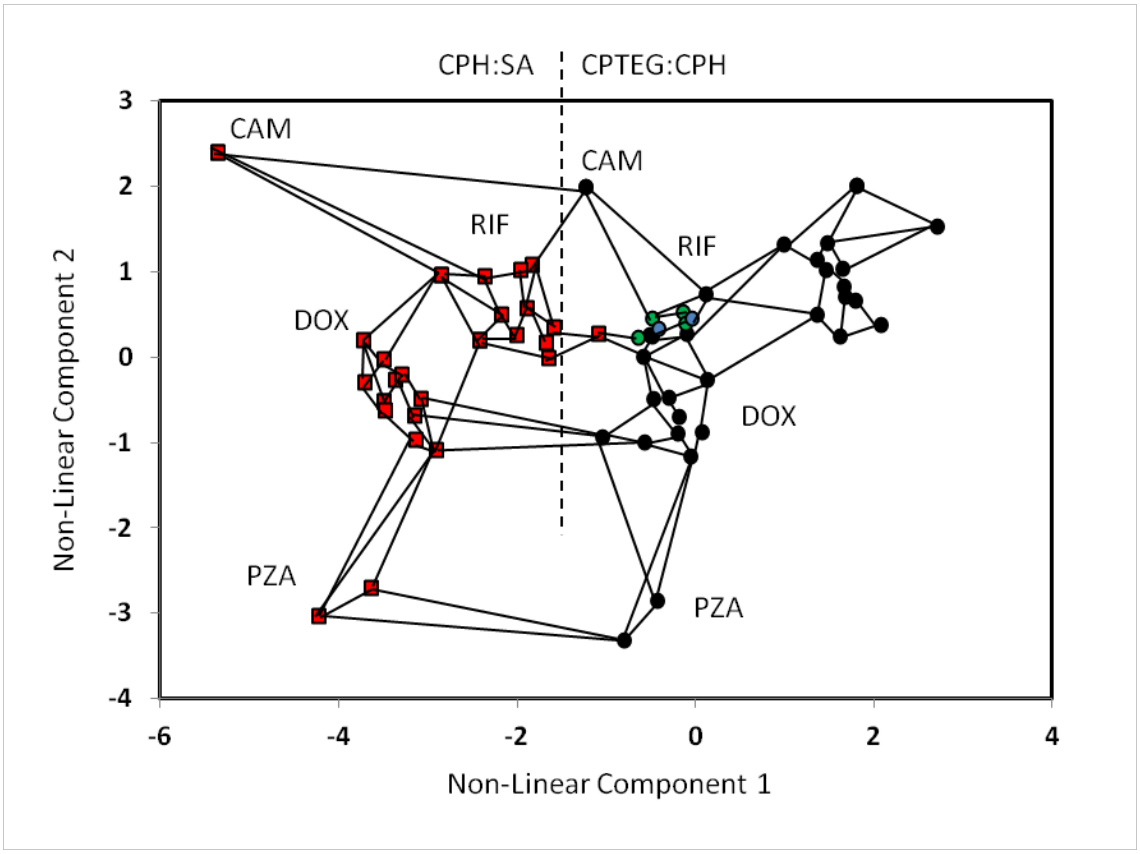

Figure 4.7 Graph theory map of formulation connectivity of release properties. Similarity between points is defined as the number of connections (solid lines) required to connect points. CPH:SA chemistries are represented by orange squares, while CPTEG:CPH chemistries are represented by circles (10:90 CPTEG:CPH in blue, 20:80 CPTEG:CPH in black, and >30:<70 CPTEG:CPH in green) This represents an approach for building a set of non-linearly derived parameters for performing high-throughput predictions. This approach was applied to a reduced descriptor set in order to develop a parameterization of the data, which ensures robustness by minimizing the number of input parameters, while incorporating non-linear relationships and maximizing variance in the data. Drug abbreviations: doxycycline (DOX), rifampicin (RIF), chloramphenicol (CAM), and pyrazinamide (PZA).

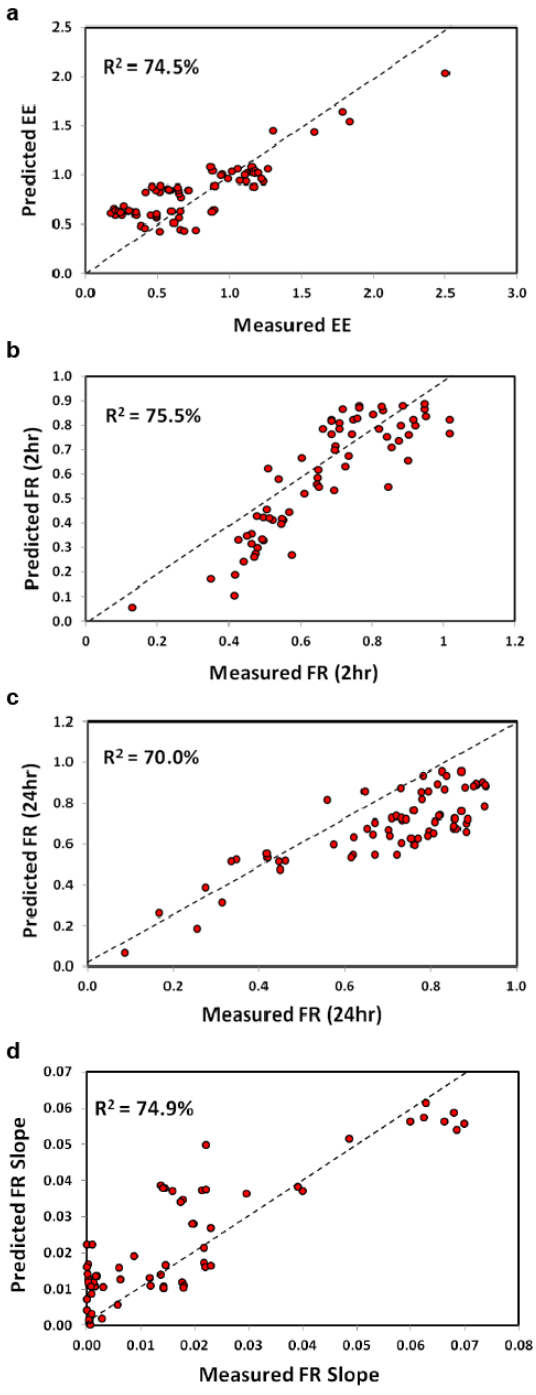

Figure 4.8 Graph theory high-throughput modeling of drug release properties. The horizontal axis is the experimental measurements. The vertical axis is the predicted encapsulation efficiency (a), 2-hour burst release (b), 24-hour burst release (c), and the d2-d7 release profile slope values from our model based on the reduced descriptor set. These calculations are based on a new hybrid informatics approach where non-linear manifold projections serve as the input, thereby accounting for greater complexity in descriptor-property relationships while also increasing the robustness of the models. The models are reasonably accurate for all tested release properties.

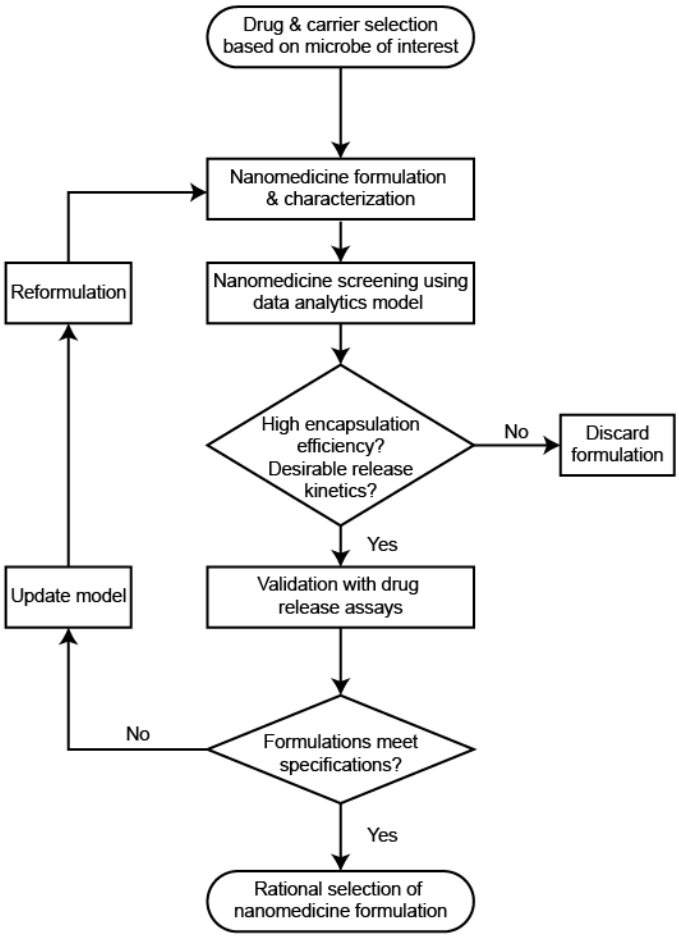

Figure 4.9 Data analytics framework for rapid nanomedicine design and screening

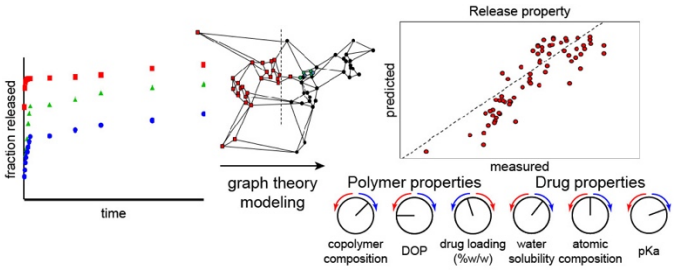

Figure 4.10 Table of contents graphic

4.10 Supporting Information

Supporting Table 4.1 Dendrogram raw input data

Formulation	FR (2h)	FR (24h)	d2-d7 slope	EE	zeta potential	diameter	PDI	DOP	Mn	Tm (Drug)	water solubility
20:80 CPH:SA 5% DOX	0.878	0.921	3.11275E-05	0.649	-24.2	295.0	0.11606438	29.34	15385	201	630
20:80 CPH:SA 10% DOX	0.878	0.928	0.000682253	0.451	-19.9	290.2	0.0944491	29.34	15385	201	630
20:80 CPTEG:CPH 5% DOX	0.810	0.816	0	0.663	16.1	187.0	0.13094153	16.69	5902	201	630
20:80 CPTEG:CPH 10% DOX	0.861	0.871	0.000267517	0.519	10.8	198.0	0.09410895	16.69	5902	201	630
20:80 CPH:SA 5% DOX	0.821	0.882	0.001030157	0.493	-24.2	295.0	0.11606438	29.34	15385	201	630
20:80 CPH:SA 10% DOX	0.870	0.926	0.000255865	0.349	-19.9	290.2	0.0944491	29.34	15385	201	630
20:80 CPTEG:CPH 5% DOX	0.752	0.778	0.000964581	0.589	-14	188.8	0.11068015	16.69	5902	201	630
20:80 CPTEG:CPH 10% DOX	0.798	0.827	0.000407385	0.415	10.8	198.0	0.09410895	16.69	5902	201	630
20:80 CPH:SA 5% RIF	0.355	0.669	0.019842283	0.267	-21.2	326.8	0.12999352	29.34	15385	183	1400
20:80 CPTEG:CPH 5% RIF	0.622	0.762	0.014603834	0.613	-32.4	183.3	0.1262826	16.69	5902	183	1400
20:80 CPH:SA 5% RIF	0.315	0.721	0.019558135	0.385	-21.2	326.8	0.12999352	29.34	15385	183	1400
20:80 CPTEG:CPH 5% RIF	0.665	0.855	0.005726169	1.127	-13.9	164.8	0.10765556	16.69	5902	183	1400
20:80 CPH:SA 20% CAM	0.866	0.907	0.002788729	0.654	-28.8	330.1	0.09645677	29.34	15385	171	2500
20:80 CPTEG:CPH 20% CAM	0.766	0.782	0.000547523	1.235	-36.5	177.3	0.10820173	16.69	5902	171	2500
20:80 CPTEG:CPH 20% CAM	0.821	0.838	0.000423089	1.117	-36.5	177.3	0.10820173	16.69	5902	171	2500
20:80 CPH:SA 20% CAM	0.886	0.927	0.001916802	0.598	-28.8	330.1	0.09645677	29.34	15385	171	2500
20:80 CPH:SA 5% PZA	0.171	0.276	0.021718991	0.493	-21.5	282.3	0.11965848	29.34	15385	192	1.50E+04
20:80 CPTEG:CPH 5% PZA	0.057	0.086	0.008793703	0.897	-24.1	216.3	0.10769206	16.69	5902	192	1.50E+04
20:80 CPH:SA 5% PZA	0.298	0.449	0.021676638	0.349	-32.8	317.7	0.09466064	29.34	15385	192	1.50E+04
20:80 CPTEG:CPH 5% PZA	0.268	0.313	0.006047673	1.169	-35.1	181.5	0.12303395	18.47	6499	192	1.50E+04
20:80 CPH:SA 10% DOX	0.843	0.856	0.01784599	0.410	-16.4	300.1	0.14238195	66.18	14715	201	630
20:80 CPH:SA 9% DOX	0.876	0.885	0.014484272	0.516	-10.4	302.3	0.15598785	66.18	14715	201	630
20:80 CPH:SA 8% DOX	0.785	0.822	0.017440928	0.656	-7.46	329.0	0.13393998	66.18	14715	201	630
20:80 CPH:SA 7% DOX	0.823	0.860	0.01375275	0.686	-19.3	352.0	0.1488103	66.18	14715	201	630
20:80 CPH:SA 6% DOX	0.829	0.855	0.015909071	0.768	-14.7	343.2	0.14415255	66.18	14715	201	630
20:80 CPH:SA 5% DOX	0.865	0.882	0.014097678	0.895	-20.1	346.3	0.14633586	66.18	14715	201	630
20:80 CPH:SA 4% DOX	0.763	0.795	0.022073666	0.876	-13.6	337.2	0.15620233	66.18	14715	201	630
20:80 CPH:SA 3% DOX	0.785	0.807	0.021288819	1.074	-17	344.8	0.14393289	66.18	14715	201	630
20:80 CPH:SA 2% DOX	0.764	0.792	0.022058247	1.305	-18.9	342.4	0.14448117	66.18	14715	201	630
20:80 CPH:SA 1% DOX	0.675	0.702	0.029634541	1.590	-7.96	324.5	0.14340887	66.18	14715	201	630
20:80 CPTEG:CPH 10% DOX	0.799	0.905	0.000223847	0.574	-8.24	188.8	0.08952265	17.71	6230	201	630
20:80 CPTEG:CPH 9% DOX	0.836	0.900	0	0.647	-2.23	175.3	0.11657572	17.71	6230	201	630
20:80 CPTEG:CPH 8% DOX	0.823	0.878	0.000418826	0.488	-6.01	163.3	0.10179907	17.71	6230	201	630
20:80 CPTEG:CPH 7% DOX	0.760	0.833	0.001562307	0.642	-6.12	165.0	0.10244058	17.71	6230	201	630
20:80 CPTEG:CPH 6% DOX	0.656	0.731	0.001318373	0.714	-3.44	177.3	0.09540602	17.71	6230	201	630
20:80 CPTEG:CPH 5% DOX	0.736	0.794	0.000230922	0.583	-5.95	167.3	0.09709577	17.71	6230	201	630
20:80 CPTEG:CPH 4% DOX	0.709	0.777	0.000136467	0.636	-7.1	163.3	0.08765737	17.71	6230	201	630
20:80 CPTEG:CPH 3% DOX	0.546	0.646	0	0.524	-6.21	157.5	0.0797639	17.71	6230	201	630
20:80 CPTEG:CPH 2% DOX	0.422	0.558	0.001648516	0.463	-13.6	157.5	0.08989265	17.71	6230	201	630
20:80 CPTEG:CPH 1% DOX	0.329	0.462	0.000816278	0.716	-6.24	171.3	0.10018658	17.71	6230	201	630
20:80 CPH:SA 10% RIF	0.410	0.574	0.048640198	0.196	-17.3	298.3	0.12142294	66.18	14715	183	1400
20:80 CPH:SA 9% RIF	0.417	0.620	0.039920326	0.207	-17.4	329.0	0.15660778	66.18	14715	183	1400
20:80 CPH:SA 8% RIF	0.327	0.420	0.067948568	0.176	-23.3	351.9	0.1414808	66.18	14715	183	1400
20:80 CPH:SA 7% RIF	0.412	0.616	0.039087381	0.255	-16.9	352.6	0.15262713	66.18	14715	183	1400
20:80 CPH:SA 6% RIF	0.332	0.418	0.068454099	0.207	-18.1	345.2	0.12222125	66.18	14715	183	1400
20:80 CPH:SA 5% RIF	0.345	0.446	0.066219621	0.230	-24.3	350.0	0.13065327	66.18	14715	183	1400
20:80 CPH:SA 4% RIF	0.274	0.347	0.062373003	0.245	-17.3	359.5	0.13344125	66.18	14715	183	1400
20:80 CPH:SA 3% RIF	0.240	0.335	0.069931257	0.298	-20.6	366.7	0.12454902	66.18	14715	183	1400
20:80 CPH:SA 2% RIF	0.186	0.255	0.05983363	0.305	-24.4	317.3	0.13607798	66.18	14715	183	1400
20:80 CPH:SA 1% RIF	0.106	0.168	0.062846415	0.493	-23.1	338.3	0.15404764	66.18	14715	183	1400
20:80 CPTEG:CPH 10% RIF	0.556	0.709	0.011641771	1.017	-15.3	171.8	0.0920574	17.71	6230	183	1400
20:80 CPTEG:CPH 9% RIF	0.520	0.670	0.013749282	0.883	-19.5	173.3	0.09072136	17.71	6230	183	1400
20:80 CPTEG:CPH 8% RIF	0.585	0.721	0.017676351	1.161	-9.86	161.8	0.08304844	17.71	6230	183	1400
20:80 CPTEG:CPH 7% RIF	0.442	0.665	0.018013083	0.946	-24.5	168.5	0.11797225	17.71	6230	183	1400
20:80 CPTEG:CPH 6% RIF	0.427	0.621	0.021989935	1.155	-37.1	164.5	0.08225642	17.71	6230	183	1400
20:80 CPTEG:CPH 5% RIF	0.394	0.650	0.023027263	1.268	-21.8	168.0	0.08104582	17.71	6230	183	1400
20:80 CPTEG:CPH 4% RIF	0.580	0.704	0.011808479	1.175	-23.3	172.0	0.10299328	17.11	6052	183	1400
20:80 CPTEG:CPH 3% RIF	0.454	0.755	0.01425443	1.787	-25.8	169.5	0.09688981	17.71	6230	183	1400
20:80 CPTEG:CPH 2% RIF	0.420	0.769	0.014252747	2.503	-22.1	165.8	0.09975738	17.71	6230	183	1400
20:80 CPTEG:CPH 1% RIF	0.260	0.733	0.003109203	1.837	-27.3	174.5	0.09653278	17.71	6230	183	1400
10:90 CPTEG:CPH 10% RIF	0.533	0.734	0.02296554	0.991	-7.27	175.5	0.12154016	19.7	6894	183	1400
20:80 CPTEG:CPH 10% RIF	0.630	0.760	0.017949702	1.108	-1.56	162.8	0.10197021	17.67	6225	183	1400
30:70 CPTEG:CPH 10% RIF	0.715	0.819	0.006303884	0.940	-7.59	172.0	0.10670578	20.97	7412	183	1400
50:50 CPTEG:CPH 10% RIF	0.818	0.872	0.00086837	0.867	-13.1	160.3	0.08394513	16.89	6099	183	1400
10:90 CPTEG:CPH 10% RIF	0.547	0.733	0.014208586	1.177	-13.1	178.8	0.09274206	19.7	6894	183	1400
20:80 CPTEG:CPH 10% RIF	0.616	0.744	0.00785114	1.196	-15.5	175.3	0.09939584	17.67	6225	183	1400
30:70 CPTEG:CPH 10% RIF	0.698	0.809	0.005925504	1.222	-9.16	181.3	0.12844245	20.97	7412	183	1400
50:50 CPTEG:CPH 10% RIF	0.785	0.857	0.001769323	1.058	-18.2	177.0	0.09931877	16.89	6099	183	1400

Encapsulation efficiencies (EE) are formatted as fractions.

Supporting Table 4.2 Dendrogram processed input data

Formulation	FR (2h)	FR (24h)	d2-d7 slope	EE	zeta potential	diameter	PDI	DOP	Mn	Tm (Drug)	water solubility
20:80 CPH:SA 5% DOX	1.049	0.957	-0.77245373	-0.269	-0.695637879	0.8	0.11000297	-0.12	1.329	1.167277	-0.241625119
20:80 CPH:SA 10% DOX	1.049	0.990	-0.73878824	-0.731	-0.27866345	0.7	-0.9161651	-0.12	1.329	1.167277	-0.241625119
20:80 CPTEG:CPH 5% DOX	0.771	0.464	-0.77406313	-0.236	3.212285262	-0.6	0.81628394	-0.73	-0.87	1.167277	-0.241625119
20:80 CPTEG:CPH 10% DOX	0.978	0.722	-0.76023157	-0.572	2.698340035	-0.5	-0.9323134	-0.73	-0.87	1.167277	-0.241625119
20:80 CPH:SA 5% DOX	0.818	0.773	-0.7208004	-0.631	-0.695637879	0.8	0.11000297	-0.12	1.329	1.167277	-0.241625119
20:80 CPH:SA 10% DOX	1.017	0.982	-0.76083402	-0.967	-0.27866345	0.7	-0.9161651	-0.12	1.329	1.167277	-0.241625119
20:80 CPTEG:CPH 5% DOX	0.537	0.285	-0.7241909	-0.408	0.293464256	-0.6	-0.145609	-0.73	-0.87	1.167277	-0.241625119
20:80 CPTEG:CPH 10% DOX	0.725	0.516	-0.75299988	-0.815	2.698340035	-0.5	-0.9323134	-0.73	-0.87	1.167277	-0.241625119
20:80 CPH:SA 5% RIF	-1.074	-0.231	0.251852237	-1.159	-0.404725487	1.2	0.77127795	-0.12	1.329	-0.66354	-0.207450955
20:80 CPTEG:CPH 5% RIF	0.009	0.208	-0.01899388	-0.353	-1.490798419	-0.7	0.59510478	-0.73	-0.87	-0.66354	-0.207450955
20:80 CPH:SA 5% RIF	-1.239	0.014	0.237160814	-0.884	-0.404725487	1.2	0.77127795	-0.12	1.329	-0.66354	-0.207450955
20:80 CPTEG:CPH 5% RIF	0.182	0.647	-0.47800015	0.846	0.303161336	-0.9	-0.289199	-0.73	-0.87	-0.66354	-0.207450955
20:80 CPH:SA 20% CAM	1.001	0.891	-0.62987609	####	-1.141703548	1.2	-0.8208524	-0.12	1.329	-1.88408	-0.158630722
20:80 CPTEG:CPH 20% CAM	0.593	0.301	-0.74575429	1.099	-1.888378689	-0.8	-0.2632698	-0.73	-0.87	-1.88408	-0.158630722
20:80 CPTEG:CPH 20% CAM	0.818	0.567	-0.75218793	0.823	-1.888378689	-0.8	-0.2632698	-0.73	-0.87	-1.88408	-0.158630722
20:80 CPH:SA 20% CAM	1.082	0.987	-0.67495776	-0.388	-1.141703548	1.2	-0.8208524	-0.12	1.329	-1.88408	-0.158630722
20:80 CPH:SA 5% PZA	-1.821	-2.087	0.348884598	-0.631	-0.433816726	0.6	0.28063019	-0.12	1.329	0.251871	3.96E-01
20:80 CPTEG:CPH 5% PZA	-2.284	-2.983	-0.31939797	0.309	-0.6859408	-0.3	-0.2874662	-0.73	-0.87	0.251871	3.96E-01
20:80 CPH:SA 5% PZA	-1.308	-1.270	0.346694823	-0.969	-1.529586738	1.1	-0.9061224	-0.12	1.329	0.251871	3.96E-01
20:80 CPTEG:CPH 5% PZA	-1.427	-1.912	-0.46137727	0.943	-1.752619573	-0.7	0.44087769	-0.64	-0.73	0.251871	3.96E-01
20:80 CPH:SA 10% DOX	0.907	0.653	0.148636914	-0.826	0.060734342	0.8	1.35940872	1.632	1.174	1.167277	-0.241625119
20:80 CPH:SA 9% DOX	1.041	0.787	-0.02517562	-0.580	0.642559127	0.9	2.00533759	1.632	1.174	1.167277	-0.241625119
20:80 CPH:SA 8% DOX	0.671	0.490	0.127693791	-0.252	0.927653272	1.2	0.95863291	1.632	1.174	1.167277	-0.241625119
20:80 CPH:SA 7% DOX	0.823	0.671	-0.06299788	-0.182	-0.220480971	1.5	1.66458911	1.632	1.174	1.167277	-0.241625119
20:80 CPH:SA 6% DOX	0.848	0.647	0.048491452	0.008	0.225584697	1.4	1.44346644	1.632	1.174	1.167277	-0.241625119
20:80 CPH:SA 5% DOX	0.997	0.773	-0.04516392	0.304	-0.298057609	1.4	1.54711713	1.632	1.174	1.167277	-0.241625119
20:80 CPH:SA 4% DOX	0.583	0.365	0.367222585	0.261	0.332252575	1.3	2.01552003	1.632	1.174	1.167277	-0.241625119
20:80 CPH:SA 3% DOX	0.671	0.420	0.326643234	0.723	0.002551863	1.4	1.43303826	1.632	1.174	1.167277	-0.241625119
20:80 CPH:SA 2% DOX	0.585	0.349	0.366425325	1.260	-0.181692652	1.4	1.45906738	1.632	1.174	1.167277	-0.241625119
20:80 CPH:SA 1% DOX	0.224	-0.077	0.758146213	1.925	0.879167873	1.2	1.40816087	1.632	1.174	1.167277	-0.241625119
20:80 CPTEG:CPH 10% DOX	0.726	0.883	-0.76248944	-0.443	0.85201605	-0.6	-1.1500441	-0.68	-0.8	1.167277	-0.241625119
20:80 CPTEG:CPH 9% DOX	0.878	0.858	-0.77406313	-0.272	1.434810543	-0.8	0.13427868	-0.68	-0.8	1.167277	-0.241625119
20:80 CPTEG:CPH 8% DOX	0.826	0.757	-0.75240837	-0.643	1.068260928	-0.9	-0.567231	-0.68	-0.8	1.167277	-0.241625119
20:80 CPTEG:CPH 7% DOX	0.570	0.543	-0.69328637	-0.284	1.05759414	-0.9	-0.536776	-0.68	-0.8	1.167277	-0.241625119
20:80 CPTEG:CPH 6% DOX	0.145	0.060	-0.70589865	-0.118	1.317475878	-0.8	-0.8707359	-0.68	-0.8	1.167277	-0.241625119
20:80 CPTEG:CPH 5% DOX	0.470	0.357	-0.76212366	-0.422	1.074079176	-0.9	-0.7905163	-0.68	-0.8	1.167277	-0.241625119
20:80 CPTEG:CPH 4% DOX	0.363	0.280	-0.76700732	-0.299	0.962562759	-0.9	-1.2385971	-0.68	-0.8	1.167277	-0.241625119
20:80 CPTEG:CPH 3% DOX	-0.301	-0.340	-0.77406313	-0.560	1.048866769	-1.0	-1.6133331	-0.68	-0.8	1.167277	-0.241625119
20:80 CPTEG:CPH 2% DOX	-0.802	-0.757	-0.68882911	-0.702	0.332252575	-1.0	-1.1324789	-0.68	-0.8	1.167277	-0.241625119
20:80 CPTEG:CPH 1% DOX	-1.179	-1.210	-0.73185869	-0.113	1.045957645	-0.8	-0.6437825	-0.68	-0.8	1.167277	-0.241625119
20:80 CPH:SA 10% RIF	-0.852	-0.678	1.740805149	-1.324	-0.026539376	0.8	0.3643963	1.632	1.174	-0.66354	-0.207450955
20:80 CPH:SA 9% RIF	-0.825	-0.464	1.289957248	-1.299	-0.036236456	1.2	2.0347684	1.632	1.174	-0.66354	-0.207450955
20:80 CPH:SA 8% RIF	-1.187	-1.407	2.739115341	-1.372	-0.608364162	1.5	1.31662712	1.632	1.174	-0.66354	-0.207450955
20:80 CPH:SA 7% RIF	-0.845	-0.482	1.246891117	-1.187	0.012248943	1.5	1.84579016	1.632	1.174	-0.66354	-0.207450955
20:80 CPH:SA 6% RIF	-1.170	-1.417	2.76525308	-1.299	-0.104116014	1.4	0.40229543	1.632	1.174	-0.66354	-0.207450955
20:80 CPH:SA 5% RIF	-1.114	-1.286	2.649722729	-1.244	-0.705334959	1.5	0.80259871	1.632	1.174	-0.66354	-0.207450955
20:80 CPH:SA 4% RIF	-1.405	-1.753	2.450839151	-1.211	-0.026539376	1.6	0.93495577	1.632	1.174	-0.66354	-0.207450955
20:80 CPH:SA 3% RIF	-1.543	-1.810	2.841627302	-1.086	-0.346543008	1.7	0.51280454	1.632	1.174	-0.66354	-0.207450955
20:80 CPH:SA 2% RIF	-1.761	-2.185	2.319544683	-1.071	-0.715032039	1.1	1.06013267	1.632	1.174	-0.66354	-0.207450955
20:80 CPH:SA 1% RIF	-2.087	-2.599	2.475316219	-0.631	-0.588970002	1.3	1.91322802	1.632	1.174	-0.66354	-0.207450955
20:80 CPTEG:CPH 10% RIF	-0.259	-0.044	-0.17214289	0.590	0.167402219	-0.8	-1.0297088	-0.68	-0.8	-0.66354	-0.207450955
20:80 CPTEG:CPH 9% RIF	-0.407	-0.227	-0.06317719	0.277	-0.239875131	-0.8	-1.0931363	-0.68	-0.8	-0.66354	-0.207450955
20:80 CPTEG:CPH 8% RIF	-0.141	0.013	0.139866018	0.925	0.694923358	-1.0	-1.4574022	-0.68	-0.8	-0.66354	-0.207450955
20:80 CPTEG:CPH 7% RIF	-0.721	-0.252	0.157276246	0.423	-0.724729119	-0.9	0.20057743	-0.68	-0.8	-0.66354	-0.207450955
20:80 CPTEG:CPH 6% RIF	-0.783	-0.458	0.362893362	0.910	-1.946561168	-0.9	-1.4950025	-0.68	-0.8	-0.66354	-0.207450955
20:80 CPTEG:CPH 5% RIF	-0.917	-0.321	0.416526836	1.174	-0.462907965	-0.9	-1.552475	-0.68	-0.8	-0.66354	-0.207450955
20:80 CPTEG:CPH 4% RIF	-0.163	-0.066	-0.16352351	0.958	-0.608364162	-0.8	-0.5105371	-0.71	-0.84	-0.66354	-0.207450955
20:80 CPTEG:CPH 3% RIF	-0.673	0.173	-0.03705928	2.385	-0.850791155	-0.9	-0.8002944	-0.68	-0.8	-0.66354	-0.207450955
20:80 CPTEG:CPH 2% RIF	-0.811	0.242	-0.03714627	4.054	-0.491999204	-0.9	-0.6641587	-0.68	-0.8	-0.66354	-0.207450955
20:80 CPTEG:CPH 1% RIF	-1.462	0.071	-0.61330646	2.500	-0.996247352	-0.8	-0.817244	-0.68	-0.8	-0.66354	-0.207450955
10:90 CPTEG:CPH 10% RIF	-0.351	0.074	0.413335551	0.529	0.946077723	-0.8	0.36996134	-0.58	-0.64	-0.66354	-0.207450955
20:80 CPTEG:CPH 10% RIF	0.040	0.200	0.153999224	0.802	1.499780977	-0.9	-0.5591065	-0.68	-0.8	-0.66354	-0.207450955
30:70 CPTEG:CPH 10% RIF	0.388	0.475	-0.4481303	0.410	0.915047068	-0.8	-0.3342888	-0.52	-0.52	-0.66354	-0.207450955
50:50 CPTEG:CPH 10% RIF	0.806	0.726	-0.72916535	0.240	0.380737974	-1.0	-1.4148327	-0.72	-0.83	-0.66354	-0.207450955
10:90 CPTEG:CPH 10% RIF	-0.294	0.069	-0.03942957	0.962	0.380737974	-0.7	-0.9972053	-0.58	-0.64	-0.66354	-0.207450955
20:80 CPTEG:CPH 10% RIF	-0.016	0.123	-0.36813176	1.007	0.148008059	-0.8	-0.6813224	-0.68	-0.8	-0.66354	-0.207450955
30:70 CPTEG:CPH 10% RIF	0.317	0.430	-0.46769388	1.067	0.762802916	-0.7	0.69764198	-0.52	-0.52	-0.66354	-0.207450955
50:50 CPTEG:CPH 10% RIF	0.669	0.656	-0.68258294	0.684	-0.113813094	-0.8	-0.6849813	-0.72	-0.83	-0.66354	-0.207450955

The data were normalized and mean-centered.

Supporting Table 4.3 Principal component analysis raw input data

	Drug Release Properties			Particle Properties							Particle Chemistry			Drug Chemistry							Drugbank Experimental Data										
Formulation	EE	FR (2h)	FR (24h)	zeta potential	diameter	PDI	Water Contact Angle	DOP	Mn	Tg	Backbone O	Aliphatic C	Aromatic C	%C (drug)	%H (drug)	%Cl (drug)	%N (drug)	%O (drug)	Molar mass	Trn (drug)	Water Solubility	logP	pKa (strongest acid)	pKa (strongest base)	physiological charge	hydrogen acceptor count	hydrogen donor count	polar surface area	rotatable bond count	refractivity	polarizability	number of rings
20:80 CPH:SA 5% DOX	0.649	0.878	0.921	-24.2	295.0	0.116064378	50	29.34	15385	61.77	0.4	7.6	2.4	0.392857143	0.428571429	0	0.035714286	0.142857143	444.43	201	630	-0.02	-2.2	7.75	-1	9	6	181.62	2	113.89	42.88	4
20:80 CPH:SA 10% DOX	0.451	0.878	0.928	-19.9	290.2	0.094449098	50	29.34	15385	61.77	0.4	7.6	2.4	0.392857143	0.428571429	0	0.035714286	0.142857143	444.43	201	630	-0.02	-2.2	7.75	-1	9	6	181.62	2	113.89	42.88	4
20:80 CPTEG:CPH 5% DOX	0.663	0.810	0.816	16.1	187.0	0.130941533	45	16.69	5902	37.81	2.4	6.0	12.0	0.392857143	0.428571429	0	0.035714286	0.142857143	444.43	201	630	-0.02	-2.2	7.75	-1	9	6	181.62	2	113.89	42.88	4
20:80 CPTEG:CPH 10% DOX	0.519	0.861	0.871	10.8	198.0	0.094108949	45	16.69	5902	37.81	2.4	6.0	12.0	0.392857143	0.428571429	0	0.035714286	0.142857143	444.43	201	630	-0.02	-2.2	7.75	-1	9	6	181.62	2	113.89	42.88	4
20:80 CPH:SA 5% DOX	0.493	0.821	0.882	-24.2	295.0	0.116064378	50	29.34	15385	61.77	0.4	7.6	2.4	0.392857143	0.428571429	0	0.035714286	0.142857143	444.43	201	630	-0.02	-2.2	7.75	-1	9	6	181.62	2	113.89	42.88	4
20:80 CPH:SA 10% DOX	0.349	0.870	0.926	-19.9	290.2	0.094449098	50	29.34	15385	61.77	0.4	7.6	2.4	0.392857143	0.428571429	0	0.035714286	0.142857143	444.43	201	630	-0.02	-2.2	7.75	-1	9	6	181.62	2	113.89	42.88	4
20:80 CPTEG:CPH 5% DOX	0.589	0.752	0.778	-14	188.8	0.11068015	45	16.69	5902	37.81	2.4	6.0	12.0	0.392857143	0.428571429	0	0.035714286	0.142857143	444.43	201	630	-0.02	-2.2	7.75	-1	9	6	181.62	2	113.89	42.88	4
20:80 CPTEG:CPH 10% DOX	0.415	0.798	0.827	10.8	198.0	0.094108949	45	16.69	5902	37.81	2.4	6.0	12.0	0.392857143	0.428571429	0	0.035714286	0.142857143	444.43	201	630	-0.02	-2.2	7.75	-1	9	6	181.62	2	113.89	42.88	4
20:80 CPH:SA 5% RIF	0.267	0.355	0.669	-21.2	326.8	0.129993524	50	29.34	15385	61.77	0.4	7.6	2.4	0.367521368	0.495726496	0	0.034188034	0.102564103	822.94	183	1400	2.7	6.9	7.53	1	14	6	220.15	5	225.58	86.46	5
20:80 CPTEG:CPH 5% RIF	0.613	0.622	0.762	-32.4	183.3	0.126282599	45	16.69	5902	37.81	2.4	6.0	12.0	0.367521368	0.495726496	0	0.034188034	0.102564103	822.94	183	1400	2.7	6.9	7.53	1	14	6	220.15	5	225.58	86.46	5
20:80 CPH:SA 5% RIF	0.385	0.315	0.721	-21.2	326.8	0.129993524	50	29.34	15385	61.77	0.4	7.6	2.4	0.367521368	0.495726496	0	0.034188034	0.102564103	822.94	183	1400	2.7	6.9	7.53	1	14	6	220.15	5	225.58	86.46	5
20:80 CPTEG:CPH 5% RIF	1.127	0.665	0.855	-13.9	164.8	0.107655559	45	16.69	5902	37.81	2.4	6.0	12.0	0.367521368	0.495726496	0	0.034188034	0.102564103	822.94	183	1400	2.7	6.9	7.53	1	14	6	220.15	5	225.58	86.46	5
20:80 CPH:SA 20% CAM	0.654	0.866	0.907	-28.8	330.1	0.096456771	50	29.34	15385	61.77	0.4	7.6	2.4	0.34375	0.375	0.0625	0.0625	0.15625	323.132	171	2500	1.14	7.49	-2.8	0	5	3	115.38	6	73.2	28.08	1
20:80 CPTEG:CPH 20% CAM	1.235	0.766	0.782	-36.5	177.3	0.108201732	45	16.69	5902	37.81	2.4	6.0	12.0	0.34375	0.375	0.0625	0.0625	0.15625	323.132	171	2500	1.14	7.49	-2.8	0	5	3	115.38	6	73.2	28.08	1
20:80 CPTEG:CPH 20% CAM	1.117	0.821	0.838	-36.5	177.3	0.108201732	45	16.69	5902	37.81	2.4	6.0	12.0	0.34375	0.375	0.0625	0.0625	0.15625	323.132	171	2500	1.14	7.49	-2.8	0	5	3	115.38	6	73.2	28.08	1
20:80 CPH:SA 20% CAM	0.598	0.886	0.927	-28.8	330.1	0.096456771	50	29.34	15385	61.77	0.4	7.6	2.4	0.34375	0.375	0.0625	0.0625	0.15625	323.132	171	2500	1.14	7.49	-2.8	0	5	3	115.38	6	73.2	28.08	1
20:80 CPH:SA 5% PZA	0.493	0.171	0.276	-21.5	282.3	0.119658483	50	29.34	15385	61.77	0.4	7.6	2.4	0.357142857	0.357142857	0	0.214285714	0.071428571	123.113	192	1.50E+04	-0.6	13.06	-0.68	0	3	1	68.87	1	30.45	11.13	1
20:80 CPTEG:CPH 5% PZA	0.897	0.057	0.086	-24.1	216.3	0.107692057	45	16.69	5902	37.81	2.4	6.0	12.0	0.357142857	0.357142857	0	0.214285714	0.071428571	123.113	192	1.50E+04	-0.6	13.06	-0.68	0	3	1	68.87	1	30.45	11.13	1
20:80 CPH:SA 5% PZA	0.349	0.298	0.449	-32.8	317.7	0.094660637	50	29.34	15385	61.77	0.4	7.6	2.4	0.357142857	0.357142857	0	0.214285714	0.071428571	123.113	192	1.50E+04	-0.6	13.06	-0.68	0	3	1	68.87	1	30.45	11.13	1
20:80 CPTEG:CPH 5% PZA	1.169	0.268	0.313	-35.1	181.5	0.123033948	45	18.47	6499	33.8	2.4	6.0	12.0	0.357142857	0.357142857	0	0.214285714	0.071428571	123.113	192	1.50E+04	-0.6	13.06	-0.68	0	3	1	68.87	1	30.45	11.13	1
20:80 CPH:SA 10% DOX	0.410	0.843	0.856	-16.4	300.1	0.142381954	50	66.18	14715	58.44	0.4	7.6	2.4	0.392857143	0.428571429	0	0.035714286	0.142857143	444.43	201	630	-0.02	-2.2	7.75	-1	9	6	181.62	2	113.89	42.88	4
20:80 CPH:SA 9% DOX	0.516	0.876	0.885	-10.4	302.3	0.155987848	50	66.18	14715	58.44	0.4	7.6	2.4	0.392857143	0.428571429	0	0.035714286	0.142857143	444.43	201	630	-0.02	-2.2	7.75	-1	9	6	181.62	2	113.89	42.88	4
20:80 CPH:SA 8% DOX	0.656	0.785	0.822	-7.46	329.0	0.133939982	50	66.18	14715	58.44	0.4	7.6	2.4	0.392857143	0.428571429	0	0.035714286	0.142857143	444.43	201	630	-0.02	-2.2	7.75	-1	9	6	181.62	2	113.89	42.88	4
20:80 CPH:SA 7% DOX	0.686	0.823	0.860	-19.3	352.0	0.148810296	50	66.18	14715	58.44	0.4	7.6	2.4	0.392857143	0.428571429	0	0.035714286	0.142857143	444.43	201	630	-0.02	-2.2	7.75	-1	9	6	181.62	2	113.89	42.88	4
20:80 CPH:SA 6% DOX	0.768	0.829	0.855	-14.7	343.2	0.144152552	50	66.18	14715	58.44	0.4	7.6	2.4	0.392857143	0.428571429	0	0.035714286	0.142857143	444.43	201	630	-0.02	-2.2	7.75	-1	9	6	181.62	2	113.89	42.88	4
20:80 CPH:SA 5% DOX	0.895	0.865	0.882	-20.1	346.3	0.146335858	50	66.18	14715	58.44	0.4	7.6	2.4	0.392857143	0.428571429	0	0.035714286	0.142857143	444.43	201	630	-0.02	-2.2	7.75	-1	9	6	181.62	2	113.89	42.88	4
20:80 CPH:SA 4% DOX	0.876	0.763	0.795	-13.6	337.2	0.156202331	50	66.18	14715	58.44	0.4	7.6	2.4	0.392857143	0.428571429	0	0.035714286	0.142857143	444.43	201	630	-0.02	-2.2	7.75	-1	9	6	181.62	2	113.89	42.88	4
20:80 CPH:SA 3% DOX	1.074	0.785	0.807	-17	344.8	0.143932892	50	66.18	14715	58.44	0.4	7.6	2.4	0.392857143	0.428571429	0	0.035714286	0.142857143	444.43	201	630	-0.02	-2.2	7.75	-1	9	6	181.62	2	113.89	42.88	4
20:80 CPH:SA 2% DOX	1.305	0.764	0.792	-18.9	342.4	0.144481171	50	66.18	14715	58.44	0.4	7.6	2.4	0.392857143	0.428571429	0	0.035714286	0.142857143	444.43	201	630	-0.02	-2.2	7.75	-1	9	6	181.62	2	113.89	42.88	4
20:80 CPH:SA 1% DOX	1.590	0.675	0.702	-7.96	324.5	0.143408873	50	66.18	14715	58.44	0.4	7.6	2.4	0.392857143	0.428571429	0	0.035714286	0.142857143	444.43	201	630	-0.02	-2.2	7.75	-1	9	6	181.62	2	113.89	42.88	4
20:80 CPTEG:CPH 10% DOX	0.574	0.799	0.905	-8.24	188.8	0.089522654	45	17.71	6230	42.35	2.4	6.0	12.0	0.392857143	0.428571429	0	0.035714286	0.142857143	444.43	201	630	-0.02	-2.2	7.75	-1	9	6	181.62	2	113.89	42.88	4
20:80 CPTEG:CPH 9% DOX	0.647	0.836	0.900	-2.23	175.3	0.116575724	45	17.71	6230	42.35	2.4	6.0	12.0	0.392857143	0.428571429	0	0.035714286	0.142857143	444.43	201	630	-0.02	-2.2	7.75	-1	9	6	181.62	2	113.89	42.88	4
20:80 CPTEG:CPH 8% DOX	0.488	0.823	0.878	-6.01	163.3	0.101799071	45	17.71	6230	42.35	2.4	6.0	12.0	0.392857143	0.428571429	0	0.035714286	0.142857143	444.43	201	630	-0.02	-2.2	7.75	-1	9	6	181.62	2	113.89	42.88	4
20:80 CPTEG:CPH 7% DOX	0.642	0.760	0.833	-6.12	165.0	0.102440578	45	17.71	6230	42.35	2.4	6.0	12.0	0.392857143	0.428571429	0	0.035714286	0.142857143	444.43	201	630	-0.02	-2.2	7.75	-1	9	6	181.62	2	113.89	42.88	4
20:80 CPTEG:CPH 6% DOX	0.714	0.656	0.731	-3.44	177.3	0.095406021	45	17.71	6230	42.35	2.4	6.0	12.0	0.392857143	0.428571429	0	0.035714286	0.142857143	444.43	201	630	-0.02	-2.2	7.75	-1	9	6	181.62	2	113.89	42.88	4
20:80 CPTEG:CPH 5% DOX	0.583	0.736	0.794	-5.95	167.3	0.097095773	45	17.71	6230	42.35	2.4	6.0	12.0	0.392857143	0.428571429	0	0.035714286	0.142857143	444.43	201	630	-0.02	-2.2	7.75	-1	9	6	181.62	2	113.89	42.88	4
20:80 CPTEG:CPH 4% DOX	0.636	0.709	0.777	-7.1	163.3	0.087657365	45	17.71	6230	42.35	2.4	6.0	12.0	0.392857143	0.428571429	0	0.035714286	0.142857143	444.43	201	630	-0.02	-2.2	7.75	-1	9	6	181.62	2	113.89	42.88	4
20:80 CPTEG:CPH 3% DOX	0.524	0.546	0.646	-6.21	157.5	0.079763899	45	17.71	6230	42.35	2.4	6.0	12.0	0.392857143	0.428571429	0	0.035714286	0.142857143	444.43	201	630	-0.02	-2.2	7.75	-1	9	6	181.62	2	113.89	42.88	4
20:80 CPTEG:CPH 2% DOX	0.463	0.422	0.558	-13.6	157.5	0.089892648	45	17.71	6230	42.35	2.4	6.0	12.0	0.392857143	0.428571429	0	0.035714286	0.142857143	444.43	201	630	-0.02	-2.2	7.75	-1	9	6	181.62	2	113.89	42.88	4
20:80 CPTEG:CPH 1% DOX	0.716	0.329	0.462	-6.24	171.3	0.100186585	45	17.71	6230	42.35	2.4	6.0	12.0	0.392857143	0.428571429	0	0.035714286	0.142857143	444.43	201	630	-0.02	-2.2	7.75	-1	9	6	181.62	2	113.89	42.88	4
20:80 CPH:SA 10% RIF	0.196	0.410	0.574	-17.3	298.3	0.121422938	50	66.18	14715	58.44	0.4	7.6	2.4	0.367521368	0.495726496	0	0.034188034	0.102564103	822.94	183	1400	2.7	6.9	7.53	1	14	6	220.15	5	225.58	86.46	5
20:80 CPH:SA 9% RIF	0.207	0.417	0.620	-17.4	329.0	0.15660778	50	66.18	14715	58.44	0.4	7.6	2.4	0.367521368	0.495726496	0	0.034188034	0.102564103	822.94	183	1400	2.7	6.9	7.53	1	14	6	220.15	5	225.58	86.46	5
20:80 CPH:SA 8% RIF	0.176	0.327	0.420	-23.3	351.9	0.141480799	50	66.18	14715	58.44	0.4	7.6	2.4	0.367521368	0.495726496	0	0.034188034	0.102564103	822.94	183	1400	2.7	6.9	7.53	1	14	6	220.15	5	225.58	86.46	5
20:80 CPH:SA 7% RIF	0.255	0.412	0.616	-16.9	352.6	0.152627129	50	66.18	14715	58.44	0.4	7.6	2.4	0.367521368	0.495726496	0	0.034188034	0.102564103	822.94	183	1400	2.7	6.9	7.53	1	14	6	220.15	5	225.58	86.46	5
20:80 CPH:SA 6% RIF	0.207	0.332	0.418	-18.1	345.2	0.122221248	50	66.18	14715	58.44	0.4	7.6	2.4	0.367521368	0.495726496	0	0.034188034	0.102564103	822.94	183	1400	2.7	6.9	7.53	1	14	6	220.15	5	225.58	86.46	5
20:80 CPH:SA 5% RIF	0.230	0.345	0.446	-24.3	350.0	0.130653266	50	66.18	14715	58.44	0.4	7.6	2.4	0.367521368	0.495726496	0	0.034188034	0.102564103	822.94	183	1400	2.7	6.9	7.53	1	14	6	220.15	5	225.58	86.46	5
20:80 CPH:SA 4% RIF	0.245	0.274	0.347	-17.3	359.5	0.133441245	50	66.18	14715	58.44	0.4	7.6	2.4	0.367521368	0.495726496	0	0.034188034	0.102564103	822.94	183	1400	2.7	6.9	7.53	1	14	6	220.15	5	225.58	86.46	5
20:80 CPH:SA 3% RIF	0.298	0.240	0.335	-20.6	366.7	0.12454902	50	66.18	14715	58.44	0.4	7.6	2.4	0.367521368	0.495726496	0	0.034188034	0.102564103	822.94	183	1400	2.7	6.9	7.53	1	14	6	220.15	5	225.58	86.46	5
20:80 CPH:SA 2% RIF	0.305	0.186	0.255	-24.4	317.3	0.136077981	50	66.18	14715	58.44	0.4	7.6	2.4	0.367521368	0.495726496	0	0.034188034	0.102564103	822.94	183	1400	2.7	6.9	7.53	1	14	6	220.15	5	225.58	86.46	5
20:80 CPH:SA 1% RIF	0.493	0.106	0.168	-23.1	338.3	0.154047645	50	66.18	14715	58.44	0.4	7.6	2.4	0.367521368	0.495726496	0	0.034188034	0.102564103	822.94	183	1400	2.7	6.9	7.53	1	14	6	220.15	5	225.58	86.46	5
20:80 CPTEG:CPH 10% RIF	1.017	0.556	0.709	-15.3	171.8	0.092057405	45	17.71	6230	42.35	2.4	6.0	12.0	0.367521368	0.495726496	0	0.034188034	0.102564103	822.94	183	1400	2.7	6.9	7.53	1	14	6	220.15	5	225.58	86.46	5
20:80 CPTEG:CPH 9% RIF	0.883	0.520	0.670	-19.5	173.3	0.090721364	45	17.71	6230	42.35	2.4	6.0	12.0	0.367521368	0.495726496	0	0.034188034	0.102564103	822.94	183	1400	2.7	6.9	7.53	1	14	6	220.15	5	225.58	86.46	5
20:80 CPTEG:CPH 8% RIF	1.161	0.585	0.721	-9.86	161.8	0.083048439	45	17.71	6230	42.35	2.4	6.0	12.0	0.367521368	0.495726496	0	0.034188034	0.102564103	822.94	183	1400	2.7	6.9	7.53	1	14	6	220.15	5	225.58	86.46	5
20:80 CPTEG:CPH 7% RIF	0.946	0.442	0.665	-24.5	168.5	0.117972246	45	17.71	6230	42.35	2.4	6.0	12.0	0.367521368	0.495726496	0	0.034188034	0.102564103	822.94	183	1400	2.7	6.9	7.53	1	14	6	220.15	5	225.58	86.46	5
20:80 CPTEG:CPH 6% RIF	1.155	0.427	0.621	-37.1	164.5	0.082256424	45	17.71	6230	42.35	2.4	6.0	12.0	0.367521368	0.495726496	0	0.034188034	0.102564103	822.94	183	1400	2.7	6.9	7.53	1	14	6	220.15	5	225.58	86.46	5
20:80 CPTEG:CPH 5% RIF	1.268	0.394	0.650	-21.8	168.0	0.081045819	45	17.71	6230	42.35	2.4	6.0	12.0	0.367521368	0.495726496	0	0.034188034	0.102564103	822.94	183	1400	2.7	6.9	7.53	1	14	6	220.15	5	225.58	86.46	5
20:80 CPTEG:CPH 4% RIF	1.175	0.580	0.704	-23.3	172.0	0.102993275	45	17.11	6052	37.17	2.4	6.0	12.0	0.367521368	0.495726496	0	0.034188034	0.102564103	822.94	183	1400	2.7	6.9	7.53	1	14	6	220.15	5	225.58	86.46	5
20:80 CPTEG:CPH 3% RIF	1.787	0.454	0.755	-25.8	169.5	0.096889806	45	17.71	6230	42.35	2.4	6.0	12.0	0.367521368	0.495726496	0	0.034188034	0.102564103	822.94	183	1400	2.7	6.9	7.53	1	14	6	220.15	5	225.58	86.46	5
20:80 CPTEG:CPH 2% RIF	2.503	0.420	0.769	-22.1	165.8	0.099757379	45	17.71	6230	42.35	2.4	6.0	12.0	0.367521368	0.495726496	0	0.034188034	0.102564103	822.94	183	1400	2.7	6.9	7.53	1	14	6	220.15	5	225.58	86.46	5
20:80 CPTEG:CPH 1% RIF	1.837	0.260	0.733	-27.3	174.5	0.096532778	45	17.71	6230	42.35	2.4	6.0	12.0	0.367521368	0.495726496	0	0.034188034	0.102564103	822.94	183	1400	2.7	6.9	7.53	1	14	6	220.15	5	225.58	86.46	5
10:90 CPTEG:CPH 10% RIF	0.991	0.533	0.734	-7.27	175.5	0.121540161	45	19.7	6894	37.49	2.2	6.0	12.0	0.367521368	0.495726496	0	0.034188034	0.102564103	822.94	183	1400	2.7	6.9	7.53	1	14	6	220.15	5	225.58	86.46	5
20:80 CPTEG:CPH 10% RIF	1.108	0.630	0.760	-1.56	162.8	0.101970206	45	17.67	6225	41.29	2.4	6.0	12.0	0.367521368	0.495726496	0	0.034188034	0.102564103	822.94	183	1400	2.7	6.9	7.53	1	14	6	220.15	5	225.58	86.46	5
30:70 CPTEG:CPH 10% RIF	0.940	0.715	0.819	-7.59	172.0	0.106705784	45	20.97	7412	35.03	2.6	6.0	12.0	0.367521368	0.495726496	0	0.034188034	0.102564103	822.94	183	1400	2.7	6.9	7.53	1	14	6	220.15	5	225.58	86.46	5
50:50 CPTEG:CPH 10% RIF	0.867	0.818	0.872	-13.1	160.3	0.083945126	45	16.89	6099	32.04	3	6.0	12.0	0.367521368	0.495726496	0	0.034188034	0.102564103	822.94	183	1400	2.7	6.9	7.53	1	14	6	220.15	5	225.58	86.46	5
10:90 CPTEG:CPH 10% RIF	1.177	0.547	0.733	-13.1	178.8	0.092742061	45	19.7	6894	37.49	2.2	6.0	12.0	0.367521368	0.495726496	0	0.034188034	0.102564103	822.94	183	1400	2.7	6.9	7.53	1	14	6	220.15	5	225.58	86.46	5
20:80 CPTEG:CPH 10% RIF	1.196	0.616	0.744	-15.5	175.3	0.099395842	45	17.67	6225	41.29	2.4	6.0	12.0	0.367521368	0.495726496	0	0.034188034	0.102564103	822.94	183	1400	2.7	6.9	7.53	1	14	6	220.15	5	225.58	86.46	5
30:70 CPTEG:CPH 10% RIF	1.222	0.698	0.809	-9.16	181.3	0.12844245	45	20.97	7412	35.03	2.6	6.0	12.0	0.367521368	0.495726496	0	0.034188034	0.102564103	822.94	183	1400	2.7	6.9	7.53	1	14	6	220.15	5	225.58	86.46	5
50:50 CPTEG:CPH 10% RIF	1.058	0.785	0.857	-18.2	177.0	0.099318771	45	16.89	6099	32.04	3	6.0	12.0	0.367521368	0.495726496	0	0.034188034	0.102564103	822.94	183	1400	2.7	6.9	7.53	1	14	6	220.15	5	225.58	86.46	5

Encapsulation efficiencies (EE) are formatted as fractions.

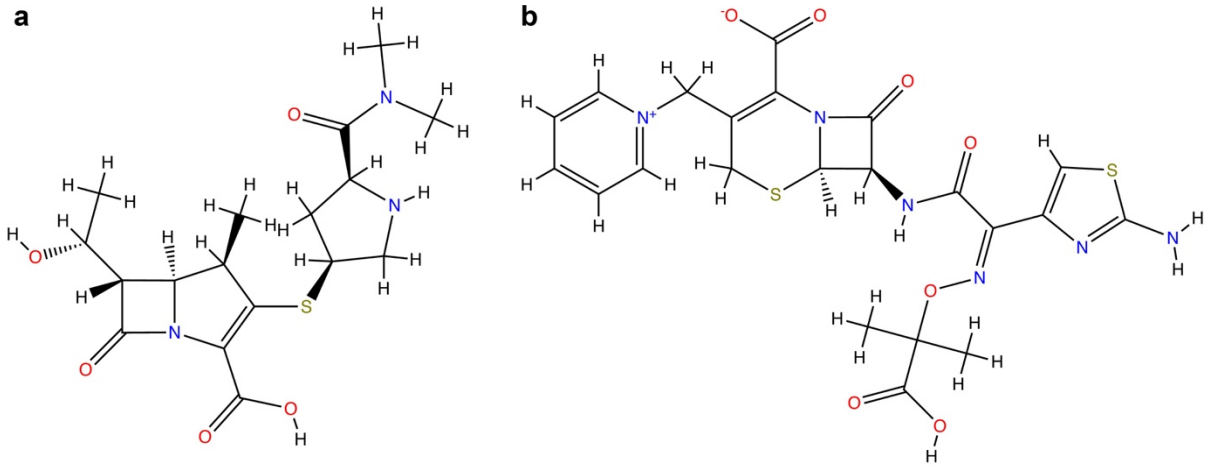

Supporting Figure 4.1 Chemical structures of antibiotics in model validation data set. Meropenem (MEM, a) and ceftazidime (CAZ, b) both contain sulfur atoms, which were not included in training data set.

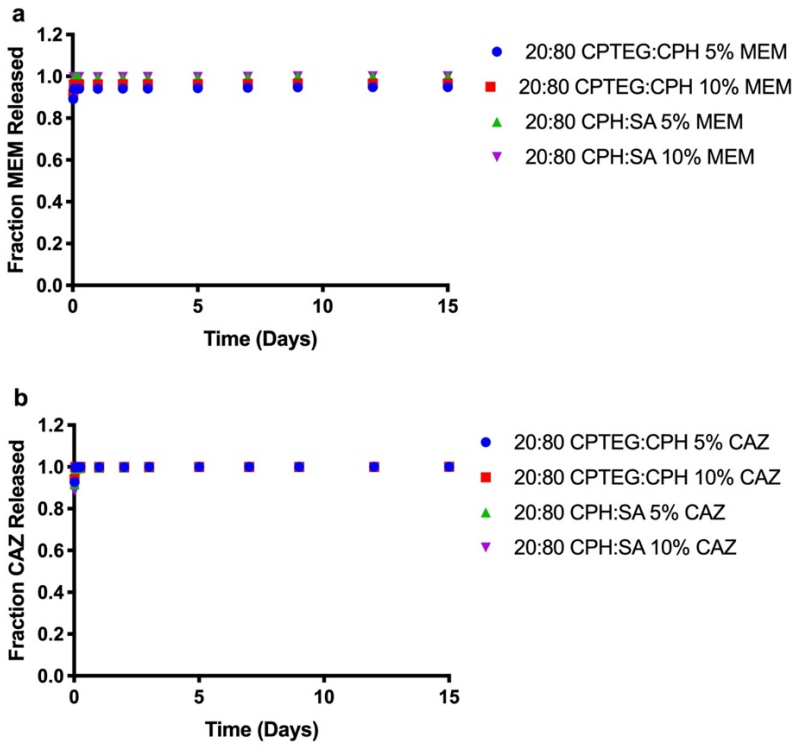

Supporting Figure 4.2 Release kinetics from nanoparticles encapsulating drugs not included in training data set. All formulations showed an extensive burst. Release property parameterization is shown in Table 4.3. Drug abbreviations: meropenem (MEM); ceftazidime (CAZ).

CHAPTER 5. HIGH-THROUGHPUT SYNTHESIS AND SCREENING OF RAPIDLY DEGRADING POLYANHYDRIDE NANOPARTICLES

A paper published in ACS Combinatorial Science, March 2020

*Adam S. Mullis, Sarah J. Jacobson, Balaji Narasimhan**

**Corresponding author*

AUTHOR ADDRESS

Department of Chemical and Biological Engineering and Nanovaccine Institute, Iowa State University, Ames, Iowa 50011, United States

KEYWORDS: polyanhydrides, high-throughput synthesis, drug delivery, nanoparticles, melting point depression, group contribution methods

5.1 Abstract

Combinatorial techniques can accelerate the discovery and development of polymeric nanodelivery devices by pairing high-throughput synthesis with rapid materials characterization. Biodegradable polyanhydrides demonstrate tunable release, high cellular internalization, and dose sparing properties when used as nanodelivery devices. This nanoparticle platform shows promising potential for small molecule drug delivery, but the pace of understanding and rational design of these nanomedicines is limited by the low throughput of conventional characterization. This study reports the use of a high-throughput method to synthesize libraries of a newly synthesized, rapidly-eroding polyanhydride copolymer based on 1,8-bis(*p*-carboxyphenoxy)-3,6-dioxaoctane (CPTEG) and sebacic acid (SA) monomers. The high-throughput method enabled efficient screening of copolymer microstructure, revealing weak block-type and alternating architectures. The high-throughput method was adapted to synthesize nanoparticle libraries encapsulating hydrophobic model

drugs. Drug release from these nanoparticles was rapid, with a majority of the payload released within three days. Drug release was dramatically slowed at acidic pH, which could be useful for oral drug delivery. Rhodamine B (RhoB) release kinetics generally followed patterns of polymer erosion kinetics, while Coomassie brilliant blue (CBB) released the fastest from the slowest degrading polymer chemistry and vice versa. These differences in trends between copolymer chemistry and release kinetics were hypothesized to arise from differences in mixing thermodynamics. A high-throughput method was developed to synthesize polymer-drug film libraries and characterize mixing thermodynamics by melting point depression. Rhodamine B had a negative χ for all copolymers tested, indicating a tendency toward miscibility. By contrast, Coomassie brilliant blue χ increased, eventually becoming positive, with increasing CPTEG content. This indicates an increasing tendency toward phase separation in CPTEG-rich copolymers. These *in vitro* results screening polymer-drug interactions showed good agreement with *in silico* predictions from Hansen solubility parameter estimation and were able to explain the observed differences in model drug release trends.

5.2 Introduction

Combinatorial and high-throughput screening of polymeric biomaterials is a burgeoning field. While early combinatorial approaches were successfully applied to drug discovery in the pharmaceutical industry, biomaterials pose several challenges for such approaches. Complex, interconnected relationships between molecular and bulk properties of materials and payloads and biological outcomes give rise to nonlinear behavior that is challenging to predict from first-principles.[1] As a result, recent years have seen an increased use of high-throughput experimentation to screen many polymer formulations in parallel.[2,3]

By pairing simultaneous synthesis of polymer libraries with material characterization techniques, combinatorial science has the potential to advance understanding and development of biomaterials much more rapidly than conventional methods. Key challenges to these "omics" approaches include the relatively small throughput of polymer screening (hundreds, at most, in parallel) relative to traditional drug screening experiments (millions of compounds), as well as the adaptation of computational and informatics tools to reveal underlying structure-property relations.[1]

While many combinatorial techniques have been applied to macro- and micro-scale polymeric devices, nanoparticle-based drug delivery devices have received less attention. Previous work from our and collaborators' laboratories has focused on combinatorial investigation of protein release,[4,5] protein stability,[6] biocompatibility,[7] and immune activation[8] of polyanhydride nanoparticles composed of sebacic acid (SA), 1,6-bis(*p*-carboxyphenoxy)hexane (CPH), and 1,8-bis(*p*-carboxyphenoxy)-3,6-dioxaoctane (CPTEG) monomers. An automated, high-throughput methodology was recently developed in our laboratory for synthesizing copolymer libraries, protein-encapsulating nanoparticle libraries, and surface-functionalized nanoparticle libraries, as well as validating through comparisons with conventionally synthesized polymers and nanoparticles.[9] Small molecule drug release from CPH:SA and CPTEG:CPH copolymer films and microparticles have been investigated conventionally.[10–12] Polyanhydride nanoparticles have also shown promising capabilities for delivery of small molecule drugs,[13–15] but the pace of understanding and rational design of these nanomedicines is limited by the low throughput of conventional methods. Additionally, newly synthesized polyanhydride copolymers, such as CPTEG:SA,[16] have limited supporting literature to guide understanding of their nano-scale drug delivery properties. These

CPTEG:SA copolymers are hypothesized to combine the favorable thermal properties of SA-rich polymers, such as high melting point (T_m), that enables room temperature nanoparticle synthesis and discrete nanoparticle morphology,[9] with the amphiphilicity, payload-stabilizing,[6] and high cellular internalization[15] properties of CPTEG-rich polymers. Furthermore, the relatively low hydrophobicity of these monomers is predicted to provide rapid polymer erosion, corresponding with faster release kinetics of encapsulated payloads from nanoparticles.

In this work, the high-throughput method developed in our laboratory was used to characterize the morphology of CPTEG:SA copolymer libraries. With this high-throughput method, CPTEG:SA nanoparticle libraries were synthesized to investigate the effect of varying copolymer composition on the release kinetics of model hydrophobic drugs. As release kinetics are known to be influenced by drug distribution in such particles,[10] a high-throughput film synthesis method was developed to test polymer-drug thermodynamic mixing interactions and illustrate the connectivity between copolymer chemistry, thermodynamic interactions, and drug release kinetics.

5.3 Experimental Methods

5.3.1 Materials

Sebacic acid was purchased from Sigma Aldrich (St. Louis, MO). Triethylene glycol was purchased from Sigma Aldrich for CPTEG monomer synthesis. Potassium carbonate, dimethyl formamide, toluene, acetonitrile, acetic acid, sulfuric acid, N,N-dimethylacetamide, and acetic anhydride was purchased from Fisher Scientific (Fairlawn, NJ) for monomer and polymer synthesis. 4-*p*-fluorobenzonitrile was purchased from Apollo Scientific (Cheshire, UK) for use in monomer synthesis. Nanoparticle synthesis utilized methylene chloride, chloroform, pentane, and hexanes from Fisher Scientific. Rhodamine B (RhoB) and

Coomassie brilliant blue G 250 (CBB) from Sigma Aldrich were used as model small molecule drugs. Deuterated chloroform was purchased from Cambridge Isotope Laboratories (Andover, MA) for ^{1}H NMR analysis. A custom-built Nanoprep 24 automated high-throughput robot (OMNI International, Kennesaw, GA) was used for polymer and nanoparticle library synthesis.

5.3.2 Polymer Library Synthesis

CPTEG monomer was synthesized as described previously (Supporting Figure 5.1).[17] Conventional CPTEG:SA copolymer was synthesized by acetylating CPTEG and SA monomers in excess acetic anhydride at 125°C for 30 min (Supporting Figure 5.2). Acetic anhydride was removed by rotary evaporation, and polymerization was carried out for one hour at 140°C and 0.2 torr. The polymer was dissolved in methylene chloride and precipitated in hexanes.[16] High-throughput synthesis of CPTEG:SA copolymer libraries was carried out with a protocol modified from that reported by Goodman et al. (Supporting Figure 5.2).[9] This method can produce up to 24 different polymers in parallel. Briefly, 15 mg/mL stocks of CPTEG and SA monomers in acetic anhydride were created, and monomers were acetylated at 125°C for 30 min. These acetylated monomer solutions were dispensed by the automated high-throughput robot into 10 mL glass test tubes (VWR International, Radnor, PA) at 100 mg per tube. The test tubes were transferred to a 180°C vacuum oven for copolymerization of the acetylated monomers. Polymer libraries were allowed to react between 5 and 10 h, starting after evaporation of acetic anhydride. Polymer libraries not intended for nanoparticle synthesis were dissolved in methylene chloride (7 mL per tube) and precipitated in hexanes in 50 mL conical tubes. The tubes were centrifuged, solvent was decanted, and the purified polymers were dried by vacuum overnight to remove residual solvent. Throughout this work, libraries of 8 different copolymer compositions in triplicate or

6 different compositions in quadruplicate were prepared. Copolymer composition, molecular weight, and purity were confirmed using ^{1}H NMR spectra gathered from a Varian MR-400 (Varian, Inc. Palo Alto, CA). ^{1}H NMR spectra were used to calculate number-average sequence lengths following the methods described in Shen et al. and Ron et al.[12,18] Differential scanning calorimetry (DSC) was used for thermal characterization (Q2000, TA Instruments, New Castle, DE).

5.3.3 Tablet Erosion

Fourteen mm diameter, 1 mm thick tablets of approximately 200 mg were prepared from conventionally synthesized CPTEG:SA copolymers. Tablets were pressed for 10 min at 5000 lb pressure at a temperature above polymer melting point. Tablets were incubated in duplicate in glass vials with 20 mL phosphate buffer saline (PBS), pH 7.4 at 37°C with agitation at 100 rpm. Fifteen mL PBS was replaced with fresh PBS daily. At regular time intervals, buffer was removed and tablets were dried by vacuum. Mass loss of the tablets was monitored by gravimetry.

5.3.4 Nanoparticle Library Synthesis

Conventional nanoparticle synthesis from high-throughput polymer libraries was carried out to determine the optimal parameter space of copolymer composition and molecular weight. Nanoparticles were synthesized by flash nanoprecipitation as described previously.[16] Briefly, CPTEG:SA polymers were weighed and dissolved in methylene chloride at 25 mg/mL. The polymer solutions were quickly poured into a pentane bath at -10°C at a solvent:antisolvent ratio of 1:250 to precipitate nanoparticles. Nanoparticles were harvested via vacuum filtration.

High-throughput synthesis of CPTEG:SA nanoparticle libraries was carried out using a modified protocol from that reported by Goodman et al.[9] Methylene chloride solutions

containing appropriate concentrations of the model drugs, RhoB or CBB, were dispensed by the robot into polymer library test tubes to dissolve polymer at 20 mg/mL. Fifty mL centrifuge tubes were filled with 45 mL of hexanes chilled to -10°C and placed in the robot's stainless-steel rack, which had been chilled in a -80°C freezer and filled with dry ice. The robot sonicated each test tube at 30% amplitude for 30 s and transferred the contents to its corresponding 45 mL centrifuge tube with its stainless-steel pipet nozzle to precipitate nanoparticles. A solvent:anti-solvent ratio of 1:9 was found to be adequate for nanoprecipitation of sub-micron particles, while maintaining the 100 mg scale desired for characterization of small molecule drug-encapsulating nanoparticle libraries. The tubes were centrifuged, hexanes were decanted, and the nanoparticle-containing pellets were dried overnight in a vacuum oven. Scanning electron microscopy (SEM, FEI Quanta 250, Hillsboro, OR) was used to characterize nanoparticle dry powders. Average size distributions were calculated from SEM micrographs using Fiji image analysis software[19] and the ParticleSizer plugin script for Fiji,[20] using 200 nanoparticles per image. Zeta potentials of particle suspensions (0.25 mg/mL) were characterized on a ZetaSizer Nano (Malvern Panalytical, Malvern, UK).

5.3.5 Drug release kinetics

Nine to eleven mg RhoB- and CBB-loaded nanoparticles were placed in 1.5 mL microcentrifuge tubes, 0.5 mL PBS (pH 7.4) was added to each tube, and the nanoparticles were dispersed by sonication. The tubes were incubated at 37°C with agitation at 100 rpm. At regular time points, the nanoparticles were pelleted by centrifugation, supernatants were extracted, and fresh PBS was added to maintain sink conditions. At the conclusion of the release experiment, 40 mM sodium hydroxide was used to extract remaining encapsulated drug and this information was used to calculate the drug encapsulation efficiency, as

previously described.[21] RhoB and CBB release in acidic conditions were similarly assayed by incubating particles in 0.1 M acetate buffer, pH 4.3 for one week, followed by base extraction. Mass drug released was quantified via fluorescence (RhoB, λ_{ex} 553 nm, λ_{em} 627 nm) and absorbance (CBB, PBS and acetate buffer λ_{abs} 580 nm, NaOH λ_{abs} 590 nm) spectrophotometry (SpectraMax M3, Molecular Devices, San Jose, CA) in 96-well plates. Drug release kinetics are presented as a cumulative mass fraction, in which mass released is normalized by total mass encapsulated.

5.3.6 Polymer-drug interaction screening

The Fedors method[22,23] was used to estimate molar volume (**V**), cohesive energy density, and the solubility parameter (δ) for representative CPTEG:SA copolymers and model drugs. The Fedors method-derived molar volume and the Hoftyzer-Van Krevelen method[22] were used to estimate solubility parameter components resulting from dispersion forces, polar forces, and hydrogen bonding. Polymer-drug compatibility was then estimated from the difference between the solubility parameter components for two species:[22]

$$\Delta\delta = \left[\left(\delta_{d,1} - \delta_{d,2}\right)^2 + \left(\delta_{p,1} - \delta_{p,2}\right)^2 + \left(\delta_{h,1} - \delta_{h,2}\right)^2\right]^{1/2} \qquad (1)$$

In Eq. 1, d represents the dispersion forces, p the polar forces, and h the hydrogen bonding forces. Good solubility is predicted to occur at small Δδ, generally below 5 $(J/cm^3)^{1/2}$. A Flory-Huggins interaction parameter, χ_{FH}, can then be estimated using:

$$\chi_{FH} = \frac{V_{seg}(\Delta\delta)^2}{RT} \qquad (2)$$

In Eq. 2, V_{seg} is the volume of a mole of lattice sites, defined here as the molar volume of the SA monomer. R is the ideal gas constant and T is the temperature. The χ_{FH}

represents the enthalpic contribution to polymer-drug interactions and complete solubility occurs at $\chi_{FH} < 0.5$.[22]

Polymer-drug interaction was investigated using melting point depression studies of polymer-drug films. In these experiments, the model drugs were dissolved in methylene chloride and dispensed with the robot into polymer library test tubes. Solvent was evaporated under nitrogen, and the films were dried by vacuum and stored under desiccation prior to DSC analysis. The melting point depression that arises from polymer-drug mixing thermodynamics can be modeled by the equation:[24]

$$\frac{1}{T_m} - \frac{1}{T_{m0}} = \frac{R}{\Delta H}\frac{V_u}{V_1}(\phi - \chi\phi^2) \qquad (3)$$

In Eq. 3, ϕ is the volume fraction of the diluting drug, R is the ideal gas constant, V_u is the molar volume of the polymer repeat unit, and V_1 is the molar volume of the diluting drug. By plotting $1/T_m - 1/T_{m0}$ against ϕ and performing a quadratic least squares regression with a y-intercept of zero, a χ value was extracted from the second-degree term.

5.4 Results

5.4.1 Polymer Library Synthesis and Characterization

CPTEG:SA copolymers were synthesized with the high-throughput method and characterized by ^{1}H NMR spectroscopy and DSC (Figures 5.1, Supporting Table 5.3, Table 5.1). This method afforded tight control over copolymer composition and produced copolymers of high purity (Figure 5.1a, Table 5.1). Copolymers of greater than 40 mol% CPTEG were sticky and either had near-zero °C T_g or were thermally unstable (Supporting Figure 5.4). The T_m and crystallinity of the copolymer decreased as the CPTEG content increased (Figure 5.1b, Table 5.1). All copolymers included in the analysis had T_m's above 37°C. Copolymers with less than 25 mol% CPTEG did not display distinct T_g's. The more

amorphous 30:70 and 35:75 CPTEG:SA copolymers showed T_g's near 20-25°C. The molar composition, molecular weight, and thermal properties of the combinatorially-synthesized CPTEG:SA copolymers were consistent with those observed in conventionally synthesized polymers (Table 5.1).

Number-average sequence lengths of the CPTEG:SA copolymer library ranging in composition from 100% poly(CPTEG) to 100% poly(SA) were calculated using ^{1}H NMR spectra (Figure 5.2). For near-equimolar compositions of CPTEG and SA, copolymers displayed moderate sequence lengths for both CPTEG and SA (Figure 5.2a). This is indicative of an alternating copolymer sequence.[12] For compositions richer in either monomer, the majority component sequence length greatly increased while the minority component remained moderate. Such divergence in number-average sequence length indicates a weak block-like microstructure.[25] Following the same methodology, reactivity ratios were calculated for this library (Figure 5.2b). At compositions between 20:80 and 80:20 CPTEG:SA, the reactivity ratios for both components were near unity. This indicates a nearly equal tendency of a chain ending in SA to add another SA monomer versus a CPTEG monomer, and conversely so for a chain ending in CPTEG. For copolymer compositions rich in one component, the minority component reactivity ratio was elevated while the majority component remained near unity, suggesting an increased affinity for minority components to self-assemble into blocks. All copolymers in the library displayed a degree of randomness near two, indicating a nearly alternating copolymer structure.[18]

The high-throughput polymer synthesis methodology facilitated rapid screening of CPTEG:SA copolymers, as up to 24 polymers can be synthesized in parallel. In conventional polymer synthesis CPTEG and SA monomer must be weighed, acetylated, evaporated, and

reacted separately. By contrast, the high-throughput method requires a single stock solution of each acetylated diacid for the entire polymer library and enables simultaneous evaporation and reaction. The robot can be programmed to autonomously precipitate the resulting polymer in hexanes, and the purified polymer can be recovered by centrifugation for characterization. Additionally, polymer libraries were synthesized at much smaller mass scales (100 mg per formulation) relative to conventional polymer synthesis (>1-2 g per formulation). This reduced the material costs of screening individual polymer compositions, particularly for CPTEG monomer which is synthesized in-house. Additionally, 100 mg is the same mass scale used in conventional synthesis of nanoparticles encapsulating small molecule drugs,[26] whereas the previously published high-throughput polymer and nanoparticle synthesis protocol[9] used a 14 mg scale which is insufficient for small molecule efficacy assays (e.g. minimum inhibitory concentration for antibiotics). Synthesizing polymer libraries at the same scale as conventional nanoparticle synthesis could facilitate translation and scaleup of lead formulations. Finally, reacting the polymer in a heated vacuum oven improved the safety of polymer synthesis by mitigating the fire risks associated with oil baths.

5.4.2 Screening CPTEG:SA material properties.

Previous experiments suggested that CPTEG:SA copolymer films rich in SA degrade more rapidly than CPTEG-rich copolymers in unbuffered water.[16] To validate these results, CPTEG:SA tablet erosion was investigated in buffered conditions at physiological pH using conventionally synthesized polymers (Figure 5.3). Only semicrystalline copolymers (<30 mol% CPTEG) were pressed into tablets. CPTEG:SA copolymers eroded rapidly, losing approximately 50% of their mass within four days and >75% of their mass within 11 days. CPTEG:SA tablets showed similar erosion rates across chemistries, with 30:70 CPTEG:SA

showing slightly lower mass lost after 11 days. All CPTEG:SA copolymers eroded more rapidly than 20:80 CPH:SA. While statistically significant differences between CPTEG:SA chemistries were not observed, SA-rich chemistries tended to show higher percent erosion than CPTEG-rich chemistries after 11 days. Regardless, these results support the hypothesis that the semicrystalline CPTEG:SA copolymers degrade more rapidly than the more well-described and more hydrophobic CPH:SA copolymers.

To aid screening of nanomedicine formulations based on CPTEG:SA copolymers, the effect of polymer molecular weight on nanoparticle size and morphology was studied. Polymer libraries between 10:90 and 50:50 CPTEG:SA were synthesized with the high-throughput method, and the reaction time was varied. As described in Supporting Table 5.1, reaction times of 4, 5, 6, and 10 hours yielded mean (across compositions) number-average molecular weights of approximately 12, 13.5, 15, and 23 kDa. These polymer libraries were precipitated following the conventional nanoparticle synthesis method, and SEM was used to determine size distributions of the resulting particles (Supporting Table 5.1, Supporting Figure 5.5). For given reaction times, increasing CPTEG content generally corresponded with an increase in particle size. There was not a strong trend between reaction time and nanoparticle size within chemistries, however increasing reaction time corresponded with increasing aggregation of nanoparticles. 50:50 CPTEG:SA polymers did not result in nanoparticles at any reaction time tested, likely due to the tackiness of this chemistry. Polymer reacted for both 4 and 5 hours yielded nanoparticles for compositions between 10:90 and 30:70 CPTEG:SA. For these reaction times, SA-rich chemistries produced more discrete particles at 5 h than at 4 h reaction time. At the 6 h reaction time, only CPTEG:SA compositions between 10:90 and 20:80 CPTEG:SA formulations resulted in nanoparticles,

while 40:60 CPTEG:SA particles were highly aggregated. At the 10 h reaction time, only 10:90 and 20:80 CPTEG:SA compositions yielded recoverable particles, both of which were nanoparticles.

These results allowed a reduction of the screening space for the various CPTEG:SA compositions with respect to particle formation. The 5 h reaction time was chosen for ongoing experiments as it yielded the most-discrete, sub-micron particles at high yield for copolymer compositions up to 30:70 CPTEG:SA. Additionally, copolymer compositions below 40:60 CPTEG:SA were selected, because they consistently returned high yields and sub-micron particles.

5.4.3 Synthesis and characterization of model drug-encapsulating nanoparticle libraries

Previous work from our laboratories described the development of a high-throughput method to synthesize nanoparticle libraries with comparable properties to conventionally synthesized particles.[9] We adapted this method for CPTEG:SA copolymers, increasing the mass scale to improve yields and to enable a wider battery of tests to be performed on individual nanoparticle lots. Methylene chloride and chloroform were tested as polymer solvents, and pentane and hexanes at 4°C, -10°C, and -20°C were tested as anti-solvents (Supporting Figure 5.6). For all experiments, the polymer concentration in the solvent was kept constant at 20 mg/mL and the solvent:anti-solvent volume ratio was kept constant at 1:9. Optimal nanoparticle synthesis conditions were found using methylene chloride as the solvent and hexanes at -10°C as the antisolvent, precipitating the nanoparticles with the lowest melting point first.

SEM was used to image the nanoparticles and size distributions were calculated from the resulting micrographs (Figure 5.4, Table 5.2). The nanoparticles gradually increased in size with increasing CPTEG copolymer content, from count mean diameters of 272.3 nm for

5:95 CPTEG:SA to 482.3 nm for 30:70 CPTEG:SA. Smaller nanoparticles could likely be achieved by reducing the mass scale and increasing the solvent:anti-solvent ratio. These unloaded nanoparticles had negative zeta potentials between -37 and -46 mV, which is attributed to terminal carboxylic acid groups that form when polyanhydrides are exposed to water.

Two hydrophobic dyes, rhodamine B (RhoB) and Coomassie brilliant blue (CBB), were selected as model small molecular weight drugs to probe release kinetics from CPTEG:SA nanoparticles. RhoB has an ALGOPS-predicted logP of 2.37 and logS of -6.02, and CBB has a logP of 4.34 and logS of-7.42.[27] As these dyes have varying degrees of hydrophobicity, they were used to simultaneously probe the effects of polymer composition and drug chemistry on release kinetics. Polyanhydrides exhibit surface erosion, and drug distribution within a particle is known to influence release kinetics.[10] Given the hydrophobicity of polyanhydrides, it was hypothesized that the more hydrophobic drug (CBB) would achieve a more homogeneous distribution within nanoparticles than the less hydrophobic drug (RhoB). Both drugs were expected to exhibit erosion-controlled release, wherein faster eroding polymer compositions (lower CPTEG) provided faster release kinetics than slower eroding compositions. The hypothesized more homogeneous distribution of CBB within the particles was expected to yield a lower burst and slower release kinetics than RhoB.

Nanoparticle libraries encapsulating these compounds at 5% (w/w) were synthesized and analyzed via SEM to calculate size distributions (Table 5.2). As observed with the unloaded particle library, mean size of nanoparticles increased as CPTEG content increased. Encapsulating payloads also increased the size of the nanoparticles. Significant differences

($P<0.05$) in count mean diameter between the model drug-encapsulating particle libraries and their unloaded counterparts were observed for CBB in 10:90 CPTEG:SA, as well as for RhoB and CBB for 20:80 – 30:70 CPTEG:SA. RhoB nanoparticles had near-neutral zeta potentials, which deviated from the unloaded library (Table 5.2). CBB nanoparticles had zeta potentials close to those measured in the unloaded library.

The effect of polymer composition on *in vitro* drug release kinetics from these model drug-encapsulating nanoparticle libraries was investigated (Figure 5.5). All RhoB formulations yielded measured encapsulation efficiencies greater than 100% (Table 5.2) and between 73-82% mass yield. This apparent "over-encapsulation" is attributed to non-uniform losses of polymer and RhoB payload during nanoparticle synthesis. Polymer is typically lost during nanoprecipitation and filtration, whereas the RhoB may be preferentially localizing in the nanoparticles collecting in the filter cake. This would therefore result in an enrichment of RhoB in the collected nanoparticles, violating the assumption of uniform losses of polymer and payload typically employed in encapsulation efficiency calculations. To compensate for the shortcoming of this assumption, these encapsulation efficiency values are interpreted as 100%. SA-rich chemistries showed the highest burst and the quickest timescale of release (Figure 5.5a). Increasing CPTEG content reduced the burst and slowed the rate of RhoB release. All formulations released the majority of their payloads in three days, although detectable amounts of RhoB were observed throughout two weeks of sampling for all chemistries. RhoB release was consistent with previous polymer film erosion kinetics results.[16] This erosion-controlled release and high encapsulation efficiency likely indicates favorable mixing thermodynamic interactions between RhoB and the CPTEG:SA polymers tested.

In contrast, CBB formulations displayed lower encapsulation efficiencies, ranging from 35-60% (Table 5.2). The only pair that showed statistically significant differences ($P < 0.05$) in encapsulation efficiency were 5:95 and 25:75 CPTEG:SA, using Tukey's multiple comparisons test. Increasing CPTEG content had a moderate positive correlation with encapsulation efficiency. CBB formulations showed chemistry-dependent release, but with an opposite trend to that seen in rhodamine B (Figure 5.5b). SA-rich chemistries displayed the lowest burst and the longest timescale of release. Increasing CPTEG content tended to increase the burst and shorten the timescale of release. These observations contradicted our earlier hypothesis that CBB would show slower release and a lower burst than RhoB. Based on the lower encapsulation efficiency and inverse correlation between the CBB release and the polymer erosion data, we hypothesized that unfavorable polymer-CBB interactions may have impacted drug distribution within the nanoparticles.

Given the fast release rate provided by CPTEG:SA copolymers and the base-catalyzed degradation of polyanhydrides,[28] CPTEG:SA nanoparticles could have promise for oral drug delivery applications. To probe the release kinetics in acidic environments that approximately model gastrointestinal tract conditions, the RhoB and CBB nanoparticle libraries were incubated in acetate buffer pH 4.3 for three days (Figure 5.5c-d). All RhoB formulations showed a small burst (less than 20% of encapsulated drug) in the acetate buffer for three hours (Figure 5.5c). RhoB formulations gradually released their payloads over three days in acetate buffer, with SA-rich chemistries releasing more of their payload at faster rates than CPTEG-rich chemistries. CBB nanoparticles showed bursts between <1% and 40% of encapsulated drug in acidic conditions, with burst prevalence generally increasing with increasing CPTEG (Figure 5.5d). The only exception to this trend was the higher burst

observed in 25:75 CPTEG:SA than 30:70 CPTEG:SA. These particles released none to very little CBB after the initial burst. No formulation released its entire payload within three days in the acetate buffer.

The release profiles of both drugs showed similar trends with changing copolymer composition in acidic conditions compared to neutral pH. CBB had more variability in burst than RhoB, while RhoB had more variability in day 1-3 release than CBB. Release kinetics from all formulations were slowed at reduced pH, as expected from the base-catalyzed hydrolysis of polyanhydrides.

5.4.4 Screening polymer-model drug interactions

Group contribution methods were used to estimate solubility parameters of CPTEG:SA copolymers and model drugs for initial *in silico* screening of polymer and drug interactions (Table 5.3) and to test their relationships with copolymer chemistry and drug release kinetics. The Fedors method yielded δ values that increased as CPTEG content increased. The δ values for both model drugs and poly(CPTEG) were similar. Given the similarity in δ values for compounds tested, the Fedors method was not sufficient to explain differences in polymer-drug compatibility in this system. This necessitated the use of an alternative method, namely the Hoftyzer-Van Krevelen method.

The Hoftyzer-Van Krevelen method yielded a greater difference in drug δ values. Copolymers had greater δ_d than the model drugs, and δ_d increased with CPTEG content. RhoB had a greater δ_p than CBB, and δ_p stayed relatively constant across copolymer composition. The largest difference in drug δ components occurred in δ_h, where RhoB had a much greater δ_h than CBB. CPTEG:SA copolymers had δ_h values similar to RhoB, and δ_h increased as CPTEG content increased. Overall δ values were calculated from these

solubility parameter components. RhoB had a similar δ to all copolymer compositions tested, whereas CBB showed a greater similarity to poly(SA) than poly(CPTEG). Δδ values were calculated for polymer-drug pairs from Eq.1. Δδ analysis predicted solubility for both model drugs in all copolymers tested in the nanoparticle library, because all Δδ values were less than 5 $(J/cm^3)^{1/2}$. Solubility for both RhoB and CBB is predicted to decrease as CPTEG content increases. These Δδ values were used to predict χ_{FH} values using Eq. 2. These χ_{FH} parameters predicted complete RhoB solubility only in 5:95 CPTEG:SA and poly(SA). No polymer in the analysis was predicted to provide complete CBB solubility.

Melting point depression experiments were used to probe the thermodynamics of polymer-model drug mixing and to validate the results from group contribution methods (Figure 5.6). Polymer-model drug film libraries were synthesized and analyzed for T_m using DSC. RhoB produced a melting point depression effect for all CPTEG:SA copolymers tested (Figure 5.6a), wherein increasing volume fractions of the drug produced a larger magnitude of difference between the polymer-drug film (T_m) and the polymer control (T_{m0}). CBB produced a mild melting point depression effect for CPTEG:SA copolymers, with less than 7°C of suppression for all films (Figure 5.6b). The 15:85 CPTEG:SA-CBB films did not show a melting point depression effect.

The Flory-Huggins χ parameter values were extracted from these melting point depression data using Eq. 3 (Figure 5.6c-d, Table 5.4). RhoB had negative χ values for all copolymers except 30:70 CPTEG:SA, which is indicative of exothermic mixing interactions.[29] The positive χ values between 30:70 CPTEG:SA and RhoB is indicative of endothermic mixing. Copolymers with ≤10 mol% CPTEG, when mixed with CBB, had negative χ values. Copolymers with ≥20 mol% CPTEG, when mixed with CBB, had positive

χ values. The absence of a melting point depression effect in 15:85 CPTEG:SA-CBB films is indicative of a lack of mixing interactions or unfavorable mixing thermodynamics, which occurs at some sufficiently positive χ value.[29]

The high-throughput method was effectively integrated with the melting point depression analysis. Twenty-four different films could be autonomously dispensed from a combinatorially-synthesized copolymer library, a stock solution of drug in methylene chloride, and a diluting stream of methylene chloride. A multiplexed nitrogen evaporator allowed simultaneous drying of the films. Using this method, a library of polymer-drug films could be synthesized, dried, and prepared for DSC analysis within one day.

5.5 Discussion

Herein, we describe the value of a previously described automated high-throughput method to rapidly screen a newly discovered rapidly degrading polyanhydride copolymer system for its ability to serve as a carrier for drug delivery. The high-throughput method enabled rapid, simultaneous synthesis of multiple CPTEG:SA copolymers, which was validated by comparison with conventionally synthesized copolymers, as shown by the NMR and DSC data in Figure 5.1. This validation enables facile scaleup when lead formulations are identified. The high-throughput method yielded precise control over copolymer composition and molecular weight could be modified by altering reaction time (Table 5.1 & Supporting Table 5.1). Favorable thermal properties (e.g., T_m values that are higher than body temperature) with respect to processability and particle synthesis were identified for a subset of copolymers between 5:95 and 25:75 CPTEG:SA.

The copolymer microstructure is of interest for drug delivery because microphase separation can affect encapsulated drug distribution and drug release profiles.[12,30] Copolymer

sequence length analysis (Figure 5.2) indicated a weakly segregated block-like microstructure for CPTEG:SA copolymers, especially for copolymer compositions that are rich in one monomer. As the copolymer composition approached 50:50, the microstructure shifted toward an alternating architecture. These gradual changes in microstructure may be attributed to the differences in hydrophobicity between the amphiphilic CPTEG monomer and the weakly hydrophobic SA monomer.[12] The high throughput, tight control over composition, and small mass scale offered by the combinatorial method proved especially advantageous to analyze this microphase separation. A high-resolution library spanning a wide range of compositions was synthesized with comparable material and time demands to a single batch of conventionally-synthesized copolymer.

Understanding the degradation rate of biodegradable polymers is important for tailoring device drug release kinetics. Erosion of degradable polymers can be affected by composition, crystallinity, and local pH changes due to monomer dissolution.[17,31] To this end, only semicrystalline CPTEG:SA copolymers were investigated to avoid confounding variables arising from compounded versus melt-pressed tablets, and a 14:1 aspect ratio was used to ensure nearly one-dimensional erosion. CPTEG:SA copolymers tablets exhibited rapid erosion, losing approximately 50% mass in four days (Figure 5.3). This CPTEG:SA mass loss rate was much faster than the 20:80 CPH:SA tablets in the same geometry (Figure 5.3). Previous experiments in 10 mm diameter 20:80 CPH:SA tablets showed a 50% mass loss in less than two days,[12] which is attributed to the much smaller tablet aspect ratio than the tablets used herein. CPTEG:SA erosion was faster than CPTEG:CPH copolymers as well, which show half-lives on the order of six days to >one month in the 10 mm tablet

geometry.[17] CPTEG:SA polymer films have been shown to degrade faster in nanopure water than CPH:SA or CPTEG:CPH polymers,[16] supporting these results.

Polymer molecular weight influences viscosity and dissolution in solvents, and therefore can impact nanoparticle synthesis by nanoprecipitation. A 5 h reaction time for CPTEG:SA libraries, corresponding to M_n's between 12-15 kDa, was found to be optimal for conventional nanoparticle synthesis (Supporting Figure 5.5). The high-throughput methodology allowed rapid screening of copolymer properties, which aided the reduction in design space to copolymers containing <40 mol% CPTEG.

Drug delivery vehicles can improve the activity of hydrophobic drugs by increasing their bioavailability.[32] Poly(lactic-*co*-glycolic acid) nanoparticles have been used to improve the bioavailability and efficacy of the hydrophobic drug ivermectin, an antiparasitic used to treat lymphatic filariasis, which suffers from poor bioavailability in deep tissues.[33] Similarly, 20:80 CPTEG:CPH nanoparticles co-delivering ivermectin and the hydrophilic drug doxycycline achieved macrofilaricidal effects with 4000-fold less drug than soluble controls.[13] RhoB and CBB were used as two hydrophobic model drugs to test the CPTEG:SA copolymers' potential for controlled release. The high-throughput method was used to synthesize drug-encapsulating, sub-micron particle libraries at high encapsulation efficiency. The nanoparticle libraries demonstrated chemistry-dependent, controlled release capabilities over three days as shown in Figure 5.5. Drug release kinetics were slower in acidic environments, while maintaining chemistry dependence, consistent with the base-catalyzed degradation of polyanhydrides.[5,34]

The rapid release from CPTEG:SA nanoparticles adds a new tool in designing polyanhydride-based drug delivery devices, because conventional CPH:SA and CPTEG:CPH

nanoparticles release their payloads on the order of several weeks to several months.[5,35,36] Some biomedical applications, such as delivery of antimicrobial therapeutics to counter acute infections, may require release over shorter timescales, such as 3-5 days. Additionally, these CPTEG:SA nanoparticles could have competitive advantages for oral drug delivery. The gastric emptying half-life is approximately 1.2 hours,[37] so the small burst release at low pH could protect labile drugs like insulin[38] or protect the stomach from toxic drugs like cancer chemotherapeutics.[39] The mean small bowel residence time is approximately four hours[37] and the downstream colonic environment can be challenging for drug transport.[39] Rapid release at more neutral pH, such as that displayed by CPTEG:SA nanoparticles, could exploit the favorable conditions for bloodstream partitioning in the intestine (i.e., high surface area of absorptive tissue and microvasculature).[39] The high-throughput method aided rapid identification of nanoparticle properties by simultaneously synthesizing a two-dimensional nanoparticle library with varying copolymer chemistry and model drugs for encapsulation.

The relationship between copolymer chemistry and drug release is driven by thermodynamic interactions between the copolymer and model drug. In microphase-separated copolymers, drugs tend to partition into compatible microdomains until a saturation threshold is reached, after which they are forced to disperse into less favorable regions.[12] Differences in hydrophilicity of polyanhydride monomers result in different rates of erosion, so partitioning of the drug directly influences the rate of drug release. Unfavorable interactions between the drug and polymer can cause the drug to migrate to the surface, resulting in a more pronounced burst effect.[40] Based on the erosion-mediated release of RhoB, we predicted favorable mixing thermodynamics for RhoB and CPTEG:SA copolymers. In contrast, the counter-intuitive release trends for CBB suggested unfavorable

interactions between the CBB and CPTEG monomer, because increasing CPTEG content increased the rate of release and the prevalence of the burst.

Solubility parameter estimation by group contribution methods was used as a rapid screening tool to predict polymer-drug interactions and to test the hypotheses about mixing thermodynamics. Hildebrand solubility parameter predictions from the Fedors method are frequently used in the polymer literature, but rely on assumptions of no specific forces within the system.[22] Given the semicrystallinity of the CPTEG:SA copolymers, the presence of polar groups in the model drugs, and the possibility of hydrogen bonding between the model drugs and the copolymers, it is unsurprising that this method failed to explain the differences in drug release in the system.[23,41] In contrast, Hansen solubility parameter predictions from the Hoftyzer-Van Krevelen method take into account dispersion forces, polar forces, and hydrogen bonding.[22] This method captured more of the hypothesized differences in polymer-drug interactions between RhoB and CBB. Based on $\Delta\delta$ and χ_{FH} predictions, RhoB was expected to be more soluble in CPTEG:SA copolymers than CBB. This result matched observations in release kinetics, where RhoB exhibited erosion controlled release while CBB showed precipitation-mediated release (Figure 5.5). For both drugs, increasing CPTEG was expected to correlate with poorer drug solubility. This prediction agrees with the increasing burst with increasing CPTEG for CBB-encapsulating particles, but no such trend was observed for RhoB. It is possible that the difference between RhoB-CPTEG:SA and CBB-CPTEG:SA $\Delta\delta$ and χ_{FH} values are large enough to discriminate solubility and insolubility between the drugs in CPTEG-rich polymers, but the heuristics for solubility in the Hoftyzer-Van Krevelen method did not have predictive power for explaining release kinetics trends.

However, the Hoftyzer-Van Krevelen method could provide useful information for polyanhydride nanomedicine design by more clearly depicting contributions of dispersion forces, polar forces, and hydrogen bonding to polymer-drug compatibility. For example, CPTEG-rich chemistries may be more appropriate for payloads with high hydrogen bonding, whereas SA-rich chemistries may be more appropriate for those with more moderate hydrogen bonding. Neither homopolymer was predicted to have high polarity (as expected, based on their hydrophobicity), so stabilizers/excipients or alternate chemistries may be needed for highly polar payloads.

Melting point depression results (Figure 5.6) showed better agreement with release kinetics trends than group contribution analysis. RhoB showed a strong diluent effect within CPTEG:SA copolymers, corresponding with a negative χ and exothermic mixing for copolymers with compositions between 5:95-25:75 CPTEG:SA (Table 5.4). Negative χ values indicate strong adhesive interactions and a tendency toward miscibility.[29] CBB showed a milder diluent effect, producing χ values that were higher than those of RhoB for the given copolymer chemistries. Copolymers with ≥15 mol% CPTEG had positive χ values, which corresponds with endothermic mixing. Positive χ values indicate strong cohesive interactions and a tendency towards phase separation.[29] Mixing interactions between the copolymer and model drugs are driven by interactions between the drugs and individual monomers, as well as by the polymer architecture. The melting point depression-derived χ values for the model drugs went from negative to positive for copolymer compositions around 15:85-25:85 CPTEG:SA (Table 5.4). This region is predicted to represent a shift from weakly segregated block-like microstructure to an alternating copolymer system (Figure 5.2). Both drugs were predicted to be more soluble in SA-rich polymers than in CPTEG-rich

polymers by group contribution methods (Table 5.3). As the copolymer becomes more alternating in sequence, there are likely fewer and smaller SA-rich domains in the copolymer for the drugs to distribute into.[42] Therefore, there is likely a critical composition threshold wherein CPTEG-model drug interactions begin to drive drug precipitation out of the copolymer. As RhoB has less unfavorable interactions with CPTEG than CBB by $\Delta\delta$ analysis, it is predicted that RhoB would have a higher precipitation threshold than CBB. Indeed, this transition appears to occur between 25:75 and 30:70 CPTEG:SA for RhoB and between 10:90 and 15:85 CPTEG:SA for CBB. However, such a threshold would be expected to correspond with an increased burst, which was not observed for 30:70 CPTEG:SA RhoB particles.

These results have identified shortcomings in the current framework of using thermodynamic mixing relationships to explain release kinetics behavior from polyanhydride nanoparticles. It is possible that polymer-drug mixing kinetics during nanoparticle synthesis are different than those in thermal analysis experiments for polymer drug films. Additionally, microphase distribution within CPTEG:SA nanoparticles may be sufficiently different from polymer films to significantly alter drug localization, thereby affecting release kinetics. Given these shortcomings, the current framework still needs further development.

Overall, the high-throughput method was capable of rapidly synthesizing libraries of polymer-drug films, which facilitated screening for favorable interactions. Pairing *in silico* thermodynamic predictions with *in vitro* validation efficiently estimated polymer-drug mixing interactions, although their predictive power for release kinetics was limited. Altogether, the proposed framework can be useful in the rational design of nanomedicine formulations for drug delivery.

5.6 Conclusions

CPTEG:SA copolymers exhibit rapid, tunable erosion and interesting nanoparticle properties for drug delivery. The high-throughput methodology described in this work enabled efficient screening of bulk polymer properties with good agreement with conventionally synthesized polymers. This high-throughput method was used to synthesize and characterize the controlled small molecule drug release from CPTEG:SA nanoparticles, revealing chemistry-dependent effects. This recently discovered copolymer system demonstrates tunable release of hydrophobic model drugs at short timescales, which is slower in acidic conditions. The high-throughput method was adapted to synthesize polymer-drug films to screen for thermodynamic mixing interactions by melting point depression, which showed mixed agreement with predictions from group contribution methods. An important trend that these methods identified is that CBB is predicted to become increasingly insoluble in the copolymer as CPTEG content increases. This supports our hypothesis that the trends in release kinetics for CBB-loaded particles is driven by partitioning of CBB to the particle surface with increasing CPTEG. These methods were less capable of explaining RhoB release, as some methods predicted partial solubility while others predicted full solubility for a model drug that showed erosion-controlled release. These polymer-drug interaction screening data were able to explain trends in drug release from nanoparticle libraries.

5.7 References

(1) Groen, N.; Guvendiren, M.; Rabitz, H.; Welsh, W. J.; Kohn, J.; De Boer, J. Stepping into the Omics Era: Opportunities and Challenges for Biomaterials Science and Engineering. *Acta Biomater.* **2016**, *34*, 133–142. https://doi.org/10.1016/j.actbio.2016.02.015.

(2) Goldberg, M.; Mahon, K.; Anderson, D. Combinatorial and Rational Approaches to Polymer Synthesis for Medicine. *Adv. Drug Deliv. Rev.* **2008**, *60* (9), 971–978. https://doi.org/10.1016/j.addr.2008.02.005.

(3) Hook, A. L.; Anderson, D. G.; Langer, R.; Williams, P.; Davies, M. C.; Alexander, M. R. High Throughput Methods Applied in Biomaterial Development and Discovery. *Biomaterials* **2010**, *31* (2), 187–198. https://doi.org/10.1016/j.biomaterials.2009.09.037.

(4) Petersen, L. K.; Chavez-Santoscoy, A. V; Narasimhan, B. Combinatorial Synthesis of and High-Throughput Protein Release from Polymer Film and Nanoparticle Libraries. *J. Vis. Exp.* **2012**, No. 67, e3882. https://doi.org/10.3791/3882.

(5) Petersen, L. K.; Sackett, C. K.; Narasimhan, B. Novel, High Throughput Method to Study in Vitro Protein Release from Polymer Nanospheres. *J. Comb. Chem.* **2010**, *12* (1), 51–56. https://doi.org/10.1021/cc900116c.

(6) Petersen, L. K.; Sackett, C. K.; Narasimhan, B. High-Throughput Analysis of Protein Stability in Polyanhydride Nanoparticles. *Acta Biomater.* **2010**, *6* (10), 3873–3881. https://doi.org/10.1016/j.actbio.2010.04.004.

(7) Adler, A. F.; Petersen, L. K.; Wilson, J. H.; Torres, M. P.; Thorstenson, J. B.; Gardner, S. W.; Mallapragada, S. K.; Wannemuehler, M. J.; Narasimhan, B. High Throughput Cell-Based Screening of Biodegradable Polyanhydride Libraries. *Comb. Chem. High Throughput Screen.* **2009**, *12* (7), 634–645. https://doi.org/10.2174/138620709788923764.

(8) Petersen, L. K.; Xue, L.; Wannemuehler, M. J.; Rajan, K.; Narasimhan, B. The Simultaneous Effect of Polymer Chemistry and Device Geometry on the in Vitro Activation of Murine Dendritic Cells. *Biomaterials* **2009**, *30* (28), 5131–5142. https://doi.org/10.1016/j.biomaterials.2009.05.069.

(9) Goodman, J. T.; Mullis, A. S.; Dunshee, L.; Mitra, A.; Narasimhan, B. Automated High-Throughput Synthesis of Protein-Loaded Polyanhydride Nanoparticle Libraries. *ACS Comb. Sci.* **2018**, *20* (5), 298–307. https://doi.org/10.1021/acscombsci.8b00008.

(10) Berkland, C.; Kipper, M. J.; Narasimhan, B.; Kim, K.; Pack, D. W. Microsphere Size, Precipitation Kinetics and Drug Distribution Control Drug Release from Biodegradable Polyanhydride Microspheres. *J. Control. Release* **2004**, *94* (1), 129–141. https://doi.org/10.1016/j.jconrel.2003.09.011.

(11) Shen, E.; Pizsczek, R.; Dziadul, B.; Narasimhan, B. Microphase Separation in Bioerodible Copolymers for Drug Delivery. *Biomaterials* **2001**, *22* (3), 201–210. https://doi.org/10.1016/S0142-9612(00)00175-7.

(12) Shen, E.; Kipper, M. J.; Dziadul, B.; Lim, M.-K. M. K. M.-K.; Narasimhan, B. Mechanistic Relationships between Polymer Microstructure and Drug Release Kinetics in Bioerodible Polyanhydrides. *J. Control. Release* **2002**, *82* (1), 115–125. https://doi.org/10.1016/S0168-3659(02)00125-6.

(13) Binnebose, A. M.; Haughney, S. L.; Martin, R.; Imerman, P. M.; Narasimhan, B.; Bellaire, B. H. Polyanhydride Nanoparticle Delivery Platform Dramatically Enhances Killing of Filarial Worms. *PLoS Negl. Trop. Dis.* **2015**, *9* (10), e0004173. https://doi.org/10.1371/journal.pntd.0004173.

(14) Brenza, T. M.; Ghaisas, S.; Ramirez, J. E. V.; Harischandra, D.; Anantharam, V.; Kalyanaraman, B.; Kanthasamy, A. G.; Narasimhan, B. Neuronal Protection against Oxidative Insult by Polyanhydride Nanoparticle-Based Mitochondria-Targeted Antioxidant Therapy. *Nanomedicine Nanotechnology, Biol. Med.* **2017**, *13* (3), 809–820. https://doi.org/10.1016/j.nano.2016.10.004.

(15) Phanse, Y.; Lueth, P.; Ramer-Tait, A. E.; Carrillo-Conde, B. R.; Wannemuehler, M. J.; Narasimhan, B.; Bellaire, B. H. Cellular Internalization Mechanisms of Polyanhydride Particles: Implications for Rational Design of Drug Delivery Vehicles. *J. Biomed. Nanotechnol.* **2016**, *12* (7), 1544–1552. https://doi.org/10.1166/jbn.2016.2259.

(16) Kelly, S. M.; Mitra, A.; Mathur, S.; Narasimhan, B. Synthesis and Characterization of Rapidly Degrading Polyanhydrides as Vaccine Adjuvants. *ACS Biomater. Sci. Eng.* **2020**, *6* (1), 265–276. https://doi.org/10.1021/acsbiomaterials.9b01427.

(17) Torres, M. P.; Vogel, B. M.; Narasimhan, B.; Mallapragada, S. K. Synthesis and Characterization of Novel Polyanhydrides with Tailored Erosion Mechanisms. *J. Biomed. Mater. Res. - Part A* **2006**, *76* (1), 102–110. https://doi.org/10.1002/jbm.a.30510.

(18) Ron, E.; Mathiowitz, E.; Mathiowitz, G.; Domb, A.; Langer, R. NMR Characterization of Erodible Copolymers. *Macromolecules* **1991**, *24* (9), 2278–2282. https://doi.org/10.1021/ma00009a024.

(19) Schindelin, J.; Arganda-Carreras, I.; Frise, E.; Kaynig, V.; Longair, M.; Pietzsch, T.; Preibisch, S.; Rueden, C.; Saalfeld, S.; Schmid, B.; et al. Fiji: An Open-Source Platform for Biological-Image Analysis. *Nat. Methods* **2012**, *9* (7), 676–682. https://doi.org/10.1038/nmeth.2019.

(20) Wagner, T.; Eglinger, J. ParticleSizer. 2017. https://doi.org/http://doi.org/10.5281/zenodo.820296.

(21) Carrillo-Conde, B. R.; Darling, R. J.; Seiler, S. J.; Ramer-Tait, A. E.; Wannemuehler, M. J.; Narasimhan, B. Sustained Release and Stabilization of Therapeutic Antibodies Using Amphiphilic Polyanhydride Nanoparticles. *Chem. Eng. Sci.* **2015**, *125*, 98–107. https://doi.org/10.1016/j.ces.2014.08.015.

(22) Krevelen, D. W. van; Nijenhuis, K. te; Te Nijenhuis, K.; W, V. K. *Properties of Polymers : Their Correlation with Chemical Structure; Their Numerical Estimation and Prediction from Additive Group Contributions*; Elsevier Science & Technology: Oxford, NETHERLANDS, 2009.

(23) Kipper, M. J.; Seifert, S.; Thiyagarajan, P.; Narasimhan, B. Understanding Polyanhydride Blend Phase Behavior Using Scattering, Microscopy, and Molecular Simulations. *Polymer (Guildf).* **2004**, *45* (10), 3329–3340. https://doi.org/10.1016/j.polymer.2004.03.052.

(24) Rodriguez, F. *Principles of Polymer Systems.*, 5th ed.; Taylor & Francis: New York, 2003.

(25) Kipper, M. J.; Hou, S.-S.; Seifert, S.; Thiyagarajan, P.; Schmidt-Rohr, K.; Narasimhan, B. Nanoscale Morphology of Polyanhydride Copolymers. *Macromolecules* **2005**, *38* (20), 8468–8472. https://doi.org/10.1021/ma051267r.

(26) Mullis, A. S.; Broderick, S. R.; Binnebose, A. M.; Peroutka-Bigus, N.; Bellaire, B. H.; Rajan, K.; Narasimhan, B. Data Analytics Approach for Rational Design of Nanomedicines with Programmable Drug Release. *Mol. Pharm.* **2019**, *16* (5), 1917–1928. https://doi.org/10.1021/acs.molpharmaceut.8b01272.

(27) Tetko, I. V.; Gasteiger, J.; Todeschini, R.; Mauri, A.; Livingstone, D.; Ertl, P.; Palyulin, V. A.; Radchenko, E. V.; Zefirov, N. S.; Makarenko, A. S.; et al. Virtual Computational Chemistry Laboratory - Design and Description. *J. Comput. Aided. Mol. Des.* **2005**, *19* (6), 453–463. https://doi.org/10.1007/s10822-005-8694-y.

(28) Lopac, S. K.; Torres, M. P.; Wilson-Welder, J. H.; Wannemuehler, M. J.; Narasimhan, B. Effect of Polymer Chemistry and Fabrication Method on Protein Release and Stability from Polyanhydride Microspheres. *J. Biomed. Mater. Res. - Part B Appl. Biomater.* **2009**, *91* (2), 938–947. https://doi.org/10.1002/jbm.b.31478.

(29) Marsac, P. J.; Li, T.; Taylor, L. S. Estimation of Drug–Polymer Miscibility and Solubility in Amorphous Solid Dispersions Using Experimentally Determined Interaction Parameters. *Pharm. Res.* **2009**, *26* (1), 139–151. https://doi.org/10.1007/s11095-008-9721-1.

(30) Larobina, D.; Mensitieri, G.; Kipper, M. J.; Narasimhan, B. Mechanistic Understanding of Degradation in Bioerodible Polymers for Drug Delivery. *AIChE J.* **2002**, *48* (12), 2960–2970. https://doi.org/10.1002/aic.690481221.

(31) Göpferich, A. Mechanisms of Polymer Degradation and Erosion. *Biomaterials* **1996**, *17* (2), 103–114. https://doi.org/10.1016/0142-9612(96)85755-3.

(32) Narasimhan, B.; Goodman, J. T.; Vela Ramirez, J. E. Rational Design of Targeted Next-Generation Carriers for Drug and Vaccine Delivery. *Annu. Rev. Biomed. Eng* **2016**, *18* (1), 25–49. https://doi.org/10.1146/annurev-bioeng-082615-030519.

(33) Ali, M.; Afzal, M.; Verma, M.; Bhattacharya, S. M.; Ahmad, F. J.; Samim, M.; Abidin, M. Z.; Dinda, a. K. Therapeutic Efficacy of Poly (Lactic-Co-Glycolic Acid) Nanoparticles Encapsulated Ivermectin (Nano-Ivermectin) against Brugian Filariasis in Experimental Rodent Model. *Parasitol. Res.* **2014**, *113* (2), 681–691. https://doi.org/10.1007/s00436-013-3696-5.

(34) Determan, A. S.; Graham, J. R.; Pfeiffer, K. A.; Narasimhan, B. The Role of Microsphere Fabrication Methods on the Stability and Release Kinetics of Ovalbumin Encapsulated in Polyanhydride Microspheres. *J. Microencapsul.* **2006**, *23* (8), 832–843. https://doi.org/10.1080/02652040601033841.

(35) Ulery, B. D.; Kumar, D.; Ramer-Tait, A. E.; Metzger, D. W.; Wannemuehler, M. J.; Narasimhan, B. Design of a Protective Single-Dose Intranasal Nanoparticle-Based Vaccine Platform for Respiratory Infectious Diseases. *PLoS One* **2011**, *6* (3), 1–8. https://doi.org/10.1371/journal.pone.0017642.

(36) Carrillo-Conde, B. R.; Darling, R. J.; Seiler, S. J.; Ramer-Tait, A. E.; Wannemuehler, M. J.; Narasimhan, B. Sustained Release and Stabilization of Therapeutic Antibodies Using Amphiphilic Polyanhydride Nanoparticles. *Chem. Eng. Sci.* **2015**, *125*, 98–107. https://doi.org/10.1016/j.ces.2014.08.015.

(37) Read, N. W.; Al-Janabi, M. N.; Holgate, A. M.; Barber, D. C.; Edwards, C. A. Simultaneous Measurement of Gastric Emptying, Small Bowel Residence and Colonic Filling of a Solid Meal by the Use of the Gamma Camera. *Gut* **1986**, *27* (3), 300–308. https://doi.org/10.1136/gut.27.3.300.

(38) Wong, C. Y.; Martinez, J.; Dass, C. R. Oral Delivery of Insulin for Treatment of Diabetes: Status Quo, Challenges and Opportunities. *J. Pharm. Pharmacol.* **2016**, *68*, 1093–1108. https://doi.org/10.1111/jphp.12607.

(39) Sharpe, L. A.; Daily, A. M.; Horava, S. D.; Peppas, N. A. Therapeutic Applications of Hydrogels in Oral Drug Delivery. *Expert Opin. Drug Deliv.* **2014**, *11* (6), 901–915. https://doi.org/10.1517/17425247.2014.902047.

(40) Narasimhan, B.; Langer, R. Zero-Order Release of Micro- and Macromolecules from Polymeric Devices: The Role of the Burst Effect. *J. Control. Release* **1997**, *47* (1), 13–20. https://doi.org/10.1016/S0168-3659(96)01611-2.

(41) Marsac, P. J.; Shamblin, S. L.; Taylor, L. S. Theoretical and Practical Approaches for Prediction of Drug–Polymer Miscibility and Solubility. *Pharm. Res.* **2006**, *23* (10), 2417–2426. https://doi.org/10.1007/s11095-006-9063-9.

(42) Kipper, M. J.; Seifert, S.; Thiyagarajan, P.; Narasimhan, B. Morphology of Polyanhydride Copolymers: Time-Resolved Small-Angle X-Ray Scattering Studies of Crystallization. *J. Polym. Sci. Part B Polym. Phys.* **2005**, *43* (5), 463–477. https://doi.org/10.1002/polb.20351.

5.8 Tables

Table 5.1 Characterization of CPTEG:SA copolymers synthesized using the high-throughput method. Values in parentheses indicate averages for conventionally-synthesized copolymers.[16]

Copolymer	Actual Molar Ratio	M_n (Da)	T_m (°C)	Reaction Time (h)
05:95 CPTEG:SA	04:96 (04:96)	30,100 (24,700)	76.8 (74.6)	7
10:90 CPTEG:SA	11:89 (09:91)	27,100 (29,800)	71.8 (70.0)	7
15:85 CPTEG:SA	16:84 (14:86)	23,900 (25,900)	65.9 (64.5)	7
20:80 CPTEG:SA	21:79 (20:80)	19,500 (21,100)	65.2 (58.9)	7
25:75 CPTEG:SA	25:75 (23:77)	20,900 (36,300)	60.2 (52.3)	7
30:70 CPTEG:SA	30:70	18,300	54.6	7
35:65 CPTEG:SA	35:65	16,700	48.9	7
40:60 CPTEG:SA	42:58	14,400	TD	6
50:50 CPTEG:SA	51:49	16,500	N/A	6

Table 5.2 Characterization of non-encapsulating and model drug-encapsulating nanoparticle libraries. Count mean size distributions were calculated from SEM micrographs. Rhodamine B formulations showed >100% measured encapsulation efficiency (values in parentheses), which are interpreted as 100%. Data are presented as mean ± standard deviation.

	Unloaded		**5% Rhodamine B**			**5% Coomassie brilliant blue**		
Copolymer	**Diameter (nm)**	**Zeta Potential (mV)**	**Diameter (nm)**	**Zeta Potential (mV)**	**Encapsulation Efficiency**	**Diameter (nm)**	**Zeta Potential (mV)**	**Encapsulation Efficiency**
05:95 CPTEG:SA	272 ± 90	-37.7 ± 3.4	299 ± 101	-6.4 ± 0.4	100% (128%)	291 ± 95	-34.3 ± 0.6	35.7%
10:90 CPTEG:SA	319 ± 107	-46.0 ± 1.0	295 ± 105	7.2 ± 1.2	100% (131%)	356 ± 141	-41.7 ± 0.9	42.1%
15:85 CPTEG:SA	342 ± 129	-38.0 ± 1.1	328 ± 121	-6.7 ± 1.4	100% (129%)	366 ± 145	-49.2 ± 0.7	46.7%
20:80 CPTEG:SA	363 ± 126	-42.9 ± 0.3	425 ± 165	12.0 ± 0.8	100% (146%)	442 ± 194	-50.0 ± 2.0	44.3%
25:75 CPTEG:SA	418 ± 156	-41.7 ± 1.9	552 ± 231	17.7 ± 1.5	100% (119%)	535 ± 240	-46.6 ± 1.3	58.0%
30:70 CPTEG:SA	482 ± 167	-38.4 ± 3.8	705 ± 277	-0.6 ± 2.2	100% (102%)	599 ± 266	-46.0 ± 1.4	46.2%

Table 5.3 Group contribution method estimation of polymer and model drug solubility parameters. Units are as follows: **V** (cm^3/mol), δ's $(J/cm^3)^{1/2}$. Δδ and χ_{FH} values at 298 K were predicted using Eq. 1 and 2, respectively.

	Fedors		**Hoftyzer-Van Krevelen**							
Polymer or Compound	**V (cm^3/mol)**	**δ $(J/cm^3)^{1/2}$**	**δ_d**	**δ_p**	**δ_h**	**δ**	**Δδ RhoB**	**Δδ CBB**	**χ_{FH} RhoB**	**χ_{FH} CBB**
0:100 CPTEG:SA	17247	21.0	17.9	0.6	7.5	19.4	2.5	3.4	0.44	0.84
5:95 CPTEG:SA	17722	21.2	18.1	0.5	7.7	19.7	2.6	3.6	0.47	0.94
10:90 CPTEG:SA	18196	21.4	18.4	0.5	7.8	20.0	2.7	3.8	0.51	1.03
15:85 CPTEG:SA	18670	21.6	18.6	0.5	7.9	20.2	2.8	4.0	0.56	1.14
20:80 CPTEG:SA	19144	21.8	18.8	0.5	8.0	20.5	2.9	4.1	0.62	1.24
25:75 CPTEG:SA	19618	21.9	19.0	0.5	8.2	20.7	3.1	4.3	0.68	1.35
30:70 CPTEG:SA	20092	22.1	19.2	0.5	8.3	20.9	3.2	4.5	0.75	1.46
100:0 CPTEG:SA	26730	23.6	21.2	0.5	9.2	23.2	5.0	6.4	1.82	2.96
Rhodamine B	339	23.0	17.3	2.9	7.3	19.0				
Coomassie Brilliant Blue	581	23.0	17.2	1.6	4.4	17.9				

Table 5.4 Interaction parameters calculated from melting point depression of polymer-model drug films. χ values were predicted from Figure 5.8 data using Eq (3). No melting point depression effect was observed for 15:85 CPTEG:SA-CBB films.

Copolymer	χ RhoB	χ CBB
05:95 CPTEG:SA	-18.3	-2.6
10:90 CPTEG:SA	-9.9	-2.6
15:85 CPTEG:SA	-8.7	N/A
20:80 CPTEG:SA	-0.2	0.6
25:75 CPTEG:SA	-4.9	1.4
30:70 CPTEG:SA	2.3	2.7

5.9 Figures

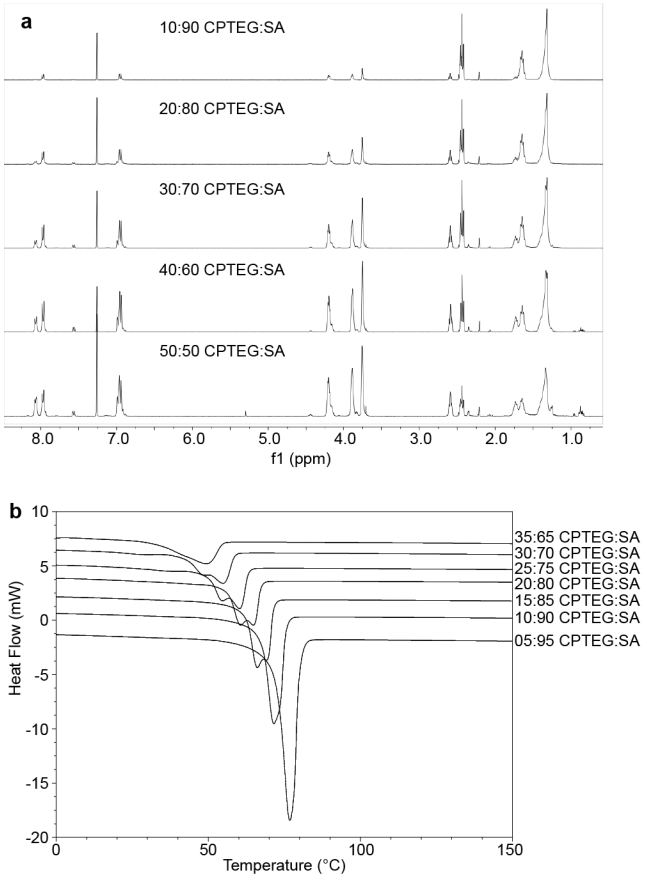

Figure 5.1 Representative ^{1}H NMR spectra and DSC thermograms of CPTEG:SA copolymer libraries. (a) ^{1}H NMR spectra of CPTEG:SA copolymers. (b) DSC thermograms of CPTEG:SA copolymers.

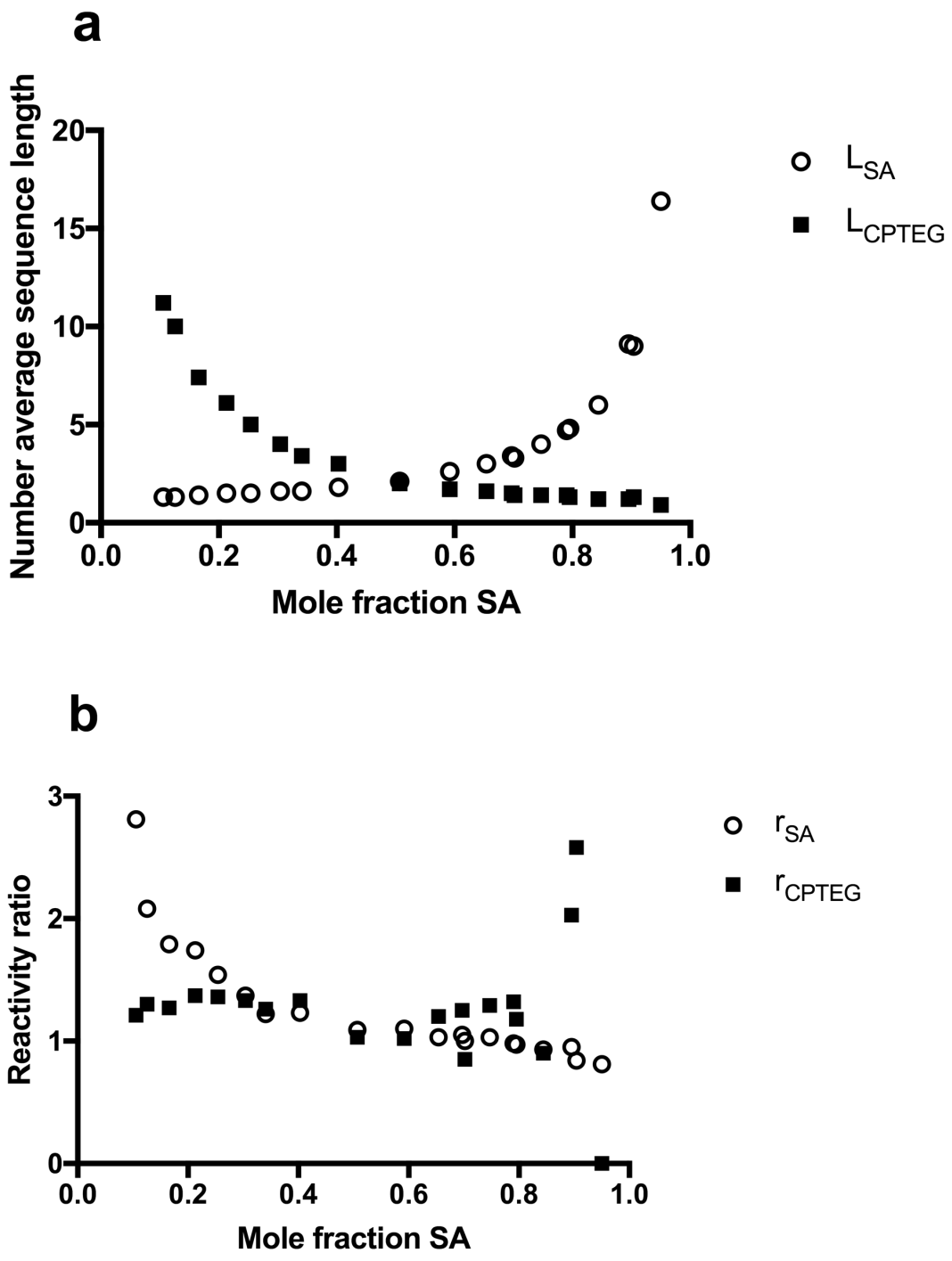

Figure 5.2 CPTEG:SA copolymer microphase composition analysis. (a) CPTEG:SA number average sequence length, determined from ^{1}H NMR. (b) CPTEG:SA reactivity ratio, determined from ^{1}H NMR.

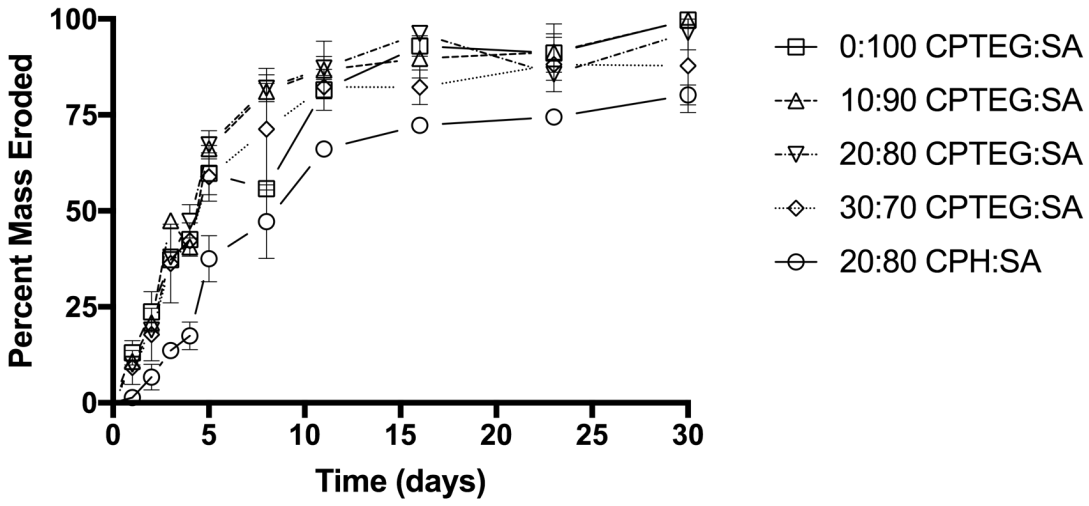

Figure 5.3 Percent mass lost from tablets of CPTEG:SA copolymersin PBS, pH7.4. Data are presented as mean ± standard deviation.

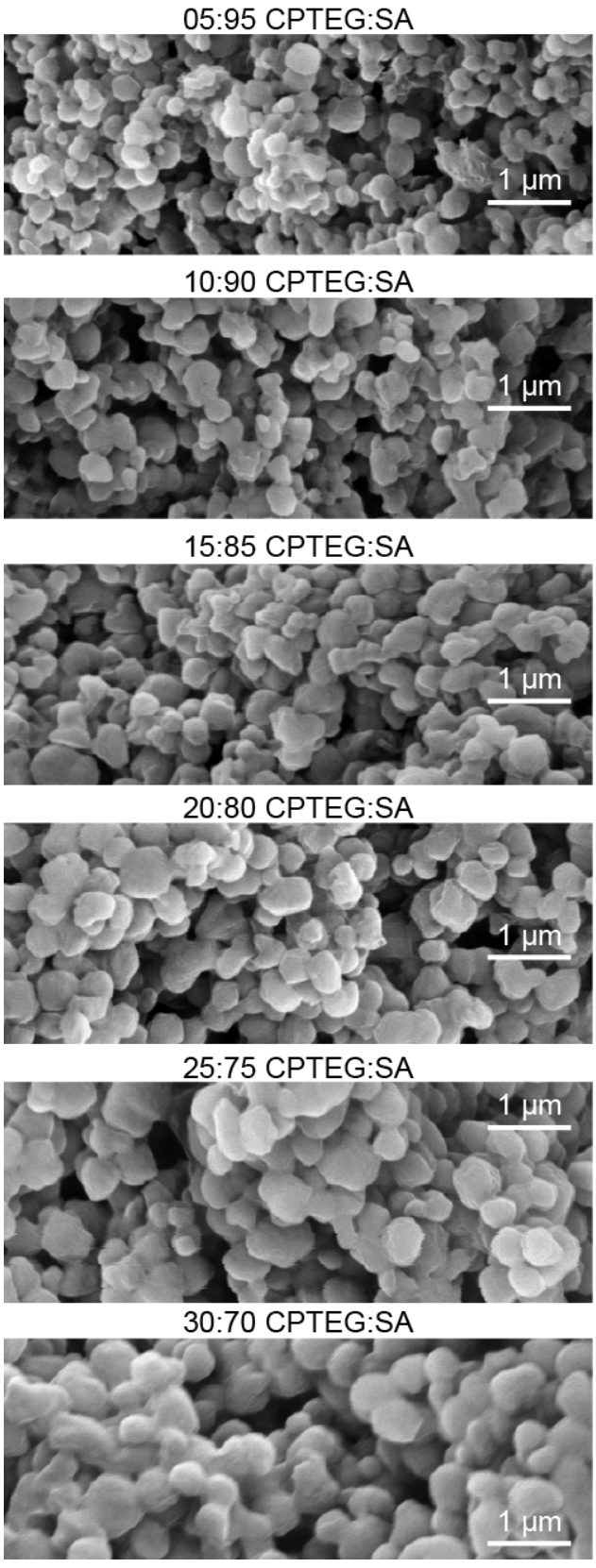

Figure 5.4 Scanning electron micrographs of empty CPTEG:SA nanoparticle library.

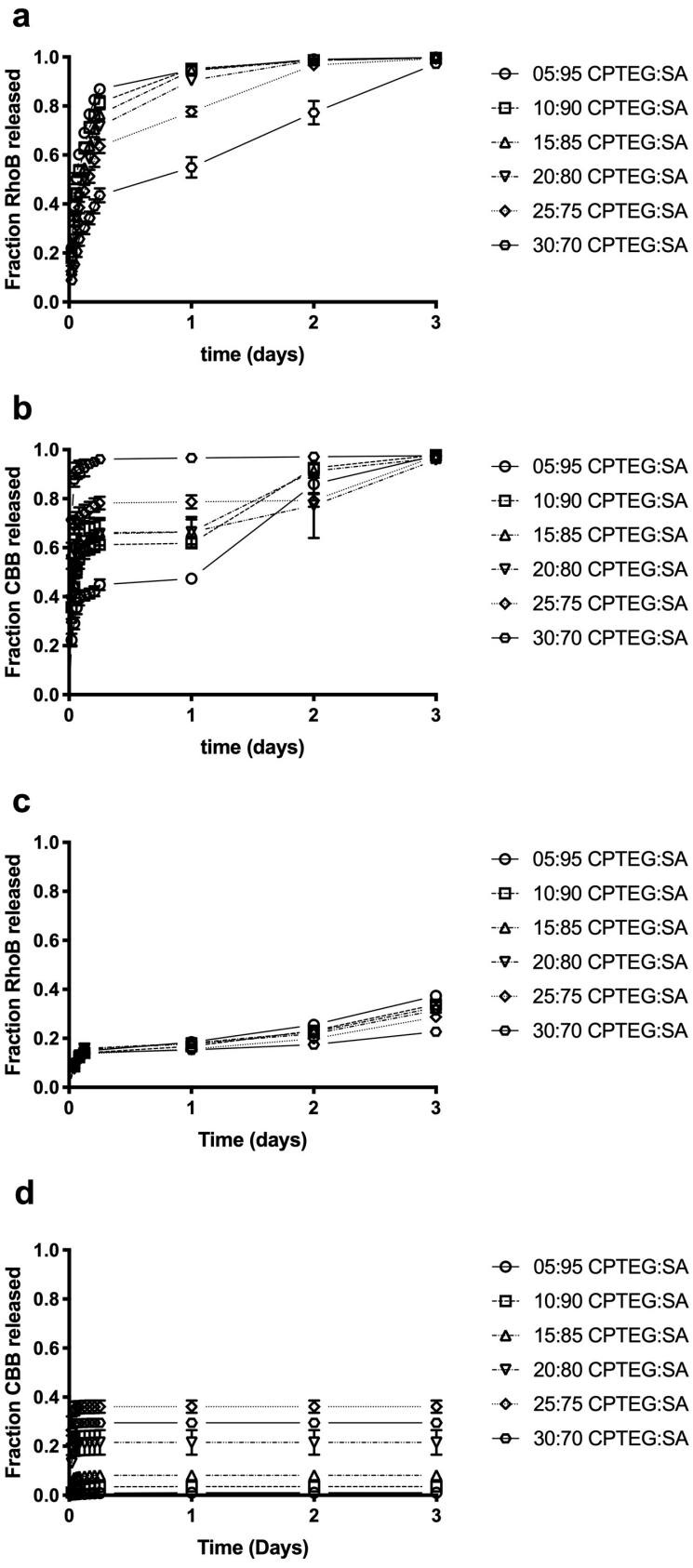
a
Fraction RhoB released
time (days)
b
Fraction CBB released
time (days)
c
Fraction RhoB released
Time (days)
d
Fraction CBB released
Time (Days)
05:95 CPTEG:SA
10:90 CPTEG:SA
15:85 CPTEG:SA
20:80 CPTEG:SA
25:75 CPTEG:SA
30:70 CPTEG:SA

Figure 5.5 Model drug release from nanoparticle libraries. (a,b) RhoB (a) or CBB (b) release from 5% loaded (w/w) CPTEG:SA nanoparticles in PBS, pH 7.4. (c,d) RhoB (c) or CBB (d) release from 5% loaded CPTEG:SA nanoparticles in acetate buffer, pH 4.3. In both buffers, RhoB release profiles follow erosion trends from polymer tablets, while CBB release profiles are inverted from these trends. Data are presented as mean ± standard deviation.

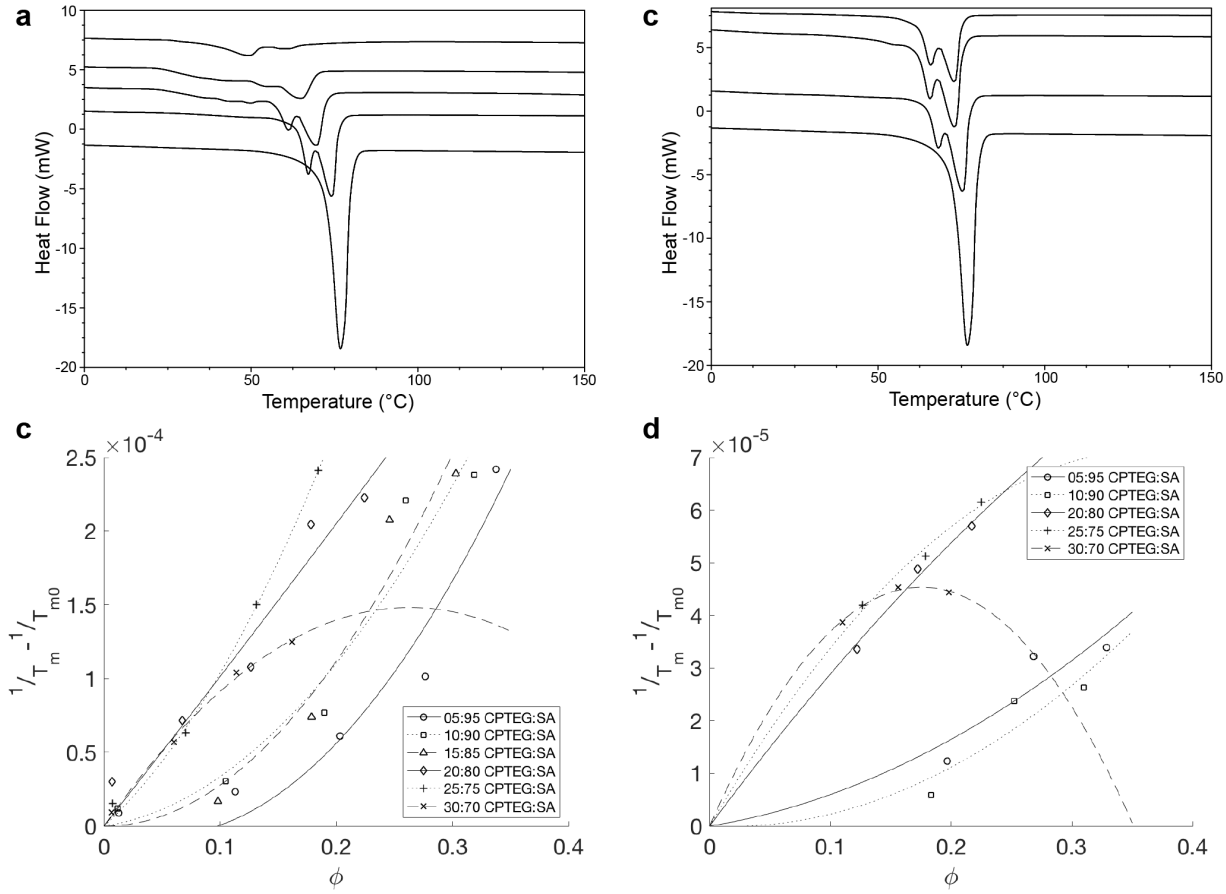

Figure 5.6 Melting point depression of polymer-model drug films. (a) DSC thermograms of 05:95 CPTEG:SA-RhoB films at 0%, 9%, 17%, 23%, and 29% (w/w) RhoB, from bottom to top. The melting point is gradually decreased with increasing (b) DSC thermograms of 05:95 CPTEG:SA-CBB films at 0%, 17%, 23%, and 29% (w/w) CBB, from bottom to top. (c,d) Determination of the polymer-model drug interaction parameters from melting point depression data for RhoB (c) and CBB (d). Quadratic curves were fitted and χ values were extracted using Eq. (3).

5.10 Supporting Information

Supporting Table 5.1 Effect of reaction time on copolymer molecular weight and nanoparticle size distribution. Molecular weight was determined by ^{1}H NMR, and nanoparticle diameter was determined by SEM. Cells left blank indicate no nanoparticles were recovered. Size distributions are presented as mean ± standard deviation.

	Reaction time:	4 hours	5 hours	6 hours	10 hours
10:90 CPTEG:SA	**Mn (Da)**	14,000	14,800	15,300	27,900
	Diameter (nm)	297 ± 125	291 ± 107	370 nm ± 165	286 ± 98
20:80 CPTEG:SA	**Mn (Da)**	12,000	13,600	14,000	24,300
	Diameter (nm)	445 ± 114	657 ± 257	492 ± 155	355 ± 126
30:70 CPTEG:SA	**Mn (Da)**	11,800	12,200	14,600	24,800
	Diameter (nm)	796 ± 189	868 ± 313	1,054 ± 350	N/A
40:60 CPTEG:SA	**Mn (Da)**	10,600	14,000	14,400	18,400
	Diameter (nm)	295 ± 123	1,505 ± 204	N/A	N/A
50:50 CPTEG:SA	**Mn (Da)**	11,200	12,700	16,500	20,800

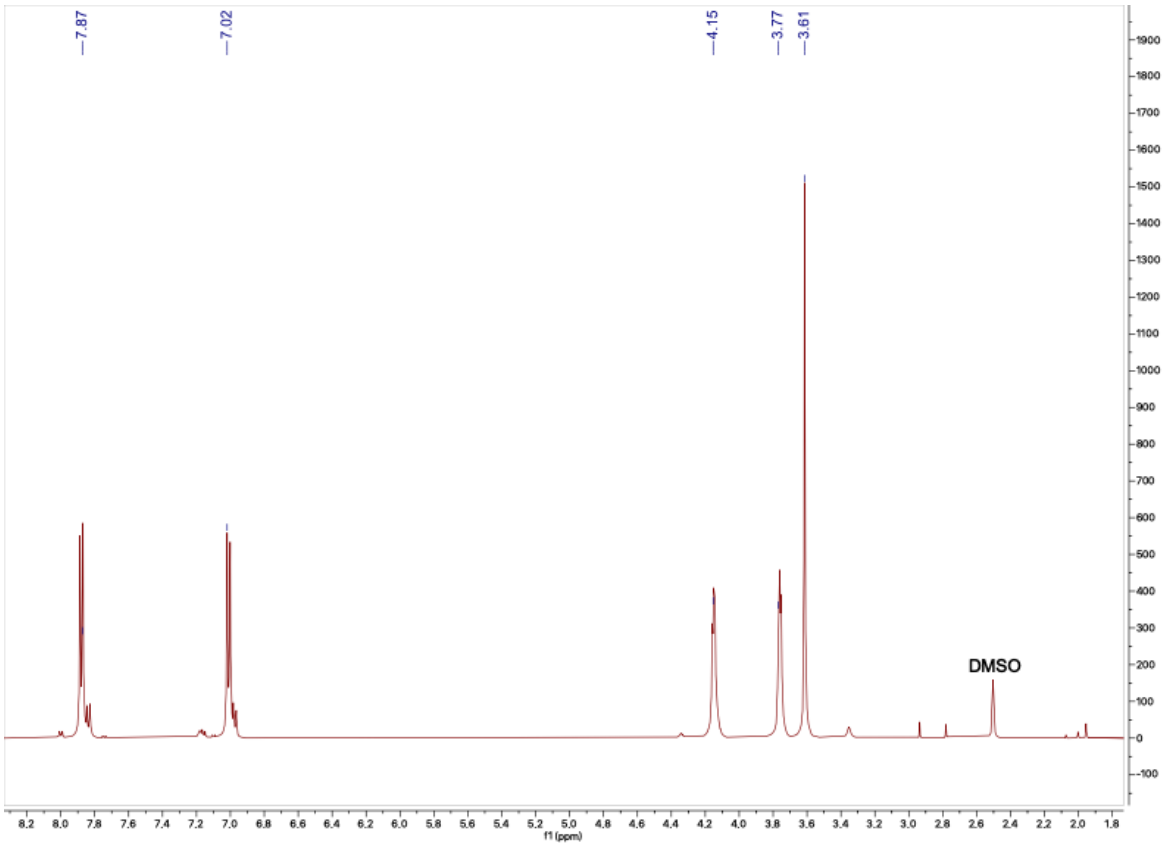

Supporting Figure 5.1 ^{1}H NMR spectrum of CPTEG diacid.

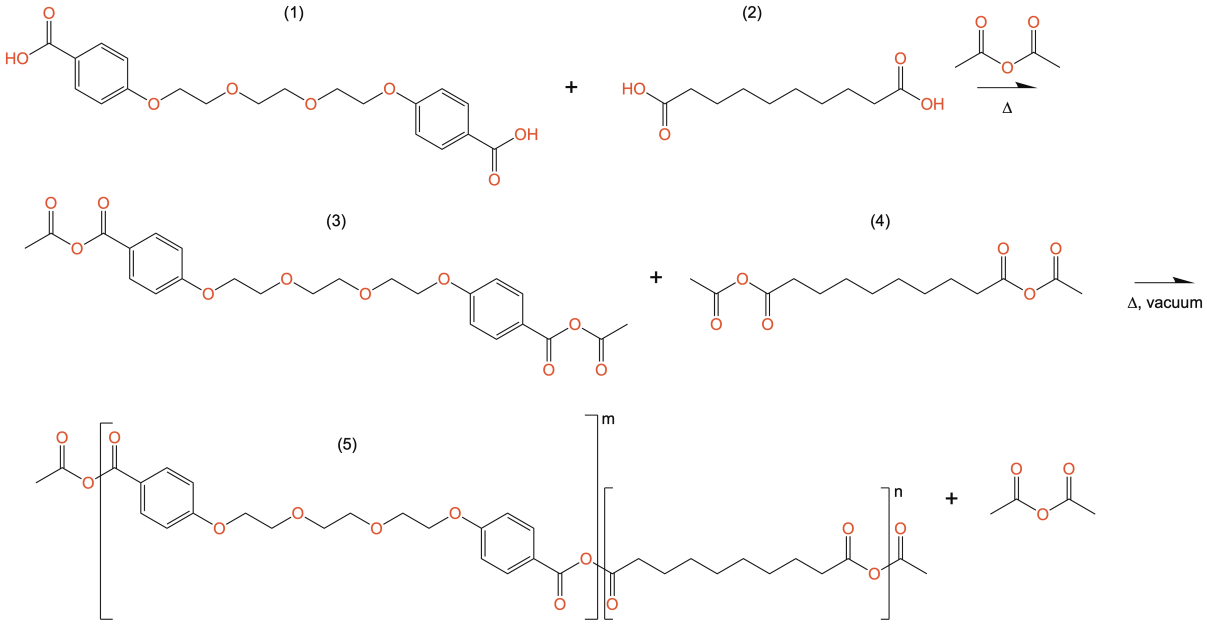

Supporting Figure 5.2 CPTEG:SA copolymerization scheme. CPTEG (1) and SA (2) dicarboxylic acid monomers are acetylated in acetic anhydride, yielding CPTEG (3) and SA (4) prepolymers. Acetic anhydride is removed by rotary evaporation and the remaining prepolymers are reacted under vacuum to yield CPTEG:SA copolymers (5). Polymerization used a melt polycondensation mechanism, where acetic anhydride is produced and continually removed by vacuum.

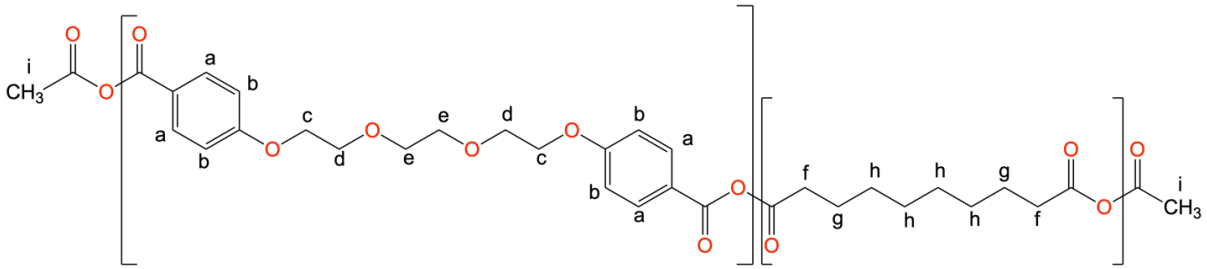

Hydrogen	Shift	# of H	Splitting
a	8.0	4	d
b	7.0	4	d
c	4.2	4	t
d	3.9	4	m
e	3.75	4	m
f	2.6	2	t
f'	2.45	2	t
g	1.65	4	m
h	1.32	8	m
i	2.22	6	s

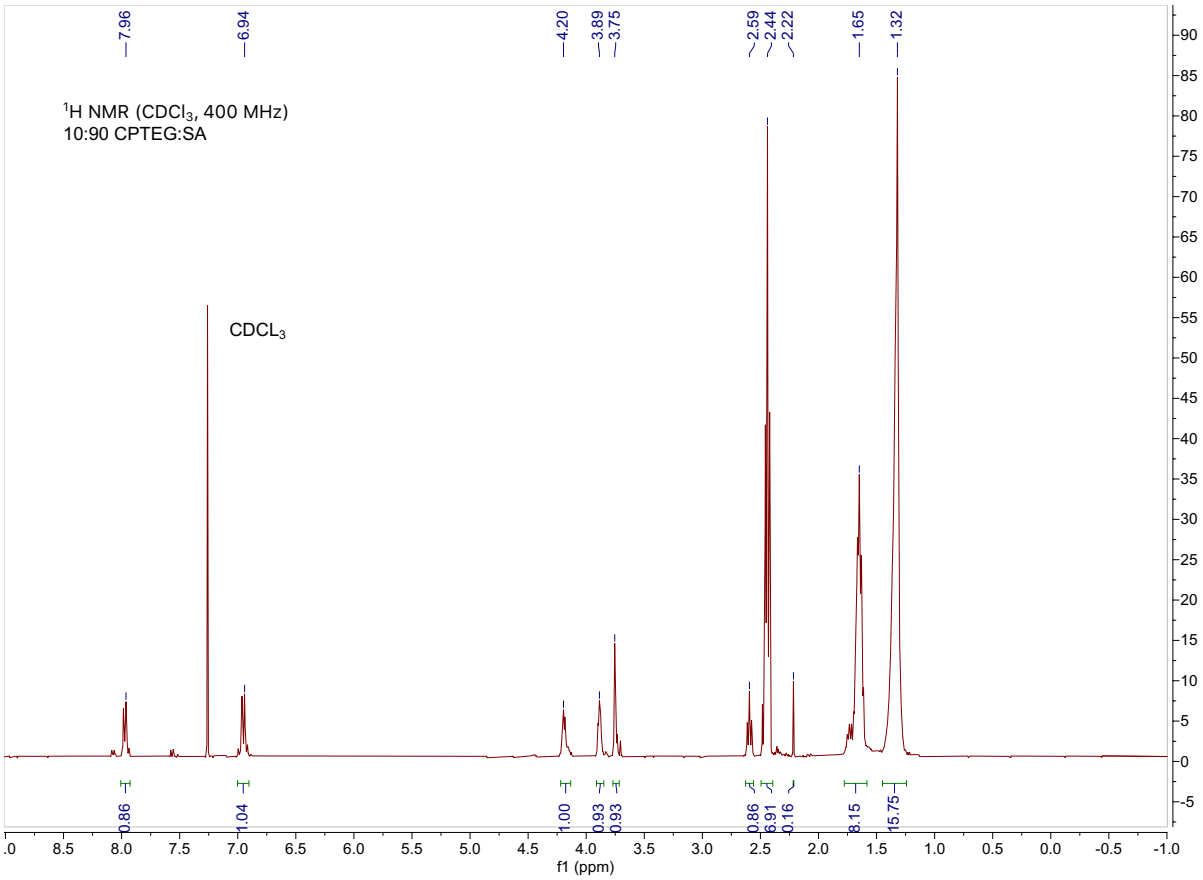
7.96
6.94
4.20
3.89
3.75
2.59
2.44
2.22
1.65
1.32
^{1}H NMR ($CDCl_3$, 400 MHz)
10:90 CPTEG:SA
$CDCL_3$
0.86
1.04
1.00
0.93
0.93
0.86
6.91
0.16
8.15
15.75
f1 (ppm)

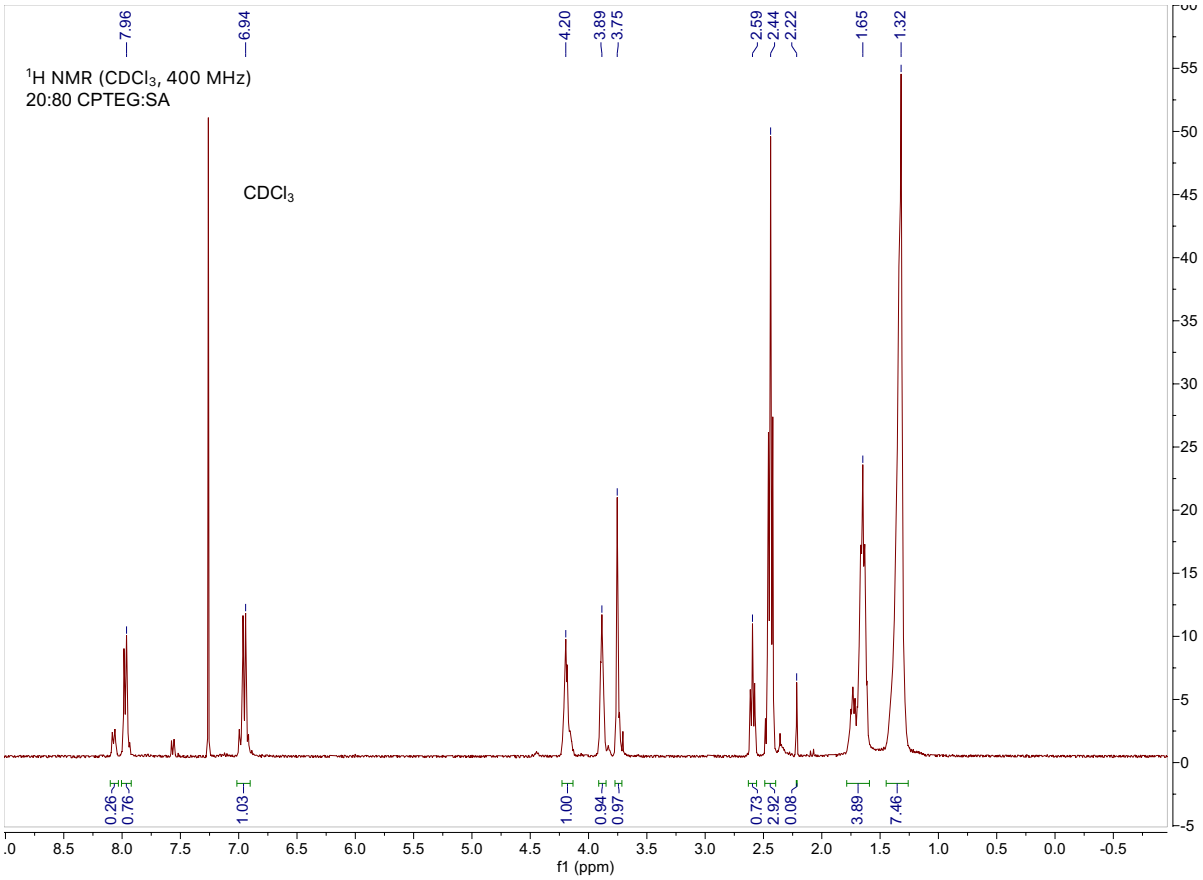
7.96
6.94
4.20
3.89
3.75
2.59
2.44
2.22
1.65
1.32
^{1}H NMR ($CDCl_3$, 400 MHz)
20:80 CPTEG:SA
$CDCl_3$
0.26
0.76
1.03
1.00
0.94
0.97
0.73
2.92
0.08
3.89
7.46
f1 (ppm)

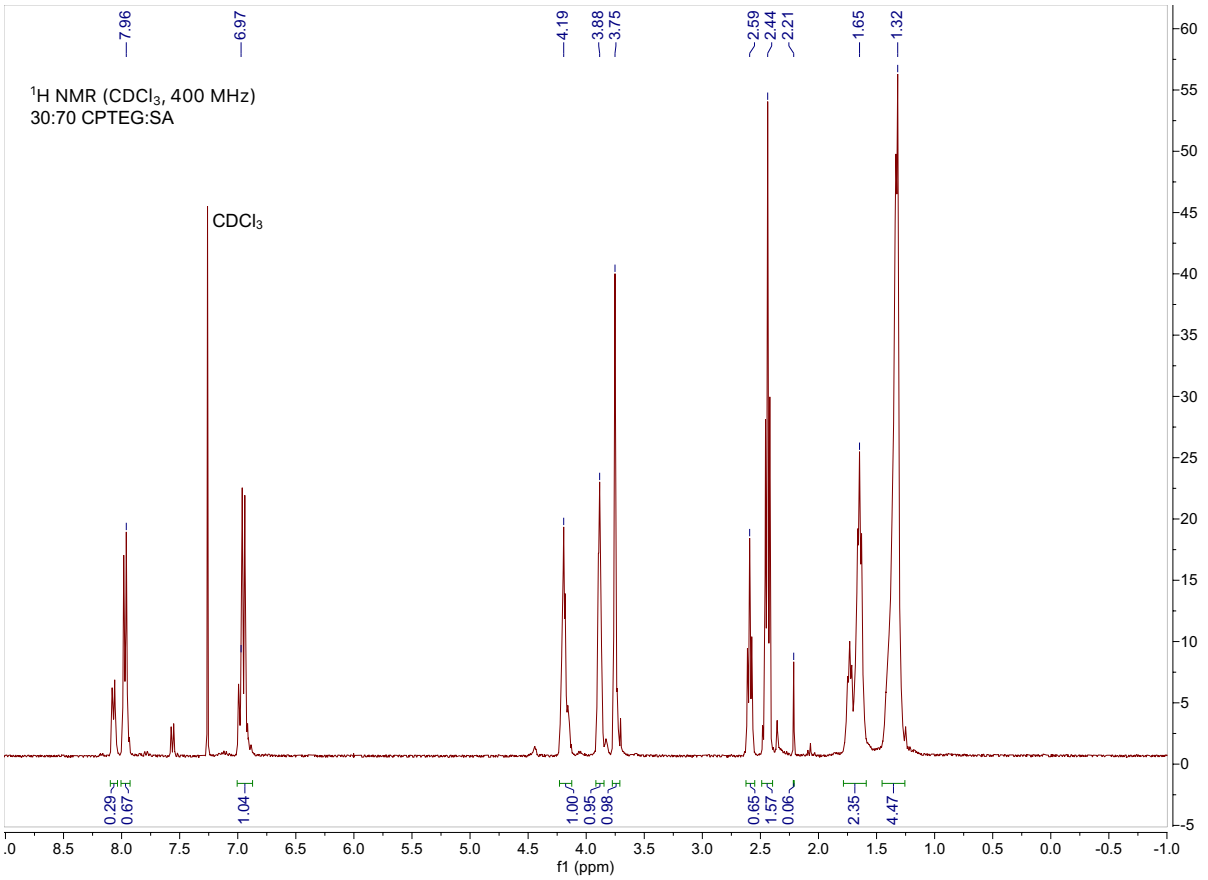
7.96
6.97
4.19
3.88
3.75
2.59
2.44
2.21
1.65
1.32
^{1}H NMR ($CDCl_3$, 400 MHz)
30:70 CPTEG:SA
$CDCl_3$
0.29
0.67
1.04
1.00
0.95
0.98
0.65
1.57
0.06
2.35
4.47
f1 (ppm)

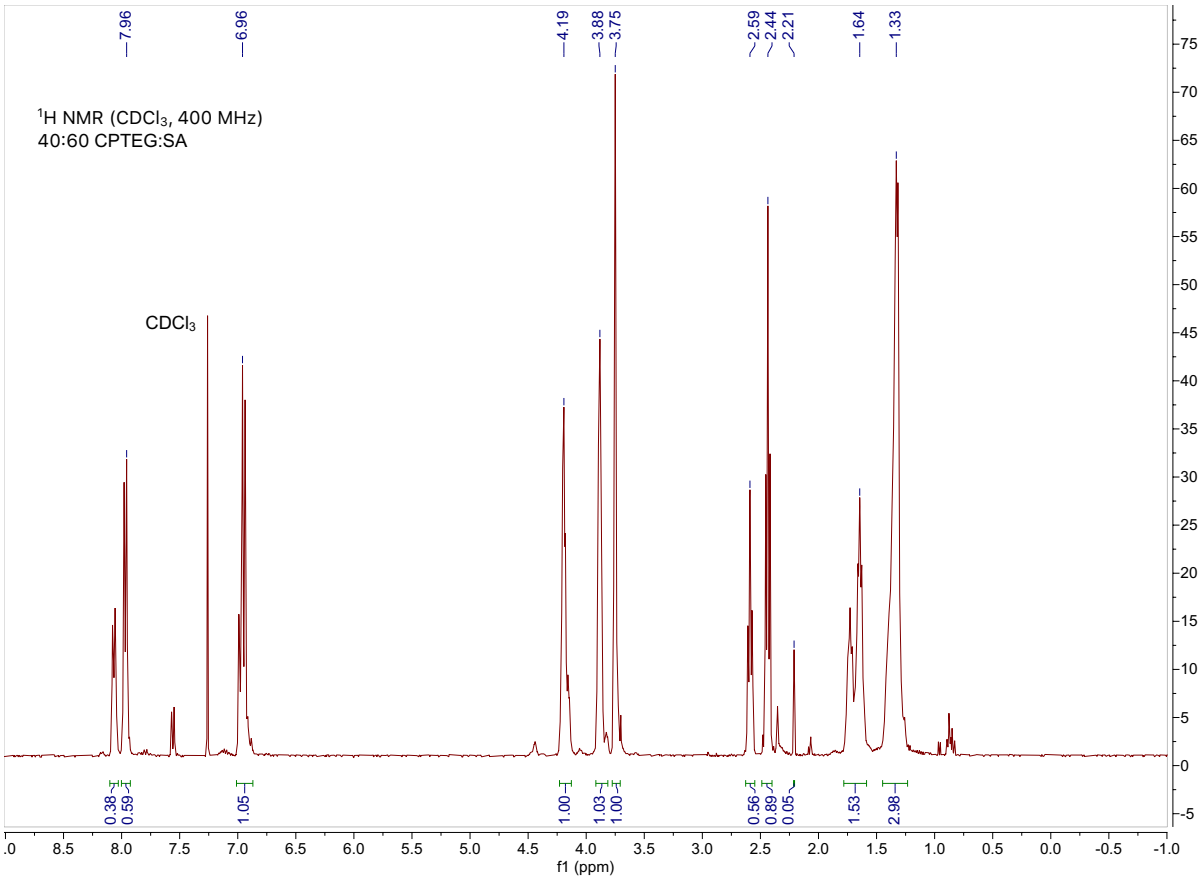
7.96
6.96
4.19
3.88
3.75
2.59
2.44
2.21
1.64
1.33
^{1}H NMR ($CDCl_3$, 400 MHz)
40:60 CPTEG:SA
$CDCl_3$
0.38
0.59
1.05
1.00
1.03
1.00
0.56
0.89
0.05
1.53
2.98
f1 (ppm)

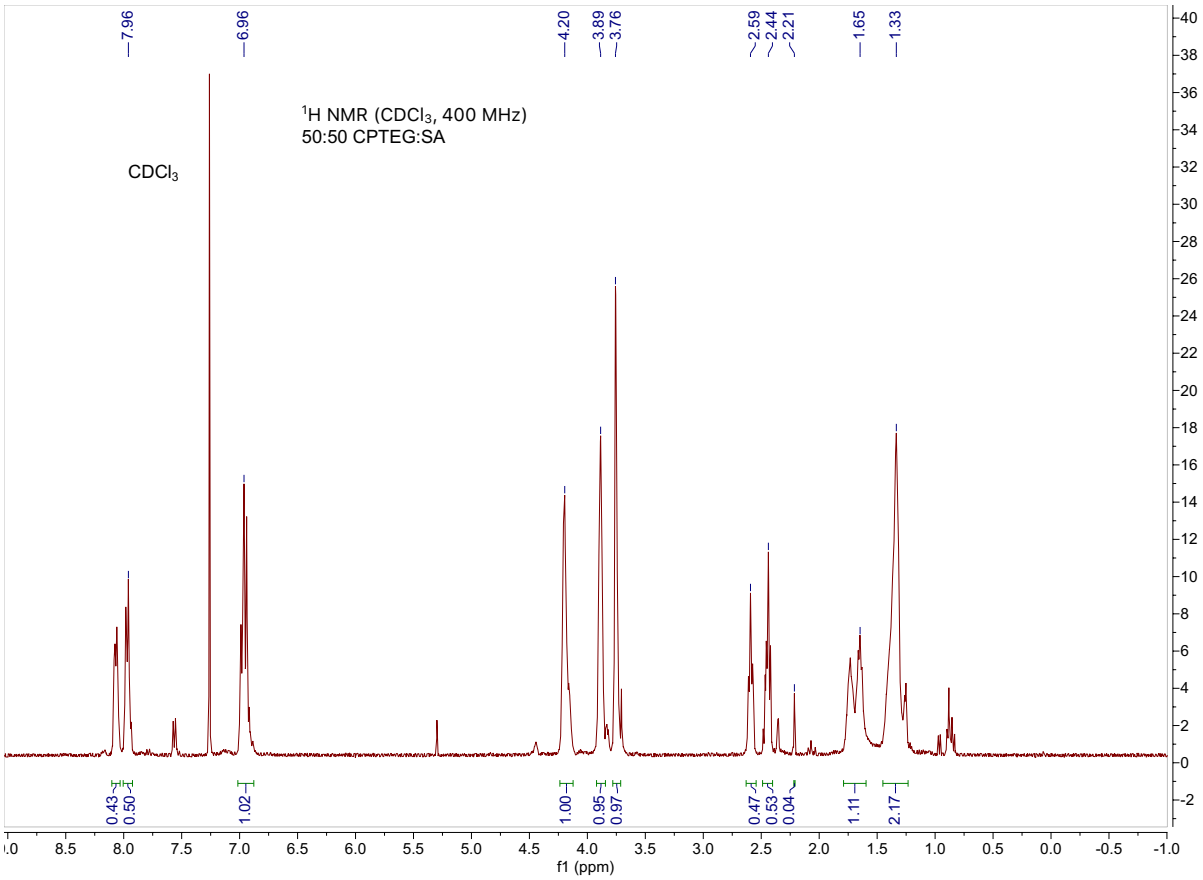

Supporting Figure 5.3 CPTEG:SA ^{1}H NMR peak assignment and labeled spectra of high-throughput polymer library.

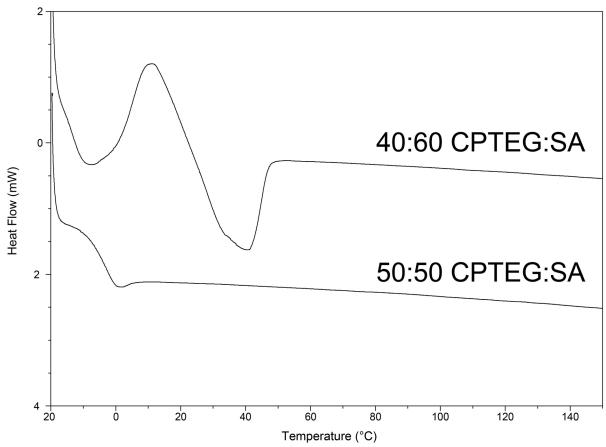

Supporting Figure 5.4 DSC thermograms of CPTEG-rich copolymers. 40:60 CPTEG:SA was thermally unstable and 50:50 CPTEG:SA showed a near-zero °C T_g.

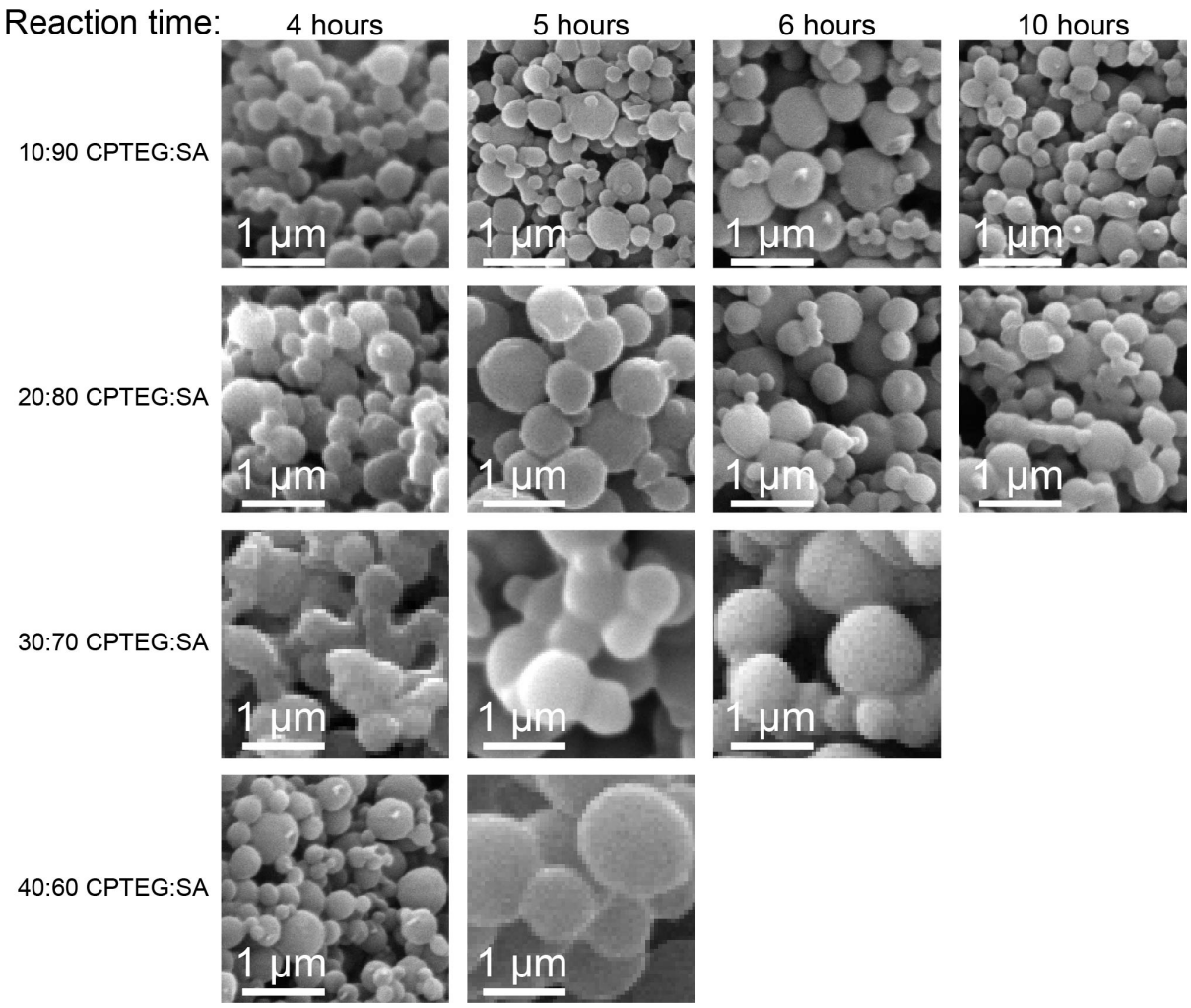

Supporting Figure 5.5 Screening high-throughput CPTEG:SA copolymers for conventional nanoparticles. Size distributions are provided in Supporting Table 5.1. Empty spaces indicate that no particles were able to be recovered due to polymer tackiness. The 5 hour reaction time was selected for ongoing experiments as it produced the most discrete, sub-micron particles with high yield for chemistries with 30 mol % or less CPTEG.

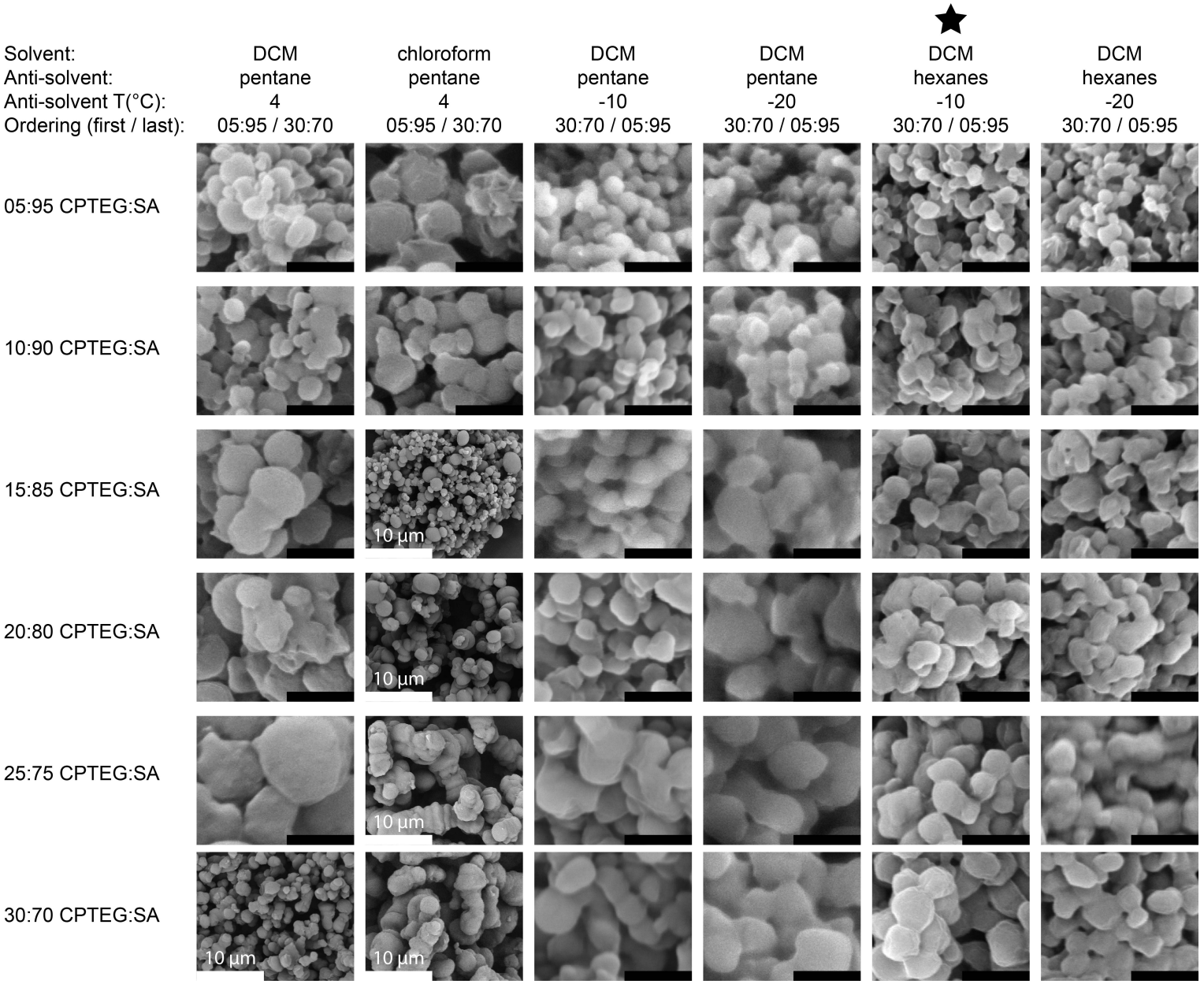
Solvent: DCM chloroform DCM DCM DCM DCM
Anti-solvent: pentane pentane pentane pentane hexanes hexanes
Anti-solvent T(°C): 4 4 -10 -20 -10 -20
Ordering (first / last): 05:95 / 30:70 05:95 / 30:70 30:70 / 05:95 30:70 / 05:95 30:70 / 05:95 30:70 / 05:95
05:95 CPTEG:SA
10:90 CPTEG:SA
15:85 CPTEG:SA
20:80 CPTEG:SA
25:75 CPTEG:SA
30:70 CPTEG:SA
10 µm

Supporting Figure 5.6 Optimization of high-throughput nanoparticle synthesis conditions. Methylene chloride (DCM) and chloroform were tested as solvents, and pentane and hexanes were tested as anti-solvents at 4, –10, and –20°C. For all, polymer concentration in methylene chloride was kept constant at 20 mg//mL and solvent to anti-solvent ratio was kept constant at 1:9. Scale bars represent 1 μm (black), unless noted otherwise (white, 10μm). Star represents the optimal conditions for synthesizing spherical, sub-micron particles, which were used for all other nanoparticle libraries.

CHAPTER 6. RATIONAL DESIGN OF ANTIMICROBIAL NANOMEDICINES AGAINST OPPORTUNISTIC, RESISTANT PATHOGENS USING A HYBRID ANALYTICS APPROACH

A manuscript to be submitted to Acta Biomaterialia

*Adam S. Mullis[a], *Scott R. Broderick[b], *Kruttika S. Phadke[c,d], Nathan Peroutka-Bigus[c,d], Bryan H. Bellaire[c,d,e], Krishna Rajan[b,e], and Balaji Narasimhan[a,e,+]

[a]Department of Chemical and Biological Engineering, Iowa State University, Ames, Iowa 50011, United States

[b]Department of Materials Design and Innovation, University at Buffalo, Buffalo, NY 14260, United States

[c]Department of Veterinary Microbiology and Preventive Medicine, Iowa State University, Ames, Iowa 50011, United States

[d]Interdepartmental Microbiology Graduate Program, Iowa State University, Ames, Iowa 50011, United States

[e]Nanovaccine Institute, Iowa State University, Ames, Iowa 50011, United States

*Co-first authors

+Corresponding author

6.1 Abstract

Nanoparticle carriers can improve antibiotic functional efficacy by altering drug biodistribution. However, the dataspace is massive, limiting the feasibility of traditional screening approaches. Informatics-assisted screening could streamline screening, but nanoparticle efficacy is governed by nonlinear relationships with descriptors that are challenging to model. A hybrid informatics approach was used to identify polymer, drug, and

nanoparticle properties that determine the antimicrobial activity of nanomedicines against the opportunistic, intrinsically resistant pathogen *Burkholderia cepacia*, and to develop a model for predicting nanomedicine performance. Polymer T_g, polymer backbone N_{group}, drug LogP3, nanoparticle diameter and zeta potential, the fractional drug released at two hours, and the mass of drug released at 24 hours were identified as key descriptors associated with particle antimicrobial performance. Graph analysis provided dimensionality reduction of the descriptor space while preserving nonlinear descriptor-property relationships, enabling accurate modeling of nanomedicine performance. Out-of-library validation confirmed the model's accuracy, supporting its use in prioritizing candidate formulations and cocktails for *in vitro* testing based on predicted performance. This approach provides an important step toward the development of a framework to rationally design nanomedicines with improved potency to counter antimicrobial resistant infections.

6.2 Introduction

Burkholderia cepacia complex (BCC) bacteria are a group of hard-to-treat opportunistic pathogens primarily affecting immunocompromised and cystic fibrosis (CF) patients [1]. BCC bacteria are only present in a minority of CF infections, approximately 2–4% of CF patients [2,3]. BCC infections can be highly virulent, in some cases causing necrotizing pneumonia and septicemia, and are "correlate[d] with poorer prognosis, longer hospital stays[,] and an increased risk of death" for CF patients [1]. All species of BCC bacteria exhibit intrinsic resistance to multiple antibiotic classes due to efflux pumps, β-lactamases, trimethoprim-resistant dihydrofolate reductase, and lipopolysaccharide moieties that have been implicated in resistance [1]. Additionally, a *B. cepacia* clinical isolate has shown the ability to enter and survive within cultured human macrophages and epithelial cells [4]. This intracellular lifestyle establishes the host cell membrane as an additional

diffusional barrier to antibiotics, further contributing to the resistance of BCC pathogens. Due to these factors, BCC infections can be extremely challenging to treat, to the extent that 94% and 50% of *B. cenocepacia* and *B. multivorans* infections become chronic despite antimicrobial therapy, respectively [2]. There exists an unmet need for effective antimicrobial therapies against BCC pathogens, as a recent review identified a complete lack of high-quality studies investigating either therapies to eradicate BCC infections or to prevent or delay chronic BCC infections [2].

Nanoscale delivery vehicles constitute a modern approach to the challenge of antibiotic delivery for intracellular infections. Such technologies can improve the intracellular localization of antibiotics by guiding the drugs past complex biological barriers such as the host cell membrane [5,6]. Polyanhydride nanoparticles, synthesized from biodegradable copolymers with high biocompatibility [7–9], are internalized by the phagocytic cells targeted by BCC pathogens and distribute into intracellular niches wherein such pathogens reside [5]. By this mechanism, antibiotic-loaded polyanhydride nanoparticles have been shown to improve the *in vitro* activity of doxycycline of against intracellular *Brucella abortus* [5], and to improve the *in vitro and in vivo* performance of rifampicin against *Brucella melitensis* [10]. These nanoparticles have also been shown to achieve faster killing rates and lower effective concentrations against parasitic filarial worms than soluble drugs by co-delivering an antiparasitic drug and doxycycline, which targets an endosymbiotic bacterium of the worms [11]. Additionally, the antibiotic release kinetics from these nanoparticles can be tuned based on drug and polymer chemistry as well as nanoparticle size [12]. This controlled release, coupled with their passive targeting of intracellular niches, can

alter the absorption, distribution, metabolism, and excretion properties of the drug to maintain consistent selective pressure against pathogens.

While polyanhydride nanoparticles have demonstrated the potential to contribute improved therapies against bacteria, to date the identification of such formulations has relied on a traditional screening approach. This poses an immense feasibility challenge as the data space expands significantly from individual microbial susceptibility factors and drug physicochemical properties to now include polymer chemical and material properties as well as nanoparticle gross material properties. Hierarchical modeling offers a pragmatic solution to this problem, wherein key descriptors are identified and correlated to antimicrobial performance. Our group has previously used such an approach to develop a graph-theory based framework to predict release kinetics based on key polymer, drug, and nanoparticle physicochemical properties [12].

The focus of this work was to expand upon the existing framework by identifying polymer, drug, and nanoparticle properties that strongly influence the *in vitro* antimicrobial potency of individual nanoformulations. The major goal was the development of a predictive model to suggest untested nanoformulations or combinations of nanoformulations with high antimicrobial activity to improve screening efficiency. This would constitute an important step toward our long-term goal of developing predictive analytics frameworks to enable rational design of nanomedicines for therapeutic applications.

6.3 Materials & Methods

6.3.1 Materials

Monomer and polymer synthesis used sebacic acid (SA), triethylene glycol, 4-*p*-hydroxybenzoic acid, 1-methyl-2pyrrolidinone, and 1,6-dibromohexane purchased from MilliporeSigma (Burlington, MA), potassium carbonate, dimethyl formamide, toluene,

acetonitrile, acetic acid, sulfuric acid, N,N-demethylacetamide, and acetic anhydride from Thermo Fisher Scientific (Waltham, MA), and 4-*p*-fluorobenzonitrile from Apollo Scientific (Cheshire, U.K.). Methylene chloride, pentane, and hexane from Fisher Scientific were used in polymer purification and nanoparticle synthesis. ^{1}H NMR analysis was performed in deuterated chloroform from from Cambridge Isotope Laboratories (Andover, MA). Antibiotic payloads doxycycline (DOX), rifampicin (RIF), and gentamicin (GEN) were obtained from MilliporeSigma, meropenem (MEM) from Ark Pharm (Arlington Heights, IL) and ceftazidime (CAZ) from Acros Organics (Thermo Fisher Scientific). Drug quantification used UV-transparent microplates from Greiner Bio-One (Kremsmünster, Austria), HPLC-grade acetonitrile, methanol, and trifluoroacetic acid from Thermo Fisher Scientific, and phosphoric acid and *o*-phthaldialdehyde from Sigma-Aldrich. *Burkholderia cepacia* strain UCB 717 was obtained from BEI Resources, NIAID, NIH (Bethesda, MD).

6.3.2 Polymer and Particle Synthesis and Characterization

CPTEG and CPH diacids were synthesized as described previously[8,13,14]. 20:80 CPTEG:CPH [8], 20:80 CPH:SA [12], and 10:90 CPTEG:SA [15] copolymers were synthesized by melt condensation as described previously. Briefly, appropriate masses of monomers were added to a round bottom flask and acetylated in excess acetic anhydride at 125°C for 30 min. Excess acetic anhydride was removed from these prepolymers by rotary evaporation. CPTEG:CPH was polymerized for 6-8 h at <0.1 Torr to a number average molecular weight (M_n) of 5-10 kDa, while CPH:SA and CPTEG:SA polymers were polymerized for 80 min at 0.25 – 0.3 Torr to a M_n of 15-20 kDa. Polymers were purified by precipitation in chilled hexanes. Polymer composition and M_n were characterized by ^{1}H NMR spectra acquired on a Varian MR-400 (Varian, Inc., Palo Alto, CA) and thermal properties were characterized by DSC (Q2000, TA Instruments, New Castle, DE).

Antibiotic-loaded particles were synthesized using a previously described high-throughput flash nanoprecipitation method [12]. Briefly, polymer and drugs were dissolved/dispersed in methylene chloride and dispensed using a high-throughput, automated robot into 10 mL borosilicate tubes at a final polymer concentration of 20 mg/mL. The robot sonicated the mixed solutions and dispensed into 50 mL conical polypropylene tubes containing 45 mL hexanes (-10°C for CPTEG:CPH, room temperature for CPH:SA and CPTEG:SA) to precipitate the particles. Gentamicin-loaded particles were synthesized by conventional flash nanoprecipitation [12] as the antibiotic was too insoluble in methylene chloride to be dispensed with the robot. Multiple particle batches for each formulation were pooled and recovered by vacuum filtration. Scanning electron microscopy (SEM, FEI Quanta 250, Hillsboro, OR) was used to image all nano- particles, and size distributions were calculated using Fiji image analysis software [16] and the ParticleSizer plugin script for Fiji [17]. Particle ζ-potential was measured using a Zetasizer Nano (Malvern Instruments Ltd., Worcester, U.K.).

Particle release kinetics were characterized as described previously [12]. Briefly, 9-11 mg particles were dispersed in 0.5 mL phosphate buffered saline (PBS), and supernatants containing released drug were extracted at regular time points. After one week of release in PBS, 40 mM sodium hydroxide was added to rapidly degrade the polymer, freeing any remaining entrapped drug. Meropenem and ceftazidime in release and base extraction samples were quantified by RP-HPLC-UV (1200 series, Agilent Technologies, Santa Clara, CA). For brevity, HPLC protocol details are provided in Supplemental Table 6.1. Doxycycline and rifampicin were quantified by UV spectrophotometry in UV-transparent 96-well plates using absorbance at 350 and 333 nm, respectively (SpectraMax M3, Molecular

Devices, San Jose, CA). Gentamicin samples were derivatized with *o*-phthaldialdehyde [18] prior to quantification using absorbance at 340 nm. Encapsulation efficiency (EE) was calculated from the cumulative sum of drug mass released in PBS and base extraction samples [12]. In some samples >100% EE was observed, likely due to greater masses of polymer than payload being lost during particle synthesis [12]. For these situations, EE is interpreted as a "normalized EE" of 100%. Drug release kinetics are presented as fraction released, where the cumulative drug mass release is normalized by the total encapsulated drug mass. Release kinetics were parameterized for the informatics analysis by calculating the fraction released at 2 h and 24 h (burst release) and the slope of the release profile at 2 h and 24 h using the nearest neighbors in the time domain.

6.3.3 Antimicrobial Susceptibility Assays

Growth inhibition assays followed CLSI guidelines for broth microdilution antimicrobial susceptibility testing. Cultures of *B. cepacia* UCB 717 in Mueller Hinton Media were diluted to an OD_{600} value of 0.5. Fifty µL aliquots of a 1:100 dilution of this solution were added to well plates, and 50 µL of the treatment was added to yield a final volume of 100 µL. Resazurin reduction was used to quantify changes in bacterial viability. From these viability curves, half maximal inhibitory concentrations (IC_{50}) were extracted for soluble drug controls and nanoparticle treatments. Nanoparticle IC_{50} values were normalized by EE to reflect the maximal potential dose from nanoparticles regardless of release kinetics. As we are interested in identifying nanoparticle candidates that improve antibiotic activity, the Log_2 ratio of the nanoparticle to soluble IC_{50} was defined as the objective function for antimicrobial performance.

6.3.4 Informatics Analysis

Log_2 ratios for individual nanoparticle formulations and cocktails, along with polymer, drug, and nanoparticle properties, were normalized and mean centered. Three different informatics approaches were integrated in a hybrid approach to identify interesting features in the data, develop structure-function relationships, and model nanoparticle antimicrobial performance. Principal component analysis (PCA), a linear manifold learning approach, was used to reduce the dimensionality of the data to analyze the impact of individual descriptors on nanoparticle performance [19–21]. Through eigenvector decomposition, PCA defines composite orthogonal axes that are constructed from linear combinations of descriptors, maximizing the variance captured within a minimal set of these axes (termed principal components or PCs). The original data are decomposed into two matrices: the loadings and scores. Loadings describe the contributions of input descriptors to each PC, while scores describe the objective function (i.e. Log_2) of each formulation or cocktail in the PC space. From the loadings matrix, the variable importance projection (VIP) was calculated for each descriptor using Eq. 1. In this case, T = Log_2 ratio, and x = 2 because two PCs captured >80% of the variance. VIP analysis provides an estimation of the correlation of individual descriptors to the objective function.

Eq. 1 $$VIP = \frac{PC_x^T \times PC_x^i}{\sum PC_x^T \times PC_x^i}$$

PC regression modeling of Log_2 values was found to be insufficient (data not shown), likely due to nonlinearity which is lost in the Euclidean decomposition of PCA. Graph analysis, using the Isomap algorithm, was used for nonlinearity-preserving dimensional reduction to parameterize the descriptor space [22,23]. This nonlinear manifold learning approach functions on the principal that for data lying on a non-linear manifold in high-

dimensional space, points that are far apart by geodesic distances might appear closely related by Euclidean distance [22]. Graph theory generates a graph connecting closely related data points along the high-dimensional manifold via geodesic distances, and then projects onto a low-dimensional manifold. The manifold unravels in two or three dimensions, allowing visualization of the curvilinear relationships between formulations in high-dimensional space as connecting lines in the low-dimensional projection. Therefore, graph analysis yields composite dimensions or parameters (in this case, five) based on nonlinear combinations of descriptors. Finally, a multilinear regression using these parameters was derived for modeling Log_2 values of nanoparticles and cocktails.

6.4 Results

6.4.1 Particle Library Synthesis and Characterization

For this analysis, we focused on nano- and microparticles synthesized from CPTEG, CPH, and SA copolymers (Figure 6.1a-c). Such nanoparticles demonstrate high internalization in phagocytic cells that are infected by *Burkholderia spp* [5,15,24], localize in intracellular compartments where these bacteria reside [24,25], and have been shown to improve the antimicrobial activity of encapsulated small molecule drugs [5,10,11]. Five antibiotics with orthogonal antimicrobial mechanisms and a range of physicochemical properties were used in these studies, namely rifampicin (transcription inhibition), doxycycline and gentamicin (translation inhibition), and meropenem and ceftazidime (cell wall synthesis inhibition) (Figure 6.1d-h). These antibiotics are all FDA-approved and have well-characterized pharmacokinetic, pharmacodynamic, and structural data available on the DrugBank database [26]. Meropenem and ceftazidime are commonly administered in the acute phase of *Burkholderia pseudomallei* treatment, while doxycycline was included in a

cocktail along with chloramphenicol and co-trimoxazole that served as the primary acute phase treatment until 1985 [27].

These antibiotics were encapsulated within polyanhydride nano- and microparticles using high-throughput flash nanoprecipitation method at 5% and 10% loadings (w/w%) [28,29]. Gentamicin was too insoluble in methylene chloride for this high-throughput method, and was synthesized by conventional flash nanoprecipitation. This particle library was analyzed for size distributions, ζ-potential, release kinetics, and EE (Supplementary Figure 6.1, Table 6.1). Particle size was primarily influenced by polymer chemistry, with CPTEG:CPH and CPH:SA forming nanoparticles with mean diameters of approximately 150 nm and 500 nm. CPTEG:SA formed microparticles with mean diameters of approximately 1.3 μm. A moderately negative zeta potential was observed for nearly all particle formulations. Gentamicin formulations tended to have near-zero zeta potentials.

Release kinetics from the particle library are shown in Supplementary Figure 6.2. All antibiotics except rifampicin showed burst-dominated release kinetics. CPTEG:CPH–rifampicin formulations showed a high burst followed by a trickling sustained release through two weeks. CPTEG:SA–rifampicin formulations showed a similarly high burst followed by a steady sustained release through one week. CPH:SA–rifampicin formulations showed the most sustained-release of all chemistries tested, characterized by a moderate (<40%) burst followed by near zero-order release through two weeks.

6.4.2 Antimicrobial Screening

Broth microdilution antimicrobial susceptibility assays with *Burkholderia cepacia* strain UCB 717 were used to characterize nanoparticle efficacy. Resazurin reduction was used to calculate the IC_{50} for nanoparticles and soluble drug controls. Nanoparticles show lower effective concentrations, and improved antimicrobial activity relative to soluble

controls at negative $\log_2$ ratios. These formulations are referred to as "hits". Conversely, a positive Log_2 ratio corresponds with poorer nanoparticle activity compared to soluble drug. For example, if the soluble drug IC_{50} is 10 μg/mL and the nanoparticle IC_{50} is 5 μg/mL, the Log_2 ratio would be –1.

Single formulation antimicrobial activity is presented in Table 6.2. Strong hits (defined as $Log_2 < –0.5$) tended to occur in ceftazidime and meropenem-based nanomedicines. For ceftazidime, this may be related to the relatively higher soluble IC_{50} compared to the other drugs. Doxycycline-based nanomedicines produced a mix of weaker ($–0.5 < Log_2 < 0$) hits and non-hits ($Log_2 > 1$), and showed the greatest inter-replicate variability of the four drugs tested. Rifampicin nanoparticles performed the worst, as no formulation showed improved activity over soluble drug. This is likely due to the delayed release kinetics in rifampicin nanoparticles (Supplementary Figure 6.2a) rather than increased resistance to the drug, as the soluble IC_{50} values for rifampicin are similar to doxycycline and meropenem. With respect to particle chemistry, CPH:SA–meropenem formulations showed a stronger tendency toward improved activity compared to CPTEG:CPH–meropenem formulations. By contrast, all other drugs showed comparable Log_2 values across particle chemistries. Based on these results, ceftazidime-, meropenem-, and doxycycline-based nanomedicines show the potential to improve antimicrobial activity compared to soluble drug.

Treating resistant infections with antibiotics using orthogonal antimicrobial mechanisms could provide improved killing and reduce the risk of persistence. Dual drug nanomedicine cocktails at differing drug mass ratios were tested and compared to soluble drug mixes (Table 6.3). Hits were exclusively composed of cocktails of ceftazidime-,

meropenem-, and doxycycline-based nanomedicines at 1:1 drug ratios. Altering the mass ratio of these antibiotics from 1:1 tended to reduce the antimicrobial performance, producing non-hits. However, some of these altered drug ratios reduced the soluble IC_{50} value. No nanomedicine cocktail including rifampicin produced a hit.

Paired doxycycline and rifampicin were highly represented in the ten lowest soluble cocktail IC_{50} values. This supports the above hypothesis that orthogonal antibiotic mechanisms can improve antimicrobial activity, as rifampicin and doxycycline inhibit bacterial transcription and translation, respectively. By contrast, pairs of doxycycline, meropenem, and ceftazidime were highly represented in the ten highest soluble cocktail IC_{50} values. For meropenem and ceftazidime, this result may be due to similar mechanisms of action, namely inhibition of cell wall biosynthesis. In accordance with these soluble drug cocktail results, the ten nanomedicine cocktails with the lowest IC_{50} values tended to include 20:80 CPTEG:CPH–DOX and 20:80 CPTEG:CPH–RIF nanoparticles. Drug pairs of rifampicin with either meropenem or ceftazidime was strongly represented in the ten highest nanomedicine cocktail IC_{50} values. No strong particle chemistry effect was observed in these ten nanomedicine cocktails with high IC_{50} values.

From these results in single formulations and nanomedicine cocktails, we conclude that both drug and particle chemistry influence antimicrobial activity in *B. cepacia* UCB 717. However, beyond gross generalizations about certain high- or low-performing drugs or particle chemistries, it is difficult to draw conclusions regarding the underlying reasons these formulation inputs are performing well. This means expanding our particle library outside the drug and particle chemistry dataspace represented in Table 6.2 and 6.3 requires repetition of the physical screening of these new formulations. This would require a massive endeavor

particularly for the nanomedicine cocktails, as the dataspace significantly expands with each new formulation. Accordingly, we sought to use these antimicrobial activity data to define QSPRs (expand) and enable virtual exploration of potential new nanomedicine-based single formulations and cocktails.

6.4.3 Identifying Factors Influencing Antimicrobial Performance

A hierarchical modeling approach was used to define these QSPRs, wherein key descriptors are identified based on correlations to nanomedicine performance and used as inputs to model antimicrobial activity. A descriptor set was defined from polymer material characteristics, polymer chemical structure (based on molecular descriptors describing molar average monomers previously used by Li *et al.*) [30], drug physicochemical properties (acquired from the Drugbank database) [26], nanoparticle material characteristics, and parameterized release kinetics and encapsulation efficiency (Table 6.4).

To characterize the relative influence of these descriptors on antimicrobial activity in *B. cepacia*, we performed a PCA. This analysis compressed the 58 descriptor dimensions into composite axes (or PCs). In this case, two PCs captured 80.51% of the variability. PCs are ordered by decreasing variability captured, with PC1 capturing 59.97% and PC2 capturing 20.56%. The contributions of each descriptor (Table 6.4) to each PC are plotted in a loadings plot (Figure 6.2), where each point is a different descriptor. Polymer material characteristics and polymer chemical structure adhered primarily along PC1. Nanoparticle material descriptors fell primarily along PC1, with a minor contribution to PC2. Drug physicochemical properties and nanoparticle release kinetics descriptors scattered across both PC1 and PC2. As the previous descriptor groups lied along PC1, PC2 was primarily composed of these drug physicochemical and release kinetics descriptors. All input descriptor groups contributed to PC1. The objective function, the Log_2 ratio of nanoparticle

IC_{50} to Soluble IC_{50}, did not adhere to either PC axis, indicating antimicrobial activity is influenced by all groups of polymer, drug, and nanoparticle physicochemical properties. While unsurprising, this result matches our conclusion from section 6.4.2.

The Log_2 values of individual particle formulations and cocktails are plotted in the compressed dimensional space in a scores plot (Figure 6.3). As the Log_2 ratio was located in the bottom left quadrant in the loadings plot (Figure 6.2), more negative Log_2 values (and corresponding improved antimicrobial performance relative to soluble drug) would follow a trajectory toward the upper right corner of the scores plot. Similarly, formulations with worse antimicrobial performance relative to soluble would fall to the bottom left of the plot. Nanomedicine cocktails tended to fall closer to the top right corner than individual nanomedicine formulations, indicating that cocktails provide improved antimicrobial activity over individual formulations.

To assess the relative contributions of individual descriptors to the antimicrobial performance, a VIP analysis was performed. The correlation of each descriptor (Table 6.4) to the objective function was calculated from the loading matrix (Figure 6.4). In this plot, positive values indicate positive correlation (worse antimicrobial performance) and negative values indicate inverse correlation (better antimicrobial performance) with Log_2 ratio. Of the 57 descriptors included in the analysis, 21 descriptors were highly correlated to the objective function. Polymer M_n and T_g (#2 & 3, respectively) were positively correlated with Log_2 ratio. Within polymer chemical structural descriptors, only N_group (#17) was identified. It was inversely correlated with Log_2 ratio. Of drug physicochemical properties, LogP1, LogP4, pKa (strongest acid), pKa (strongest base), physiological charge, and polarizability (#30, 33, 35–37, 43) were positively correlated, while water solubility 2 and LogP3 (#31–32) were

inversely correlated with Log_2 ratio. Within the nanoparticle material characteristics group, all nanoparticle size descriptors except count geometrical mean diameter (#45–48) were strongly positively correlated and zeta potential (#49) was inversely correlated with Log_2 ratio. For release kinetics, fraction of drug released, fractional release slope, and mass released at 24 hours (#53, 55, 57) were positively correlated, while fraction released and fraction release slope at two hours (#52, 54) were inversely correlated with Log_2 ratio. These results indicate that faster, more burst-heavy release kinetics provide better nanomedicine antimicrobial performance than slower, sustained release kinetics.

Hierarchical modeling requires the definition of a minimal descriptor space to maximize robustness. VIP analysis enables the identification of descriptors that contribute significant information, while also identifying descriptors that are correlated. This latter function allows the exclusion of variables that fail to contribute sufficient orthogonal information to other variables. Accordingly, polymer T_g, polymer backbone N_{group}, drug LogP3, nanoparticle diameter and zeta potential, the fraction drug released at two hours, and the mass of drug released at 24 hours (#3, 17, 32, 46, 49, 54, 57) were identified as key descriptors associated with particle antimicrobial performance.

6.4.4 Modeling Nanomedicine Antimicrobial Performance

The relationships between the particle input descriptors (Tables 6.1 & 6.4) and antimicrobial activity (Tables 6.2-6.3) are extensively non-linear. This nonlinearity limits the utility of linear techniques, like principal component regression, for modeling these data. Neural networks have been used to capture such nonlinearity; however, these models need to be trained on hundreds to thousands of points for robust predictions. We used a graph theory-based modeling approach, which has the advantages of capturing nonlinear data structures while avoiding the overfitting problems of neural networks within smaller data sets.

A graph analysis was performed on the polymer, drug, and particle descriptors for all formulations and cocktails in the library, including those without IC_{50} or Log_2 data, compressing these 57 descriptors into five composite dimensions. A projection of the first two dimensions are shown in Figure 6.5, wherein each point is a particle formulation or cocktail. The graph analysis preserves curvilinear distances between formulations by projecting the geodesic distances along the higher-dimensional non-Euclidean manifold onto Euclidean distances in the lower-dimensional (Euclidean) representation [22]. In this map, similar formulations or cocktails are connected by a line, whose Euclidean distance represents the geodesic distance along the higher-dimensional manifold. This connectivity was used to interrogate design pathways between formulations, for example examining the impact of changing the antibiotic payload or polymer chemistry on antimicrobial performance.

Beyond analyzing formulation connectivity, the nonlinearity-preserving dimensionality reduction offered by graph theory can be used to develop a multilinear regression modeling antimicrobial performance for individual particle formulations and cocktails (Figure 6.6). Inclusion of all 57 input descriptors into this model reduces the risk of over-fitting the small data set. Formulations and cocktails without nanomedicine IC_{50} values were included in the graph analysis to create a parameter space that can be used to predict the performance of such untested systems. The Log_2 value model was fairly accurate within the training data, with an R^2 value of 70.8%. Cross-validation indicated reasonable robustness. The model is limited by a relatively outlying cocktail ({20:80 CPH:SA 10% CAZ} : {20:80 CPH:SA 10% RIF} 1:1) which has a Log_2 value of 4.498. Elimination of this outlier improves the model accuracy to 77.8%. However, the model still predicted this cocktail to be

have the highest Log_2 value, which matches experimental observations. Additionally, variability between replicates of some samples contributed to the error of the model. For example, the {20:80 CPH:SA 5% CAZ} : {20:80 CPH:SA 5% DOX}1:1 cocktail had observed Log_2 values of 1.80 and 0.17 and a predicted Log_2 value of 0.354. Given these constraints, the seemed to perform well for the training data. By predicting Log_2 ratios of individual nanomedicine formulations and cocktails, the graph theory-based model enables virtual exploration of untested treatments against *B. cepacia*.

6.4.5 Model Validation

To validate the use of this model to predict the performance of untested formulations and cocktails, out-of-library testing was performed. Four new nanomedicine formulations encapsulating a new drug chloramphenicol (CAM) within 20:80 CPH:SA and 10:90 CPTEG:SA nanoparticles were synthesized and evaluated for their release kinetics (Supplementary Figure 6.3). Importantly, chloramphenicol contains two chlorine atoms and a nitro group (Supplementary Figure 6.4), which were not present in the training data set. The model was used to predict Log_2 values for these previously untested formulations (Table 6.5). The model predicted that 20:80 CPH:SA 10% chloramphenicol would have a Log_2 value of 0.874 (near half the potency of soluble drug), while the measured Log_2 value was 0.357. This formulation showed the largest deviation from predictions of the four, however the model predicted it as a non-hit. The model predicted the remaining three formulations to have slightly negative Log_2 values (i.e. weak hits, with slightly lower IC_{50} than soluble drug) (Table 6.5). Experimental results matched these predictions more closely than the previous formulation, with measured Log_2 values between -0.10 and +0.10. 10:90 CPTEG:SA 10% chloramphenicol was the only formulation to have a different measured Log_2 sign than the predictions; however, this formulation had the predicted Log_2 value closest to zero. While the

model had some error in its Log_2 predictions, it successfully predicted the relative performance of these four out-of-library formulations. This justifies the use of this model to rank-order particle candidates for antimicrobial testing. Overall, based on the model predictions we would have expected these out-of-library candidates to provide either marginal improvements or worse performance than soluble drug, and would have assigned them a low priority for testing. Indeed, such a conclusion was validated by experimental results.

We also sought to use the model to predict hits and non-hits from within a pool of potential nanoparticle cocktails. Previously untested 10:90 CPTEG:SA microparticles encapsulating ceftazidime, meropenem, or doxycycline were paired with either previously tested nanoparticle formulations or the new chloramphenicol formulations at 1:1 drug ratios, for a total of 33 potential cocktails. Predicted Log_2 ratios for these potential cocktails were generated using the model and three cocktails, including two predicted well-performing (#12 and #25) and one poor-performing (#32) were tested against *B. cepacia* (Table 6.5 and Supporting Table 6.2) in experimental studies. The predicted Log_2 values for #12 and #25 (-1.683 and -1.066, respectively) were in good agreement with their measured values of -1.829 and -0.886, respectively. The model showed more error for the poor-performing #33, with a predicted Log_2 value of 1.968 and an experimental value of 3.016. Overall, the model successfully predicted the hit and non-hit status of untested particle cocktails. As seen with the new formulations, the model successfully predicted the relative performance of the experimentally validated cocktails, supporting this model's capability to rank candidate nanomedicine cocktails for antimicrobial testing.

6.5 Discussion

Antimicrobial resistant (AR) infections constitute an existential threat to the modern healthcare system. The 2019 CDC report on antimicrobial resistance highlighted the fact that we are living in a post-antibiotic era [32]. The report underscored the need for new approaches to kill AR bacteria and methods to protect the potency of the existing antibiotic supply [32]. Nanomedicines based on polyanhydride nanoparticles have demonstrated the capacity to overcome certain deficiencies of conventional antibiotic therapies. By guiding antibiotics past challenging biological barriers, they have been shown to improve the activity of encapsulated antimicrobials [5,10,11,33]. This function could be exploited to bring the potency of underused antibiotics into therapeutic significance, potentially contributing new, orthogonal therapies. Alternately, this capacity could be leveraged to repurpose antibiotics that are currently limited due to resistance.

Conventional antibiotics also pose challenges from a patient compliance perspective. High doses of antibiotics are currently used to overcome the host cell barrier for intracellular bacteria, increasing the risk of toxicity [34,35]. The high local dose generated by nanomedicines could reduce the systemic dose needed [33], reducing the risk of side effects. Antibiotic regimens tend to be frequent, lengthy, and many are invasive. Polyanhydride nanoparticles' ability to package multiple drugs [11] coupled with their controlled release [12,36] and needle-free capabilities [37] could ease compliance for patients. Improving adherence to antibiotic regimens could slow the development of resistance [38]. By contributing new therapies for AR bacteria and improving compliance, nanomedicines have the potential contribute to the next generation of antimicrobial therapies.

Unfortunately, conventional high-throughput screening approaches used to identify promising antimicrobial compounds are not a realistic solution for finding lead nanomedicine

candidates. The massive dataspace occupied by these nanomedicine formulations makes screening antimicrobial against biosafety level 1–2 pathogens like *B. cepacia* impractical, even more so for high biosafety level organisms like the potential bioweapons *Burkholderia pseudomallei* and *mallei*. Data analytics approaches, like the hybrid informatics hierarchical modeling approach used herein, could improve the efficiency of screening efforts by suggesting candidates with high-likelihood of success based on trends from existing screens, which could be validated experimentally. This approach has the benefit of improving predictive accuracy over time, as new data can be incorporated to iteratively refine the model.

In this work, a library of polyanhydride nanoparticles with varying polymer chemistry and payload type were synthesized (Figure 6.1 and Supporting Figure 6.1), characterized for release kinetics (Supplementary Figure 6.2), and evaluated for antimicrobial activity against *B. cepacia* (Tables 6.2–6.3). QSPRs were developed by analyzing the correlations of polymer, drug, and nanoparticle descriptors to antimicrobial activity using VIP analysis (Figure 6.4). Twenty-one descriptors, comprising polymer material characteristics and chemical structure, drug physicochemical properties, and nanoparticle material and release kinetics factors, were strongly correlated with nanomedicine antimicrobial performance. While it is unsurprising that antimicrobial performance is a function of such a complex mix of properties, this result motivates the use of nonlinear manifold learning models, like graph theory, to deconvolute such complexity to capture subtle trends that impact performance. Of note, VIP analysis identified that nanomedicines with faster, more burst-heavy release kinetics provide better antimicrobial activity than slower, sustained release formulations. This provides evidence for our hypothesis that faster release kinetics would be more

efficacious against AR bacteria by providing a rapid, suppressive pressure against growth, given adequate nanoparticle localization.

Graph theory was used to define a set of composite input parameters, based on dimensional reduction of polymer, drug, and particle descriptors, which were used to model the relative antimicrobial activity of single particle formulations and particle cocktails compared to soluble drug. This model showed good accuracy within the training data set, and successfully predicted whether candidate formulations or cocktails would significantly improve antimicrobial activity, provide no improvement in activity, or provide worse activity than soluble drug. The model also successfully predicted the relative performance of these untested formulations and cocktails in relation to each other. To our knowledge, this is the first time an informatics approach has successfully predicted the antimicrobial activity of antibiotic nano- and micro-carriers. Because the input descriptor space is defined from generalized physicochemical characteristics describing the nanocarrier and drug payload (Table 6.4), this modeling approach could easily incorporate new systems that are not represented in the training data set. For example, meropenem has several closely related chemical cousins within the carbapenem antibiotic family. The model could be used to identify the carbapenem derivative with the highest likelihood for nanoparticle improvement in activity. Alternatively, other carrier chemistries, such as altered compositions of CPH, CPTEG, and SA copolymers or poly(lactic-co-glycolic acid) (PLGA), could be virtually explored for promising antimicrobial activity using this modeling approach.

We can only make confident quantitative predictions for systems that are represented within the training data space. There are likely systems with unique behavior outside this space which this approach will fail to quantitatively describe. This was observed, to some

extent, with the higher error in the out-of-library testing compared to the training data set. However, the objective of this approach for systems containing elements and chemical groups not in our training data is to identify polymer and drug combinations that have promising characteristics. This qualitative feature allows this approach to prioritize chemical spaces where more experimentation is needed, whose results can be iteratively fed back into the analysis to refine the model.

Given these results, we propose a framework for rational design and selection of nanomedicine formulations and cocktails with improved antibiotic potency (Scheme 1). In the first step, nanomedicine libraries are synthesized from varying polymer chemistries and drug types via high-throughput methods, and the particles are evaluated for size distribution, zeta potential, and release kinetics. These nanomedicine candidates, along with cocktailed combinations thereof at multiple drug ratios, are then fed into the multilinear graph theory to generate predicted Log_2 values. Formulations with Log_2 values less than –0.5 (nanomedicine IC_{50} < 70% soluble IC_{50}) can be discarded, and such cocktails can be disregarded. The formulations and cocktails with the most negative Log_2 values can be prioritized for *in vitro* minimum inhibitory concentration testing, ideally providing new lead candidates for testing in more complex models. A feedback loop provides iterative improvement to the model and gradual optimization of candidates when formulations or cocktails fail to meet the efficacy threshold.

This framework is designed to be modular, and could be interfaced with predictive frameworks for other performance criteria like drug release kinetics [12], cellular internalization for intracellular bacteria, and intracellular viability. This methodology uses publicly available drug chemistry information and standard polymer and nanoparticle

characterization techniques; therefore it could readily incorporate other nanocarrier platforms and antibiotic classes. This latter function could leverage the massive public and corporate investment [39], regardless of clinical approval outcome, into antibiotic development to provide new therapies against resistant bacteria like *B. cepacia*. Furthermore, identification of nanomedicine formulations and cocktails with improved drug activity could allow repurposing of antibiotics limited by resistance. In these ways, this hybrid analytics framework contributes an important step toward the rational design of antimicrobial nanomedicines to counter resistant infections.

6.6 Conclusions

A hybrid informatics approach was used to identify polymer, drug, and nanoparticle properties that determine the antimicrobial activity of nanomedicines against the opportunistic, intrinsically resistant pathogen *Burkholderia cepacia*, and to develop a model for predicting nanomedicine performance. Polymer T_g, polymer backbone N_{group}, drug LogP3, nanoparticle mass mean diameter and zeta potential, the fraction drug released at two hours, and the mass of drug released at 24 hours were identified as key descriptors associated with particle antimicrobial performance. Graph analysis provided dimensionality reduction of the descriptor space while preserving nonlinear descriptor-property relationships, enabling accurate modeling of nanomedicine performance. Out-of-library validation confirmed the model's accuracy, supporting its use in prioritizing candidate formulations and cocktails for *in vitro* testing based on predicted performance. This hybrid analytics approach provides an important step toward the development of a framework to rationally design nanomedicines to counter antimicrobial resistant infections by selecting appropriate carriers and payloads for improved antibiotic potency.

6.7 References

[1] E. Mahenthiralingam, T.A. Urban, J.B. Goldberg, The multifarious, multireplicon Burkholderia cepacia complex, Nat. Rev. Microbiol. 3 (2005) 144–156. https://doi.org/10.1038/nrmicro1085.

[2] K.H. Regan, J. Bhatt, Eradication therapy for burkholderia cepacia complex in people with cystic fibrosis, Cochrane Database Syst. Rev. 2019 (2019). https://doi.org/10.1002/14651858.CD009876.pub4.

[3] P. Drevinek, E. Mahenthiralingam, Burkholderia cenocepacia in cystic fibrosis: Epidemiology and molecular mechanisms of virulence, Clin. Microbiol. Infect. 16 (2010) 821–830. https://doi.org/10.1111/j.1469-0691.2010.03237.x.

[4] D.W. Martin, C.D. Mohr, Invasion and intracellular survival of Burkholderia cepacia, Infect. Immun. 68 (2000) 24–29. https://doi.org/10.1128/IAI.68.6.3792-3792.2000.

[5] Y. Phanse, P. Lueth, A.E. Ramer-Tait, B.R. Carrillo-Conde, M.J. Wannemuehler, B. Narasimhan, B.H. Bellaire, Cellular Internalization Mechanisms of Polyanhydride Particles: Implications for Rational Design of Drug Delivery Vehicles, J. Biomed. Nanotechnol. 12 (2016) 1544–1552. https://doi.org/10.1166/jbn.2016.2259.

[6] K.A. Ross, T.M. Brenza, A.M. Binnebose, Y. Phanse, A.G. Kanthasamy, H.E. Gendelman, A.K. Salem, L.C. Bartholomay, B.H. Bellaire, B. Narasimhan, Nano-enabled delivery of diverse payloads across complex biological barriers, J. Control. Release. 219 (2015) 548–559. https://doi.org/10.1016/j.jconrel.2015.08.039.

[7] E. Shen, M.J. Kipper, B. Dziadul, M.K.M.-K. Lim, B. Narasimhan, Mechanistic relationships between polymer microstructure and drug release kinetics in bioerodible polyanhydrides, J. Control. Release. 82 (2002) 115–125. https://doi.org/10.1016/S0168-3659(02)00125-6.

[8] M.P. Torres, B.M. Vogel, B. Narasimhan, S.K. Mallapragada, Synthesis and characterization of novel polyanhydrides with tailored erosion mechanisms, J. Biomed. Mater. Res. - Part A. 76 (2006) 102–110. https://doi.org/10.1002/jbm.a.30510.

[9] L. Huntimer, A.E. Ramer-Tait, L.K. Petersen, K. a. Ross, K. a. Walz, C. Wang, J. Hostetter, B. Narasimhan, M.J. Wannemuehler, Evaluation of Biocompatibility and Administration Site Reactogenicity of Polyanhydride-Particle-Based Platform for Vaccine Delivery, Adv. Healthc. Mater. 2 (2013) 369–378. https://doi.org/10.1002/adhm.201200181.

[10] P. Lueth, S.L. Haughney, A.M. Binnebose, A.S. Mullis, N. Peroutka-Bigus, B. Narasimhan, B.H. Bellaire, Nanotherapeutic provides dose sparing and improved antimicrobial activity against Brucella melitensis infections, J. Control. Release. 294 (2019) 288–297. https://doi.org/10.1016/j.jconrel.2018.12.024.

[11] A.M. Binnebose, S.L. Haughney, R. Martin, P.M. Imerman, B. Narasimhan, B.H. Bellaire, Polyanhydride Nanoparticle Delivery Platform Dramatically Enhances Killing of Filarial Worms, PLoS Negl. Trop. Dis. 9 (2015) e0004173. https://doi.org/10.1371/journal.pntd.0004173.

[12] A.S. Mullis, S.R. Broderick, A.M. Binnebose, N. Peroutka-Bigus, B.H. Bellaire, K. Rajan, B. Narasimhan, Data Analytics Approach for Rational Design of Nanomedicines with Programmable Drug Release, Mol. Pharm. 16 (2019) 1917–1928. https://doi.org/10.1021/acs.molpharmaceut.8b01272.

[13] E. Shen, R. Pizsczek, B. Dziadul, B. Narasimhan, Microphase separation in bioerodible copolymers for drug delivery, Biomaterials. 22 (2001) 201–210. https://doi.org/10.1016/S0142-9612(00)00175-7.

[14] A. Conix, Poly[1,3-bis(p-carboxyphenoxy)-propane anhydride], Macromol. Synth. 2 (1966) 95–98.

[15] S.M. Kelly, A. Mitra, S. Mathur, B. Narasimhan, Synthesis and characterization of novel rapidly-degrading polyanhydrides as vaccine adjuvants, ACS Biomater. Sci. Eng. (2019) Submitted.

[16] J. Schindelin, I. Arganda-Carreras, E. Frise, V. Kaynig, M. Longair, T. Pietzsch, S. Preibisch, C. Rueden, S. Saalfeld, B. Schmid, J.-Y.Y. Tinevez, D.J. White, V. Hartenstein, K. Eliceiri, P. Tomancak, A. Cardona, Fiji: an open-source platform for biological-image analysis, Nat. Methods. 9 (2012) 676–682. https://doi.org/10.1038/nmeth.2019.

[17] T. Wagner, J. Eglinger, ParticleSizer, (2017). https://doi.org/http://doi.org/10.5281/zenodo.820296.

[18] J. Gubernator, Z. Drulis-Kawa, A. Kozubek, A simply and sensitive fluorometric method for determination of gentamicin in liposomal suspensions, Int. J. Pharm. 327 (2006) 104–109. https://doi.org/10.1016/j.ijpharm.2006.07.039.

[19] S.R. Broderick, C. Suh, J. Provine, C.S. Roper, R. Maboudian, R.T. Howe, K. Rajan, Application of principal component analysis to a full profile correlative analysis of FTIR spectra, Surf. Interface Anal. 44 (2012) 365–371. https://doi.org/10.1002/sia.3813.

[20] M. Ashton, R.G. Hennig, S.R. Broderick, K. Rajan, S.B. Sinnott, Computational discovery of stable M2AX phases, Phys. Rev. B. 94 (2016) 054116. https://doi.org/10.1103/PhysRevB.94.054116.

[21] L. Ericksson, T. Byrne, E. Johansson, J. Trygg, C. Vikstrom, Multi- and megavariate data analysis : basic principles and applications, Umetrics Ab, Umea, 2001.

[22] J. Tenenbaum, V. Silva, J. Langford, A Global Geometric Framewok for Nonlinear Dimensionality Reduction, Science (80-.). 290 (2000) 2319–2323.

[23] S. Srinivasan, S.R. Broderick, R. Zhang, A. Mishra, S.B. Sinnott, S.K. Saxena, J.M. LeBeau, K. Rajan, Mapping Chemical Selection Pathways for Designing Multicomponent Alloys: An informatics framework for materials design, Sci. Rep. 5 (2015) 1–8. https://doi.org/10.1038/srep17960.

[24] B.D. Ulery, Y. Phanse, a. Sinha, M.J. Wannemuehler, B. Narasimhan, B.H. Bellaire, Polymer chemistry influences monocytic uptake of polyanhydride nanospheres, Pharm. Res. 26 (2009) 683–690. https://doi.org/10.1007/s11095-008-9760-7.

[25] B.D. Ulery, L.K. Petersen, Y. Phanse, C.S. Kong, S.R. Broderick, D. Kumar, A.E. Ramer-Tait, B. Carrillo-Conde, K. Rajan, M.J. Wannemuehler, B.H. Bellaire, D.W. Metzger, B. Narasimhan, Rational Design of Pathogen-Mimicking Amphiphilic Materials as Nanoadjuvants, Sci. Rep. 1 (2011) 1–9. https://doi.org/10.1038/srep00198.

[26] D.S. Wishart, Y.D. Feunang, A.C. Guo, E.J. Lo, A. Marcu, J.R. Grant, T. Sajed, D. Johnson, C. Li, Z. Sayeeda, N. Assempour, I. Iynkkaran, Y. Liu, A. MacIejewski, N. Gale, A. Wilson, L. Chin, R. Cummings, Di. Le, A. Pon, C. Knox, M. Wilson, DrugBank 5.0: A major update to the DrugBank database for 2018, Nucleic Acids Res. 46 (2018) D1074–D1082. https://doi.org/10.1093/nar/gkx1037.

[27] D. Dance, Treatment and prophylaxis of melioidosis, Int. J. Antimicrob. Agents. 43 (2014) 310–318. https://doi.org/10.1016/j.ijantimicag.2014.01.005.

[28] J.T. Goodman, A.S. Mullis, L. Dunshee, A. Mitra, B. Narasimhan, Automated High-Throughput Synthesis of Protein-Loaded Polyanhydride Nanoparticle Libraries, ACS Comb. Sci. 20 (2018) 298–307. https://doi.org/10.1021/acscombsci.8b00008.

[29] A.S. Mullis, S.J. Jacobson, B. Narasimhan, High-throughput synthesis and screening of rapidly-degrading polyanhydride nanoparticles, ACS Comb. Sci. (2019) Submitted.

[30] X. Li, L. Petersen, S. Broderick, B. Narasimhan, K. Rajan, Identifying Factors Controlling Protein Release from Combinatorial Biomaterial Libraries via Hybrid Data Mining Methods, ACS Comb. Sci. 13 (2011) 50–58. https://doi.org/10.1021/co100019d.

[31] J. Bicerano, Prediction of polymer properties, 2nd ed., Marcel Dekker, Inc., 1996.

[32] CDC, Antibiotic Resistance Threats in the United States, Atlanta, GA, U.S. Dep. Heal. Hum. Serv. CDC. (2019). https://doi.org/CS239559-B.

[33] R.Y. Pelgrift, A.J. Friedman, Nanotechnology as a therapeutic tool to combat microbial resistance, Adv. Drug Deliv. Rev. 65 (2013) 1803–1815. https://doi.org/10.1016/j.addr.2013.07.011.

[34] G. Pappas, P. Papadimitriou, L. Christou, N. Akritidis, Future trends in human brucellosis treatment, Expert Opin. Investig. Drugs. 15 (2006) 1141–1149. https://doi.org/10.1517/13543784.15.10.1141.

[35] R. Lang, B. Shasha, E. Rubinstein, Therapy of experimental murine brucellosis with streptomycin alone and in combination with ciprofloxacin, doxycycline, and rifampin, Antimicrob. Agents Chemother. 37 (1993) 2333–2336. https://doi.org/10.1128/AAC.37.11.2333.

[36] L.K. Petersen, C.K. Sackett, B. Narasimhan, Novel, high throughput method to study in vitro protein release from polymer nanospheres, J. Comb. Chem. 12 (2010) 51–56. https://doi.org/10.1021/cc900116c.

[37] T.M. Brenza, L.K. Petersen, Y. Zhang, L.M. Huntimer, A.E. Ramer-Tait, J.M. Hostetter, M.J. Wannemuehler, B. Narasimhan, Pulmonary Biodistribution and Cellular Uptake of Intranasally Administered Monodisperse Particles, Pharm. Res. 32 (2014) 1368–1382. https://doi.org/10.1007/s11095-014-1540-y.

[38] M.S. Niederman, Principles of appropriate antibiotic use, Int. J. Antimicrob. Agents. 26 (2005) 170–175. https://doi.org/10.1016/S0924-8579(05)80324-3.

[39] J.A. DiMasi, H.G. Grabowski, R.W. Hansen, Innovation in the pharmaceutical industry: New estimates of R&D costs, J. Health Econ. 47 (2016) 20–33. https://doi.org/10.1016/j.jhealeco.2016.01.012.

6.8 Tables

Table 6.1 Particle library material characterization and release kinetics parameterization.

	Material Characterization			Release Kinetics Parameterization				
Formulation	**Count Mean Diameter (nm)**	**Count PdI**	**Zeta Potential (mV)**	**Encapsulation Efficiency**	**FR @ 2 h**	**FR @ 24 h**	**Slope @ 2 h (FR/day)**	**Slope @ 24 h (FR/day)**
20:80 CPTEG:CPH 5% rifampicin	131 ± 44	0.11	-39.8 ± 1.1	100.0% ± 5.3%	0.693	0.797	1.84794	0.00627
20:80 CPTEG:CPH 10% rifampicin	124 ± 50	0.16	-19.9 ± 2.6	100.0% ± 3.3%	0.731	0.860	2.02316	0.01528
20:80 CPTEG:CPH 5% doxycycline	139 ± 58	0.17	-7.6 ± 1.6	92.6% ± 1.2%	0.983	0.986	0.16841	0.00060
20:80 CPTEG:CPH 10% doxycycline	146 ± 62	0.18	-11.8 ± 1.1	83.5% ± 1.9%	0.960	0.987	0.76509	0.00049
20:80 CPTEG:CPH 5% gentamicin	264 ± 100	0.15	-1.1 ± 1.8	94.1% ± 3.0%	0.960	0.960	0.00427	0.00017
20:80 CPTEG:CPH 10% gentamicin	276 ± 93	0.12	-3.0 ± 0.6	82.0% ± 0.9%	0.978	0.979	0.01223	0.00010
20:80 CPTEG:CPH 5% meropenem	142 ± 56	0.15	-29.5 ± 0.8	100.0% ± 3.7%	0.941	0.941	0.00101	0.00018
20:80 CPTEG:CPH 10% meropenem	142 ± 50	0.12	-31.4 ± 0.3	100.0% ± 9.4%	0.962	0.962	0.00044	0.00020
20:80 CPTEG:CPH 5% ceftazidime	153 ± 58	0.14	-23.7 ± 3.1	100.0% ± 0.1%	1.000	1.000	0.00536	0.00001
20:80 CPTEG:CPH 10% ceftazidime	132 ± 51	0.15	-29.4 ± 1.8	100.0% ± 0.6%	1.000	1.000	0.00452	0.00000
20:80 CPH:SA 5% rifampicin	475 ± 186	0.15	-32.9 ± 1.4	53.1% ± 1.9%	0.101	0.259	1.07480	0.03574
20:80 CPH:SA 10% rifampicin	549 ± 188	0.12	-32.0 ± 4.5	37.6% ± 0.9%	0.169	0.359	1.35118	0.04430
20:80 CPH:SA 5% doxycycline	438 ± 130	0.09	-11.6 ± 2.0	83.4% ± 4.2%	0.985	0.998	0.40645	0.00072
20:80 CPH:SA 10% doxycycline	560 ± 155	0.08	-10.6 ± 0.7	84.5% ± 2.5%	0.985	0.999	0.38889	0.00045
20:80 CPH:SA 5% gentamicin	543 ± 153	0.08	-34.2 ± 3.3	100.0% ± 1.1%	0.982	0.983	0.00360	0.00087
20:80 CPH:SA 10% gentamicin	547 ± 183	0.11	5.2 ± 0.2	80.8% ± 4.2%	0.989	0.990	0.01438	0.00063
20:80 CPH:SA 5% meropenem	588 ± 173	0.09	-26.8 ± 2.0	34.5% ± 1.6%	0.993	0.993	0.00000	0.00013
20:80 CPH:SA 10% meropenem	525 ± 133	0.07	-16.8 ± 0.9	61.7% ± 1.6%	0.997	0.997	0.00235	0.00072
20:80 CPH:SA 5% ceftazidime	549 ± 135	0.06	-26.4 ± 1.3	91.8% ± 11.2%	0.992	0.995	0.04184	0.00079
20:80 CPH:SA 10% ceftazidime	505 ± 127	0.06	-30.4 ± 0.5	100.0% ± 11.1%	0.991	0.994	0.02604	0.00178
10:90 CPTEG:SA 5% rifampicin	1317 ± 682	0.27	-21.9 ± 1.2	85.3% ± 0.9%	0.418	0.848	5.26043	0.07717
10:90 CPTEG:SA 10% rifampicin	1367 ± 661	0.23	-24.9 ± 1.1	81.2% ± 2.4%	0.502	0.856	4.67598	0.06003
10:90 CPTEG:SA 5% doxycycline	1402 ± 633	0.20	-41.6 ± 1.1	66.3% ± 1.4%	0.992	1.000	0.03368	0.00033
10:90 CPTEG:SA 10% doxycycline	1484 ± 723	0.24	-35.7 ± 0.4	81.2% ± 5.7%	0.995	1.000	0.02554	0.00018
10:90 CPTEG:SA 5% gentamicin	1213 ± 644	0.28	4.1 ± 0.5	54.9% ± 1.8%	0.970	0.986	0.04481	0.00722
10:90 CPTEG:SA 10% gentamicin	1162 ± 524	0.20	4.4 ± 1.6	55.0% ± 2.0%	0.985	0.992	0.02632	0.00354
10:90 CPTEG:SA 5% meropenem	1325 ± 623	0.22	-34.6 ± 2.4	15.2% ± 3.5%	0.995	0.995	0.08333	0.00000
10:90 CPTEG:SA 10% meropenem	1310 ± 727	0.31	-47.8 ± 1.8	44.3% ± 2.6%	0.999	1.000	0.04167	0.00000
10:90 CPTEG:SA 5% ceftazidime	1341 ± 687	0.26	-55.0 ± 2.1	95.0% ± 0.8%	1.000	1.000	0.00091	0.00003
10:90 CPTEG:SA 10% ceftazidime	1296 ± 693	0.29	-50.3 ± 0.9	86.7% ± 1.2%	1.000	1.000	0.00230	0.00001

FR fraction released. Data are presented as mean ± SD.

Table 6.2 Nanomedicine Antimicrobial Activity Against Burkholderia cepacia.

Particle Formulation	Soluble IC_{50} (μg/ml)	Nanoparticle IC_{50} (μg/ml) (adj for EE)	Log_2 (Nanoparticle IC_{50} / Soluble IC_{50})
20:80 CPTEG:CPH 5% CAZ	11.450	5.964	-0.941
20:80 CPH:SA 5% CAZ	9.318	5.813	-0.681
20:80 CPH:SA 10% CAZ	12.714	14.330	0.173
20:80 CPTEG:CPH 5% DOX	5.588	3.694	-0.597
20:80 CPTEG:CPH 10% DOX	7.190	5.960	-0.271
20:80 CPH:SA 10% DOX	6.484	5.510	-0.235
20:80 CPH:SA 5% DOX	7.190	6.400	-0.168
20:80 CPTEG:CPH 5% DOX	7.190	6.570	-0.130
20:80 CPH:SA 10% DOX	7.190	6.760	-0.089
20:80 CPH:SA 5% DOX	6.588	7.322	0.152
20:80 CPTEG:CPH 10% DOX	5.769	7.073	0.294
20:80 CPH:SA 5% MEM	7.775	4.392	-0.824
20:80 CPH:SA 5% MEM	6.180	3.640	-0.764
20:80 CPTEG:CPH 5% MEM	7.589	5.909	-0.361
20:80 CPH:SA 10% MEM	7.660	6.263	-0.290
20:80 CPTEG:CPH 10% MEM	7.355	7.747	0.075
20:80 CPTEG:CPH 10% MEM	6.180	6.790	0.136
20:80 CPTEG:CPH 5% MEM	6.180	9.090	0.557
50:50 CPTEG:CPH 10% RIF	7.100	9.150	0.366
10:90 CPTEG:CPH 10% RIF	7.100	13.220	0.897
30:70 CPTEG:CPH 10% RIF	7.100	13.240	0.899
20:80 CPTEG:CPH 10% RIF	7.100	15.070	1.086
20:80 CPTEG:CPH 5% RIF	7.700	19.340	1.329
20:80 CPTEG:CPH 10% RIF	6.822	22.488	1.721
20:80 CPTEG:CPH 10% RIF	7.700	32.720	2.087
20:80 CPH:SA 5% RIF	7.383	32.000	2.116
20:80 CPH:SA 10% RIF	6.870	32.000	2.220

Table 6.3 Nanomedicine Cocktail Antimicrobial Activity Against Burkholderia cepacia.

Particle Cocktail	Soluble Drug Cocktail IC_{50} (μg/ml)	Nanoparticle Cocktail IC_{50} (μg/ml) (adj for EE)	Log_2 (Nanoparticle IC_{50} / Soluble IC_{50})
{20:80 CPH:SA 5% DOX} : {20:80 CPH:SA 5% MEM} 1:1	7.154	4.270	-0.745
{20:80 CPH:SA 5% CAZ} : {20:80 CPH:SA 10% MEM} 1:1	11.439	7.390	-0.630
{20:80 CPH:SA 5% MEM} : {20:80 CPH:SA 10% DOX} 1:1	7.448	5.161	-0.529
{20:80 CPTEG:CPH 5% DOX} : {20:80 CPTEG:CPH 10% CAZ} 1:1	3.329	2.340	-0.509
{20:80 CPTEG:CPH 5% DOX} : {20:80 CPH:SA 5% MEM} 1:1	5.464	3.930	-0.475
{20:80 CPH:SA 5% DOX} : {20:80 CPH:SA 5% MEM} 1:1	6.540	5.012	-0.384
{20:80 CPTEG:CPH 5% MEM} : {20:80 CPTEG:CPH 5% CAZ} 1:1	7.590	5.900	-0.363
{20:80 CPH:SA 10% MEM} : {20:80 CPH:SA 10% CAZ} 1:1	12.663	11.019	-0.201
{20:80 CPTEG:CPH 5% MEM} : {20:80 CPH:SA 5% CAZ} 1:1	7.860	6.921	-0.184
{20:80 CPH:SA 10% CAZ} : {20:80 CPH:SA 10% DOX} 1:1	5.334	4.851	-0.137
{20:80 CPH:SA 10% MEM} : {20:80 CPH:SA 10% DOX} 1:1	7.195	6.886	-0.063
{20:80 CPTEG:CPH 5% DOX} : {20:80 CPTEG:CPH 10% MEM} 1:1	7.870	7.930	0.011
{20:80 CPH:SA 10% CAZ} : {20:80 CPH:SA 10% MEM} 1:1	6.605	7.008	0.085
{20:80 CPTEG:CPH 10% DOX} : {20:80 CPTEG:CPH 5% MEM} 1:1	5.305	5.689	0.101
{20:80 CPTEG:CPH 5% DOX} : {20:80 CPTEG:CPH 5% RIF} 1:2	3.487	3.813	0.129
{20:80 CPTEG:CPH 5% DOX} : {20:80 CPTEG:CPH 5% RIF} 1:2	1.743	1.907	0.130
{20:80 CPTEG:CPH 10% DOX} : {20:80 CPTEG:CPH 10% MEM} 1:1	6.148	6.856	0.157
{20:80 CPH:SA 5% CAZ} : {20:80 CPH:SA 5% DOX} 1:1	6.351	7.149	0.171
{20:80 CPTEG:CPH 5% DOX} : {20:80 CPTEG:CPH 5% MEM} 1:0.625	4.293	4.922	0.197
{20:80 CPTEG:CPH 5% DOX} : {20:80 CPTEG:CPH 5% MEM} 1:0.625	6.869	7.876	0.197
{20:80 CPTEG:CPH 5% DOX} : {20:80 CPTEG:CPH 5% CAZ} 1:1	6.297	7.400	0.233
{20:80 CPH:SA 5% RIF} : {20:80 CPH:SA 5% MEM} 1:1	3.885	4.573	0.235
{20:80 CPTEG:CPH 10% MEM} : {20:80 CPTEG:CPH 10% CAZ} 1:1	7.517	9.509	0.339
{20:80 CPTEG:CPH 5% MEM} : {20:80 CPH:SA 5% DOX} 1:1	4.654	6.094	0.389
{20:80 CPTEG:CPH 10% DOX} : {20:80 CPTEG:CPH 5% CAZ} 1:1	2.370	3.191	0.429
{20:80 CPTEG:CPH 10% MEM} : {20:80 CPH:SA 10% RIF} 1:1	7.424	10.677	0.524
{20:80 CPTEG:CPH 5% MEM} : {20:80 CPTEG:CPH 5% RIF} 1:2	1.593	2.531	0.668
{20:80 CPTEG:CPH 5% MEM} : {20:80 CPTEG:CPH 5% RIF} 1:2	3.185	5.063	0.669
{20:80 CPTEG:CPH 5% MEM} : {20:80 CPTEG:CPH 10% RIF} 1:2	3.156	5.199	0.720
{20:80 CPTEG:CPH 5% MEM} : {20:80 CPTEG:CPH 10% RIF} 1:2	6.312	10.399	0.720
{20:80 CPTEG:CPH 5% MEM} : {20:80 CPTEG:CPH 10% CAZ} 1:1	13.477	23.065	0.775
{20:80 CPTEG:CPH 10% MEM} : {20:80 CPTEG:CPH 5% RIF} 1:2	3.383	6.173	0.868
{20:80 CPTEG:CPH 10% MEM} : {20:80 CPTEG:CPH 5% RIF} 1:2	6.766	12.347	0.868
{20:80 CPH:SA 10% RIF} : {20:80 CPH:SA 10% DOX} 1:1	3.783	7.377	0.964
{20:80 CPTEG:CPH 5% DOX} : {20:80 CPTEG:CPH 10% RIF} 1:2	3.760	7.344	0.966
{20:80 CPTEG:CPH 5% DOX} : {20:80 CPTEG:CPH 10% RIF} 1:2	1.879	3.672	0.967
{20:80 CPTEG:CPH 5% MEM} : {20:80 CPH:SA 5% RIF} 1:1	4.326	8.487	0.972
{20:80 CPH:SA 10% MEM} : {20:80 CPH:SA 10% RIF} 1:1	3.616	7.489	1.050
{20:80 CPTEG:CPH 5% DOX} : {20:80 CPH:SA 5% RIF} 1:1	2.267	5.141	1.181
{20:80 CPH:SA 5% DOX} : {20:80 CPH:SA 5% RIF} 1:1	3.505	8.855	1.337
{20:80 CPH:SA 5% CAZ} : {20:80 CPH:SA 10% DOX} 1:1	2.982	8.071	1.436
{20:80 CPTEG:CPH 10% RIF} : {20:80 CPTEG:CPH 10% MEM} 2:1	6.114	16.846	1.462
{20:80 CPTEG:CPH 10% RIF} : {20:80 CPTEG:CPH 10% MEM} 2:1	3.057	8.423	1.462
{20:80 CPH:SA 10% CAZ} : {20:80 CPH:SA 10% RIF} 1:1	6.609	18.493	1.484
{20:80 CPTEG:CPH 10% DOX} : {20:80 CPTEG:CPH 5% RIF} 1:2	1.187	3.398	1.517
{20:80 CPTEG:CPH 10% DOX} : {20:80 CPTEG:CPH 5% RIF} 1:2	2.374	6.796	1.517
{20:80 CPH:SA 10% DOX} : {20:80 CPH:SA 10% CAZ} 1:1	2.290	7.169	1.646
{20:80 CPH:SA 5% CAZ} : {20:80 CPH:SA 5% DOX} 1:1	2.250	7.857	1.804
{20:80 CPTEG:CPH 10% DOX} : {20:80 CPTEG:CPH 10% RIF} 1:2	1.506	5.399	1.842
{20:80 CPTEG:CPH 10% DOX} : {20:80 CPTEG:CPH 10% RIF} 1:2	0.751	2.699	1.846
{20:80 CPH:SA 5% CAZ} : {20:80 CPTEG:CPH 5% DOX} 1:1	2.360	8.513	1.851
{20:80 CPH:SA 5% RIF} : {20:80 CPH:SA 5% CAZ} 1:1	7.102	29.207	2.040
{20:80 CPTEG:CPH 10% CAZ} : {20:80 CPTEG:CPH 5% RIF} 1:2	3.751	15.864	2.080
{20:80 CPTEG:CPH 10% CAZ} : {20:80 CPTEG:CPH 5% RIF} 1:2	1.875	7.932	2.081
{20:80 CPH:SA 10% CAZ} : {20:80 CPH:SA 10% RIF} 1:1	1.871	42.289	4.498

Table 6.4 Material and Molecular Descriptors Correlated to Antimicrobial Activity.

Descriptor Group	ID	Descriptor	Description
Polymer Material Characterization	1	DOP	degree of polymerization
	2	M_n (Da)	number average molecular weight
	3	***Tg (°C)***	glass transition temperature
Polymer Chemical Structure[a]	4	0χ	atomic indices
	5	$0\chi v$	atomic indices
	6	1χ	connectivity indices
	7	$1\chi v$	connectivity indices
	8	N_C	total non-hydrogen atom number in one repeat unit
	9	N_O	backbone index1 (12.19)
	10	N_H	number of atoms in the shortest path across the backbone of a polymeric repeat unit, N_SP ≤ N_BB (2.11)
	11	M	number of carbon atoms in a polymeric repeat unit
	12	N_ester_n	number of hydrogen atoms in a polymeric repeat unit
	13	N_ester_c	number of backbone −COO− (nonconjugated)
	14	N_ether	number of backbone −COO− (one-sided conjugation with aromatic ring)
	15	Nmv	number of aromatic rings in a polymeric repeat unit
	16	N_alkyl_ether	number of CH2 in a polymeric repeat unit
	17	***N_group***	numer of −O− in a polymeric repeat unit
	18	N_rot	Nmv = 2*N_ester + 3*N_ether (3.14)
	19	N_backbone_O	N_K = −3*N_ether_quote-3*N_acrylic_ester (12.27)
	20	N_dc	the total number of rotational degrees of freedom parameter
	21	N	number of backbone oxygen atoms in a polymeric repeat unit
	22	BB_index1	N_dc = 7*N_backbone_O + 12*N_sideGroup_O (9.11)
	23	BB_index2	number of oxygen atoms in a polymeric repeat unit
	24	SG_index	mole weight of the repeat unit
	25	N_K	backbone index 2 (12.20)
	26	N_SP	backbone index 4 (12.22)
	27	N_aromaticRing	the number of ether (R−O−R′) linkages between two units R and R′ both of which are connected to the alkyl carbon atom
	28	N_CH2	N_group = −N_alkyl_ether + 7*N_CO + 2*N_otherCO (5.10)
Drug Physicochemical Properties[b]	29	Molar Mass (g/mol)	
	30	LogP1	octanol-water partition coefficient, experimental
	31	Water Solubility2 (mg/mL)	experimental
	32	***LogP3***	octanol-water partition coefficient, predicted by ALGOPS
	33	LogP4	octanol-water partition coefficient, predicted by ChemAxon
	34	LogS5	Solubility, predicted by ALGOPS
	35	pKa (strongest acid)	acid dissociation constant, predicted by ChemAxon
	36	pKa (strongest base)	acid dissociation constant, predicted by ChemAxon
	37	Physiological Charge	predicted by ChemAxon
	38	Hydrogen Acceptor Count	predicted by ChemAxon
	39	Hydrogen Donor Count	predicted by ChemAxon
	40	Polar Surface Area ($Å^2$)	predicted by ChemAxon
	41	Rotatable Bond Count	predicted by ChemAxon
	42	Refractivity (m^3/mol)	predicted by ChemAxon
	43	Polarizability ($Å^3$)	predicted by ChemAxon
Nanoparticle Material Characterization	44	Count Geo Mean Diameter (nm)	
	45	Count PdI	polydispersity index
	46	***Mass Mean Diameter (nm)***	
	47	Mass Geo Mean Diameter (nm)	
	48	Mass PDI	polydispersity index
	49	***Zeta potential average (mV)***	function of particle surface charge
Nanoparticle Release Kinetics	50	Encapsulation Efficiency (%)	ratio of drug encapsulated to drug loaded at synthesis
	51	Final Loading (% wt/wt)	nominal drug loading normalized by encapsulation efficiency
	52	Fraction Released @ 2 h	
	53	Fraction Released @ 24 h	
	54	***Fraction Released Slope @ 2 h***	
	55	Fraction Released Slope @ 24 h	
	56	Mass Released @ 2 h (µg / mg particles)	
	57	***Mass Released @ 24 h (µg / mg particles)***	

Key descriptors identified by variable importance projection analysis (Figure 6.4) are italicized and bolded. aDescriptors were previously used by Li et al. [30] and equation numbers refer to corresponding equations in Bicerano [31]. bDescriptors were gathered from the DrugBank database [26].

Table 6.5 Out-of-library validation of antimicrobial activity predictions.

Formulation or Cocktail	Predicted Log_2 (Nanoparticle IC50 / Soluble IC50)	Soluble IC_{50} (µg/ml)	Nanoparticle IC_{50} (µg/ml) (adj for EE)	Measured Log_2 (Nanoparticle IC50 / Soluble IC50)
20:80 CPH:SA 20% chloramphenicol	-0.215	7.12	6.89	-0.048
10:90 CPTEG:SA 20% chloramphenicol	-0.030	7.12	7.02	-0.021
10:90 CPTEG:SA 10% chloramphenicol	-0.024	7.12	7.43	0.061
20:80 CPH:SA 10% chloramphenicol	0.874	7.12	9.11	0.357
#12 {10:90 CPTEG:SA 5% DOX} : {20:80 CPH:SA 10% CAM} 1:1	-1.683	3.46	0.97	-1.829
#25 {10:90 CPTEG:SA 5% MEM} : {10:90 CPTEG:SA 10% CAM} 1:1	-1.066	6.58	3.56	-0.886
#32 {10:90 CPTEG:SA 5% CAZ} : {10:90 CPTEG:SA 5% RIF} 1:1	1.968	2.72	22.00	3.016

6.9 Figures

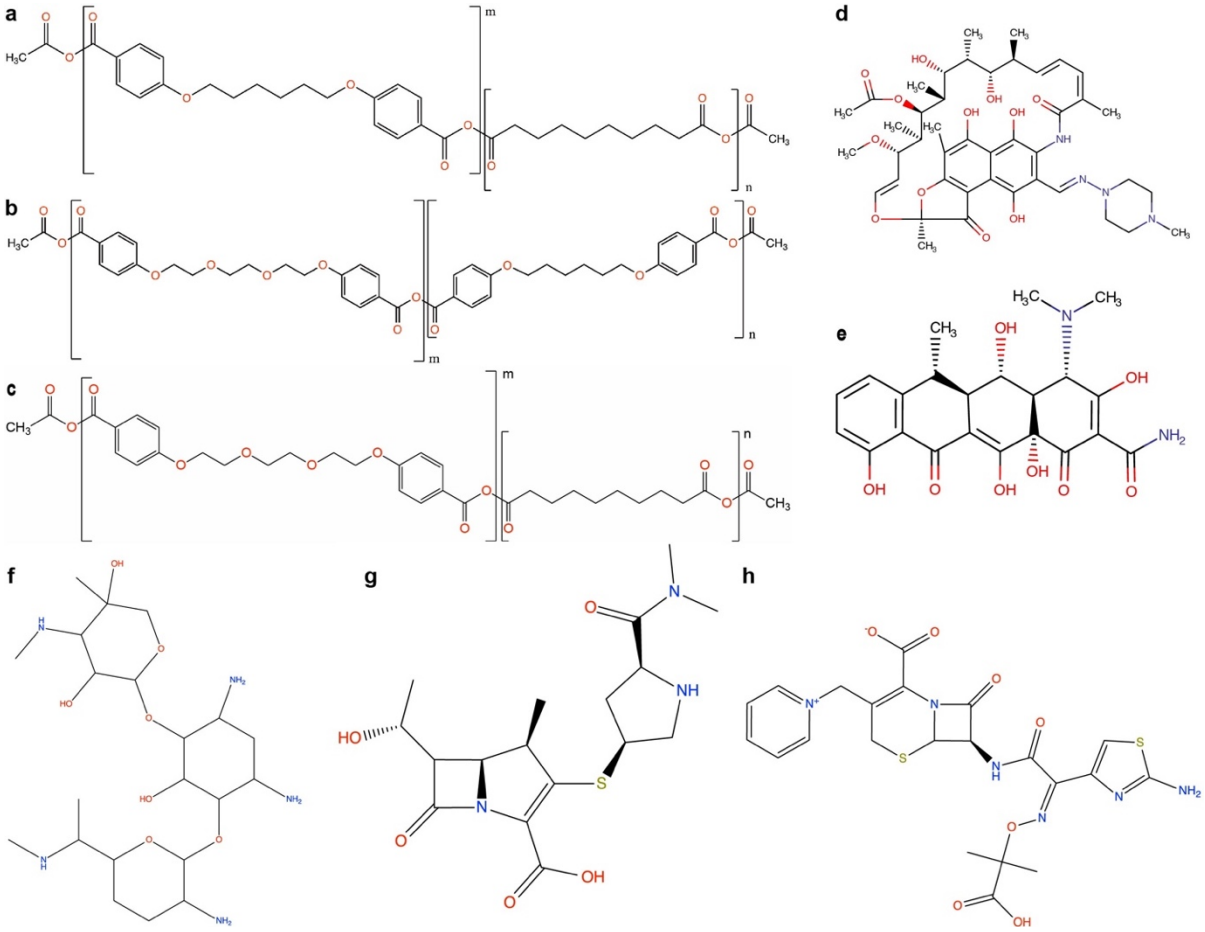

Figure 6.1 Chemical structures of polymers and antibiotics used in particle library. Structures of CPH:SA (a), CPTEG:CPH (b), and CPTEG:SA (c) copolymers, where m and n are the number of repeats for each unit. (d-h) Structure of rifampicin (RIF, d), doxycycline (DOX, e), gentamicin (GEN, f), meropenem (MEM, g), and ceftazidime (CAZ, h).

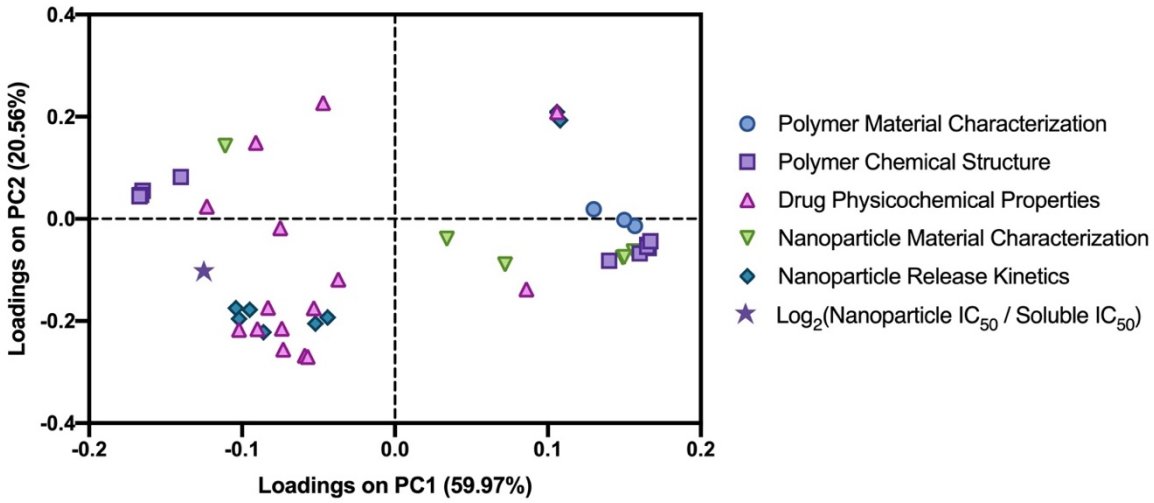

Figure 6.2 PCA loadings plot mapping individual descriptor contributions to each principal component. PC1 is composed of contributions from each input descriptor group. PC2 is primarily composed of drug physicochemical properties and nanoparticle release kinetics. Nanoparticle antimicrobial performance (purple star) does not adhere to either PC, indicating that each descriptor group contributes to nanoparticle antimicrobial activity.

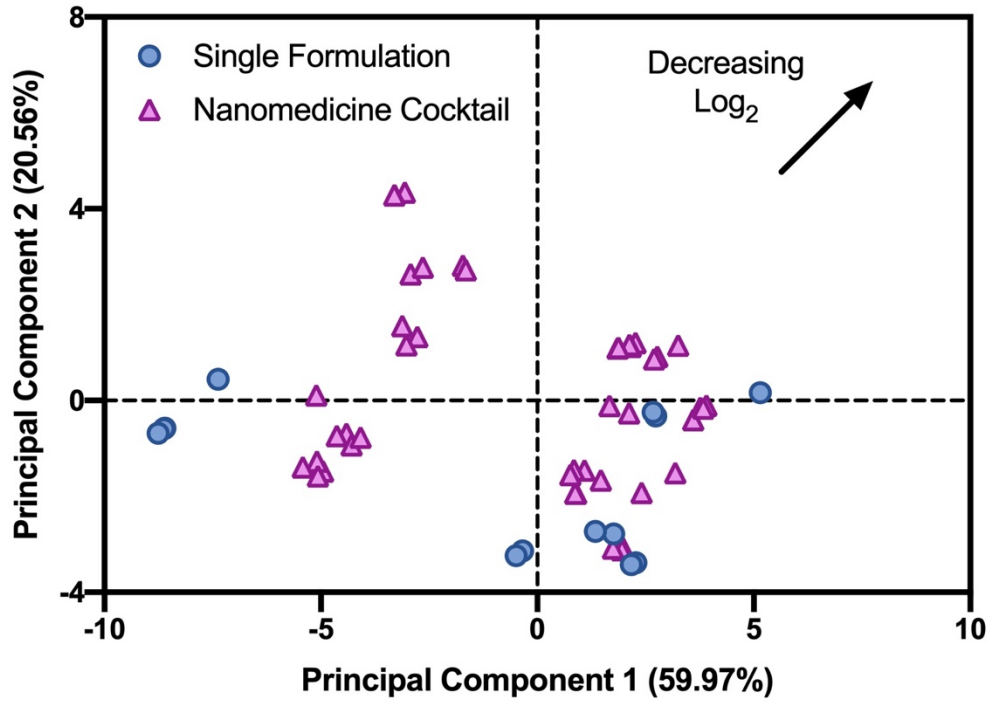

Figure 6.3 PCA scores plot mapping the antimicrobial activity of individual nanoparticle formulations and cocktails. Improved nanoparticle performance compared to soluble drug follows a trajectory toward the top right corner. Generally, nanoparticle cocktails provide better antimicrobial activity than single formulations.

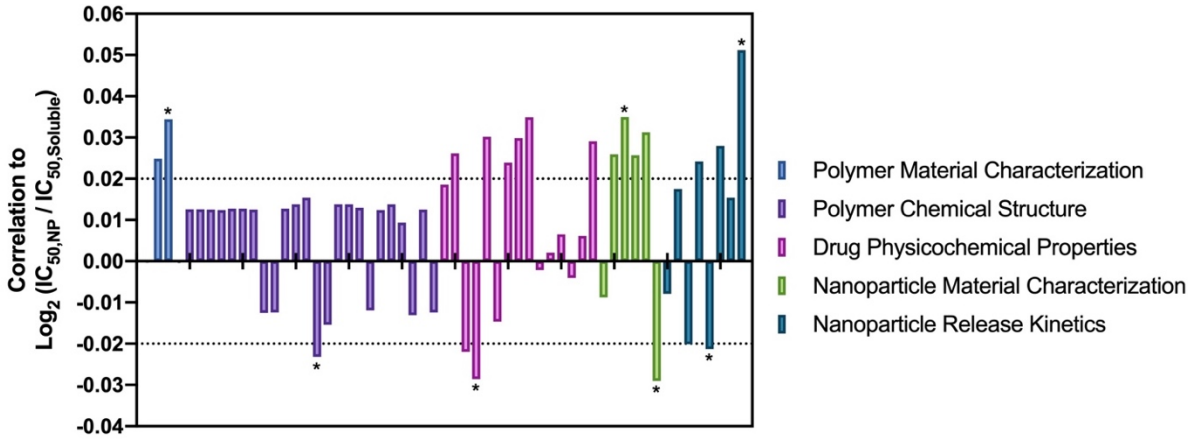

Figure 6.4 Correlation of descriptors with nanoparticle antimicrobial performance. Positive values correspond to positive correlation and negative values to inverse correlation. Twenty descriptors (of 57) were highly correlated with Log_2 ratio. VIP analysis enabled elimination of cross-correlated descriptors, resulting in a minimal descriptor set of seven descriptors (marked by *). Table 6.4 includes the full descriptor list.

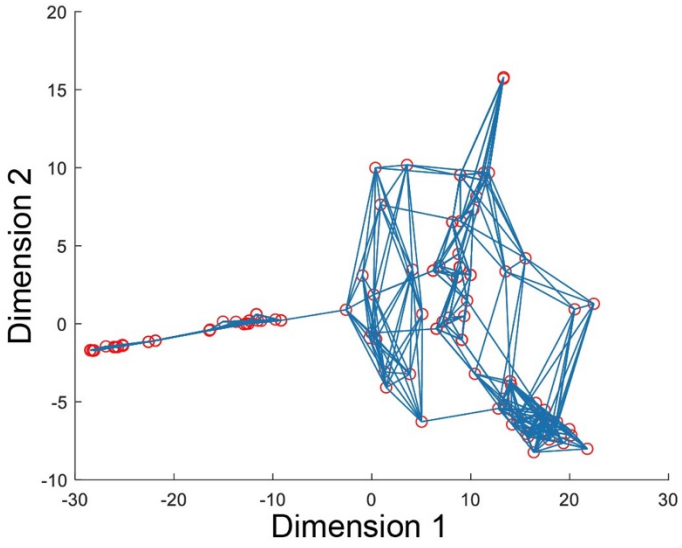

Figure 6.5 Graph analysis for parameterizing the descriptor space. Graph analysis was used for dimensional reduction of the 57 input descriptors (Table 6.4) into five composite parameters while preserving nonlinearity via geodesic distances. A projection along the first two (most important) dimensions is depicted. Each point represents a particle formulation or cocktail, and similar points are connected by a line. These paths of connectivity can be used to interrogate design relationships between formulations. Untested formulations and cocktails of interest (Tables 6.5-6.6) were included to create a parameter space suitable for predicting their behavior. The dimensionally reduced parameters from this graph analysis were used as inputs for the predictive model in Figure 6.6.

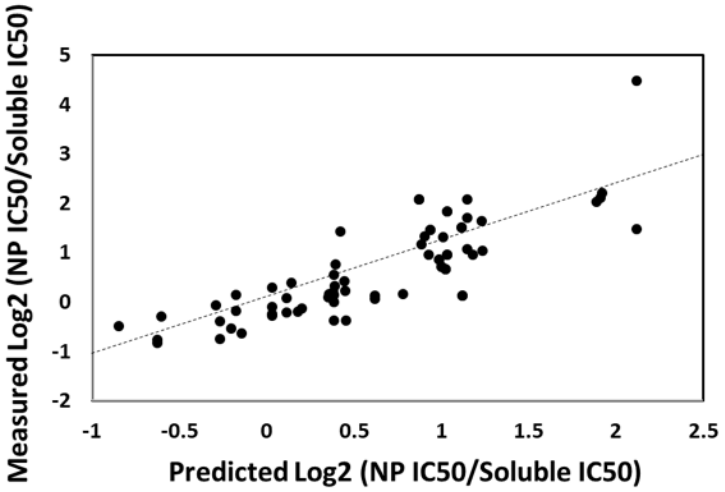

Figure 6.6 Graph theory-based model predicts nanoparticle formulation and cocktail antimicrobial performance. The model had an R^2 value of 70.8%, and therefore was reasonably accurate within the training data set. Cross-validation analysis showed reasonable robustness. These calculations are based on a hybrid informatics approach where nonlinear manifold projections serve as the input, which maintains complexity in descriptor-property relationships while minimizing the risk of over-fitting and reducing computational power.

6.10 Supplementary Materials

Supplementary Table 6.1 High-pressure liquid chromatography separation and detection protocols for ceftazidime and meropenem.

Drug	Meropenem		Ceftazidime	
Sample Solvent	PBS, pH 7.4	40 mM Sodium Hydroxide	PBS, pH 7.4	40 mM Sodium Hydroxide
Injection volume	20 µL			
Column	Zorbax Eclipse XDB-c8 5-micron 4.6x150mm			
Flow Rate	1 mL/min			
Temperature	25 °C			
Solvent A	Water	Water 0.1% Trifluoroacetic Acid	Water	Water 0.1% Trifluoroacetic Acid
Solvent B	Methanol	Acetonitrile 0.1% Trifluoroacetic Acid	Methanol	Acetonitrile 0.1% Trifluoroacetic Acid
Starting % B	0.1	0.1	0.1	15
Gradient peak % B	50	50	50	40
Gradient time	15 min	15 min	10 min (after 5 min hold)	5 min (after 1 min hold)
Drug wavelength (nm)	299	299	260	260

Supplementary Table 6.2 Predictions for all nanomedicine cocktail candidates.

ID	Formulation Cocktail	Predicted Log_2 (Nanoparticle IC50 / Soluble IC50)	Measured Log_2 (Nanoparticle IC50 / Soluble IC50)
1	{10:90 CPTEG:SA 5% MEM} : {10:90 CPTEG:SA 5% CAZ} 1:1	-2.364	
2	{10:90 CPTEG:SA 5% CAZ} : {20:80 CPH:SA 20% CAM} 1:1	-2.134	
3	{10:90 CPTEG:SA 5% MEM} : {20:80 CPTEG:CPH 5% DOX} 1:1	-2.105	
4	{10:90 CPTEG:SA 5% MEM} : {20:80 CPH:SA 20% CAM} 1:1	-2.091	
5	{10:90 CPTEG:SA 5% CAZ} : {20:80 CPTEG:CPH 5% MEM} 1:1	-2.087	
6	{10:90 CPTEG:SA 5% MEM} : {10:90 CPTEG:SA 20% CAM} 1:1	-2.087	
7	{10:90 CPTEG:SA 5% MEM} : {20:80 CPH:SA 10% CAM} 1:1	-1.865	
8	{10:90 CPTEG:SA 5% CAZ} : {20:80 CPTEG:CPH 5% DOX} 1:1	-1.852	
9	{10:90 CPTEG:SA 5% CAZ} : {20:80 CPH:SA 5% CAZ} 1:1	-1.794	
10	{10:90 CPTEG:SA 5% MEM} : {20:80 CPTEG:CPH 5% MEM} 1:1	-1.717	
11	{10:90 CPTEG:SA 5% MEM} : {20:80 CPTEG:CPH 5% CAZ} 1:1	-1.706	
12	{10:90 CPTEG:SA 5% DOX} : {20:80 CPH:SA 10% CAM} 1:1	-1.683	-1.829
13	{10:90 CPTEG:SA 5% CAZ} : {10:90 CPTEG:SA 20% CAM} 1:1	-1.682	
14	{10:90 CPTEG:SA 5% CAZ} : {20:80 CPTEG:CPH 5% CAZ} 1:1	-1.669	
15	{10:90 CPTEG:SA 5% MEM} : {20:80 CPH:SA 5% CAZ} 1:1	-1.668	
16	{10:90 CPTEG:SA 5% MEM} : {10:90 CPTEG:SA 5% DOX} 1:1	-1.637	
17	{10:90 CPTEG:SA 5% DOX} : {20:80 CPH:SA 20% CAM} 1:1	-1.612	
18	{10:90 CPTEG:SA 5% CAZ} : {10:90 CPTEG:SA 10% CAM} 1:1	-1.474	
19	{10:90 CPTEG:SA 5% MEM} : {20:80 CPTEG:CPH 5% RIF} 1:1	-1.440	
20	{10:90 CPTEG:SA 5% CAZ} : {20:80 CPH:SA 10% CAM} 1:1	-1.437	
21	{10:90 CPTEG:SA 5% DOX} : {10:90 CPTEG:SA 20% CAM} 1:1	-1.365	
22	{10:90 CPTEG:SA 5% MEM} : {20:80 CPH:SA 5% DOX} 1:1	-1.235	
23	{10:90 CPTEG:SA 5% MEM} : {20:80 CPH:SA 5% MEM} 1:1	-1.190	
24	{10:90 CPTEG:SA 5% CAZ} : {10:90 CPTEG:SA 5% DOX} 1:1	-1.160	
25	{10:90 CPTEG:SA 5% MEM} : {10:90 CPTEG:SA 10% CAM} 1:1	-1.066	-0.886
26	{10:90 CPTEG:SA 5% CAZ} : {20:80 CPH:SA 5% MEM} 1:1	-1.037	
27	{10:90 CPTEG:SA 5% CAZ} : {20:80 CPTEG:CPH 5% RIF} 1:1	-1.009	
28	{10:90 CPTEG:SA 5% DOX} : {10:90 CPTEG:SA 10% CAM} 1:1	-0.952	
29	{10:90 CPTEG:SA 5% CAZ} : {20:80 CPH:SA 5% DOX} 1:1	-0.502	
30	{10:90 CPTEG:SA 5% MEM} : {20:80 CPH:SA 5% RIF} 1:1	0.905	
31	{10:90 CPTEG:SA 5% MEM} : {10:90 CPTEG:SA 5% RIF} 1:1	1.322	
32	{10:90 CPTEG:SA 5% CAZ} : {10:90 CPTEG:SA 5% RIF} 1:1	1.968	3.016
33	{10:90 CPTEG:SA 5% CAZ} : {20:80 CPH:SA 5% RIF} 1:1	2.069	

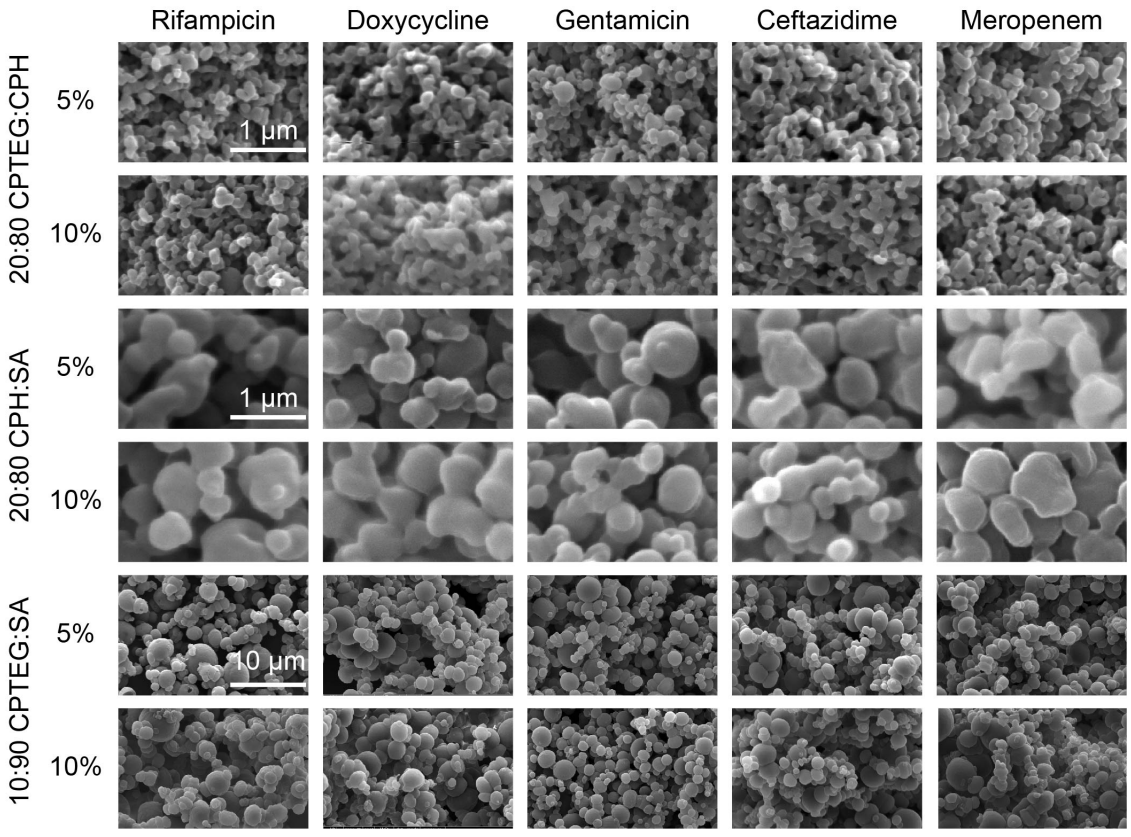

Supplementary Figure 6.1 Scanning electron micrographs of the particle library. Particle size and morphology was primarily dependent on particle chemistry, not on payload. Note: scale bar changes for 10:90 CPTEG:SA formulations.

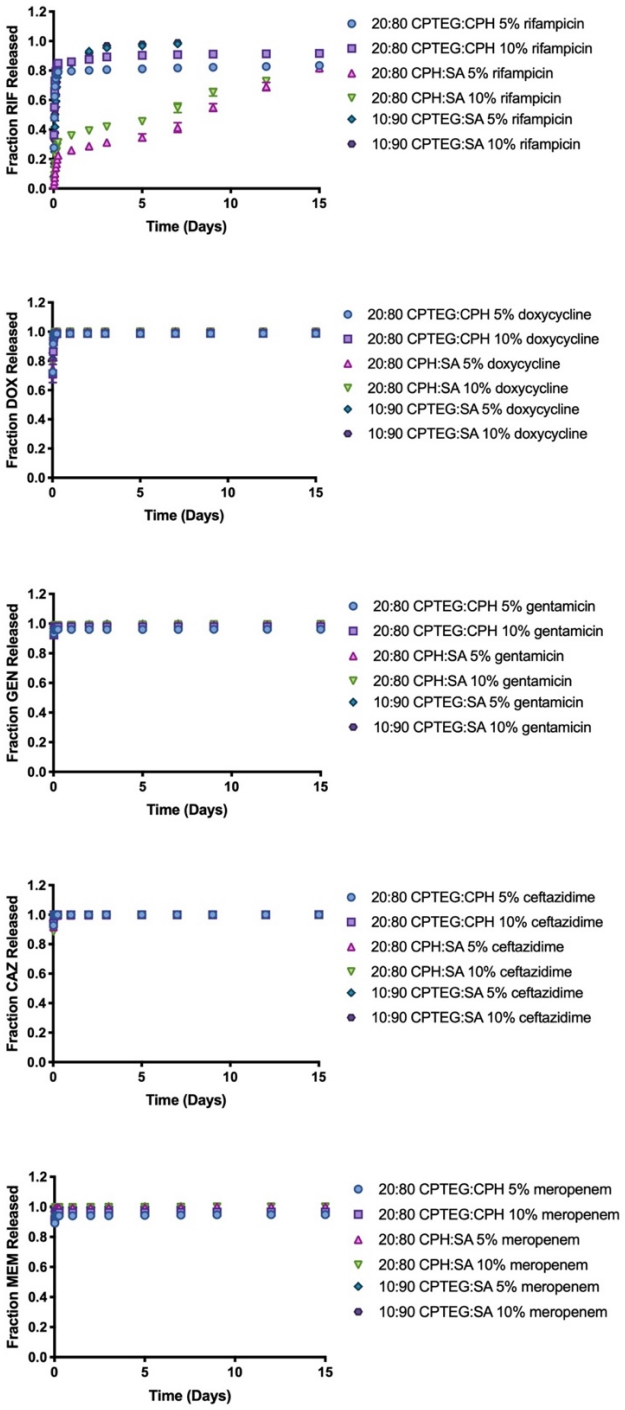

Supplementary Figure 6.2 Antibiotic release kinetics from particles in library encapsulating rifampicin (RIF, a), doxycycline (DOX, b), gentamicin (GEN, c), meropenem (MEM, d), and ceftazidime (CAZ, e). Data are presented as mean ± SD. Error bars are not depicted in cases where the error bar height is smaller than the symbol. Release profiles were parameterized into a 2 h burst, a 24 h burst, and slopes of release at 2 h and 24 h. The release kinetics from 20:80 CPTEG:CPH and 20:80 CPH:SA meropenem- and ceftazidime-encapsulating formulations were used as validation data in [12].

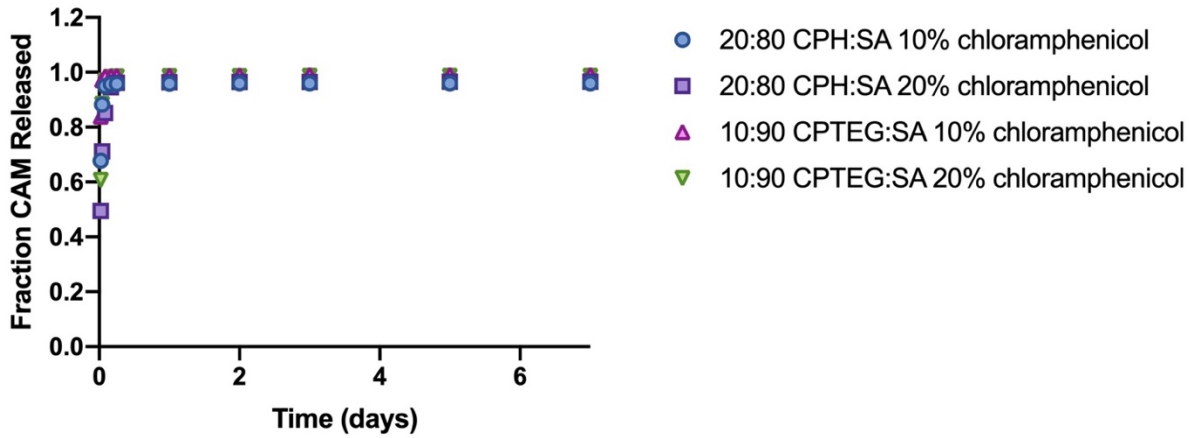

Supplementary Figure 6.3 Antibiotic release kinetics from nanoparticles used in out-of-library validation. Chloramphenicol (CAM) nanoparticles show a burst-heavy release profile. Data are presented as mean ± SD.

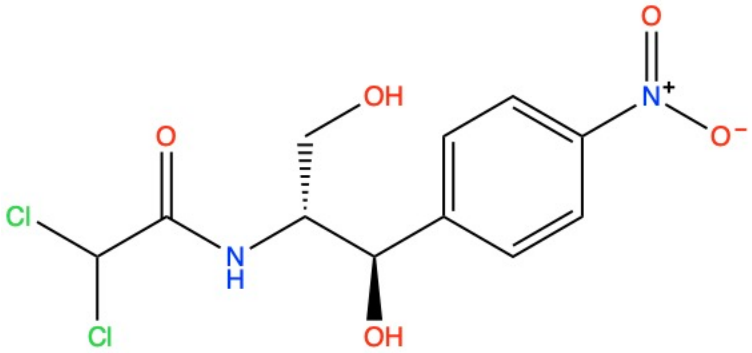

Supplementary Figure 6.4 Chemical structure of chloramphenicol. Chloramphenicol (CAM) contains two chlorine atoms and a nitro group, which were not present in the training data set.

CHAPTER 7. CONCLUSIONS AND ONGOING/FUTURE WORK

7.1 Conclusions

Antimicrobial-resistant infections are a defining healthcare challenge of our age. Antibiotics, tools that built the modern healthcare system, are losing their efficacy, and the drug discovery and development pipeline is woefully underpopulated to meet society's needs. This threat requires innovative solutions to provide new therapies against resistant pathogens and preserve our existing antibiotic supply. Polyanhydride-based nanomedicines have shown the striking capability to improve antibiotic efficacy, and deserve to be explored as one such solution. These nanomedicines provide control over the release rate of the drug, alter the biodistribution of the drug by enhancing its bioavailability, lower drug dose, reduce or eliminate off-target effects, and can be targeted for delivery to specific tissues or cross complex biological barriers, such as the insect cuticle, the bacterial cell wall, or the blood-brain-barrier. By improving antimicrobial activity, nanomedicines could allow repurposing of existing antibiotics and contribute new therapies against resistant bacteria. To maximize nanomedicine success, modernized screening approaches are needed to compensate for the massive dataspace conferred by carrier chemistry, drug chemistry, and nanoparticle material properties. Informatics-assisted screening provides such an advance by efficiently developing structure-function relationships to guide selection of lead candidates. This approach would help deconvolute complex, interconnected relationships between drug type, carrier chemistry, particle properties, and biological activity that are notoriously difficult to model a priori, and provide a framework for rational design of antimicrobial nanomedicines to kill resistant pathogens.

In Chapter 4, a multivariate data analytics approach was developed to identify polymer and drug properties that significantly impacted drug encapsulation efficiency and release kinetics. A multilinear map of nanoparticle formulations captured non-linear behavior governing relationships between drug type, polymer chemistry, and nanoparticle release properties, enabling interrogation of nanomedicine design pathways. Predictive models for drug release kinetics of untested drugs were developed from this map. Release kinetics predictions of two drugs containing atoms not included in the model showed good agreement with experimental results, validating the model and indicating its potential to virtually explore new polymer and drug pairs. This multilinear modeling approach provides the first steps towards development of a framework that can be used to rationally design nanomedicine formulations by selecting the appropriate carrier for a drug payload to program desirable release kinetics profiles.

In Chapter 5, a high-throughput method was adapted to rapidly screen the novel CPTEG:SA copolymer chemical space for interesting drug delivery properties. CPTEG:SA copolymers were shown to erode more rapidly than traditional polyanhydride copolymers, giving rise to rapid, chemistry-dependent drug release within three days. This rapid release could be beneficial for fast-growing pathogens by providing a quick, suppressive dose of antibiotic that is maintained over several days. The high-throughput method was adapted to synthesize polymer-drug films to screen for thermodynamic mixing interactions by melting point depression studies, which showed mixed agreement with predictions from group contribution methods. The interaction parameters estimated from these methods were able to explain trends in model drug release kinetics from nanoparticle libraries. Overall, these methods could improve nanomedicine screening by allowing parallel, semi-automated

synthesis of up to 24 different formulations and enabling high-throughput characterization of polymer-drug mixing thermodynamics.

Finally, in Chapter 6, a particle library with varying polymer and nanoparticle chemistry was synthesized using the high-throughput methodology from Chapter 5. Single nanoparticle formulations and binary combinations of formulations were tested for antimicrobial efficacy against *Burkholderia cepacia*, an opportunistic, resistant pathogen. The multivariate data analytics approach was applied to identify drug, polymer, and carrier properties that determine antimicrobial performance of single nanoparticles and cocktails of nanoparticles encapsulating different drugs. A graph theory-based model, used in Chapter 4 to model release kinetics, was developed to predict nanoparticle and cocktail efficacy. The model successfully discriminated high performing candidates from those with no improvement or worse efficacy than soluble drug. This hybrid informatics approach constitutes another step toward rational design of antimicrobial nanomedicines by identifying polymer and drug combinations that improve antibiotic potency.

Overall, this dissertation has contributed improved nanomedicine screening methods and enabled the development of a framework to rationally select antibiotic-loaded nanoparticle candidates. The high-throughput method can accelerate the synthesis of antibiotic-loaded nanoparticle libraries and rapidly screen for polymer-drug compatibility. This enabled the characterization of the nano-delivery device capabilities based on a novel, rapidly degrading CPTEG:SA copolymer system. This work developed structure-function relationships between input polymer, drug, and nanoparticle properties and their controlled release and antimicrobial performance. An informatics approach to identify nanoparticle candidates with controlled release and improved antimicrobial efficacy was successfully

developed. In all these ways, this dissertation has provided the first steps toward a framework for the rational design of antimicrobial nanomedicines capable of killing resistant organisms and controlling drug release. Lead candidates identified by this framework could provide new therapies against resistant pathogens and enable repurposing of existing antibiotics limited by resistance.

7.2 Ongoing and Future Work

Ongoing work is focused on refining the structure-function relationships between the drug, polymer, and nanoparticle properties and biological activity by expanding the chemical and biological dataspace. Through multiple fruitful collaborations with the Bellaire group, we have generated *in vitro* biological activity data for nanomedicine formulations in bacterial and parasitic biological systems. The same nanoparticle library used in Chapter 6 is currently being evaluated for performance against potential bioweapons *Burkholderia pseudomallei* and *mallei*. These data could be mined to identify pathogen-specific and -nonspecific factors that influence nanomedicine efficacy, which could provide information about the generalizability of the trends identified in Chapter 6.

We have ongoing collaborations with the Coats group to explore the biodistribution of polyanhydride particles in insect vectors. This work will provide preliminary evidence for the use of drug delivery devices for vector control. While experiments thus far have focused on mosquitoes, future experiments will investigate American cockroaches. Our goal is to investigate how differences in copolymer chemistry and particle size impact biodistribution.

7.2.1 Generalizing the Antimicrobial Efficacy Model to Other Pathogens

Drug-resistant tuberculosis infections pose a current challenge for global healthcare systems. The bacterium's intracellular niche provides a barrier to achieving a high local antibiotic concentration, and its slow growth rate limits the effectiveness of antimicrobials

that act on actively replicating cells.[1] Multidrug-resistant TB infections are often incurable by frontline drugs, and in 2006 “extensively drug-resistant” TB infections were defined to describe a subset of MDR-TB infections that are resistant second line therapies.[2] The slowing rate of antibiotic discovery has also limited the development of therapies for parasitic infections. *Acanthamoeba* spp. infections in immunosuppressed individuals can cause granulomatous amebic encephalitis, which is often fatal due to a prodromal period, limited diagnostic tools, and a lack of effective antimicrobial treatments.[3] *Acanthamoeba* can also cause a corneal infection called *Acanthamoeba* keratitis, which can impair vision and require enucleation if left untreated.[4] Effective antimicrobial therapies capable of killing both the metabolically-active trophozoite and cyst forms of *Acanthamoeba* remain elusive. Polyanhydride nanoparticles have a demonstrated potential for increasing the potency of antimicrobial drugs and providing dose sparing effects,[5,6] but conventional screening methods are too inefficient to adequately cover the large nanoparticle dataspace. Ideally, the trends between input descriptors and antimicrobial performance identified in Chapter 6 could be applied to these systems to guide candidate selection. However, the generalizability of that model to other biological systems is unknown. Here, we use data gathered in collaboration with the Bellaire lab to propose some new directions to characterize this generalizability.

An *in vitro* assay has been developed by Dr. Andrea Binnebose from the Bellaire lab to characterize the effectiveness of drugs released from nanoparticles in *Mycobacterium marinum*. In this work, 20:80 CPTEG:CPH nanoparticles dual-encapsulating the anti-tubercular drugs pyrazinamide/rifampicin (PZA/RIF) and isoniazid/ethambutol (IZD/ETHAM) were synthesized, and incubated in PBS to release their drug payloads. At regular time points, the particles were centrifuged, supernatants were collected, and fresh

PBS was added. These 24 h, 48 h, and 72 h supernatants containing all four drugs were used to treat *M. marinum* broth cultures, and CFUs were counted at regular intervals (Figure 7.1). At 24 h, there was no significant difference between the groups. At 120 h, the 24 h and 48 h supernatants generated more growth suppression than the soluble control, while the 72 h supernatants wasn't as effective as the soluble control. At 168 h, both the 24 h and 48 h supernatants showed more activity than the soluble control, and the 72 h supernatant was indistinguishable from the soluble control. At both later timepoints, all soluble and nanoparticle groups were significantly different from untreated control. These results give a sense of combined release kinetics and efficacy of drugs released from nanoparticles. The released drug from nanoparticles loses potency at later time points, likely because less drug is released at these time points due to the burst release from the particles. Additionally, this assay provides an estimate of the overall potency of nanoparticle formulations encapsulating multiple payloads, for which drug release kinetics can be challenging to determine.

Acanthamoeba were treated with rifampicin-encapsulating nanoparticles *in vitro* in collaboration with Nathan Peroutka-Bigus from Dr. Bellaire's lab. The cells in groups treated by either soluble rifampicin or 5% rifampicin-loaded 10:90, 20:80, or 30:70 CPTEG:CPH nanoparticles were counted by Trypan blue exclusion hemocytometer counts and normalized to untreated controls to generate a percentage growth inhibition (Figure 7.2). At 12.5 μg/mL of rifampicin, only the 30:70 CPTEG:CPH nanoparticles had significantly different cell counts than the untreated control. There were no significant differences in percent growth inhibition between different chemistries or the soluble control at this low concentration. At 25 μg/mL of rifampicin, both 20:80 and 30:70 CPTEG:CPH nanoparticles had significantly different cell counts than the untreated control. At this higher concentration, 20:80 and 30:70

CPTEG:CPH nanoparticles showed significantly higher growth inhibition than soluble drug, which was indistinguishable from the untreatable control and the 10:90 CPTEG:CPH nano-formulation. These results show that polyanhydride nanoparticles encapsulating rifampicin can significantly reduce the growth of pathogenic *Acanthamoeba*. Furthermore, these studies illustrate that both dose and nanoparticle chemistry impact nanotherapeutic efficacy. These data from *Mycobacterium* and *Acanthamoeba* could be leveraged to provide additional insights into nanoparticle inputs that govern efficacy. It is hypothesized that some proportion of the factors that influenced nanoparticle efficacy against *B. cepacia* in Chapter 6 would maintain their influence in other biological systems, while others would likely be genus- or species-specific.

As a case in point, we tested the antimicrobial performance of a subset of the nanoparticle library used in Chapter 6 against the potential bioweapon *B. pseudomallei* (Table 7.1). This project involves collaboration with the Bellaire group at ISU for microbiological performance of the nanoparticles, as well as with Dr. Scott Broderick and the Rajan group at the University of Buffalo for the informatics analysis. Like *B. cepacia*, *B. pseudomallei* are intracellular pathogens with intrinsic antibiotic resistance.[7] *B. pseudomallei* is a biodefense threat because it is easily aerosolized and causes the disease melioidosis, which can be highly lethal and requires invasive, frequent, and lengthy antibiotic treatment.[8,9] *B. pseudomallei* had much more negative $\log_2$ values for hits than were observed previously in *B. cepacia* (Table 7.1), indicating that nanoparticles provided greater improvements in potency compared to soluble drug. A PCA analysis was performed to compare the nanoparticle performance in *B. cepacia* and *pseudomallei*. In the scores plot in Figure 7.3, *B. pseudomallei* were generally located closer to the top right corner than *B. cepacia*, indicating

a higher susceptibility toward nanoparticles. However, some *B. pseudomallei* data points lie on a trajectory orthogonal to the *B. cepacia* $\log_2$ vector. This indicates that, to some extent, different physics govern antimicrobial performance in the two species. More comprehensive testing of the nanoparticle library is needed to characterize the magnitude of the difference in performance, as well as to evaluate the organism-dependency of input descriptors' effects on antimicrobial performance. Understanding the generalizability of the conclusions from Chapter 6 would improve translation of nanoparticle design between different pathogens by (1) identifying antimicrobial performance structure-property relationships that are broadly valid, if any, and (2) identifying descriptors that show the most variability in effect between pathogens.

7.2.2 Enabling Design of Nanomedicines for Vector Control: Biodistribution of Nanoparticles in Insects

Nanoparticles could improve vector control strategies by altering the biodistribution of hydrophobic agents in mosquitoes. These delivery technologies could enable lower effective doses of insecticides, target insecticides to tissues of action within pests, and enable treatment with novel insecticide candidates whose biodistribution and activity is encumbered by hydrophobicity. Through collaborations with Dr. Edmund Norris, previously of the Coats group at ISU, and Dr. Yash Phanse of the Bartholomay group at the University of Wisconsin, we sought to identify polyanhydride chemistries and nanoparticle sizes that are internalized by yellow fever mosquitoes and American cockroaches.

We have developed a method of end group-functionalizing 20:80 CPH:SA and 20:80 CPTEG:CPH with the fluorophore rhodamine B. When microparticles and nanoparticles are synthesized from these functionalized polymers, there is a persistent fluorescent signal from the conjugated label. In *in vitro* experiments using Aag2 and C636 insect cells, we

determined that majority of cells are labeled within two hours, and that nanoparticles achieve higher uptake than microparticles of the same chemistry (data not shown).

We exposed mosquitoes to rhodamine B-labeled particles in surface contact experiments where mosquitoes are entrapped in a plastic cone containing a filter paper with a layer of nanoparticles. The mosquitoes were dissected and particle association was quantified by epifluorescence. We observed higher association of the nanoparticles with the legs and whole bodies than microparticles, confirming the results of in vitro experiments. CPH:SA nanoparticles showed a higher association with legs, whereas CPTEG:CPH nanoparticles showed a higher association with the bodies. We also investigated the biodistribution of nanoparticles in mosquito internal tissues after surface contact exposure. CPTEG:CPH nanoparticles showed much higher labeling in ovary, midgut, and Malpighian tubules (which function similarly to human kidneys) tissues than CPH:SA nanoparticles (Figure 7.4). In contrast, CPH:SA nanoparticles showed only a modest increase in fluorescence compared to non-treated controls in the midgut and Malpighian tubules.

We also tested a topical application route of exposure. This route generated much more extensive labeling of internal tissues than surface contact (Figure 7.5). Both CPH:SA and CPTEG:CPH nanoparticles showed a statistically significant labeling of ovary, midgut, and Malpighian tubules tissues compared to untreated control. For each tissue, CPTEG:CPH nanoparticles labeled more extensively than CPH:SA nanoparticles.

The above work in mosquitoes has resulted in a manuscript, which is being submitted to *PLOS Negl Trop Dis*. Future work will test nanoparticle biodistribution after different exposure routes in cockroaches. The larger size of this insect model in comparison to mosquitoes will likely enable us to characterize nanoparticle localization in the spinal cord.

Successful completion of this project will enable us to design vector-control nanomedicines for maximum potency by delivering neuroactive compounds to their tissues and sites of action.

7.3 References

(1) Smith, I. Mycobacterium Tuberculosis Pathogenesis and Molecular Determinants of Virulence. *Clin. Microbiol. Rev.* **2003**, *16* (3), 463–496. https://doi.org/10.1128/CMR.16.3.463.

(2) Seung, K. J.; Keshavjee, S.; Rich, M. L. Drug-Resistant Tuberculosis. *Cold Spring Harb Perspect Med* **2015**, *5*, 1–20.

(3) Visvesvara, G. S.; Moura, H.; Schuster, F. L. Pathogenic and Opportunistic Free-Living Amoebae: Acanthamoeba Spp., Balamuthia Mandrillaris, Naegleria Fowleri, and Sappinia Diploidea. *FEMS Immunol. Med. Microbiol.* **2007**, *50* (1), 1–26. https://doi.org/10.1111/j.1574-695X.2007.00232.x.

(4) Lorenzo-Morales, J.; Khan, N. A.; Walochnik, J. An Update on *Acanthamoeba* Keratitis: Diagnosis, Pathogenesis and Treatment. *Parasite* **2015**, *22*, 10. https://doi.org/10.1051/parasite/2015010.

(5) Phanse, Y.; Lueth, P.; Ramer-Tait, A. E.; Carrillo-Conde, B. R.; Wannemuehler, M. J.; Narasimhan, B.; Bellaire, B. H. Cellular Internalization Mechanisms of Polyanhydride Particles: Implications for Rational Design of Drug Delivery Vehicles. *J. Biomed. Nanotechnol.* **2016**, *12* (7), 1544–1552. https://doi.org/10.1166/jbn.2016.2259.

(6) Binnebose, A. M.; Haughney, S. L.; Martin, R.; Imerman, P. M.; Narasimhan, B.; Bellaire, B. H. Polyanhydride Nanoparticle Delivery Platform Dramatically Enhances Killing of Filarial Worms. *PLoS Negl. Trop. Dis.* **2015**, *9* (10), e0004173. https://doi.org/10.1371/journal.pntd.0004173.

(7) Allwood, E. M.; Devenish, R. J.; Prescott, M.; Adler, B.; Boyce, J. D. Strategies for Intracellular Survival of Burkholderia Pseudomallei. *Front. Microbiol.* **2011**, *2* (AUG). https://doi.org/10.3389/fmicb.2011.00170.

(8) Cheng, A. C.; Currie, B. J. Melioidosis: Epidemiology, Pathophysiology, and Management. *Clinical Microbiology Reviews*. 2005, pp 383–416. https://doi.org/10.1128/CMR.18.2.383-416.2005.

(9) CDC. Melioidosis https://www.cdc.gov/melioidosis/index.html (accessed Dec 3, 2019).

7.4 Tables

Table 7.1 Nanoparticle Antimicrobial Activity Against *Burkholderia pseudomallei*

Particle Formulation	Soluble IC_{50} (µg/ml)	Nanoparticle IC_{50} (µg/ml) (adj for EE)	Log_2 (Nanoparticle IC_{50} / Soluble IC_{50})
20:80 CPTEG:CPH 5% DOX	0.603	0.536	-0.170
20:80 CPTEG:CPH 5% DOX	0.570	0.490	-0.219
20:80 CPTEG:CPH 10% DOX	0.603	0.441	-0.453
20:80 CPTEG:CPH 10% DOX	0.604	0.552	-0.130
20:80 CPH:SA 10% MEM	0.749	0.798	0.091
10:90 CPTEG:SA 5% RIF	8.186	Not Detected	N/A
10:90 CPTEG:SA 10% RIF	8.186	Not Detected	N/A
10:90 CPTEG:SA 5% MEM	0.646	0.107	-2.590
10:90 CPTEG:SA 5% CAZ	3.157	1.276	-1.307
10:90 CPTEG:SA 5% CAZ	0.567	0.540	-0.071
10:90 CPTEG:SA 5% CAZ	3.079	1.228	-1.326
10:90 CPTEG:SA 10% CAZ	3.157	1.050	-1.588
10:90 CPTEG:SA 10% CAZ	0.567	0.580	0.032

7.5 Figures

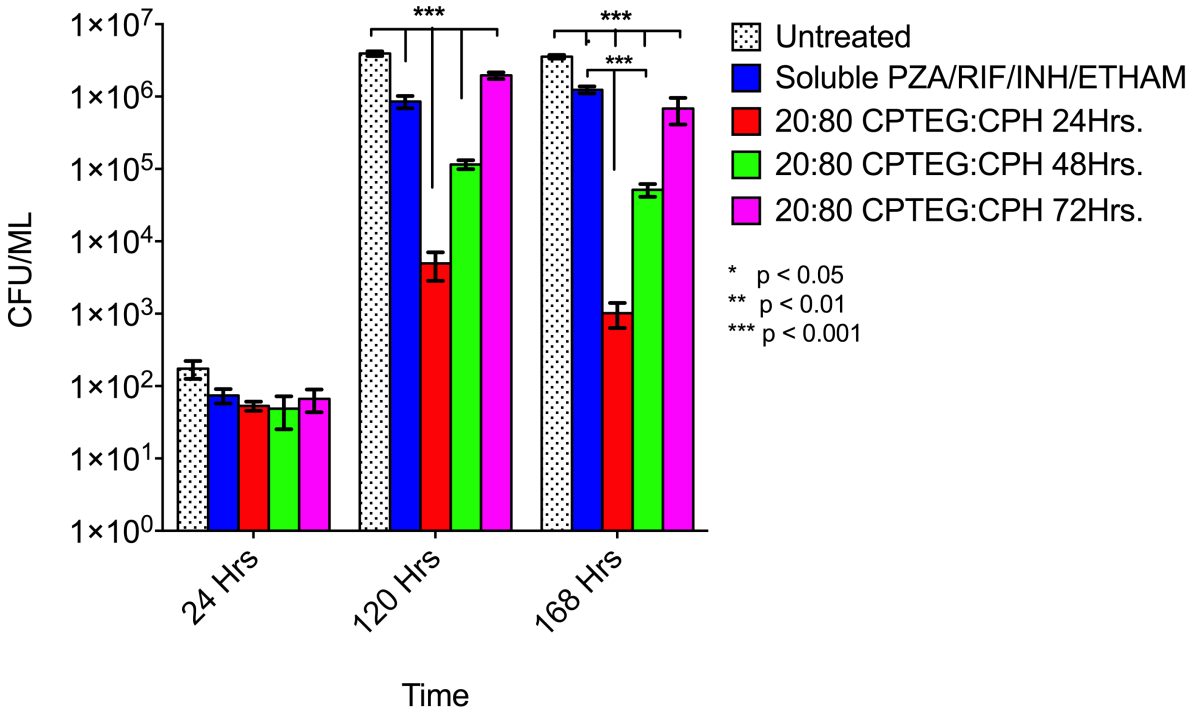

Figure 7.1 Growth inhibition of *Mycobacterium marinum* treated with nanoparticle release supernatants. The soluble group was treated with 10 µg of soluble PZA, RIF, INH, and ETHAM. Experimental groups were treated with release supernatants from nanoparticles dual-encapsulating PZA/RIF and IBH/ETHAM, gathered at the times specified in the legend. Treated groups were cultured in 7H9 broth, and plated at times listed on the x-axis on Middlebrook 7H10 or 7H11 media for CFU counting.

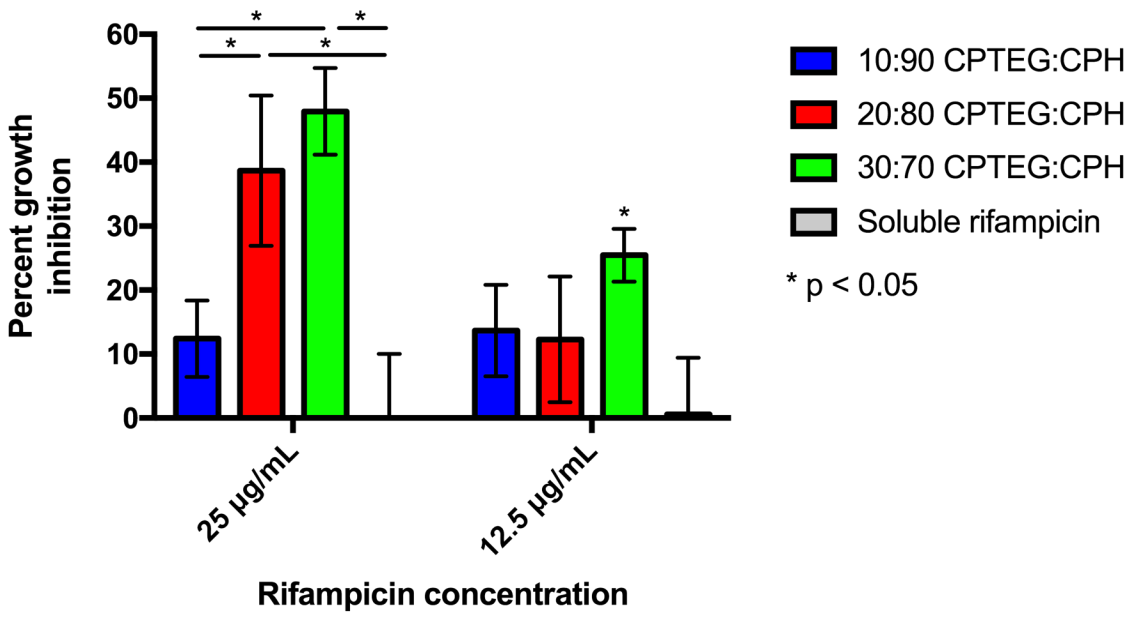

Figure 7.2 Effect of copolymer chemistry on rifampicin-medited growth inhibition of *Acanthamoeba* strain V062 at 72 hours post-treatment. Nanoparticles were loaded with 5% rifampicin (w/w). Treated groups are compared to untreated controls to generate a percentage growth inhibition.

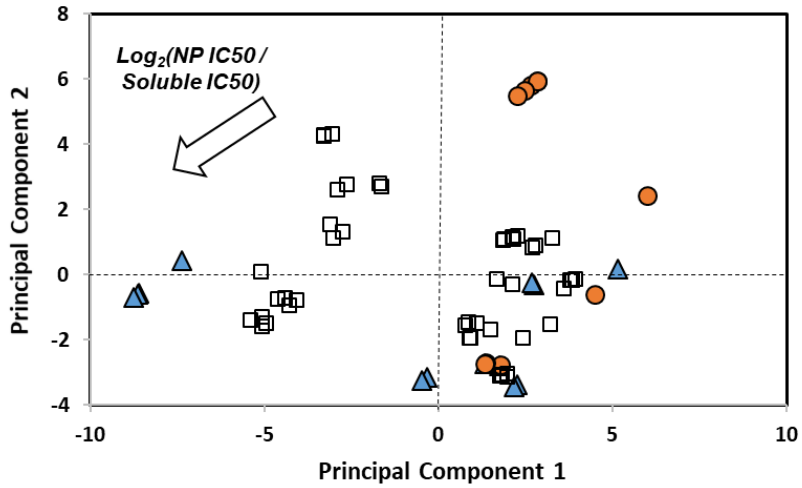

Figure 7.3 PCA scores plot comparing antimicrobial activity against *Burkholderia cepacia* and *pseudomallei*. Blue triangles represent *B. cepacia* single formulations, white squares *B. cepacia* cocktails, orange circles *B. pseudomallei* single formulations. Improved nanoparticle performance in *B. cepacia* compared to soluble drug follows a trajectory toward the top right corner. *B. pseudomallei* generally seem to be more sensitive to nanoparticles than *B. cepacia*. However, some *B. pseudomallei* lie on a trajectory orthogonal to the Log_2 vector, indicating that, to some extent, different physics govern antimicrobial performance in *B. pseudomallei* compared to *B. cepacia*. *B. cepacia* data are the same as in Figure 6.3

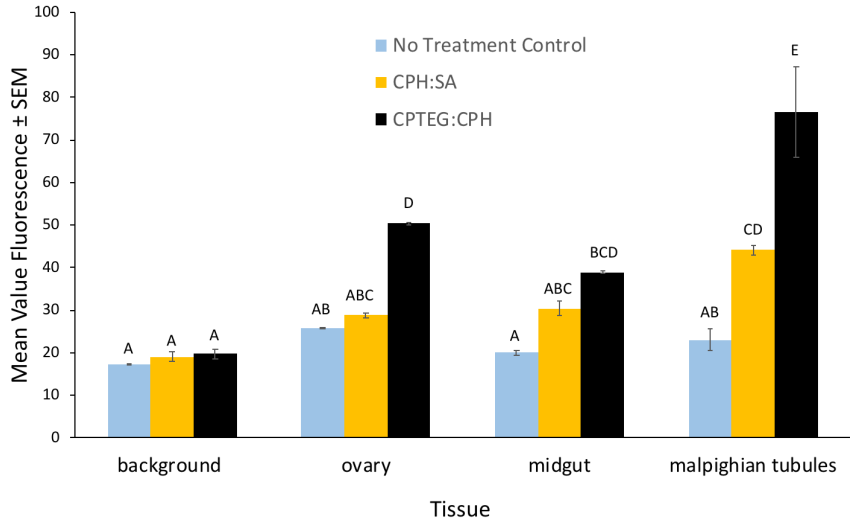

.

Figure 7.4 Rhodamine-functionalized nanoparticle internalization in mosquitoes after surface contact exposure.

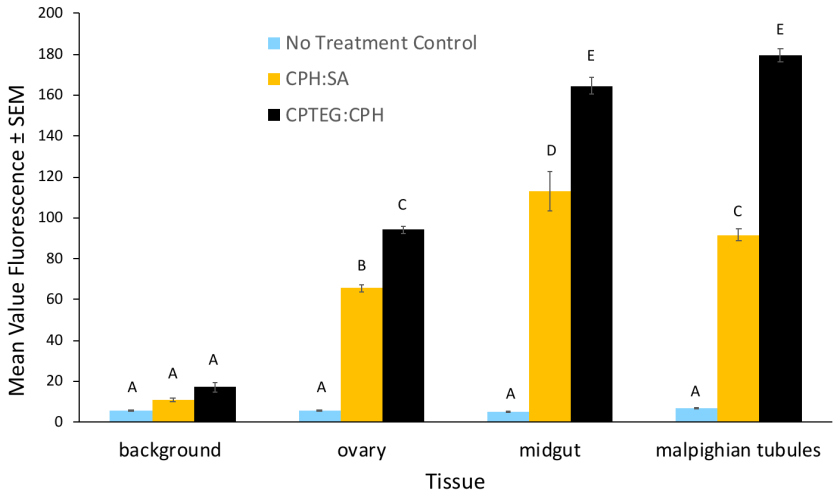

Figure 7.5 Rhodamine-functionalized nanoparticle internalization in mosquitoes after topical exposure.